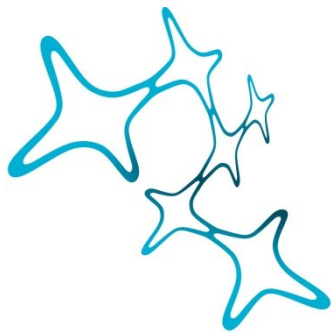

NEUROENERGETICS AND FUNCTION OF THE DEFAULT MODE NETWORK

QUANTITATIVE MEASUREMENT OF HUMAN BRAIN METABOLISM

Samira Maria Epp



Graduate School of
Systemic Neurosciences

LMU Munich



Dissertation der
Graduate School of Systemic Neurosciences der
Ludwig-Maximilians-Universität München

June 14th, 2023

Supervisor

Prof. Dr. med. Valentin Riedl

Department of Neuroradiology

Technical University of Munich

First Reviewer: Prof. Dr. med. Valentin Riedl

Second Reviewer: Dr. Lars Kunz, PD

External Reviewer: Prof. Stephen Mayhew, PhD

Date of Submission: 14th of June, 2023

Date of Defense: 10th of October, 2023

Although only 2% of our body weight, the brain uses 20% of our energy, but produces 100% of our suffering

- and 100% of our joy

ABSTRACT

Functional brain imaging relies on the fact that neuronal activity and brain metabolism are closely coupled. Changes in neuronal activity evoke vascular responses, more precisely changes in cerebral blood flow (CBF) and blood volume (CBV), as well as metabolic responses, that is oxygen and glucose consumption. Yet, in neuroimaging research, most studies are not measuring these different responses separately. Instead, most researchers acquire the blood-oxygen-level-dependent (BOLD) signal, which is relying on a mismatch between oxygen delivery and the cerebral rate of oxygen (CMRO₂). Increases in neuronal activity usually trigger larger CBF than CMRO₂ increases. Only if more oxygen is delivered than is consumed, deoxyhemoglobin (dHb) levels in venous blood drop, which gives rise to a positive BOLD response. Thus, metabolic and vascular contributions cannot be disentangled by a simple BOLD experiment. Further, impaired metabolism in different disease states or after drug administration have been shown to influence the amplitude of BOLD signals. Due to its relative nature, its amplitude is not comparable in terms of neuronal activity level across different brain regions within one subject and even less across subjects or patient populations. In contrast to fMRI BOLD, CMRO₂ is a physiological signal that directly measures oxidative brain metabolism. Apart from oxygen, the brain needs glucose to fuel its brain activity. The cerebral rate of glucose (CMRglc) quantifies glucose consumption and, via comparing CMRO₂ to CMRglc, provides information about levels of oxidative versus nonoxidative metabolism. Changes in both glucose and oxygen metabolism are supposedly more localized at the exact site of neuronal activation than CBF and BOLD changes.

In this doctoral thesis, I show the applicability of simultaneous CMRO₂ and CMRglc measurements during a visual stimulation experiment within the first study. I then extend these findings to a cognitive design within the second study. I show that multiparametric, quantitative BOLD (mqBOLD) measurements in healthy human subjects are sensitive enough to measure absolute task-induced changes in CMRO₂. Further, by comparing fMRI BOLD with CMRO₂, I provide evidence that specifically *negative* BOLD responses are not necessarily indicative of reduced oxygen metabolism and thereby cannot be interpreted as reduced excitatory brain activity. This showed in a dissociation of the sign of BOLD and CMRO₂ changes, which was more pronounced for negative than for positive BOLD signal changes and especially apparent in regions of the default mode network (DMN). While parts of the DMN with significant BOLD decreases also showed concomitant task-induced *decreases* in oxygen metabolism, around half to two-thirds of DMN voxels actually showed *increased* oxygen consumption, despite consistent negative BOLD signal changes. These results fundamentally question our commonly accepted interpretation of specifically negative BOLD responses as indicators for decreased neuronal activity.

Overall, measuring brain metabolism has several advantages over fMRI BOLD. The most important ones are its better localization at the site of neuronal activity and its potential for measuring absolute energy consumption. While there is currently no way of measuring CMRglc without the administration of radiotracers, the non-invasive measurement of CMRO₂ developed into a promising area of research. Further steps into improving the applicability of measuring cerebral oxygen consumption are important to consolidate its path into clinical routines as well as within neuroimaging research, as an extension or alternative to fMRI BOLD measurements.

CONTENT

ABSTRACT	5
LIST OF ABBREVIATIONS	8
1 GENERAL INTRODUCTION	9
1.1 How to measure human brain activity and brain energy metabolism with functional brain imaging..	10
1.1.1 Absolute glucose and oxygen consumption: CMRglc and CMRO2	10
1.1.2 Blood-oxygen-level-dependent functional imaging.....	11
1.1.3 Recent developments in quantitative imaging: quantitative MRI and fPET	16
1.2 Task-induced changes in metabolism	18
1.2.1 Visual stimulation	18
1.2.2 Default mode network	18
1.3 Aims of the current work	21
2 PROJECT I: SIMULTANEOUS MEASUREMENT OF OXYGEN AND GLUCOSE CONSUMPTION DURING VISUAL STIMULATION IN THE HUMAN CORTEX.....	23
3 PROJECT II: NEGATIVE BOLD SIGNALS DO NOT NECESSARILY INDICATE REDUCED OXYGEN METABOLISM – A QUANTITATIVE MRI STUDY	48
4 GENERAL DISCUSSION	93
4.1 Implications of Project I.....	93
4.2 Implications of Project II	94
4.3 Limitations.....	99
5 OUTLOOK.....	100
6 CONCLUSIONS.....	102
REFERENCES.....	103
ACKNOWLEDGEMENTS.....	120
CURRICULUM VITAE.....	121
LIST OF PUBLICATIONS.....	122
AFFIDAVIT / EIDESSTATTLICHE VERSICHERUNG	123
DECLARATION OF AUTHOR CONTRIBUTIONS	124

List of abbreviations

(f)MRI	(Functional) magnetic resonance imaging
(f) PET	(Functional) positron emission tomography
BOLD	Blood oxygen level dependent
mqBOLD	Multiparametric, quantitative BOLD
CBF	Cerebral blood flow
CBV	Cerebral blood volume
OEF	Oxygen extraction fraction
CMRO ₂	Cerebral metabolic rate of oxygen
CMRglc	Cerebral metabolic rate of glucose
dHb	Deoxyhemoglobin
Hct	Hematocrit
R ₂	1/T ₂ , transverse relaxation rate, irreversible, due to tissue properties
R ₂ *	1/T ₂ *, sum of reversible and irreversible decay
R ₂ '	R ₂ * - R ₂ : reversible relaxation alone, due to susceptibility differences
pCASL	Pseudo continuous arterial spin labeling
DSC	Dynamic susceptibility contrast
EPI	Echo planar imaging
[¹⁸ F]-FDG	Fluorodeoxyglucose F 18, radiotracer for CMRglc PET imaging
TE	Echo time
TR	Repetition time
FOV	Field of view
ROI	Region of interest
DMN	Default mode network
DAN	Dorsal attention network
GM	Gray matter
OGI	Oxygen-to-glucose index
EEG	Electroencephalography
PCC	Posterior cingulate cortex
SNR	Signal-to-noise ratio

1 General introduction

Humans spend around 20% of their energy on their brains, which makes them the species that spends the most energy on their brains relative to the rest of their bodies. That energy is mostly used to fuel information processing across neurons and brain regions. These signaling related processes are assumed to cost 75% of the energy in grey matter and 60% of the energy throughout the whole human brain (Engl & Attwell, 2015). Why is the human brain so energetically expensive? Evolutionary novel pathways and complex cognition processes such as memory or reading are related to increased energy use, due to a high neuromodulatory activity (Castrillon et al., 2023). Additionally, humans have a highly connected brain and the number of connections, measured by the degree of functional connectivity of a brain area, scales with increased energy (glucose) needs (Passow et al., 2015; Tomasi et al., 2013), even within single subjects (Castrillon et al., 2023). Because of the large number of synapses, more input has to be integrated, yielding information integration at the postsynaptic level that consumes 74% of the total energy spent on signaling, compared to only 34% in rodents (Attwell & Iadecola, 2002). However, this energetically expensive architecture also seems to make certain brain areas as the default mode network (DMN) more prone to be affected in various disease states. Patients with Alzheimer's disease typically show decreased glucose metabolism early on, particularly in frontoparietal and default mode network areas (Di & Biswal, and Alzheimer's Disease Neu, 2012; Leech & Sharp, 2014; Minoshima et al., 1997; Mosconi, 2005). Moreover, studies reported a reduction in metabolism throughout the brain during healthy ageing, specifically in frontal regions, while motor and sensory regions are less affected (Aanerud et al., 2012; Deery et al., 2023). Schizophrenia, as well as autistic spectrum disorder and traumatic brain injury have been connected to decreased metabolism in the posterior cingulate cortex (PCC), core region of the DMN (Leech & Sharp, 2014). A range of different diseases have been connected to functional connectivity alterations and lack of suppression in the DMN (Anticevic et al., 2012; Mohan et al., o. J.). Therefore, a better understanding of brain metabolism, specifically within DMN regions, is an important window into our further understanding of healthy brain activity and the diagnosis and characterization of pathologies.

The research projects presented in this thesis focused on new methods for non-invasive, quantitative imaging of glucose and oxygen consumption, the fuels for brain activity, via magnetic resonance imaging (MRI) and positron emission tomography (PET). The first chapter of the introduction describes the history and current work of measuring the metabolic rates of glucose (CMRglc) and oxygen (CMRO₂) within the human brain as well as its relations to functional imaging using the blood-oxygen-level-dependent (BOLD) signal. It concludes with recent methodological advances, namely multiparametric, quantitative BOLD (mqBOLD) and functional PET (fPET) imaging, which both research projects are built on. While the first chapter focuses on the methodology, the second chapter introduces the theoretical backbone of the current work, which forms the basis of our hypotheses. First, evidence for changes in CMRO₂ and CMRglc during visual stimulation is briefly described, while the second subsection focusses on the DMN. I review the history of the DMN, evidences for DMN deactivations and mixed or negative findings related to DMN deactivations. After a brief description of the aims of the current PhD work, both research projects are presented in manuscript style in sections two and three. These manuscripts are currently in preparation for submission. General findings are then discussed at the end of this thesis.

1.1 How to measure human brain activity and brain energy metabolism with functional brain imaging

The brain is an energetically expensive organ and fortunately, changes in brain signaling are coupled to changes in energy usage. In fact, from the very beginning of functional brain imaging, measuring human brain activity has been relying on the fact that neuronal activity and brain metabolism are closely coupled (Hoge & Pike, 2001; Magistretti & Pellerin, 1999). Oxygen and glucose fuel brain activity via the oxidation of glucose to produce ATP (adenosine triphosphate), the energy substrate in the body (Hoge & Pike, 2001). Yet, in early experiments in 1955, researchers failed to show that brain activity in men performing an arithmetic task was coupled to a *global* increase of cerebral blood flow (CBF) or of the metabolic rate of oxygen consumption (CMRO₂) (Sokoloff et al., 1955). However, in cats, via autoradiography, the same researcher could show in 1961 that CBF increased *regionally* in the visual cortex after stimulation, being the first example of functional neuroimaging. This technique unfortunately was too invasive for application in humans. Only the development of the positron-emission-tomography (PET) in the 1970s made functional neuroimaging possible *in vivo* in humans (Reivich et al., 1979; Ter-Pogossian et al., 1975). For excellent reviews on the development of functional neuroimaging and its relationship with oxidative metabolism see Hoge & Pike (2001) and Sokoloff (2008a).

1.1.1 Absolute glucose and oxygen consumption: CMR_{glc} and CMRO₂

With the development of PET imaging, scientists could now measure *regional* glucose consumption via the injection of fluorodeoxyglucose ([¹⁸F]-FDG) (Huang et al., 1980; Reivich et al., 1979). Also, measurements of CBF via the injection of H₂¹⁵O were possible. Further, as Kety and Smith have already shown much earlier (1945), Fick's formula could be applied to any substance which is removed from the blood by the brain. This made the calculation of the metabolic rate of oxygen (CMRO₂) possible through multiplication of CBF with the oxygen content of arterial blood and the oxygen extraction fraction (OEF), measured via inhaled gas (P. Fox et al., 1988; P. T. Fox & Raichle, 1986a). This basic principle still applies today, even though the different parameters can now be acquired non-invasively via MRI instead of PET, see section 1.1.3.

During rest, regional correlation of CBF and CMRO₂ (P. T. Fox & Raichle, 1986a; Henriksen et al., 2021), CBF and CMR_{glc} (Henriksen et al., 2018) and CMRO₂ and CMR_{glc} (F. Hyder et al., 2016) are usually high, although regional variability exists (Ances et al., 2008; Blazey, Snyder, Su, et al., 2018; Henriksen et al., 2018; Vaishnavi et al., 2010). Yet, the correlation of task-induced changes across parameters is less consistent. Task-induced increases in CBF and CMR_{glc} are mostly coupled (P. Fox et al., 1988; Newberg et al., 2005; Paulson et al., 2010), although pharmacological intervention in animals can lead to increases in glucose consumption without increases in CBF, suggesting both CBF and CMR_{glc} are triggered in parallel by neuronal activity (Magistretti & Pellerin, 1999). The uncoupling between increases in CBF and CMRO₂, on the other hand, was striking from the very beginning (P. T. Fox & Raichle, 1986a). Early studies showed large increases in CBF, between 29% and 50%, even though increases in CMRO₂ were small (around 5%) (P. Fox et al., 1988; P. T. Fox & Raichle, 1986a). Initially, the extent of CBF-CMRO₂ uncoupling remained a debated topic: while some studies found no uncoupling at all in the rat brain, that is similar increases for CMRO₂, CMR_{glc} and CBF (F. Hyder et al., 1996), others found no increase in CMRO₂ during stimulation in the rat striatum despite increases in CBF and CMR_{glc} (Lowry & Fillenz, 1997). However, after the very early PET studies, subsequent research reported consistent increases in CMRO₂ during visual stimulation in

humans that ranged between 10-30% (Donahue et al., 2009; Fujita et al., 2006; Hoge & Pike, 2001; S.-G. Kim et al., 1999; Liu et al., 2019; R. G. Shulman et al., 2001). CBF increases were usually 2-4 times larger (Ances et al., 2008; Buxton, 2010; Buxton et al., 2014), but the exact degree of uncoupling between CBF and CMRO₂ has shown to vary across brain regions and depends on the type of stimulation. One example are subcortical structures as the hippocampus, where the uncoupling of CBF and CMRO₂ increases is less pronounced, probably due to different vessel densities compared to neocortex (Shaw et al., 2021). Attention also seems to play a crucial role; visual stimuli that are attended increase the CMRO₂ response more, resulting in less pronounced uncoupling between CMRO₂ and CBF (Moradi et al., 2012). The uncoupling between increases in CMRO₂ and increases in CBF or CMRglc during focal neuronal activity resulted in two important discoveries.

First, uncoupling between task-induced increases in CMRglc versus CMRO₂ indicated that not all metabolic needs of the brain are uniquely met by oxidative metabolism. If fractional CMRglc increased more than fractional CMRO₂, there needed to be a task-induced increase in non-oxidative metabolism (P. Fox et al., 1988). During the full oxidation of glucose, six moles of oxygen and one mole of glucose are metabolized, so the oxygen-to-glucose index (OGI) for the full oxidation of glucose should be around 6, but drops significantly during focal activity (A.-L. Lin et al., 2008; Paulson et al., 2010; Uludağ et al., 2004; Vafaei et al., 2012). However, even in the resting state, the average OGI of the brain is around 5.5, with frontoparietal and default mode regions showing a lower OGI and thus higher levels of non-oxidative metabolism (Blazey, Snyder, Goyal, et al., 2018; Blazey, Snyder, Su, et al., 2018; Vaishnavi et al., 2010). Blazey and colleagues deduced that around 10% of the energy needs in the resting state are met via non-oxidative metabolism (Blazey, Snyder, Goyal, et al., 2018). Please note that this view has been rejected by (F. Hyder et al., 2016) who propose a uniform OGI during rest. So far, no single hypothesis exists that explains the existence of non-oxidative metabolism or aerobic glycolysis in the brain and its increase during neuronal activity. Aerobic glycolysis is the definition for a state where, despite sufficient oxygen being present, glucose is not fully oxidized, leading to increases in lactate levels. A role of lactate may as a signaling molecule in long-term learning and synaptic plasticity has been discussed (Magistretti & Allaman, 2018; Yang et al., 2014), because stimulation-induced decreases of the OGI in task-relevant areas last longer than the actual task duration (Madsen et al., 1995).

Second, the task-induced uncoupling between CBF and CMRO₂ is the basis for another technique that since its discovery in the 1990s (Ogawa et al., 1990, 1993) has taken over the majority of functional brain imaging research: the blood-oxygen-level-dependent (BOLD) signal. It takes advantage of this luxury perfusion, i.e. the overcompensatory increase in blood flow that is usually 2-4 times higher than the increase in CMRO₂. In the following sections we will see how the measurement of fMRI (functional magnetic resonance imaging) BOLD is based on the uncoupling between blood supply and oxygen consumption and look at the physiological model behind the BOLD signal and how to interpret it.

1.1.2 Blood-oxygen-level-dependent functional imaging

fMRI BOLD imaging has several advantages over classical PET imaging and has therefore, since its discovery, taken over a large fraction of neuroimaging research. It has both good temporal and spatial resolution, making it possible to investigate local changes in a temporally resolved way, without the injection of any exogenous tracer. It needs much less time than a PET experiment and allows to measure several task conditions in one imaging session. Nevertheless, as a conglomerate signal, the BOLD response does not reflect one biophysical process but mainly relies on the mismatch between

blood flow and CMRO₂ response (Hoge & Pike, 2001). Additionally, the BOLD response is a relative and not an absolute signal, fluctuating around an arbitrary baseline, which only allows measuring changes in the signal, but does not allow for comparison of baseline activity. Still, it is widely accepted that the BOLD signal is a proxy for underlying neuronal activity because its time course correlates strongly with local field potentials (LFPs), which consist of a combination of post-synaptic and pre-synaptic activity (A. Ekstrom, 2010; A. D. Ekstrom, 2021; Hillman, 2014; D. S. F. Hyder, 2010a; Logothetis, 2003, 2008). The correlation of spike rates, measured by multi-unit activity (MUA), with the BOLD signal is weaker (Attwell & Iadecola, 2002; Logothetis, 2003; Logothetis et al., 2001) and may not be a direct correlation, but mediated by the correlations between LFPs and spike rate. See Ekstrom (2010) for an excellent review of how and when the fMRI BOLD signal relates to underlying neural activity.

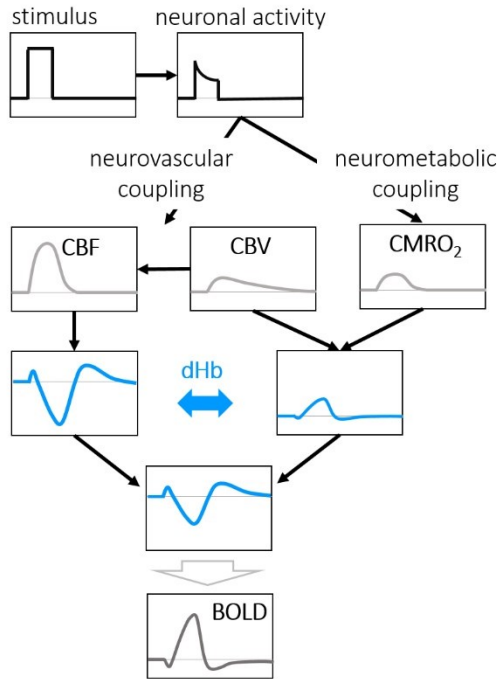
Basics of the canonical positive BOLD response

What is the physiological model behind the canonical, positive BOLD response? As its name indicates, the blood-oxygen-level-dependent signal is dependent on the oxygenation, more precisely on the deoxyhemoglobin (dHb) levels of venous blood, which is measured via T₂* weighted MRI. dHb is paramagnetic and thus elicits small disturbances in the magnetic field, leading to increased dephasing of the protons and thus to a reduced T₂* signal. Following stimulus-induced neuronal activation, vessels dilate and arterial CBV rises as smooth muscles around the arteries relax, this is called neurovascular coupling (see Figure M1|A). Consequently, CBF increases and washes out dHb in the veins and capillaries, leading to an overall decrease in dHb, less dephasing and thus an increase in the T₂* or BOLD signal (Byrne et al., 2014; Drew, 2019). However, neuronal activity usually also goes hand in hand with an increase in oxidative metabolism (Fujita et al., 2006; Hoge & Pike, 2001), thus results in increased oxygen consumption which leads to an increase in dHb in the venous blood. This is called neurometabolic coupling (see Figure M1|A) (D. S. F. Hyder, 2010b). This increase in CMRO₂, as well as the slow, venous increase of CBV counteracts the aforementioned wash-out of dHb by the blood flow, but is usually not strong enough to give rise to a negative BOLD response (Blockley et al., 2013; Buxton, 2010). Experimental evidence shows that the rise in CBF is usually 2-4 times larger than the rise in CMRO₂, so the higher the luxury perfusion, the stronger the positive BOLD signal (Ances et al., 2008; Buxton, 2010; Buxton et al., 2014; Davis et al., 1998, S. 199; A.-L. Lin et al., 2010; Uludağ et al., 2004). The canonical positive BOLD response and its underlying fractional changes in CMRO₂ and CBF are also displayed and explained in Figure M1|B a).

However, there are different factors that influence this canonical positive BOLD response. First, the exact coupling between task-induced CBF and CMRO₂ responses, the coupling ratio n , depends on both brain regions and stimulus. It has been shown that in subcortical areas as the hippocampus, the n -ratio is smaller than in the neocortex, leading to weaker BOLD responses (Ances et al., 2008; Restom et al., 2008; Shaw et al., 2021). This could in part be explained by the vascular density, which varies across regions and is lower in the hippocampus than e.g. in V1 (A. D. Ekstrom, 2021; Shaw et al., 2021). The vascular density is also higher in sensory cortices in comparison to association cortices, facilitating a stronger blood flow and blood volume response and giving rise to a higher BOLD signal (Harrison, 2002). The type of stimulation also has an impact on the amplitude of the BOLD response by modulating the size of the CMRO₂ increase. Attention seems to influence the CBF and even more the CMRO₂ response, but only influences the BOLD response minimally. During attention periods, the CBF response tripled, while the CMRO₂ increase was nearly 8-fold, compared to the non-attended condition (Moradi et al., 2012). Second, the baseline blood flow and oxygenation influences the strength of the BOLD signal. The amount of dHb in the baseline state is a scaling factor

for the BOLD response and sets its limit, i.e. when all dHb is washed out, the BOLD response cannot increase further despite possible increases in CBF (Buxton, 2010; Griffeth et al., 2012; Whittaker et al., 2016). For excellent reviews on the basis of the BOLD response and its interpretation see (Buxton, 2010; Drew, 2019; A. Ekstrom, 2010; A. D. Ekstrom, 2021).

A | Physiological BOLD model



B | Biophysical Davis model

$$\text{BOLD}[\%] = M \left[1 - \left(\frac{\text{CBF}}{\text{CBF}_0} \right)^{\alpha-\beta} \left(\frac{\text{CMRO}_2}{\text{CMRO}_{2_0}} \right)^{\beta} \right]$$

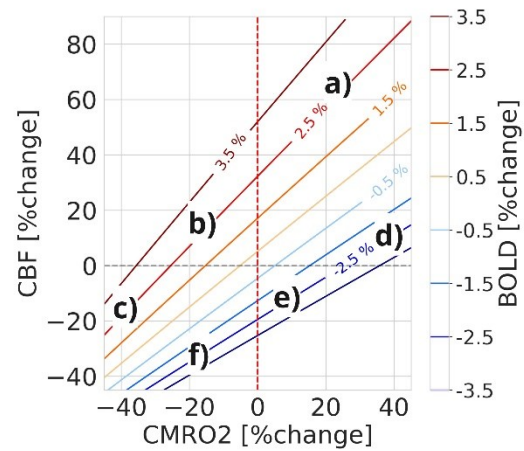


Figure M1. A | Physiological model of the canonical positive BOLD response. Increased neuronal activity causes elevated energy metabolism (CMRO₂) and blood volume (CBV), both resulting in higher dHb in venous blood. At the same time, cerebral blood flow (CBF) increases oxygen delivery, lowering dHb levels. A positive BOLD signal arises with stimulus-induced decreases of dHb levels in the venous blood, resulting from CBF increases that are larger than concomitant increases in oxygen consumption. **B |** The biophysical Davis model and its visualization across a range of fractional CBF and CMRO₂ changes. BOLD responses (%BOLD), displayed by the colored lines, are modeled in relation to changes in CMRO₂ on the x-axis and changes in CBF on the y-axis (%CBF and %CMRO₂), using $M = 10$, $\alpha = -0.05$, $\beta = 0.98$, following Gagnon et al. (2016). CBF_0 and CMRO_{2_0} denote the baseline. According to the model, the sign and amplitude of the BOLD response depend on the combined changes in CBF and CMRO₂. A positive BOLD response, resulting from decreased dHb levels and displayed in hot colors, arises either a) when oxygen delivery via CBF surpasses oxygen consumption, called ‘canonical’ BOLD response, b) with increased CBF, but decreased CMRO₂, or c) when decreases in CBF are smaller than decreases in CMRO₂. A negative BOLD response, resulting from increased dHb levels and displayed in cool colors, arises either d) when oxygen consumption, i.e. CMRO₂ surpasses oxygen delivery via CBF, e) with increased CMRO₂, but decreased CBF, or f) when decreases in CBF are larger than decreases in CMRO₂.

The Davis model: a biophysical model for BOLD-signal changes

As we have seen, the amplitude of the BOLD signal depends on the exact relation between the CBF and CMRO₂ responses as well as on the baseline dHb content. The Davis model (Davis et al., 1998) is a biophysical model that relates changes in the BOLD-signal to changes in CBF and CMRO₂ and has served as the basis for calibrated BOLD experiments. Its robustness has since been proven by

multiple studies (Ances et al., 2008; Gagnon et al., 2016; Griffeth et al., 2015). The formula and its visualization is displayed in Figure M1|B. M is a global scaling factor that accounts for baseline dHb and scanning parameters such as field strength and echo time (Buxton et al., 2004; Davis et al., 1998). α is the power-law exponent used to describe the coupling of changes in CBV to changes in CBF by a power-law relationship. It was set to $\alpha = 0.38$ by Grubb et al. (1974), but newer papers report lower values between 0.16 and 0.3, while β is dependent on the magnetic field strength with $\beta = 1.5$ at 3T (J. J. Chen & Pike, 2009; Hua et al., 2019; Wesolowski et al., 2019; Zhang et al., 2020). Optimized modeling, treating α and β as free parameters, result in better estimates of CMRO2, specifically in the case when CBF decreases, but remove their physiological meaning (Griffeth et al., 2013). A subsequent paper found different optimal values of α and β depending on the field strength, using evidence from oxygen-sensitive two-photon microscopic measurements of the cortical microvasculature (Gagnon et al., 2016). In Figure M1|B the Davis model is displayed based on $\alpha = -0.05$, $\beta = 0.98$. These are the suggested values for 3T, based on the optimized modeling values (Gagnon et al., 2016). Hence, the Davis model is the mathematical framework that formalizes dependencies between fractional changes in CMRO2, CBF and BOLD signal, based on a fixed baseline oxygenation (M-factor) and coupling between CBF and CBV. Both positive as well as negative BOLD responses can be formalized within this framework.

Negative BOLD responses (NBRs)

In the first section, I have described the ‘canonical’ positive BOLD response, which arises when oxygen delivery via CBF surpasses oxygen consumption. Can we expect the same, yet inverted, neurovascular coupling for negative BOLD signals, i.e. a decrease of CBF that is larger than the decrease in CMRO2? Negative BOLD signals and their interpretation have been a matter of debate. The Davis model is usually used in the calibrated BOLD context to determine dynamic changes in CMRO2 by measuring changes in BOLD and CBF, and determining the scaling parameter M in a calibration experiment, using mostly gas inhalation (Blockley et al., 2012, 2013; Bright et al., 2019; Davis et al., 1998; Zhang et al., 2020). Independent of the different parameters used to determine the change in CMRO2, the Davis model gives interesting insights about possible values of %CMRO2 and %CBF that result in a NBR. This could result from an ‘inverse’ neurovascular coupling in the sense that instead of an increase in CBF, there is a decrease in CBF coupled to a smaller decrease in CMRO2, as assumed by Raichle et al. (2001) and displayed in Figure M1|B f). Note that the spacing of the lines in graph M1|B is not equally distributed. The spacing between lines is smaller 1) in the negative domain (left side of the graph) with decreases in CBF and CMRO2, and 2) in general for negative BOLD responses (blue lines) compared to positive BOLD responses (red lines). Spacing is largest in the upper left quadrant, where CBF increases are larger than CMRO2 increases, indicating canonical neurovascular coupling. In graph sections with smaller line spacing, small variations in the CBF and CMRO2 response have a larger impact on the BOLD response. Concretely, a decrease of -40% CBF coupled to a decrease of -20% CMRO2 would result in a BOLD *decrease* of -3.5%, according to the model, while the same constellation in the positive domain would only lead to a BOLD *increase* of 1.5%. In general, negative BOLD responses are more sensitive to the exact CBF-CMRO2 coupling than positive BOLD responses. The Davis model also shows that NBRs are not only to be found when the CBF decrease is larger than the CMRO2 decrease, named ‘inverse’ canonical BOLD response and marked as f) in Figure M1|B. An increase in dHb levels and thus a NBR also arises when either 1) %CMRO2 increase is larger than the %CBF increase, marked as d) in Figure M1|B, or 2) when an increase in %CMRO2 is coupled to a decrease in %CBF, marked as d) in Figure M1|B. In this latter

case, the strongest negative BOLD response arises because both decreasing CBF and increasing CMRO2 are increasing the level of dHb.

While these are only theoretical considerations, it has been shown empirically in rats by Schridde et al. (2008) that negative BOLD signals can arise despite increased neuronal activity in the hippocampus, due to the fact that the CMRO2 increase exceeded the CBF increase. Another example was described in transgenic mice, where optogenetic stimulation of astrocytes resulted in a negative BOLD signal due to oxygen consumption, but without neuronal activation (Takata et al., 2018). In a different study, Shih et al. (2011) found a negative BOLD response despite elevated levels of spiking activity due to noxious forepaw stimulation in rats, which was caused by decreases of CBF in contrast to non-significant changes in CMRO2 and CMRglc. So in all of these cases, a negative BOLD response could not be interpreted in terms of decreased neuronal activity, whereas the only study with similar results in humans is, to my knowledge, the study of (Stiernman et al., 2021). Here, the authors observed a negative BOLD response in regions of the DMN despite constant or increased glucose consumption. As they did not measure CBF, it is not clear whether this was either a result of increased oxygen consumption, but not matched by constant or slightly increased CBF responses, or CBF decreased together with constant or increased CMRO2 responses.

In general, neurovascular coupling underlying NBRs seems to be different from positive BOLD responses (PBRs). First of all, high-resolution studies showed laminar differences in the NBR, rather located in deeper layers compared to the PBR (Boillat et al., 2020; Goense et al., 2012; Huber et al., 2014). Even though most studies report a neuronal basis of the NBR and similar neurovascular coupling as in the PBR, the exact CBF-CMRO2 coupling ratio was reported to be different for NBRs versus PBRs in a number of studies. In a study of Mullinger et al. (2014), unilateral nerve stimulation resulted in a PBR in contralateral and a NBR in ipsilateral sensorimotor cortex. The authors showed that both CBF and CMRO2 decreased in ipsilateral areas, but the %CBF-%CMRO2 coupling ratio was very close to one and significantly different from regions with PBR. For the NBR, CBF and CMRO2 amplitudes were nearly matching, resulting in only a very small BOLD decrease. The authors draw the conclusion that neurovascular coupling is different for positive and negative BOLD responses, as also suggested by Devi et al. (2022b). Yet, this contradicts other studies which found similar coupling ratios for both positive and negative BOLD responses (P. Lin et al., 2011; Pasley et al., 2007; Shmuel et al., 2002; Stefanovic et al., 2004).

Overall, while it has been suggested that negative BOLD signals are linked to inhibitory brain activity, thus decreases in overall neuronal activity (Boorman et al., 2010; Gu et al., 2019a; Koush et al., 2021a; Mayhew et al., 2022a; Mullinger et al., 2014), the exact coupling of the NBR to CBF, CBV and CMRO2 remains unclear. The NBR has been reported to differ from the PBR in a number of studies regarding the exact coupling between CBF and CMRO2, the time-course of the elicited HRF and cortical depth (Devi et al., 2022b; Goense et al., 2012; Huber et al., 2014; Moon et al., 2021; Mullinger et al., 2014). Yet, besides the Stiernman et al. study, the aforementioned studies looked at the NBR in somatosensory cortices with dense capillaries and consistent neurovascular coupling. But neurovascular coupling of the negative BOLD response might also be region-specific and be different in association cortices than in somatosensory cortices (A. D. Ekstrom, 2021). Along these lines, neurovascular coupling specifically in DMN regions has shown to be reverted during hypoxia (Rossetti et al., 2021a), see also the section 1.2.2 about the default mode network below. To sum it up, slight differences in neurovascular coupling between the NBR and PBR seem to exist in somatosensory cortices. These differences could be inherent to the negative BOLD signal, but could be more pronounced or even have a different origin in other brain areas.

Localization of the BOLD response

A final problem of the BOLD signal that I briefly want to mention is its localization. BOLD-responses, measured by gradient-echo EPI sequences are usually biased towards large, pial veins that drain the deoxygenated blood (Beckett et al., 2020). Additionally, as Sokoloff (2008b) pointed out, no cells have ‘their own private blood flow’. That means that active neurons will increase the CBF response within a larger area, thus producing a BOLD-response that is more widespread and less localized than the focal increase in glucose or oxygen metabolism. The metabolic response should thus be closer to the locus of increased neuronal activity than the BOLD response.

1.1.3 Recent developments in quantitative imaging: quantitative MRI and fPET

As has been shown above, the fMRI BOLD signal alone cannot resolve questions about underlying metabolic or neuronal activity in the brain. Also, it is a relative signal, so its baseline is not interpretable and questions about how regions differ in their baseline metabolism or neuronal activity levels cannot be answered. To answer these questions, quantitative methods for the estimation of CMRO₂ and CMRglc in the human brain are necessary. In the following, I will shortly review methods for the estimation of quantitative CMRO₂ and CMRglc, which represent the methodological basis for research projects I and II of this thesis.

Measuring CMRO₂

For measuring fractional changes in CMRO₂, the Davis model (Davis et al., 1998), introduced above, has been used in the calibrated BOLD framework, via mapping of the M-factor by a gas challenge. Instead of gas calibration, R₂' calibration methods have been suggested to quantitatively evaluate the cerebral dHb content and calculate the M-factor (Blockley et al., 2012, 2013, 2015; J. J. Chen et al., 2022; Fujita, 2003; Shu et al., 2016) necessary for calibration. For an extensive review over different calibration methods see the review of Bright et al. (2019). Recently, based on work of Yablonskiy and Haake (1994) studying the MRI signal behavior in the static dephasing regime, a multiparametric, quantitative BOLD (mqBOLD) method has been developed (Christen et al., 2012; He & Yablonskiy, 2007). Since then, it has been optimized (Baudrexel et al., 2009; Hirsch et al., 2014; Hirsch & Preibisch, 2013; Kaczmarz et al., 2020; Preibisch et al., 2008), applied to a patient population (Göttler et al., 2019) and compared to PET measurements (Kufer et al., 2022). The main difference to calibrated BOLD is that it does not rely on the Davis model, thus its main goal is not to calculate the M-factor in order to calculate changes in CMRO₂. Instead, via multiparametric measurements, quantitative OEF and CMRO₂ maps are derived by measuring R₂' and CBV separately, yielding an OEF map, that, multiplied by CBF, is equivalent to the CMRO₂ map. This approach is based on Fick's formula, as already used in the Kety – Schmidt paper to measure global CBF (Kety & Schmidt, 1945) and applied in early PET papers to calculate CMRO₂ (P. T. Fox & Raichle, 1986b; Mintun et al., 1984). Instead of acquiring PET measurements, the mqBOLD approach relies on acquiring the same parameters via non-invasive magnetic resonance imaging. This means that one can bypass several assumptions and problems inherent to the calibrated BOLD approach. First, gas challenges, where the participants breath a mixture of gas either high in CO₂ (hypercapnia, usually around 5% CO₂ and ‘normal’ levels of O₂) or high in O₂ (hyperoxia, usually around 25-100% O₂) require a complicated set-up. This often elicits heightened drop-outs, as subjects are feeling uncomfortable due to the breathing masks or because of experiencing shortness of breath while in the scanner. Second,

calibration experiments assume that gas challenges are not influencing the metabolism and brain activity patterns they want to measure (Bright et al., 2019). Third, the Davis model assumes one CBV-CBF power-law coupling factor α , even though it has been shown that α varies across brain regions as well as due to the field strength and type of stimulation (J. J. Chen & Pike, 2009; Gagnon et al., 2016; Hua et al., 2019; Wesolowski et al., 2019; Zhang et al., 2020).

In this thesis, we used the mqBOLD approach as described in (Bulte et al., 2012; Göttler et al., 2019; Kaczmarz et al., 2020; Kufer et al., 2022) for the first time in a task-design in healthy subjects, during visual stimulation (Project I) as well as across a range of cognitive tasks (Project II). This required separate measurements of CBF and $R2'$ for each condition. Additionally, we measured the hematocrit levels of each subject, thus optimizing estimation of subject-specific OEF and CMRO₂. Furthermore, we started measuring CBV maps with contrast agent infusion for two conditions in a row, instead of only measuring CBV in the baseline condition. This was possible because we only gave half the clinical dosage of contrast agent per scan. This enabled us to estimate task effects, even though only in two conditions and only for total CBV, as we had no means of separating arterial and venous compartments. For the exact methods on how to infer CMRO₂ from T₂, T₂^{*}, pseudo-continuous ASL (pCASL) and dynamic susceptibility contrast (DSC) images, please refer to the methods sections of Project I and II below.

Measuring CMR_{glc}

As described in section 1.1.1., PET was the first neuroimaging method to measure brain activity via measurements of glucose consumption and CBF, OEF and CBV. The measurement of glucose consumption was done via an intravenous bolus injection of [18F]-FDG and the quantification of the cerebral metabolic rate of glucose (CMR_{glc}) via compartment modeling, which implies measuring the tracer concentration in the arterial blood (Reivich et al., 1979). The basics of this technique have not changed much until today. The PET scanner measures the accumulation of FDG in brain tissue, as the radiotracer cannot be fully metabolized and is therefore trapped at the location of neuronal activity. Researchers traditionally analyze an average image over the complete scanning time. This means that in order to measure task-induced changes in CMR_{glc}, it is necessary to acquire a baseline and a task scan in different scanning sessions, for the tracer activity to have fully decayed. This is time-consuming and requires the injection of the radioactive tracer multiple times, which can be avoided since recently due to the introduction of functional PET (fPET) (Villien et al., 2014). Here, instead of a bolus application of FDG, the tracer is applied continuously over the entire scanning period in order to create a constant plasma supply of FDG, so that task-induced dynamic changes in glucose metabolism can be measured. A number of studies have replicated this approach successfully, measuring glucose metabolism in different conditions during the same scanning session, quantitatively as well as non-quantitatively (Hahn et al., 2016, 2017, 2020; Jamadar et al., 2021; Jamadar, Ward, Carey, et al., 2019; Jamadar, Ward, Li, et al., 2019; Rischka et al., 2018, 2021; Stiernman et al., 2021). Rischka et al. (2018) optimized the temporal resolution by injecting a bolus of 20% of the total tracer volume in the beginning, thus increasing the signal-to-noise-ratio (SNR). We employed the same fPET technique as them in Project I to quantify CMR_{glc} in a resting state baseline compared to a visual stimulation condition. In summary, the fPET approach is not very different from the traditional PET approach, but allows to measure condition-specific CMR_{glc} within one scanning session via continuous tracer injection.

1.2 Task-induced changes in metabolism

The aim of neuroimaging research from the beginning has been to measure task-induced changes in brain activity and visual or motor tasks are usually the first to be tested, as one can expect rather large effects and a clear localization (P. Fox et al., 1988; Kushner et al., 1988; Reivich et al., 1979; Sokoloff, 2008a; Sokoloff et al., 1955).

1.2.1 Visual stimulation

Visual stimulation, mostly in the form of a flickering checkerboard, is known to evoke large BOLD and CMRglc changes in the occipital cortex and is therefore often employed in order to validate new scanning methods (Fujita et al., 2006; S.-G. Kim et al., 1999; Villien et al., 2014). While the increase in CMRO2 in visual areas was rather small in the first PET papers, around 5% in contrast to a CBF increase of 50% (P. Fox et al., 1988), subsequent studies found higher rates of %CMRO2. The increase in CMRO2 typically ranges between 5-30% (Donahue et al., 2009; Fujita et al., 2006; Hoge & Pike, 2001; A.-L. Lin et al., 2010; Liu et al., 2019; Mintun et al., 2001; R. G. Shulman et al., 2001; Simon & Buxton, 2015), while concomitant increase in CBF range between 30 and 65%. CMRglc increases range between 6-50% (P. Fox et al., 1988; Hahn et al., 2016; Newberg et al., 2005), but most studies reported CMRglc increases around 25-30% (Kushner et al., 1988; Newberg et al., 2005; Rischka et al., 2018; Villien et al., 2014; Vlassenko et al., 2006). We used visual stimulation in Project I to elicit and compare changes in CBF, CBV, BOLD-signal, CMRO2 and CMRglc in the visual cortex in order to validate our quantitative and simultaneous CMRglc – CMRO2 measurement setup.

1.2.2 Default mode network

While visual stimulation or generally somatosensory stimulation is known to elicit robust and consistent increases in both the BOLD-response as well as CBF, CMRO2 and CMRglc, this is not necessarily true for other brain regions (A. D. Ekstrom, 2021). BOLD changes in association cortices can be different from BOLD responses in somatosensory areas because of vascularization differences (A. D. Ekstrom, 2021; Harrison, 2002). That is why we have decided to test a cognitive design in Project II, which aimed to elicit BOLD activations and deactivations in association cortices, specifically in default mode regions. Particularly the neuronal basics for negative BOLD responses are a matter of discussion, as elaborated in section 1.1.2. Negative BOLD responses can also be elicited in somatosensory cortices, for example in ipsilateral motor cortex via unilateral nerve stimulation (Mullinger et al., 2014). These negative BOLD have usually been interpreted as suppression of cortical activity and have shown to decrease in amplitude and extent during healthy ageing (Mayhew et al., 2022b). Yet, BOLD decreases in the default mode network (DMN) have shown to not decline in amplitude across the lifespan (Mayhew et al., 2022b) and are less intuitive to interpret. In the following, I will describe how the default mode network was defined and why it has a special role.

History and functional interpretation of the DMN

Regions that later defined the DMN were first described in a review of several PET studies by Shulman and colleagues (G. L. Shulman, Corbetta, et al., 1997), where they detected consistent blood flow decreases when comparing an active to a passive task or to a resting state. The naming stems

from an influential paper of the same group (Raichle et al., 2001), proposing the resting state as a baseline state of brain function with homogeneous OEF across the cortex, attaching meaning to certain brain regions that got suspended during goal-directed behaviors. These regions usually comprise midline core structures including the posterior cingulate, retrosplenial, ventral and dorsal medial prefrontal cortex as well as lateral structures, including the inferior parietal lobule and lateral temporal cortex, plus the hippocampal formation (R. Buckner et al., 2008).

Subsequently, a number of studies replicated CBF and above all fMRI BOLD decreases in the DMN (Huijbers et al., 2012; Koshino et al., 2011; P. Lin et al., 2011; Mayer et al., 2009; Pfefferbaum et al., 2011; G. L. Shulman et al., 2007). It has even been shown that task-induced fMRI BOLD deactivations scaled with performance (Anticevic et al., 2010; Daselaar et al., 2004; Gilbert et al., 2012; Singh & Fawcett, 2008). Decreases have been interpreted as neuronal deactivations or suppression of internally guided processes during externally focused tasks (Anticevic et al., 2012; Singh & Fawcett, 2008). Additionally, Greicius and colleagues (2003) could show with fMRI BOLD data that default mode regions were functionally connected in the resting state. Further evidence from functional connectivity studies came from Fox and colleagues who showed that the DMN is anti-correlated to regions involved in external attention (M. D. Fox et al., 2005) and subsequently called the DMN a 'task-negative network'.

Still, the role of the DMN and the reasons behind its 'shut-down' during goal directed tasks is not clear. Activity in the DMN is usually associated to self-referential processing such was mind wandering, but also episodic retrieval and internal mentation (Andrews-Hanna, 2012; Andrews-Hanna et al., 2014a; Anticevic et al., 2012; R. Buckner et al., 2008; Davey et al., 2016; H. Kim, 2012; Mason et al., 2007). Gradual suppression of the DMN, depending on the task difficulty, is thought to support externally-oriented cognition (Daselaar et al., 2004; Singh & Fawcett, 2008). Interestingly, regions of the DMN, especially the posterior cingulate cortex (PCC) are also among the first to show alteration in neurodegenerative disorders as e.g. Alzheimer's disease (Anticevic et al., 2012; R. Buckner et al., 2008; Leech & Sharp, 2014; Mevel et al., 2011; Scherr et al., 2019) and even during normal ageing (Mevel et al., 2011). Finally, DMN regions have been associated with high metabolic costs. Functional connectivity analyses have shown that several hubs with a very high connectivity degree, responsible for long-range connectivity throughout the brain, are located within the DMN and high connectivity scales with metabolic costs (Castrillon et al., 2023; Leech et al., 2012; Liang et al., 2013; Passow et al., 2015; Tomasi & Volkow, 2011). DMN regions were also among the regions that showed higher rates of non-oxidative metabolism, compared to sensory regions (Blazey, Snyder, Su, et al., 2018; Vaishnavi et al., 2010). These studies all point towards a special role of the DMN, being highly connected to other brain regions, supposedly having higher metabolic costs and a higher rate of non-oxidative metabolism and being amongst the first to show decline in neurodegenerative disorders.

Within recent years, the formerly prevalent assumption of the DMN being a task-negative network has changed. It has been shown that it can be 'activated', as it showed a positive BOLD response in a number of self-referential tasks as autobiographical or semantic memory tasks (Andrews-Hanna et al., 2014a; Kernbach et al., 2018; H. Kim, 2012; Leech et al., 2011; Wang et al., 2017). Also, functional connectivity analyses showed that parts of it get recruited during task execution, mostly coupled to the frontoparietal control network (A. C. Chen et al., 2013; Crittenden et al., 2015; Smallwood et al., 2012; Spreng et al., 2010). Finally, an increasing number of studies has been showing that the DMN might not be as homogenous as expected by deactivation studies. In fact, researchers proposed a midline core, rather involved in self-referential processing, a temporal subsystem, rather involved in memory processes and a parcellation of the PCC in ventral and dorsal parts (Andrews-Hanna et al.,

2010; H. Kim, 2012; Leech et al., 2011). Several meta-studies have also shown task-based specialization in DMN regions (Andrews-Hanna et al., 2014a; Kernbach et al., 2018; Wang et al., 2017). There have also been successful attempts to find functional DMN subnetworks within the individual, see (DiNicola et al., 2019; Gordon et al., 2020), which showed that a subparcellation of the DMN may be individually very specific. Thus, the role and function of the DMN is still under debate, but it becomes clear that it is probably more heterogeneous than previously thought. For an excellent review on this topic please refer to Buckner and DiNicola (2019).

Evidence for DMN deactivations

Consistent task-induced decreases of the BOLD signal were observed across the whole DMN in a number of CBF and fMRI BOLD studies (Daselaar et al., 2004; Huijbers et al., 2012; Koshino et al., 2011; P. Lin et al., 2011; Mayer et al., 2009; Pfefferbaum et al., 2011; G. L. Shulman et al., 2007; Singh & Fawcett, 2008). Both in human as in animal data, there is also electrophysiological evidence for DMN deactivations. Hayden and colleagues (Hayden et al., 2009) found significant, tonic suppression of single-unit-activity in 35% of the neurons, but also significant enhancement in 9.4% of the neurons in the posterior cingulate cortex (PCC) of two macaques during an attentive task compared to the responses in the inter-trial interval. LFP activity in the gamma band, linked to BOLD / synaptic activity, was also suppressed by active task performance. Very similar results were obtained in another study with two macaques where short activation, followed by sustained suppression in LFP power and oxygen levels was measured during a passive visual stimulation task (Bentley et al., 2016). Additional support comes from human electrophysiological data: in 14 epileptic participants with depth electrodes, Ossandón and colleagues could show that DMN areas showed suppression of gamma band during task engagement, in an easy and hard visual search task (Ossandon et al., 2011). Also, quicker target detection was associated with stronger gamma suppression in mPFC and vIPFC. Furthermore, Foster and colleagues could show in another sample of eight epileptic participants (Foster et al., 2012) with intracranial recordings that gamma-power was suppressed during a calculation condition in 24% of overall posteromedial cortex (PMC) and increased during the self-episodic condition in 33% of overall PMC (the other electrodes did not respond above threshold). In yet another study by (K. C. R. Fox et al., 2018), 13 epileptic subjects showed activations in intracranial high-frequency EEG recordings during an autobiographical memory task and deactivation during a calculation task in PMC (PCC + areas 7m/31), although activation during memory was larger than the deactivation during the calculation task. GABA and glutamate spectroscopy data in human subjects showed that the glutamate/GABA ratio positively correlated with task-induced BOLD deactivations and that deactivations were stronger in the PCC during a 2back compared to a 1back working-memory task (Gu et al., 2019b).

Mixed or negative findings

Nevertheless, despite large experimental evidence for a neuronal deactivation underlying the negative BOLD response in the DMN, there has been some controversy. It was shown that BOLD responses, especially in the PCC, key region of the DMN, is heavily influenced by physiological noise. Renvall and colleagues (Renvall et al., 2015) stated that fMRI responses are 'alarmingly inconsistent across acquisition parameters', for DMN regions but not for visual regions. Singhal and colleagues (Singhal et al., 2020) similarly showed that activity in PCC and precuneus regions do not survive when using smaller flip angles, a common tool to reduce physiological noise. Adding to this picture, Stiernman and colleagues (Stiernman et al., 2021) did not find any evidence for metabolic (CMRglc)

decreases in DMN areas during a working-memory task, despite consistent fMRI BOLD deactivations. Additionally, BOLD deactivations in the hippocampus can go hand in hand with increases in neuronal activity, probably due to differences in vascularization (Schridde et al., 2008; Shaw et al., 2021). Finally, several studies from the Mullins group showed that the DMN takes a special role within the cortex. Hypoxia increased CBF throughout the brain, but CBF decreased in the DMN, leading to a reversed pattern of BOLD responses and suggesting a difference in neurovascular coupling specifically within the DMN (Lawley et al., 2017; Rogan et al., 2022; Rossetti et al., 2021b).

One reason for these inconsistent findings is the complex nature of hemodynamic coupling that gives rise to the BOLD signal. The canonical positive BOLD response arises when the CBF response is higher than the CMRO₂ response, resulting in a wash-out of deoxy-hemoglobin at the location of neuronal activity. But neurovascular coupling changes across cortical regions and is stimulus-dependent. The exact coupling of the CBF and CMRO₂ responses (the coupling ratio n) has a large influence on the BOLD amplitude and has been shown to vary across the cortex for positive BOLD responses (Ances et al., 2008; Buxton et al., 2014; J. J. Chen & Pike, 2009), but research on underlying CBF-CMRO₂ coupling of negative BOLD responses is sparse. As association cortices, compared to visual and primary sensory regions, have less dense capillaries, this could give rise to weaker or even absent BOLD responses (A. D. Ekstrom, 2021; Harrison, 2002). All in all, a number of studies that target negative BOLD responses came to the conclusion that the neurovascular mechanisms for negative BOLD responses (NBR) was different from positive BOLD responses (PBR) (Huber et al., 2014; Mullinger et al., 2014; Rossetti et al., 2021b).

All these findings speak in favor of a special architecture of the DMN and regionally specific differences in neurovascular coupling that perhaps favor the appearance of negative BOLD results. Understanding the metabolic background of DMN deactivations will thus shed more light on its function and underlying architecture.

1.3 Aims of the current work

In contrast to BOLD fMRI, quantitative metabolic imaging makes it possible to compare different brain regions within a baseline state, as well as during task execution. Furthermore, parameters as blood flow, oxygen and glucose consumption track biophysical processes and are thus directly interpretable. Within this thesis, the first aim was to establish the multiparametric, quantitative BOLD approach for cognitive designs in healthy subjects. This method has been applied, to our knowledge, only during a baseline condition without any task (Christen et al., 2012; Kufer et al., 2022) or comparing patient populations to a control group (Göttler et al., 2019; Kaczmarz et al., 2020). Therefore, our first goal was to prove that quantitative metabolic imaging was sensitive enough to detect task-induced changes in CMRO₂.

Additional to measuring mqBOLD, we wanted to implement the recent fPET approach, which allows for running two task conditions within the same PET experiment, thus quantifying task-induced changes in CMRglc. The first project was a proof-of-concept to show that the simultaneous measurement of both CMRglc and CMRO₂ was possible. This is why we ran a simple visual stimulation design in Project I to measure CMRO₂ simultaneously with CMRglc, comparing oxygen and glucose metabolism in the visual cortex. Also, we aimed to fully quantify both CMRglc, by taking arterial samples throughout the scan, and CMRO₂, by measuring each participant's hematocrit, arterial oxygen concentration values, and total CBV values via injection of a contrast agent. With this rather complicated set-up, we expected to get task-induced increases in CBF and CBV and decreases

in OEF, all together yielding increases in both CMRO₂ and CMR_{glc} within the visual cortex. We also expected stronger increases in CMR_{glc} than in CMRO₂ due to a task-induced rise in non-oxidative metabolism, similar to the very first studies of Fox and Raichle (P. Fox et al., 1988), but this time on an integrated PET-MR scanner, measuring fPET and mqBOLD simultaneously.

The aim of Project II was to apply the mqBOLD method during cognitive tasks in order to investigate the metabolic basics for BOLD deactivations, specifically within default-mode regions. Here, we employed complex cognitive tasks that induced consistent BOLD activation and deactivation patterns, and compared them to patterns of quantitative CMRO₂ consumption. The acquisition of simultaneous CMR_{glc} was not possible in one scanning session, as scanning time would have doubled compared to Project I, being already 90min long. Additionally, we expected cognitive tasks to evoke smaller effects. We therefore acquired data on a different scanner than for Project I. Compared to the PET-MR Siemens scanner with a 12K head-coil, used in Project I, we expected improved data quality on the relatively new Philips 3T scanner with a 32k head-coil. We wanted to know whether BOLD signal decreases reliably captured decreases in metabolic activity in healthy human subjects, thus whether negative BOLD responses in the DMN were simply an inverse of the canonical positive BOLD response. Alternatively, we would find deviations from the canonical neurovascular and neurometabolic coupling mechanisms in negative BOLD regions generally. This would suggest that negative BOLD responses do not necessarily reflect decreased metabolism and thus decreased brain activity. This finding could be DMN-specific or a characteristic of negative BOLD responses in general.

2 PROJECT I: Simultaneous measurement of oxygen and glucose consumption during visual stimulation in the human cortex

The current chapter includes the research article “Simultaneous measurement of oxygen and glucose consumption during visual stimulation in the human cortex”. This article is currently under preparation for submission, so the authors retain the copyright for the manuscript. If the manuscript will be accepted for publication, it will be subject to the Copyright terms of the respective journal.

Authors

Samira M. Epp & Antonia Bose, Roman Belenya, Gabriel Castrillón, Katarzyna Kurcyus, Eric Ceballos Dominguez, Andreas Ranft, Eliana Salas Villa, Moritz Bursche, Christine Preibisch, Valentin Riedl

Contributions

Samira M. Epp, as the author of this thesis, is the shared first author of this manuscript together with Antonia Bose.

SME & AB were responsible for data collection, design optimization, participant organization, data analysis, SME wrote the manuscript with contributions of AB, GC and VR, and finalized all figures. RB performed the quantification of the fPET data, GC assisted with data analysis, data management and manuscript editing, KK assisted with data collection and conceptualization of the design, ECD assisted with the quantification of the fPET data, AR was the responsible medical doctor during data collection, ESV helped with the quantification of the fPET data, MB helped with data collection, CP was responsible for sequence optimization and for the mqBOLD analysis pipeline, VR supervised the project, was responsible for conceptualization, funding and manuscript review.

My contribution to this manuscript in detail:

For this manuscript, I was, together with AB, responsible for the project organization, all data collection & subject management, optimization of design and data quality checks. Further, I analyzed the imaging data via partial least squares analyses and calculated the OGI on the final CMRO2 and CMRglc maps. Finally, I interpreted all final analyses, wrote the manuscript draft, with contributions of AB, and finalized all figures.

Simultaneous, quantitative measurement of oxygen and glucose consumption during visual stimulation in the human cortex

Samira M. Epp^{1,2,*} & Antonia Bose^{1,2,*}, Roman Belenya^{1,2}, Katarzyna Kurcyus¹, Eric Ceballos Dominguez¹, Moritz Bursche¹, Andreas Ranft¹, Eliana Salas Villa³, Christine Preibisch¹, Gabriel Castrillón¹, Valentin Riedl^{1,4}

*Shared first authors: Samira M. Epp and Antonia Bose contributed equally to this manuscript

1 Department of Neuroradiology, Neuroimaging Center, Technical University of Munich, Munich, Germany

2 Graduate School of Systemic Neurosciences, Ludwig-Maximilians-University, Munich, Germany

3 Department of Bioengineering, Universidad de Antioquia, Medellín, Colombia

4 Department of Neuroradiology, Friedrich-Alexander-University, Erlangen, Germany

ABSTRACT

The human brain relies on oxygen and glucose consumption to fuel its signaling activity. With the help of new techniques as functional positron emission tomography and multiparametric, quantitative BOLD, this study is the first to quantify both oxygen as well as glucose metabolism simultaneously in the human brain during visual stimulation compared to a resting state. We found significant increases in both the cerebral metabolic rate of oxygen (CMRO₂) and glucose (CMR_{glc}) in primary visual regions, and a decrease in the oxygen-to-glucose-index (OGI), which indicates a heightened level of aerobic glycolysis during visual stimulation. The combined measurement of oxygen and glucose metabolism across different cognitive states and brain regions provides new insights into the understanding of neuronal activity and disease states.

Keywords: *Multiparametric, quantitative MRI (mqBOLD); functional positron emission tomography (fPET); fMRI BOLD; cerebral rate of oxygen (CMRO₂); cerebral blood flow (CBF); oxygen extraction fraction (OEF); visual stimulation*

INTRODUCTION

We, as humans, are the species that uses more energy on the brain relative to our body mass than any other species. This is due to highly energy-demanding complex cognitive processes and evolutionarily novel connections (Castrillon et al., 2023). Further, 85% of the energy used in the brain is spent on neuronal signaling, mostly on postsynaptic processes (Attwell & Iadecola, 2002). Measuring brain energy metabolism is thus a unique opportunity to measure and quantify brain activity, which is fueled by oxygen and glucose metabolism.

We simultaneously measured glucose and oxygen consumption in the healthy human brain, using functional 18F-FDG-PET (fPET) and multiparametric, quantitative BOLD (mqBOLD) imaging, respectively, to quantify the metabolic rates of glucose (CMR_{glc}) and oxygen (CMRO₂) during visual stimulation (STIM) compared to rest (REST). Early PET studies have measured either CMR_{glc} or CMRO₂ in different scanning sessions, but not within one single, comparable session (P. Fox et al., 1988; P. T. Fox & Raichle, 1986; Leenders et al., 1990; Vafaei et al., 2012; Vlassenko et al., 2006). Owing to recent developments in PET methodologies, it is now possible to measure different conditions within the same scanning session in a block design, named functional PET (fPET). This is done by constant radiotracer infusion instead of a bolus injection (Hahn et al., 2016; Jamadar et al., 2019; Rischka et al., 2018; Villien et al., 2014). CMRO₂ can be measured either via labeled water PET (P. Fox et al., 1988; Hyder et al., 2016; Vaishnavi et al., 2010), which again requires different scanning sessions, via calibrated BOLD (Kim et al., 1999; Lin et al., 2008a), which requires gas inhalation, or via gas-free techniques such as R₂' calibration (Fujita et al., 2006; Liu et al., 2019). Calibrated BOLD experiments often only measure fractional changes in CMRO₂ (Blockley et al., 2013), because the full quantification of CMRO₂ is mostly limited by the measurement of the oxygen extraction fraction (Liu et al., 2019). Therefore, we used the mqBOLD approach, which quantifies CMRO₂ from cerebral blood flow (CBF), the reversible transverse relaxation rate (R₂') and the cerebral blood volume (CBV) as well as arterial oxygen content of blood (Bright et al., 2019; Christen et al., 2012; Kufer et al., 2022).

Measuring changes in both oxygen and glucose consumption does not only track neuronal activity, but can also shed light on the level of oxidative energy metabolism. The brain's energy source ATP (adenosine triphosphate) is generated via the oxygenation of glucose. If completely oxidized, one mole of glucose together with six moles of oxygen can generate 32 ATP. Without oxygen, one mole of glucose is metabolized to pyruvate and lactate via the glycolytic pathway, namely aerobic glycolysis, generating 2 ATP (Byrne et al., 2014). Under normal resting conditions, the ratio of oxygen to glucose consumption is about 5.5 but can substantially drop with an increase in neuronal activity, leading to an increase in aerobic glycolysis (Shulman et al., 2001). Aerobic glycolysis is the definition for a state where, despite sufficient oxygen being present, glucose is not fully oxidized.

While earlier PET studies measured strong blood flow responses of around 50% during visual stimulation, but only weak CMRO₂ responses of around 5% (P. Fox et al., 1988), calibrated BOLD studies found higher CMRO₂ increases in visual regions of around 12-30% (Donahue et al., 2009; Fujita et al., 2006; Hoge & Pike, 2001; Kim et al., 1999; Liu et al., 2019; Shulman et al., 2001). Thus, in this study, we expected to measure significant increases in CBF, CMR_{glc} and CMRO₂. We also expected higher increases in CMR_{glc} than in CMRO₂ and a decrease in OGI in visual regions, as it is well established that the stimulus-evoked increase in glucose consumption is partly due to an increase in aerobic glycolysis (Lin et al., 2008b; Paulson et al., 2010).

This study had two aims, first, to propose a proof of concept to measure both CMR_{glc} and CMRO₂ fully quantitatively and simultaneously, combining two relatively new approaches, mqBOLD and fPET; second, to calculate the OGI across the whole cortex, contrasting it between STIM and REST conditions within visual regions, expecting a decrease due to aerobic glycolysis.

METHODS

Subjects

We acquired data of 18 right-handed healthy subjects for our main study. Five subjects had to be discarded due to unreasonable T2* values, severe motion, other imaging artefacts, or problems due to contrast agent delivery. All analyses depicted here were performed on the same 13 healthy subjects (mean age 32.9 ± 9.0 y, 7 women). All participants gave informed written consent to procedures approved by the Ethics Review Board of the Klinikum Rechts der Isar, Technische Universität München.

Experimental procedure and data acquisition

Participants were asked to fast for 6 hours prior to their scan, that is not to eat or drink anything except water to keep their blood sugar levels low upon arrival. We measured body weight, BMI and body fat via a balance (OMRON Healthcare), blood sugar levels via a blood glucose meter (Accu-Chek, Roche Diagnostics, United States), heart rate and pulse via a blood pressure meter and arterial oxygen concentration via a pulse oximeter (Nonin 7500FO, Nonin Medical B.V., The Netherlands). Hematocrit, hemoglobin and creatinine values were measured via venous blood and sent to our in-house clinical chemistry laboratory. Additionally, creatinine values were checked and the contrast agent was only delivered if creatinine values were in a normal range to ensure healthy kidney function.

The venous catheter was placed by a medical doctor; the arterial catheter was placed by an anesthesiologist, specifically. Data were acquired via an integrated PET/MR (3T) Siemens Biograph MR scanner (Siemens, Erlangen, Germany), using a 12-channel phase-array head coil for the MRI acquisition. Blocks of full-field visual stimulation (STIM, checkerboard moving with 8Hz) alternating with resting-state blocks (REST, white fixation cross on black background) were presented through a mirror mounted on the head coil that reflected a monitor behind the scanner bore. The PET measurement started at the same time as the visual presentation (Neurobehavioral Systems, Inc., Berkeley, USA) and the infuse pump (Harvard Apparatus, Cambridge, Massachusetts, United States) which delivered [¹⁸F]FDG through the venous catheter. We aimed for a decay-corrected total dose of 3,6MBq per 1kg body weight. 20% of the total syringe volume was given as a bolus with a flow of 1ml/s, whereas the remaining 80% was given continuously over the time-course of 70min with a flow of 0.2ml/s. PET data were collected for 70min, starting with the bolus injection, while automatic arterial blood samples were taken continuously from the radial artery via a Twilite blood sampling system (Swisstrace, Zurich, Switzerland) to measure radioactivity in the arterial blood. Please refer to Fig. 1E for an overview of the scanning protocol.

The multi-parametric, quantitative BOLD MRI included the following sequences:

- **Multi-echo spin-echo T2 mapping**, only in REST; 3D gradient spin echo (GRASE) readout as described previously (Kaczmarz et al. 2020) with 8 echoes; echo times (TE) TE1 = Δ TE = 16ms; TR=4870ms; $\alpha=90^\circ$; voxel size $2 \times 2 \times 3.3 \text{mm}^3$; 36 slices (32 slices in one subject); acquisition time = 6:16min (for 36 slices).
- **Multi-echo gradient-echo T2* mapping**, in STIM and REST; as described previously (Hirsch et al., 2014; Kaczmarz et al., 2020) with 12 echoes, TE1 = 6ms, Δ TE = 5ms, TR=2340ms; $\alpha=30^\circ$; voxel size $2 \times 2 \times 3.3 \text{mm}^3$ (including 10% distance factor); 36 slices (32 slices in one subject); 4 concatenations (1 concatenation in first subject); correction for magnetic background gradients with a standard exponential excitation pulse (Baudrexel et al., 2009; Hirsch & Preibisch, 2013); acquisition of half-resolution data in k-space center for motion correction (Nöth et al., 2014); total acquisition time = 7:32min (for 36 slices).
- **Dynamic susceptibility imaging (DSC)**, in STIM and REST (in 2 subjects only in REST); as described previously (Hedderich et al., 2019). Single-shot GRE-EPI; EPI factor 128; 80

dynamics, TE=30ms; TR = 1890ms; $\alpha=70^\circ$; acquisition voxel size $2 \times 2 \times 3.5 \text{mm}^3$; 27 slices (26 slices in one subject); acquisition time = 2:38min (for 27 slices). DSC includes the injection of a gadolinium-based contrast agent as a bolus after 5 dynamic scans, 0.1ml/kg, minimum 6ml, maximum 8ml per scan (16ml for two injections in a row), corresponding to half a clinical dosage, flow rate: 4ml/s, plus flushing with 25ml NaCl.

- **Pseudo-continuous arterial spin labeling (pCASL)**, in STIM and REST; following (Alsop et al. 2015), as implemented in (Göttler et al., 2019; Kaczmarz et al., 2020); PLD 1800ms; label duration 1800ms; 2D EPI readout; TE=22.12ms; TR=4600ms; $\alpha=180^\circ$; 24 slices; EPI factor 31; voxel size $3 \times 3 \times 6.6 \text{mm}^3$; gap 0.6mm; 30 dynamics including a proton density weighted M0 scan; acquisition time = 5:09min.

The BOLD fMRI task-localizer was acquired using single-shot EPI, EPI factor 64, voxel size = $3.0 \times 3.0 \times 3.0 \text{mm}^3$, FOV $192 \times 192 \times 192 \text{mm}^3$, TE=30ms, TR=2.0s, $\alpha=90^\circ$, 120 dynamic scans plus 2 dummy scans, 36 slices, interleaved acquisition, total acquisition time: 4:08min together with B0 field mapping data (2 echoes, TR/TE1/TE2=400ms/4.92ms/7.38ms, $\alpha=60^\circ$, voxel size = $3.0 \times 3.0 \times 3.0 \text{mm}^3$, 36 slices, interleaved acquisition, total acquisition time: 0:54s).

Additionally, a T1-weighted 3D MPRAGE pre-and post-gadolinium (TI/TR/TE/ α = 900ms/2300ms/2.98ms/ 9° ; 160 slices; voxel size $1.0 \times 1.0 \times 1.0 \text{mm}^3$, acquisition time=5:03min) and T2-weighted 2D FLAIR (TR/TE/ α = 5000/394/ 40° , 140 slices, voxel size $0.5 \times 0.5 \times 1 \text{mm}^3$, EPI factor 130, acquisition time=3:27min) were acquired for anatomical reference and to exclude brain lesions.

fPET and CMRglc calculation

We reconstructed the raw long-listmode data offline based on the ordered subsets expectation maximization (OSEM) algorithm, divided into 93 x 45s frames (plus a last frame of 15s), with the following parameters: matrix: 344, 3D iterative reconstruction method, zoom: 2.0, filter: allpass, iterations: 4, subsets: 21, scatter correction: relative. The reconstructed PET images were motion corrected, spatially smoothed (Gaussian filter, FWHM = 6 mm) and low-pass filtered (360s). For the non-quantified analyses, the polynomial fit of each voxel was calculated and regressed out, so that time-series could be used without the constant increase due to the infusion. The median TAC within the group mask (visual regions which showed significantly elevated blood flow during STIM on a group level, Fig. 2A) followed the expected stimulation model.

For the CMRglc calculation, subject specific arterial input functions (AIF) were derived from the arterial blood samples. Preprocessing was done with in-house scripts in python (Python Software Foundation, version 3.8). First, the blood delay was estimated as the time between injection start and peak in the blood data. Then, background radioactivity was estimated and the blood TAC were modeled by fitting a sum of three exponential functions to the raw blood data (Feng et al., 1993). Blood TAC were then converted to plasma TAC, using the reference FDG plasma/blood ratio function (Phelps et al., 1979) together with each subject's hematocrit value. For two subjects, the arterial blood sampling did not work properly, hence average AIF from all other participants was used to calculate a population based AIF, as described elsewhere (Castrillon et al., 2023; Vriens et al., 2009). To account for the delay of measurable FDG uptake, we shifted the task onsets by two minutes as suggested previously (Stiernman et al., 2021). To calculate CMRglc values separately for the STIM and the REST conditions, we split the PET-time-series data into four REST and four STIM periods. We calculated the net uptake rate constant (Ki) using the Patlak plot model (Patlak & Blasberg, 1985), based on the (shifted) STIM and REST frames of the preprocessed PET images and the individual, preprocessed AIF. Next, we calculated voxel-wise CMRglc separately for each STIM and REST period by multiplying the Ki map with the plasma glucose concentration value of each subject, multiplied by 100 to get values per 100g, and divided it by a lumped constant of 0.65 (Wu, 2003). In a final step, the averaged CMRglc maps across all four STIM and REST blocks were calculated and normalized to standard MNI 2mm space (Montreal Neurological Institute, McGill University) via the mean PET and anatomical images.

Quantitative parameter calculation using mqBOLD

The calculation of the quantitative parameter maps was performed with in-house scripts in Matlab and SPM12 (Wellcome Trust Centre for Neuroimaging, UCL, London, UK). Fig.1 displays all steps and subject-averaged parameter maps in native space. Quantitative T2 and T2* maps were obtained by mono-exponential fits of the multi-echo spin and gradient echo data as described previously (Hirsch et al., 2014; Kaczmarz et al., 2020; Preibisch et al., 2008). Correction was performed for macroscopic magnetic background fields (Hirsch & Preibisch, 2013) and motion using redundant acquisitions of k-space center (Nöth et al., 2014). R2' maps were calculated via

$$R2' = \frac{1}{T2^*} - \frac{1}{T2} \quad [1]$$

yielding the transverse, reversible relaxation rate that is dependent on the vascular dHb content (Blockley et al., 2013, 2015; Bright et al., 2019). However, confounds from uncorrectable strong magnetic field inhomogeneities at air-tissue boundaries, iron deposition in deep GM structures as well as white matter structure need to be considered (Hirsch & Preibisch, 2013; Kaczmarz et al., 2020). The cerebral blood volume (CBV) was derived from DSC MRI via full integration of leakage-corrected $\Delta R2^*$ -curves (Boxermann, J.L., Schmainda, K.M., Weisskoff, R.M., 2006) and normalization to a white matter value of 2.5% (Leenders et al., 1990) as described previously (Hedderich et al., 2019; Kluge et al., 2016). The oxygen extraction fraction (OEF) was then calculated from R2' and CBV parameter maps via the mqBOLD-approach as

$$OEF = \frac{R2'}{c \cdot CBV} \quad [2]$$

(Christen et al., 2012; Hirsch et al., 2014; Yablonskiy & Haacke, 1994), with $c = \gamma \cdot \frac{4}{3} \cdot \pi \cdot \Delta\chi_0 \cdot \text{hct} \cdot B_0$, the gyromagnetic ratio $\gamma = 2.675 \cdot 10^8 \text{ s}^{-1} \text{ T}^{-1}$, the susceptibility difference between fully deoxygenated and oxygenated hemoglobin $\Delta\chi_0 = 0.264 \cdot 10^{-6}$, the magnetic field strength $B_0 = 3\text{T}$ and the small-vessel hematocrit hct, which was assumed to be 85% of our empirically measured (large-vessel) hematocrit value of each subject (Eichling et al., 1975; Hirsch et al., 2014). CBF maps were calculated from pCASL data as in the first equation in (Alsop et al., 2015) to calculate CBF from averaged, pairwise differences of motion-corrected label and control images and a proton-density weighted image.

For each subject and condition, we calculated the voxelwise CMRO2 by combining all parameter maps via Fick's principle:

$$\text{CMRO2} = \text{OEF} \cdot \text{CBF} \cdot \text{C}_{a\text{O}_2} \quad [3]$$

where C_{aO_2} is the oxygen carrying capacity of hemoglobin and was calculated as $\text{C}_{a\text{O}_2} = 0.334 \cdot \text{Hct} \cdot 55.6 \cdot \text{O}_2\text{sat}$, where O_2sat is the oxygen saturation measured by a pulse oximeter and Hct being each subject's hematocrit value (Bright et al., 2019; Ma et al., 2020). All parameter maps of each individual subject were registered to the first echo of their multi echo T2 data.

Venous versus arterial CBV

It is well known that CBV measurements that are based on the injection of intravascular contrast agents as gadolinium measure total CBV, including arterial as well as venous blood volume within each voxel (Hua et al., 2019). For stimuli shorter than 40s, CBV increases may be ignored due to the passive, slow increase of venous CBV (Simon & Buxton, 2015). However, for prolonged stimulation, studies have found that between 29% (Huber et al., 2014) and 50% (Kim & Ogawa, 2012) of total CBV increase is venous. Thus, considering the total CBV increase might underestimate CMRO2 changes, specifically during visual or somatosensory stimulation, where large total CBV increases are usually observed. As our visual stimulation persisted over a few minutes, we measured changes in CBV by acquiring two DSC scans, one per condition. DSC is a measure of total CBV, therefore, we

calculated CMRO2 group results with three scenarios: 1) original total CBV changes, 2) no changes in CBV, and 3) assuming 30% of total CBV changes being venous, based on results on 7T during visual stimulation in human subjects (Huber et al., 2014). Results in the main analysis were based on scenario 3, results for scenarios 1) and 2) are in the supplements.

Artifact and GM masking

To exclude voxels from brain areas affected by artifacts, we calculated the temporal signal-to-noise ratio (tSNR) from the fMRI BOLD images per subject and voxel in standard 2mm space. We then masked out voxels that were in the lowest 15th percentile in over 66% of participants. These were mainly located in common susceptibility areas, i.e., fronto- and temporo-basal brain areas. Additionally, we masked out the cerebellum and only considered voxels with a gray-matter (GM) probability > 0.5. The final SNR-GM-mask in standard space was applied to the input matrices of the partial least squares analyses. For the analyses in native space (histograms in Fig. 1, boxplots in Fig. 2B), we additionally used native-space parameter maps to mask cerebrospinal-fluid influenced areas ($T_2 > 120\text{ms}$), susceptibility-influenced areas ($R_2' > 11\text{ s}^{-1}$), voxels with a high percentage of blood volume ($CBV > 10\%$, probably driven by larger veins/arteries) and voxels with values that are higher than physiologically expected ($T_2^* > 120\text{ms}$, $OEf > 1$, $CBF > 100$). For calculating the oxygen-to-glucose index (OGI, see next section), voxels with $R_2' > 10\text{s}^{-1}$, median across all subjects in standard space, were not included. This is because CMRO2 values are calculated via R_2' which in turn is driven by susceptibility artifacts. That leads to unreasonably high CMRO2 and in turn high OGI values in areas with high susceptibility, influencing whole-brain measurements in standard space where these areas are included.

Oxygen-to-glucose-index (OGI)

The OGI compares how much oxygen in comparison to glucose is metabolized and is an indicator of oxidative metabolism. Two major pathways are responsible for energy production, that is ATP (adenosine triphosphate) generation: 1) glycolysis, generating two ATP via one mole of glucose, and also producing pyruvate, and 2) oxidation, producing another 30 ATP via further oxidation of pyruvate via 6 moles of oxygen (Byrne et al., 2014). If fully oxidized, theoretically one mole of glucose should be coupled to six moles of oxygen, thus the OGI in this case is 6. An OGI smaller than 6 indicates some percentage of non-oxidative glycolysis being present (Hyder et al., 2016; Shulman et al., 2001). The OGI was calculated on a voxel basis, each voxel being the median across all subjects in standard space.

$$OGI = \frac{CMRO2}{CMRglc} \quad [4]$$

fMRI BOLD processing and task analysis

The BOLD fMRI localizer data was pre-processed using fMRIPrep 20.2.4 (Esteban, 2019) as a docker container, based on Nipype 1.6.1 (Gorgolewski et al., 2011). This included segmentation, estimation of motion-parameters and other confounds, susceptibility distortion correction, co-registration in native T1w space and normalization to MNI152 ICBM 2mm Non-linear 6th Generation Asymmetric Average Brain Stereotaxic Registration Model (Montreal Neurological Institute, McGill University). fMRIPrep uses FSL 5.0.9 (Jenkinson et al., 2012; Smith et al., 2004) boundary-based registration, BBR, to register BOLD fMRI EPI time series to T1w data, FSL FAST for brain tissue segmentation and spatial normalization to standard space using ANTs 2.3.3, (Avants et al., 2008)) registration in a multiscale, mutual-information based, nonlinear registration scheme, concatenating all transforms and applying all registration steps at once. This final normalization matrix was then also applied to all quantitative mqBOLD parameter maps, after 6-dof (degrees of freedom) co-registration to native T1w space, to transform all images to MNI 2mm standard space. Further, task-analysis was done following recommendations in (Esteban et al., 2020), setting up a general linear model (GLM) with CSF and white-matter signal, dvars, framewise-displacement and translations and

rotations in x-, y- and z-axis as confounds, high-pass filter of 120s and 6mm smoothing. For analyses based on native GLM masks, we used individual 1st level z-maps, $z > 3.1$.

Partial least squares analysis

Partial least squares (PLS) analyses were run using the Python pypls library (Python Software Foundation, version 3.8). Mean-centered PLS is a data-reduction method that computes latent variables and corresponding brain patterns, which optimally relate brain signals to experimental design, contrasting, e.g., groups or conditions (McIntosh & Lobaugh, 2004). In our case, the input data matrix contained one row for each subject including all voxels within the SNR-GM-mask in standard 2mm space, and stacked STIM and REST conditions. In the case of BOLD fMRI data, median values of percent signal change (deviation from median REST value) across 20s (10TRs) per task condition were used, excluding the first 10s per task block to account for the hemodynamic response lag. In the case of non-quantified fPET data, median values of percent signal change (deviation from median REST value) across the whole length of the condition blocks were used, but shifted by 6 TRs to account for continuous increase (STIM) or decrease (REST) during the blocks, so that the ‘peaks’ and ‘valleys’ in the time-course do not cancel out when calculating the median. In the case of the quantitative data, OEF, CBF, CMRO2 or CMRglc values per voxel and subject were used and stacked for the REST and the STIM conditions. With the help of a dummy-coding matrix, the pypls library computes within-condition averages, which are column-wisely mean-centered (Krishnan et al., 2011). This matrix, $R_{mean-centered}$ ($q \times p$), which comprises q conditions and p voxels, is then subjected to singular value decomposition. This results in:

$$R'_{mean-centered} = USV' \quad [5]$$

$U_{p \times q}$ are the voxel weights (brain saliences), one row per latent variable (LV) i , that reflect how much this voxel contributes to the effect captured by LV_i . $V_{q \times q}$ are the task saliences (one row per LV) that indicate how each condition contributes to the spatial pattern identified by LV_i . $S_{q \times q}$ are the singular values per LV that reflect the strength of the relationship extracted by LV_i (McIntosh & Mišić, 2013). The significance of the latent variables, i.e., the entire multivariate pattern, is tested via permutation tests (we used 2000 permutations), the reliability of the brain saliences, i.e., the voxel’s contribution to the latent variables, is deduced via bootstrap resampling (we used 2000 samples). Brain regions showing significant effects are identified via the ratio of the brain saliences to the bootstrap standard error (BSR), where a $BSR > +2 / < -2$ is akin to a confidence interval of 95%, if the bootstrap distribution is normal (Krishnan et al., 2011; McIntosh & Mišić, 2013). In this paper, we used the PLS analyses to perform group level statistics in order to identify brain regions that differentiate best between the STIM versus the REST condition. As the same analyses were applied to both BOLD fMRI, fPET and quantitative data, resulting statistical result maps could be compared across the different parameters. The statistical maps were thresholded with a BSR of ± 2 and only clusters with more than 30 voxels were kept for creating the visual masks that were used in Fig. 2, Fig. 3 and Fig. 4. Please note that for correct interpretation, BSR maps must be compared to the design scores (design variables multiplied by brain saliences) of each condition within each LV to know the direction of task differences that is captured within the BSR pattern. In this manuscript, a blue-red BSR pattern indicates a positive task effect, that is voxels with higher values during STIM compared to REST, whereas blue voxels show the opposite contrast.

Other statistical analyses

Most statistics, except the native-space analyses (boxplots in Fig. 1, right column in Fig. 2C) were based on median voxel values within a group visual region of interest (ROI) in standard space, by taking the across-subjects median value per voxel in STIM and in REST. Delta values for OEF, CBF, CMRO2 and CMRglc were calculated for each voxel (STIM minus REST) and tested against zero via two-sample related permutation tests, 2000 permutations. We used permutation tests as most of the voxel distributions were not normally distributed. Permutation tests were also used to test for

significance in OGI, across voxels, when comparing REST versus STIM (Fig. 4A). Also, in general, we used median values as these are more robust against outliers than mean values. The %CBF/%CMRO2 coupling ratio, or n-ratio (Buxton et al., 2014), displayed in Fig. 4B, was calculated for each voxel (on the median voxel value across subjects) by dividing the change in CBF by the change in CMRO2 and then averaged (median across voxels).

For the native space analysis (boxplots in Fig. 1, right column in Fig. 2C), we calculated median values within each native-space activation ROI (output of the first level GLM, thresholded with $z > 3.1$) per subject and tested significant differences in REST compared to STIM via paired-samples t-tests, across subjects.

RESULTS

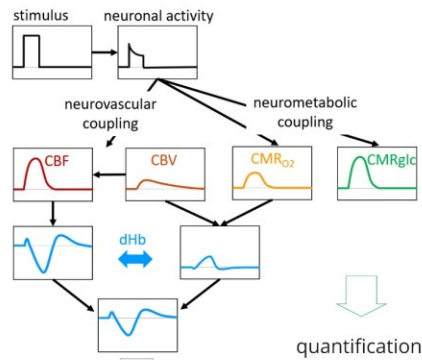
In order to fully quantify CMRglc and CMRO2 within both REST and STIM conditions, we performed simultaneous fPET and mqBOLD imaging. As the physiological model in Fig. 1A shows, we expected an increase in neuronal activity following visual stimulation, leading to an increase in both cerebral blood flow (CBF) and blood volume (CBV), called neurovascular coupling. In parallel, as more energy is needed, oxygen and glucose consumption are expected to increase, i.e. the cerebral metabolic rate of oxygen (CMRO2) and glucose (CMRglc) go up, which is called neurometabolic coupling. Both neurometabolic as well as neurovascular coupling influence the BOLD response. As the CBF increase is usually very large, it overcompensates for CMRO2 increases, leading to decreased dHb levels and a positive BOLD response. This is what we expected to happen in our data. We simultaneously measured the CMRO2 response and the CMRglc response to a flickering checkerboard during extended blocks of 5-7min, and subsequently the BOLD response during a block-design with 4 x 30s blocks. Median values across all empirical quantitative parameter maps were in biologically plausible ranges, see Table 1.

Table 1

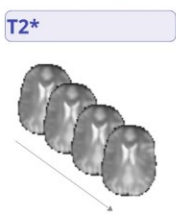
Baseline REST values, mean \pm SD across subjects, within gray matter.

T2	T2*	R2'	CBV	OEF	CBF	CMRO2
[ms]	[ms]	[1/s]	[%]	[ratio]	[ml/100g/min]	[μ mol/100g/min]
81.4 \pm 2.0	57.4 \pm 1.3	7.69 \pm 0.34	5.03 \pm 0.19	0.46 \pm 0.03	51.2 \pm 9.6	27.4 \pm 7.9

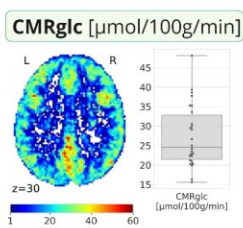
A | Physiological BOLD model



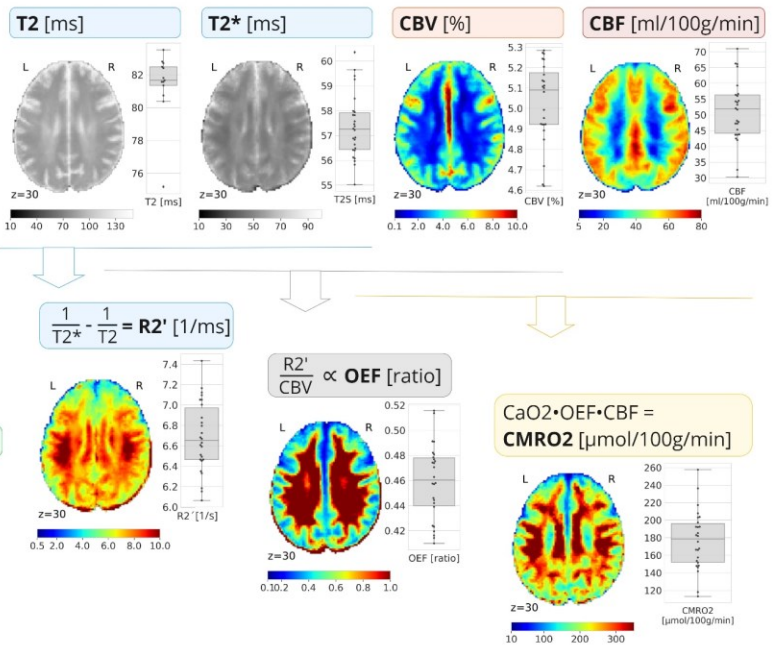
B | fMRI



C | fPET



D | Multiparametric, quantitative BOLD (mqBOLD) imaging



E | Data acquisition

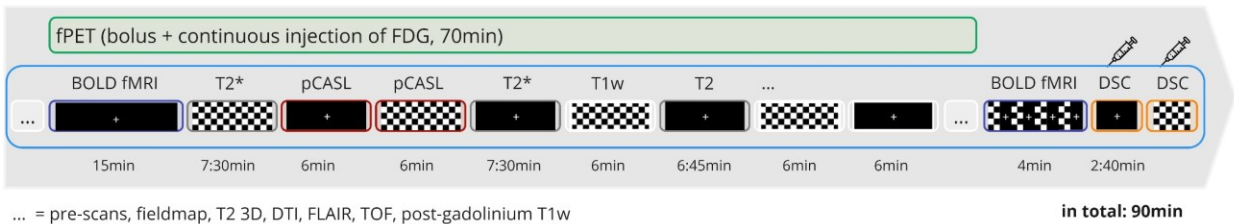


Fig. 1. Hemodynamic model, data acquisition and task design. **A**) Schematic of the physiological model of the BOLD signal. Increased neuronal activity causes elevated cerebral blood flow (CBF), lowering dHb in venous blood. In parallel, it triggers increases in energy metabolism (CMRO₂) and blood volume (CBV), resulting in higher dHb. In addition to increased oxygen metabolism, glucose metabolism (CMR_{glc}) is altered, without influences on the dHb content of the blood. **B**) Positive BOLD responses arise with lowered dHb content, i.e. when CBF increases overcompensate oxygen consumption. **C**) The fPET signal reflects glucose consumption and is independent from the venous dHb content. We quantified CMR_{glc} by continuously measuring the radioactive decay of arterial blood. **D**) Multi-parametric BOLD fMRI allows CMRO₂ calculation during rest (REST) and visual stimulation (STIM) via quantification of transverse relaxation times T₂ and T₂^{*} as well as cerebral blood volume (CBV) and CBF. Subject-average parameter maps (in REST) are depicted together with boxplots of average gray matter values per subject and condition (line: median; box limits: upper and lower quartiles). The reversible transverse relaxation rate (R₂') reflects the overall dHb content in a voxel. The oxygen extraction fraction (OEF) is proportional to the ratio of R₂' to CBV (from dynamic susceptibility contrast (DSC) MRI). Voxel-wise CMRO₂ is then obtained as the product of OEF, CBF (from pseudo-continuous arterial spin labeling, pCASL MRI), and the arterial oxygen content of blood (CaO₂). **E**) One scanning session of around 90min encompassed simultaneous fPET (green box) and MRI (blue box) measurements. After an initial resting block of 15min, STIM and REST blocks were alternately shown until the end of the fPET acquisition. Before the DSC acquisitions that contained the delivery of a contrast agent, BOLD fMRI was acquired in a 30sec block design, 4 repetitions per condition.

Significant group level changes in CBF, OEF, CMRglc and CMRO2 in visual areas

In all parameters, the group PLS analysis revealed significant stimulation-induced changes. For BOLD, fPET, CMRglc, CBF, OEF and CMRO2, the first latent variable of the PLS analysis was significant, respectively, showing a statistical pattern with increased relative BOLD and fPET signal in visual areas as well as increased absolute CBF, absolute CMRglc, absolute CMRO2 and decreased absolute OEF, see Fig. 2A. The sign of OEF is to be expected as with canonical neurovascular coupling, increased neuronal activity goes hand in hand with a decrease in oxygen extraction due to an overcompensation by blood flow. All activation areas were located within primary visual regions, see contours in the axial slices which include Yeo's visual regions A and B, from the 17 network parcellation atlas (Yeo et al., 2011). The BOLD statistical map expressed a more extended activation cluster whereas both CBF and OEF clusters were more localized. The relative fPET activation map and even more the absolute CMRglc and CMRO2 activation maps exposed an even more focal and rather small activation cluster. Surprisingly, the first latent variable of the CBF data also showed areas with significant flow decreases across the cortex during STIM, which were not examined in this manuscript. We then used the binarized group ROIs from the BOLD and fPET analysis as regions of interest (ROIs), restricted to activation regions, i.e. orange-red voxels in the fPET and BOLD group maps, to mask the quantitative parameter maps (Fig. 2B). The 3286 voxels within the BOLD group activation ROI showed a median BOLD-signal increase of 1.49% and a median PET-signal increase of 1.19% during STIM compared to REST. The 214 voxels within the fPET group activation ROI showed a median BOLD-signal increase of 3.46% and a median fPET signal increase of 3.28%. In native space, using the subject-specific, thresholded first level BOLD results as ROIs, we found a median BOLD increase of 1.69% across subjects and a 1.1% increase in fPET.

Within the same ROIs, we tested whether there were concomitant changes in CBF, OEF, CMRO2 and CMRglc. CBV, CMRO2 and CMRglc increased significantly in both group ROIs, see Table 2.

Table 2

Median values across voxels (IQR) within BOLD and fPET ROIs.

ROI	BOLD %	CBF [ml/100g/min]		CMRO2 [μ mol/100g/min]		CMRglc [μ mol/100g/min]	
		REST	Δ CBF	REST	Δ CMRO2	REST	Δ CMRglc
			% Δ CBF		%CMRO2		%CMGglc
BOLD ROI	1.5 (1.7)	45.7 (10.3)	4.8** (7.1) 11.6% (16.2)	198.9 (59.2)	5.8** (15.7) 3.3% (8.6)	25.4 (12.9)	2.6** (8.7) 8.2% (41.9)
fPET ROI	3.5 (1.6)	27.5 (6.4)	12.8** (3.4) 27.6% (8.5)	176.8 (43.5)	15.0** (17.5) 8.3% (9.1)	28.6 (13.7)	9.3** (11.6) 31.0% (44.2)

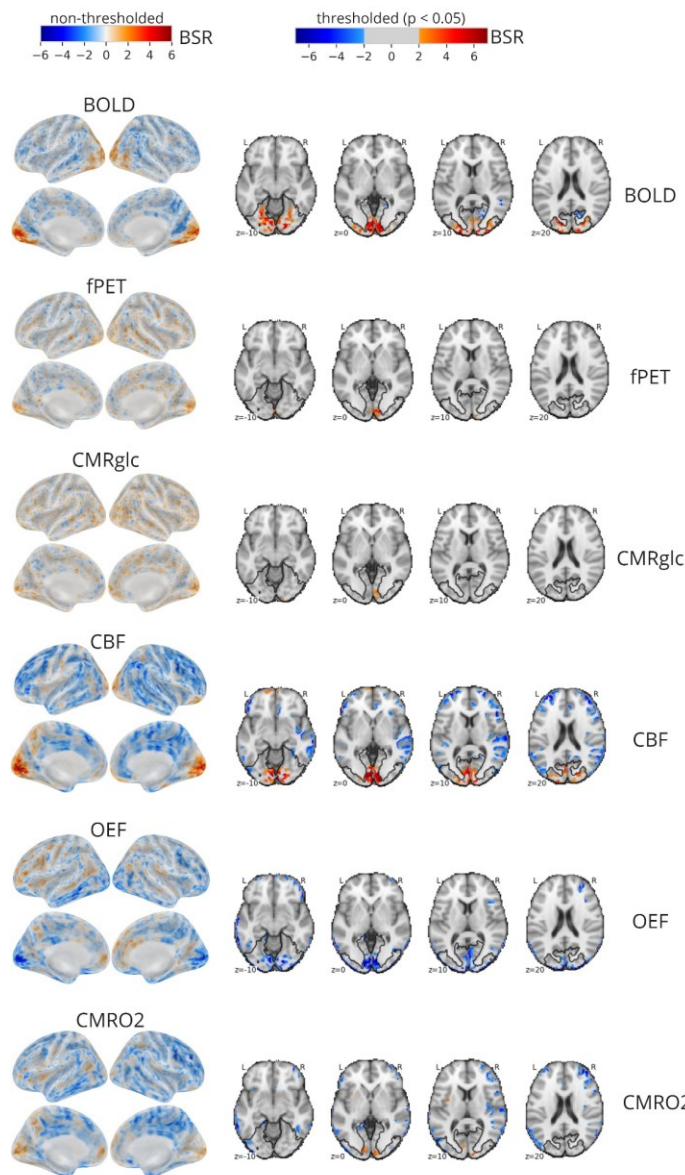
Note. This table reports median values across voxels within each BOLD ROI, based on subject-averaged voxel values. Absolute CBF, CMRO2 and CMRglc are displayed both in REST and as delta values (STIM minus REST), along with percent change values for each contrast. As voxel delta values were not normally distributed, median values along with interquartile ranges (IQR) are reported. ** $p < .001$, based on two-sample related permutation tests, 2000 permutations.

Across subjects, in native space ROIs, CMR_{glc} increased by 24.73% (median) (REST 31.0 $\mu\text{mol}/100\text{g}/\text{min} \pm 7.0$, STIM 38.1 $\mu\text{mol}/100\text{g}/\text{min} \pm 10$, paired samples two-tailed t-test: $t(12)=4.5$, $p < .001$). CBF increased about 14.5% (REST 49.1 $\text{ml}/100\text{g}/\text{min} \pm 11.9$, STIM 55.4 $\text{ml}/100\text{g}/\text{min} \pm 11.8$, paired samples two-tailed t-test: $t(12)= 4.5$, $p = < .001$) across subjects within 1st level BOLD ROIs. Yet, in native space, CMRO₂ increase were not significant (REST 180.5 $\mu\text{mol}/100\text{g}/\text{min} \pm 45.7$, STIM 185.9 $\mu\text{mol}/100\text{g}/\text{min} \pm 41.8$).

The OEF decreased significantly across voxels within the group ROIs; -0.04 or -7.3% in the BOLD ROI and 0.07 or -14.2% within the fPET ROI, delta values tested via permutation tests against zero, 2000 permutations, $p < .001$. Across subjects, in native space, OEF decreased -7.6% on median (REST 0.48 ± 0.05 , STIM 0.45 ± 0.05 , paired samples two-tailed t-test: $t(12)= -4.8$, $p = < .001$).

Please note that both OEF and CMRO₂ were calculated as described in Methods, correcting for arterial CBV increase, i.e. considering 70% of total CBV increase as arterial. It is well known that changes in CBV measured with contrast-agent include both arterial as well as venous changes, thus measure total CBV. In our data, shown in Fig. S1, total CBV (CBV_t) measured by DSC on average increased by 12.54% within the BOLD activation ROI, and up to 50% across voxels. We observed that changes in R₂' and CBV were negatively correlated (Fig. S1A). R₂' is dependent on the dHb content of the blood and is growing with increased dHb content. This means that increases in venous CBV, which lead to increases in dHb content, should lead to increased R₂'; thus increases in venous CBV and %R₂' should be positively coupled. As the opposite is the case, i.e. we observed a negative correlation, we assumed that most of the CBV changes were indeed arterial, thus not increasing but rather decreasing the dHb content. In Fig. S1 in the supplements, we show that CMRO₂ increases were larger in visual cortex when not taking changes in CBV into account and CMRO₂ changes were not significant when considering total CBV changes.

A | Group results



B | Difference values within activation ROIs

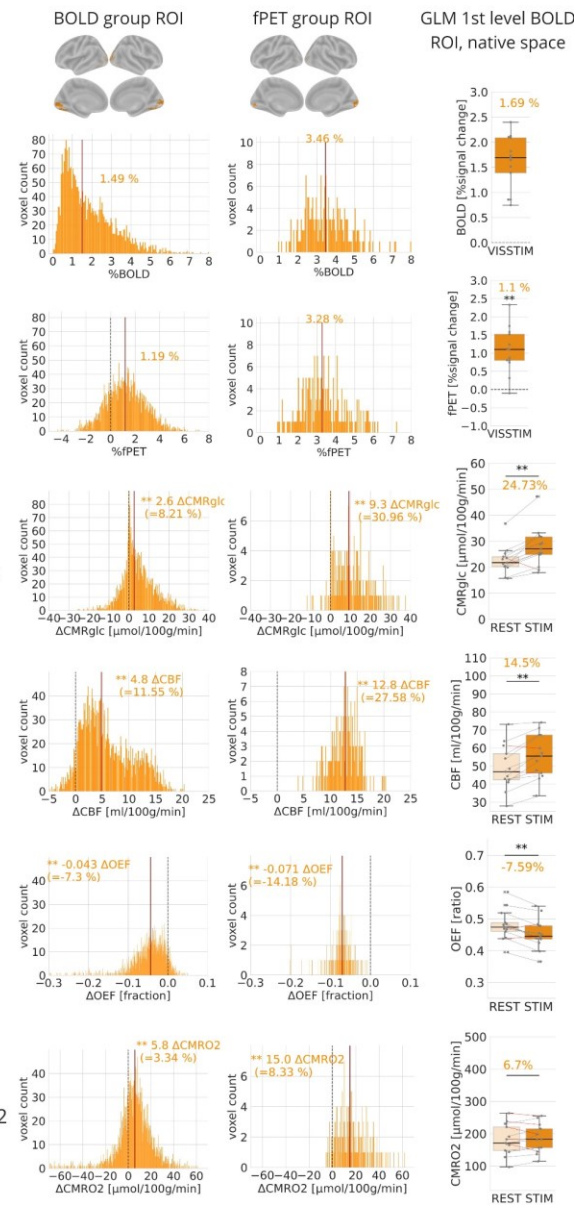


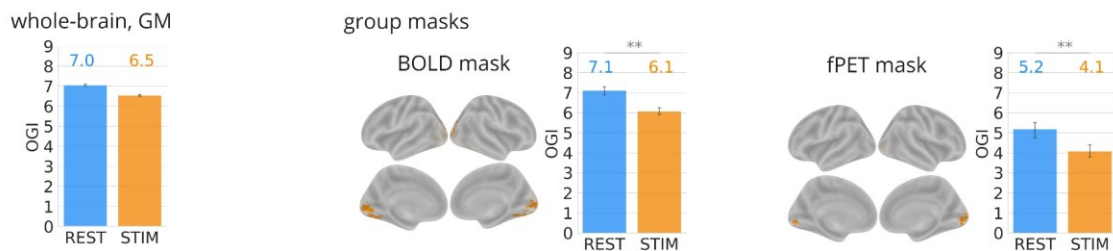
Fig. 2. Group level task results. **A**) Results of the PLS analyses of each parameter, comparing REST and STIM conditions. The left column shows statistical maps displaying the distribution of bootstrap ratios (BSR), akin to z-values, within the respective 1st latent variable, significant in all analyses ($p < .001$ for BOLD, fPET and OEF, $p < .01$ for CMRO2 and CBF, $p < .05$ for CMRglc). Axial slices show thresholded statistical maps with a BSR ± 2 , corresponding to $p < .05$. In all parameters, except CMRO2, we see significant task changes in the visual cortex, black contours show Yeo's visual areas A and B. **B**) Percent signal change and delta values within BOLD and fPET activation areas. Histograms show voxel distributions, median across subjects, for 3286 voxels within the BOLD group mask (left) and 214 voxels within the fPET group mask (right). CBF, OEF, CMRglc and CMRO2 showed significant, concomitant changes that align with BOLD and fPET increases within both masks, CMRO2 data are based on CBV values corrected for arterial increases. Delta values were tested via permutation tests against zero, ** = $p < .001$, see also Table 2. The third column shows results within native space BOLD ROIs, one dot per subject, median across voxels within the respective ROIs. We used the thresholded output of 1st level GLM per subject as masks, task changes across subjects were tested via paired samples t-tests, ** = $p < .001$. Across subjects, changes in CBF, OEF and CMRglc were significant, but changes in CMRO2 were not.

Decreases in oxygen-to-glucose-index during STIM within visual ROIs

Finally, we wanted to know whether the rate of non-oxidative glycolysis decreased during STIM compared to REST within activation ROIs. The oxygen-to-glucose-index (OGI) is an indicator of how much CMRO2 compared to CMRglc is metabolized, smaller values indicate a higher rate of non-oxidative glycolysis. Across all gray-matter voxels, there was no significant difference in OGI. Across voxels in both the BOLD as well as the fPET group masks, the OGI dropped significantly during the STIM condition, compared to REST.

All in all, our empirical voxel data were in line with the predictions of the Davis model (Fig. 4B). The scatterplots and barplots in Fig 4B summarize CBF, CMRO2, CMRglc and BOLD responses across voxels within the two group ROIs, CMRO2 calculated with 30% CBVt. The relation of %CMRO2 and %CBF predict the strength of the BOLD response, which can be summarized by the n-ratio. In the scatterplots CBF increase across voxels ranging from zero to approximately 40% are displayed, while %CMRO2 ranges up to approximately 30% and also includes some voxels with a negative CMRO2 response within the BOLD ROI. These negative voxels also decrease the CBF-CMRO2 coupling, called n-ratio, which was calculated for each voxel as the ratio of %CBF divided by %CMRO2. Within the BOLD ROI, $n = 1.46$, while within the more focal fPET mask this relation increased to $n = 2.92$. A higher n-ratio indicates a higher overcompensatory CBF response, resulting in a higher BOLD response.

A| Oxygen-to-glucose-index, REST vs STIM



B| Summary of results within activation ROIs

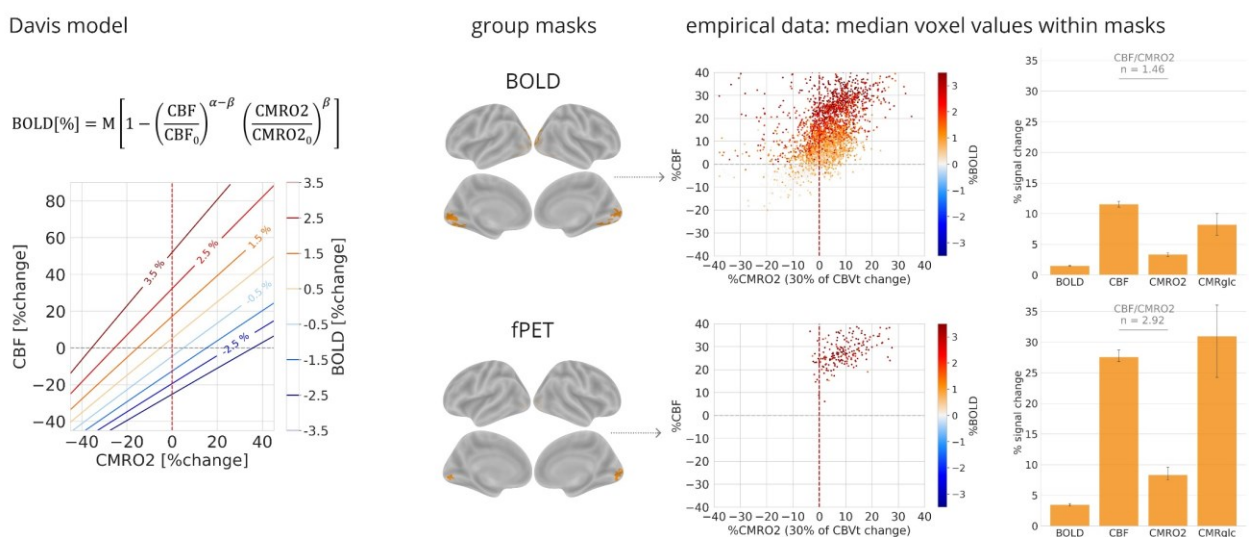


Fig. 4. Oxygen-to-glucose-index (OGI) and summary of results within the activation ROIs. A| OGI (CMRO2/CMRglc) in REST vs. STIM conditions. First column: across the whole brain, within grey matter (GM), second column: within the BOLD group ROI, third column: within the fPET group ROI. In both group masks OGI is significantly lower during STIM compared to the REST, indicating a higher rate of non-oxidative glycolysis

during STIM. Tested via permutation tests, 2000 permutations, ** $p < 0.001$. **B**] Biophysical Davis model equation and visualization, showing how changes in CMRO2 and CBF are relating to changes in BOLD, indicated by the colored contour lines. Scatterplots similarly show empirical voxel values within BOLD and fPET group masks, %CMRO2 versus %CBF, colors indicate the BOLD amplitude. The barplots in the right column show median percent-signal change values across voxels, different parameters the two ROIs, error bars display 95% confidence intervals across voxels, 2000 permutations. Within the BOLD mask (3286 voxels), the BOLD signal increased by 1.5%, CBF increased by 11.6%, CMRO2 by 3.3% and CMRglc by 8.2%. Within the fPET mask (214 voxels), the BOLD signal increased by 3.5%, CBF increased by 27.6%, CMRO2 by 8.3% and CMRglc by 31.0%. This results in a median n-factor of 1.46 (25% quantile: -0.31, 75% quantile: 3.17) within the BOLD mask and a median n-factor of 2.92 (25% quantile: 1.94, 75% quantile: 4.35) within the fPET group mask.

DISCUSSION

In this study, we used an integrated PET-MR scanner for the simultaneous measurement of mqBOLD and fPET, yielding individual quantitative CMRO2 and CMRglc maps during resting state (REST) and visual stimulation (STIM). This is, to our knowledge, the first study to quantify both metrics simultaneously during the same scanning session in multiple conditions. All measured parameters were in biologically plausible ranges, although CMRO2 values were in the upper range ($177 \pm 33.1 \mu\text{mol}/100\text{g}/\text{min}$) compared to other papers (131-153 $\mu\text{mol}/100\text{g}/\text{min}$) (Hyder et al., 2016; Raichle et al., 2001; Zhang et al., 2015), but lower than e.g. reported by Liu et al. (2019).

On a group level, we measured extended BOLD-signal increases in visual cortex and concomitant, significant changes in CBF, OEF and CMRglc. Increases in CMRO2 on the group level were only significant after correction for arterial fractional changes in CBV. Also, our increases in CMRO2 were rather low, 3.4% within the extended BOLD ROI and 8.3% within the more focal fPET ROI (Table 2) as compared to literature values where the increase in CMRO2 typically ranged between 12-30% (Donahue et al., 2009; Fujita et al., 2006; Hoge & Pike, 2001; Lin et al., 2010; Liu et al., 2019; Simon & Buxton, 2015). This could have several reasons. First, with 11.6% and 27.6% CBF increase on the group level (within BOLD and fPET ROIs), we were not in the range of 40-60% CBF increase that was reported elsewhere (P. Fox et al., 1988; Fujita et al., 2006; Huber et al., 2019; Kim et al., 1999; Lin et al., 2008a). As changes in CMRO2 were calculated via CBF (and OEF), a lower sensitivity of our CBF measurements might explain the rather low changes in CMRO2. Secondly, this might be the result of adaptation processes. It has been shown that the BOLD signal shows only little adaptation to prolonged visual stimulation (when instructed to ignore), whereas the adaptation is bigger for CBF, and even bigger for CMRO2 changes (Moradi & Buxton, 2013). Furthermore, attention has a big effect on CMRO2 changes, Moradi et al. (2012) reported a three times stronger increase in CMRO2 while participants were paying attention to visual stimulation stimuli contrasted to the same stimuli, presented in parallel, while performing another task. Additionally, it has been shown that energy demands adapted due to repeated stimulation when measured by lactate, whereas the BOLD signal did not (Mangia et al., 2007). In our experiment, the participants did not have to pay attention to the stimulus, which was shown repeatedly over a period of 5-7.5 min, so adaptation processes that influence the CMRO2 response, in particular, could explain our rather low %CMRO2 values. In contrast, an earlier water-PET study did not find adaptation of the CMRO2 response, and even significant increases during prolonged visual stimulation up to 25min, but generally reporting only weak increases in CMRO2 (5% after 25min) (Mintun et al., 2002). So, it is not sure if and how adaptation processes influenced our CMRO2 response. For CMRglc, we found significant increases within both group activation masks (BOLD: 8.21%, fPET: 31.0), which were in line with the values reported on the two first fPET studies, observing maximum increases of 6.1% in CMRglc during finger tapping (Hahn et al., 2016) and 25% during full-field checkerboard stimulation (Villien et al., 2014).

Finally, we found a significant decrease in the oxygen-to-glucose-index (OGI) within group ROIs when comparing STIM to REST blocks. The OGI consistently decreased in the activated regions, even though our overall whole-brain OGI of 7 was higher than the physiologically plausible (OGI = 6). OGI

reported in the literature is usually around 5.2-5.5 in the resting state (Blazey et al., 2018; Hyder et al., 2016; Shulman et al., 2001; Vafaei et al., 2012). This overall higher OGI is most probably due to our CMRO₂ values, which are in the higher range reported by previous literature. However, this does not affect the consistent decreases that we found within the activated ROIs. A decrease in OGI is indicative for increased non-oxidative metabolism, as expected during increased neuronal activity (Blazey et al., 2018; Shulman et al., 2001; Vafaei et al., 2012).

Limitations

By measuring R₂'₂, CBV and CBF plus hematocrit values quantitatively, we could use Fick's principle to derive subject specific CMRO₂ maps. In contrast to many other studies that did not measure CBV, but instead used CBF to estimate CBV through the use of a power-law relationship (Blockley et al., 2013, 2015; Chen et al., 2022), we measured changes in total CBV. By measuring CBV precisely, we were able to increase the validity of our CBV data. Other studies simply assumed the CBF-CBV relationship across subjects and brain regions with the same coupling factor α . This poses a problem as different studies find different coupling factors, varying also across stimuli and subjects (Chen & Pike, 2009, 2010; Wesolowski et al., 2019). The drawback of measuring CBV directly is that venous CBV is hard to measure and the CMRO₂ estimation based on total CBV changes underestimates oxygen consumption (Kim et al., 1999; Kim & Ogawa, 2012). This is why we estimated CMRO₂ in the STIM condition based on 30% of the total CBV changes being venous, as found during visual stimulation on a 7T scanner (Huber et al., 2014). We encourage future research to measure venous CBV, e.g. by specific multi-echo VASO (vascular space occupancy) techniques as SS-SI-VASO (Huber et al., 2014), the VERVE technique (venous refocusing for volume estimation) (Chen & Pike, 2010), or e.g. by combining LL-FAIR (Look-Locker flow-sensitive alternating inversion recovery) with contrast-agent techniques to measure both total and arterial CBV (Wesolowski et al., 2019). Second, while we could measure both mqBOLD and fPET on a simultaneous PET-MR scanner, the SNR was limited by a 12-channel coil. The error propagation from T₂'₂ and CBF measurements lead to noisy CMRO₂ measurements. Additionally, fPET measurements with continuous radiotracer injection have a lower signal-to-noise-ratio compared to bolus-PET acquisition, where steady-state FDG levels are reached and the whole time-series is averaged. Finally, this complex setup with continuous tracer venous injection, arterial blood withdrawal and simultaneous MRI and PET measurements is more error-prone than a unimodal imaging study. This was reflected in the incomplete data acquisition or insufficient data quality for five subjects, so only 13 out of 18 datasets survived quality checks.

CONCLUSION

All in all, we were able to acquire a completely quantitative dataset, simultaneously measuring changes in both glucose (CMR_{glc}) and oxygen metabolism (CMRO₂) during visual stimulation, based on fPET and mqBOLD. We found significant increases in visual ROIs in both CMRO₂ and CMR_{glc}, after correcting for arterial increases in blood volume. Further, we found a significant decrease in the oxygen-to-glucose-index, pointing towards increased non-oxidative metabolism during stimulation. This complete quantification of glucose and oxygen metabolism will be especially interesting to investigate changes in oxidative and non-oxidative metabolism during higher cognitive processes as well as in disease.

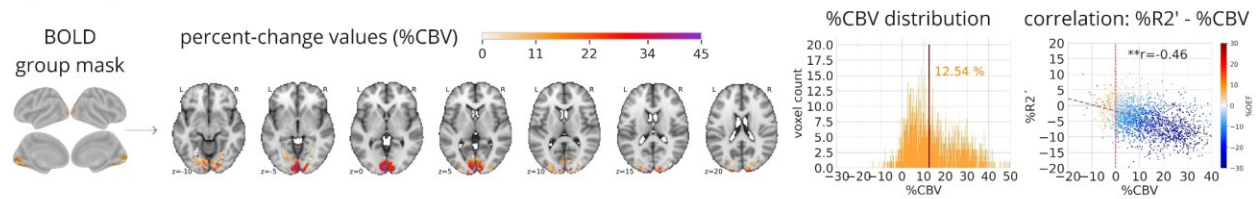
FUNDING:

CP: funded by the Deutsche Forschungsgemeinschaft (DFG, German Research Foundation) – ID 395030489.

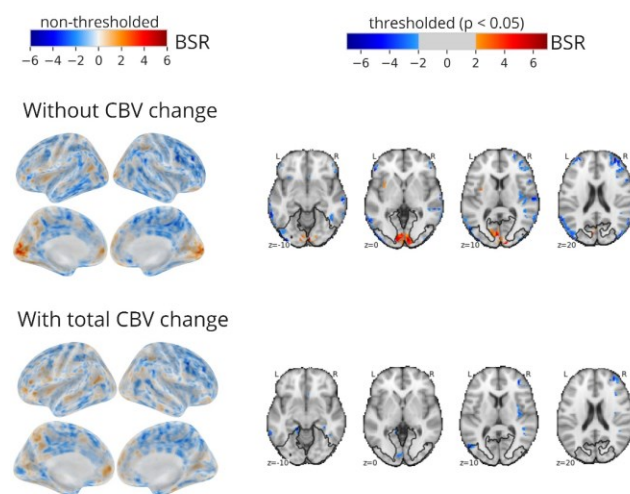
VR: funded by the European Research Council (ERC) under the European Union’s Horizon 2020 research and innovation program (ERC Starting Grant, ID 759659)

SUPPLEMENTS

A| Changes in CBV within BOLD activation ROI



B| CMRO2 group results: CBV correction



C| Delta CMRO2 within activation ROIs

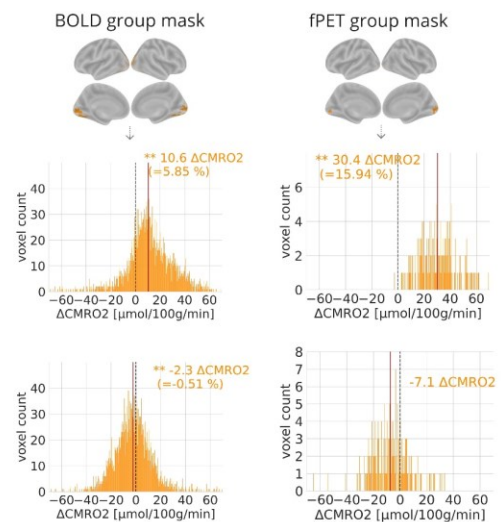


Fig. S1. Correction of CMRO2 due to arterial CBV increase. **A|** Axial slices show the distribution of percent-change CBV values, the histogram shows the distribution of voxel values, median across subjects per voxel. CBV values within the BOLD group activation mask increased about 12.54% on average (median across voxels within group mask) and up to 50%. Most likely, this was due to arterial dilation, indicated by the significant negative correlation ($r = -0.46$, $p < .001$) between changes in R2' and CBV, colored by %OEF, shown in the right scatter plot. **B|** Replication of group level CMRO2 task analysis via PLS, as in Fig. 2. First row: calculation of task CMRO2 without taking changes in CBV into account. Second row: calculation of task CMRO2 with total CBV (CBVt) increase. Maps show statistical values (bootstrap ratios, akin to z-values) within the first latent variable, $p < .001$. While there was no activation cluster in visual cortex when considering total CBV changes, we see a large visual cluster when considering no CBV changes. **C|** Distribution of absolute difference values per voxel in CMRO2, STIM minus REST condition, within BOLD and fPET group ROIs, median across subjects per voxel. Increases in CMRO2 were significant only when disregarding CBV changes (delta values tested via permutation tests against zero, $** = p < .001$) within both ROIs.

REFERENCES

- Alsop, D. C., Detre, J. A., Golay, X., Günther, M., Hendrikse, J., Hernandez-Garcia, L., Lu, H., MacIntosh, B. J., Parkes, L. M., Smits, M., van Osch, M. J. P., Wang, D. J. J., Wong, E. C., & Zaharchuk, G. (2015). Recommended implementation of arterial spin-labeled perfusion MRI for clinical applications: A consensus of the ISMRM perfusion study group and the European consortium for ASL in dementia: Recommended Implementation of ASL for Clinical Applications. *Magnetic Resonance in Medicine*, *73*(1), 102–116. <https://doi.org/10.1002/mrm.25197>
- Attwell, D., & Iadecola, C. (2002). The neural basis of functional brain imaging signals. *Trends in Neurosciences*, *25*(12), 621–625.
- Avants, B., Epstein, C., Grossman, M., & Gee, J. (2008). Symmetric diffeomorphic image registration with cross-correlation: Evaluating automated labeling of elderly and neurodegenerative brain. *Medical Image Analysis*, *12*(1), 26–41. <https://doi.org/10.1016/j.media.2007.06.004>
- Baudrexel, S., Volz, S., Preibisch, C., Klein, J. C., Steinmetz, H., Hilker, R., & Deichmann, R. (2009). Rapid single-scan T_2^* -mapping using exponential excitation pulses and image-based correction for linear background gradients: T_2^* Mapping With Field Gradient Correction. *Magnetic Resonance in Medicine*, *62*(1), 263–268. <https://doi.org/10.1002/mrm.21971>
- Blazey, T., Snyder, A. Z., Goyal, M. S., Vlassenko, A. G., & Raichle, M. E. (2018). A systematic meta-analysis of oxygen-to-glucose and oxygen-to-carbohydrate ratios in the resting human brain. *PLOS ONE*, *13*(9), e0204242. <https://doi.org/10.1371/journal.pone.0204242>
- Blockley, N. P., Griffeth, V. E. M., Simon, A. B., & Buxton, R. B. (2013). A review of calibrated blood oxygenation level-dependent (BOLD) methods for the measurement of task-induced changes in brain oxygen metabolism: A REVIEW OF CALIBRATED BOLD METHODS. *NMR in Biomedicine*, *26*(8), 987–1003. <https://doi.org/10.1002/nbm.2847>
- Blockley, N. P., Griffeth, V. E. M., Simon, A. B., Dubowitz, D. J., & Buxton, R. B. (2015). Calibrating the BOLD response without administering gases: Comparison of hypercapnia calibration with calibration using an asymmetric spin echo. *NeuroImage*, *104*, 423–429. <https://doi.org/10.1016/j.neuroimage.2014.09.061>
- Boxermann, J.L., Schmainda, K.M., Weisskoff, R.M. (2006). Relative Cerebral Blood Volume Maps Corrected for Contrast Agent Extravasation Significantly Correlate with Glioma Tumor Grade, Whereas Uncorrected Maps Do Not. *American Journal of Neuroradiology*, *27*(4), 859–867.
- Bright, M. G., Croal, P. L., Blockley, N. P., & Bulte, D. P. (2019). Multiparametric measurement of cerebral physiology using calibrated fMRI. *NeuroImage*, *187*, 128–144. <https://doi.org/10.1016/j.neuroimage.2017.12.049>
- Buxton, R. B., Griffeth, V. E. M., Simon, A. B., & Moradi, F. (2014). Variability of the coupling of blood flow and oxygen metabolism responses in the brain: A problem for interpreting BOLD studies but potentially a new window on the underlying neural activity. *Frontiers in Neuroscience*, *8*. <https://doi.org/10.3389/fnins.2014.00139>
- Byrne, J. H., Heidelberger, R., & Waxham, M. N. (Hrsg.). (2014). *From molecules to networks: An introduction to cellular and molecular neuroscience* (Third edition). Elsevier/AP, Academic Press is an imprint of Elsevier.
- Castrillon, G., Epp, S., Bose, A., Fraticelli, L., Hechler, A., Belenya, R., Ranft, A., Yakushev, I., Utz, L., Sundar, L., Rauschecker, J. P., Preibisch, C., Kurcyus, K., & Riedl, V. (2023). *An energy costly*

- architecture of neuromodulators for human brain evolution and cognition* [Preprint]. Neuroscience. <https://doi.org/10.1101/2023.04.25.538209>
- Chen, J. J., & Pike, G. B. (2009). BOLD-specific cerebral blood volume and blood flow changes during neuronal activation in humans: BOLD-SPECIFIC CHANGES IN CBV AND CBF. *NMR in Biomedicine*, 22(10), 1054–1062. <https://doi.org/10.1002/nbm.1411>
- Chen, J. J., & Pike, G. B. (2010). MRI measurement of the BOLD-specific flow–volume relationship during hypercapnia and hypocapnia in humans. *NeuroImage*, 53(2), 383–391. <https://doi.org/10.1016/j.neuroimage.2010.07.003>
- Chen, J. J., Uthayakumar, B., & Hyder, F. (2022). Mapping oxidative metabolism in the human brain with calibrated fMRI in health and disease. *Journal of Cerebral Blood Flow & Metabolism*, 42(7), 1139–1162. <https://doi.org/10.1177/0271678X221077338>
- Christen, T., Schmiedeskamp, H., Straka, M., Bammer, R., & Zaharchuk, G. (2012). Measuring brain oxygenation in humans using a multiparametric quantitative blood oxygenation level dependent MRI approach. *Magnetic Resonance in Medicine*, 68(3), 905–911. <https://doi.org/10.1002/mrm.23283>
- Donahue, M. J., Blicher, J. U., Østergaard, L., Feinberg, D. A., MacIntosh, B. J., Miller, K. L., Günther, M., & Jezzard, P. (2009). Cerebral blood flow, blood volume, and oxygen metabolism dynamics in human visual and motor cortex as measured by whole-brain multi-modal magnetic resonance imaging. *Journal of cerebral blood flow and metabolism*, 29(11), 1856–1866. <https://doi.org/10.1038/jcbfm.2009.107>
- Eichling, J. O., Raichle, M. E., Grubb, R. L., Larson, K. B., & Ter-Pogossian, M. M. (1975). In vivo determination of cerebral blood volume with radioactive oxygen-15 in the monkey. *Circulation Research*, 37(6), 707–714. <https://doi.org/10.1161/01.RES.37.6.707>
- Esteban, O. (2019). fMRIPrep: A robust preprocessing pipeline for functional MRI. *Nature Methods*, 16, 14.
- Esteban, O., Ciric, R., Finc, K., Blair, R. W., Markiewicz, C. J., Moodie, C. A., Kent, J. D., Goncalves, M., DuPre, E., Gomez, D. E. P., Ye, Z., Salo, T., Valabregue, R., Amlien, I. K., Liem, F., Jacoby, N., Stojić, H., Cieslak, M., Urchs, S., ... Gorgolewski, K. J. (2020). Analysis of task-based functional MRI data preprocessed with fMRIPrep. *Nature Protocols*, 15(7), 2186–2202. <https://doi.org/10.1038/s41596-020-0327-3>
- Feng, D., Huang, S.-C., & Wang, X. (1993). Models for computer simulation studies of input functions for tracer kinetic modeling with positron emission tomography. *International Journal of Bio-Medical Computing*, 32(2), 95–110. [https://doi.org/10.1016/0020-7101\(93\)90049-C](https://doi.org/10.1016/0020-7101(93)90049-C)
- Fox, P., Raichle, M., Mintun, M., & Dence, C. (1988). Nonoxidative glucose consumption during focal physiologic neural activity. *Science*, 241(4864), 462–464. <https://doi.org/10.1126/science.3260686>
- Fox, P. T., & Raichle, M. E. (1986). Focal physiological uncoupling of cerebral blood flow and oxidative metabolism during somatosensory stimulation in human subjects. *Proceedings of the National Academy of Sciences*, 83(4), 1140–1144. <https://doi.org/10.1073/pnas.83.4.1140>
- Fujita, N., Matsumoto, K., Tanaka, H., Watanabe, Y., & Murase, K. (2006). Quantitative study of changes in oxidative metabolism during visual stimulation using absolute relaxation rates. *NMR in Biomedicine*, 19(1), 60–68. <https://doi.org/10.1002/nbm.1001>

- Gorgolewski, K., Burns, C. D., Madison, C., Clark, D., Halchenko, Y. O., Waskom, M. L., & Ghosh, S. S. (2011). Nipype: A Flexible, Lightweight and Extensible Neuroimaging Data Processing Framework in Python. *Frontiers in Neuroinformatics*, 5. <https://doi.org/10.3389/fninf.2011.00013>
- Göttler, J., Kaczmarz, S., Kallmayer, M., Wustrow, I., Eckstein, H.-H., Zimmer, C., Sorg, C., Preibisch, C., & Hyder, F. (2019). Flow-metabolism uncoupling in patients with asymptomatic unilateral carotid artery stenosis assessed by multi-modal magnetic resonance imaging. *Journal of Cerebral Blood Flow & Metabolism*, 39(11), 2132–2143. <https://doi.org/10.1177/0271678X18783369>
- Hahn, A., Gryglewski, G., Nics, L., Hienert, M., Rischka, L., Vranka, C., Sigurdardottir, H., Vanicek, T., James, G. M., Seiger, R., Kautzky, A., Silberbauer, L., Wadsak, W., Mitterhauser, M., Hacker, M., Kasper, S., & Lanzenberger, R. (2016). Quantification of Task-Specific Glucose Metabolism with Constant Infusion of 18F-FDG. *Journal of Nuclear Medicine*, 57(12), 1933–1940. <https://doi.org/10.2967/jnumed.116.176156>
- Hedderich, D., Kluge, A., Pyka, T., Zimmer, C., Kirschke, J. S., Wiestler, B., & Preibisch, C. (2019). Consistency of normalized cerebral blood volume values in glioblastoma using different leakage correction algorithms on dynamic susceptibility contrast magnetic resonance imaging data without and with preload. *Journal of Neuroradiology*, 46(1), 44–51. <https://doi.org/10.1016/j.neurad.2018.04.006>
- Hirsch, N. M., & Preibisch, C. (2013). T2* Mapping with Background Gradient Correction Using Different Excitation Pulse Shapes. *American Journal of Neuroradiology*, 34(6), E65–E68. <https://doi.org/10.3174/ajnr.A3021>
- Hirsch, N. M., Toth, V., Förchler, A., Kooijman, H., Zimmer, C., & Preibisch, C. (2014). Technical considerations on the validity of blood oxygenation level-dependent-based MR assessment of vascular deoxygenation: BOLD-BASED ASSESSMENT OF VASCULAR DEOXYGENATION. *NMR in Biomedicine*, 27(7), 853–862. <https://doi.org/10.1002/nbm.3131>
- Hoge, R. D., & Pike, G. B. (2001). Oxidative metabolism and the detection of neuronal activation via imaging. *Journal of Chemical Neuroanatomy*, 22(1–2), 43–52. [https://doi.org/10.1016/S0891-0618\(01\)00114-4](https://doi.org/10.1016/S0891-0618(01)00114-4)
- Hua, J., Liu, P., Kim, T., Donahue, M., Rane, S., Chen, J. J., Qin, Q., & Kim, S.-G. (2019). MRI techniques to measure arterial and venous cerebral blood volume. *NeuroImage*, 187, 17–31. <https://doi.org/10.1016/j.neuroimage.2018.02.027>
- Huber, L., Goense, J., Kennerley, A. J., Ivanov, D., Krieger, S. N., Lepsien, J., Trampel, R., Turner, R., & Möller, H. E. (2014). Investigation of the neurovascular coupling in positive and negative BOLD responses in human brain at 7T. *NeuroImage*, 97, 349–362. <https://doi.org/10.1016/j.neuroimage.2014.04.022>
- Huber, L., Uludağ, K., & Möller, H. E. (2019). Non-BOLD contrast for laminar fMRI in humans: CBF, CBV, and CMRO2. *NeuroImage*, 197, 742–760. <https://doi.org/10.1016/j.neuroimage.2017.07.041>
- Hyder, F., Herman, P., Bailey, C. J., Møller, A., Globinsky, R., Fulbright, R. K., Rothman, D. L., & Gjedde, A. (2016). Uniform distributions of glucose oxidation and oxygen extraction in gray matter of normal human brain: No evidence of regional differences of aerobic glycolysis. *Journal of Cerebral Blood Flow & Metabolism*, 36(5), 903–916. <https://doi.org/10.1177/0271678X15625349>
- Jamadar, S. D., Ward, P. G., Li, S., Sforzini, F., Baran, J., Chen, Z., & Egan, G. F. (2019). Simultaneous task-based BOLD-fMRI and [18-F] FDG functional PET for measurement of neuronal metabolism in

the human visual cortex. *NeuroImage*, 189, 258–266.

<https://doi.org/10.1016/j.neuroimage.2019.01.003>

Jenkinson, M., Beckmann, C. F., Behrens, T. E. J., Woolrich, M. W., & Smith, S. M. (2012). FSL.

NeuroImage, 62(2), 782–790. <https://doi.org/10.1016/j.neuroimage.2011.09.015>

Kaczmarz, S., Hyder, F., & Preibisch, C. (2020). Oxygen extraction fraction mapping with multi-parametric quantitative BOLD MRI: Reduced transverse relaxation bias using 3D-GraSE imaging.

NeuroImage, 220, 117095. <https://doi.org/10.1016/j.neuroimage.2020.117095>

Kim, S.-G., & Ogawa, S. (2012). Biophysical and Physiological Origins of Blood Oxygenation Level-Dependent fMRI Signals. *Journal of Cerebral Blood Flow & Metabolism*, 32(7), 1188–1206.

<https://doi.org/10.1038/jcbfm.2012.23>

Kim, S.-G., Rostrup, E., Larsson, H. B. W., Ogawa, S., & Paulson, O. B. (1999). Determination of relative CMRO₂ from CBF and BOLD changes: Significant increase of oxygen consumption rate during visual stimulation. *Magnetic Resonance in Medicine*, 41(6), 1152–1161.

[https://doi.org/10.1002/\(SICI\)1522-2594\(199906\)41:6<1152::AID-MRM11>3.0.CO;2-T](https://doi.org/10.1002/(SICI)1522-2594(199906)41:6<1152::AID-MRM11>3.0.CO;2-T)

Kluge, A., Lukas, M., Toth, V., Pyka, T., Zimmer, C., & Preibisch, C. (2016). Analysis of three leakage-correction methods for DSC-based measurement of relative cerebral blood volume with respect to heterogeneity in human gliomas. *Magnetic Resonance Imaging*, 34(4), 410–421.

<https://doi.org/10.1016/j.mri.2015.12.015>

Krishnan, A., Williams, L. J., McIntosh, A. R., & Abdi, H. (2011). Partial Least Squares (PLS) methods for neuroimaging: A tutorial and review. *NeuroImage*, 56(2), 455–475.

<https://doi.org/10.1016/j.neuroimage.2010.07.034>

Kufer, J., Preibisch, C., Epp, S., Göttler, J., Schmitzer, L., Zimmer, C., Hyder, F., & Kaczmarz, S. (2022). Imaging effective oxygen diffusivity in the human brain with multiparametric magnetic resonance imaging. *Journal of Cerebral Blood Flow & Metabolism*, 42(2), 349–363.

<https://doi.org/10.1177/0271678X211048412>

Leenders, K. L., Perani, D., Lammertsma, A. A., Heather, J. D., Buckingham, P., Jones, T., Healy, M. J. R., Gibbs, J. M., Wise, R. J. S., Hatazawa, J., Herold, S., Beaney, R. P., Brooks, D. J., Spinks, T., Rhodes, C., & Frackowiak, R. S. J. (1990). CEREBRAL BLOOD FLOW, BLOOD VOLUME AND OXYGEN UTILIZATION: NORMAL VALUES AND EFFECT OF AGE. *Brain*, 113(1), 27–47.

<https://doi.org/10.1093/brain/113.1.27>

Lin, A.-L., Fox, P. T., Hardies, J., Duong, T. Q., & Gao, J.-H. (2010). Nonlinear coupling between cerebral blood flow, oxygen consumption, and ATP production in human visual cortex. *Proceedings of the National Academy of Sciences*, 107(18), 8446–8451.

<https://doi.org/10.1073/pnas.0909711107>

Lin, A.-L., Fox, P. T., Yang, Y., Lu, H., Tan, L.-H., & Gao, J.-H. (2008a). Evaluation of MRI models in the measurement of CMRO₂ and its relationship with CBF. *Magnetic Resonance in Medicine*, 60(2), 380–389. <https://doi.org/10.1002/mrm.21655>

Lin, A.-L., Fox, P. T., Yang, Y., Lu, H., Tan, L.-H., & Gao, J.-H. (2008b). Evaluation of MRI models in the measurement of CMRO₂ and its relationship with CBF. *Magnetic Resonance in Medicine*, 60(2), 380–389. <https://doi.org/10.1002/mrm.21655>

- Liu, E. Y., Guo, J., Simon, A. B., Haist, F., Dubowitz, D. J., & Buxton, R. B. (2019). The potential for gas-free measurements of absolute oxygen metabolism during both baseline and activation states in the human brain. *NeuroImage*, 116342. <https://doi.org/10.1016/j.neuroimage.2019.116342>
- Ma, Y., Sun, H., Cho, J., Mazerolle, E. L., Wang, Y., & Pike, G. B. (2020). Cerebral OEF quantification: A comparison study between quantitative susceptibility mapping and dual-gas calibrated BOLD imaging. *Magnetic Resonance in Medicine*, 83(1), 68–82. <https://doi.org/10.1002/mrm.27907>
- Mangia, S., Tkáč, I., Logothetis, N. K., Gruetter, R., Van De Moortele, P. F., & Uğurbil, K. (2007). Dynamics of lactate concentration and blood oxygen level-dependent effect in the human visual cortex during repeated identical stimuli. *Journal of Neuroscience Research*, 85, 3340–3346. <https://doi.org/10.1002/jnr.21371>
- McIntosh, A. R., & Lobaugh, N. J. (2004). Partial least squares analysis of neuroimaging data: Applications and advances. *NeuroImage*, 23, S250–S263. <https://doi.org/10.1016/j.neuroimage.2004.07.020>
- McIntosh, A. R., & Mišić, B. (2013). Multivariate Statistical Analyses for Neuroimaging Data. *Annual Review of Psychology*, 64(1), 499–525. <https://doi.org/10.1146/annurev-psych-113011-143804>
- Mintun, M. A., Vlassenko, A. G., Shulman, G. L., & Snyder, A. Z. (2002). Time-Related Increase of Oxygen Utilization in Continuously Activated Human Visual Cortex. *NeuroImage*, 16(2), 531–537. <https://doi.org/10.1006/nimg.2002.1114>
- Moradi, F., Buračas, G. T., & Buxton, R. B. (2012). Attention strongly increases oxygen metabolic response to stimulus in primary visual cortex. *NeuroImage*, 59(1), 601–607. <https://doi.org/10.1016/j.neuroimage.2011.07.078>
- Moradi, F., & Buxton, R. B. (2013). Adaptation of cerebral oxygen metabolism and blood flow and modulation of neurovascular coupling with prolonged stimulation in human visual cortex. *NeuroImage*, 82, 182–189. <https://doi.org/10.1016/j.neuroimage.2013.05.110>
- Nöth, U., Volz, S., Hattingen, E., & Deichmann, R. (2014). An improved method for retrospective motion correction in quantitative T2* mapping. *NeuroImage*, 92, 106–119. <https://doi.org/10.1016/j.neuroimage.2014.01.050>
- Patlak, C. S., & Blasberg, R. G. (1985). Graphical Evaluation of Blood-to-Brain Transfer Constants from Multiple-Time Uptake Data. Generalizations. *Journal of Cerebral Blood Flow & Metabolism*, 5(4), 584–590. <https://doi.org/10.1038/jcbfm.1985.87>
- Paulson, O. B., Hasselbalch, S. G., Rostrup, E., Knudsen, G. M., & Pelligrino, D. (2010). Cerebral Blood Flow Response to Functional Activation. *Journal of Cerebral Blood Flow & Metabolism*, 30(1), 2–14. <https://doi.org/10.1038/jcbfm.2009.188>
- Phelps, M. E., Huang, S. C., Hoffman, E. J., Selin, C., Sokoloff, L., & Kuhl, D. E. (1979). Tomographic measurement of local cerebral glucose metabolic rate in humans with (F-18)2-fluoro-2-deoxy-D-glucose: Validation of method. *Annals of Neurology*, 6(5), 371–388. <https://doi.org/10.1002/ana.410060502>
- Preibisch, C., Volz, S., Anti, S., & Deichmann, R. (2008). Exponential excitation pulses for improved water content mapping in the presence of background gradients. *Magnetic Resonance in Medicine*, 60(4), 908–916. <https://doi.org/10.1002/mrm.21730>

- Raichle, M. E., MacLeod, A. M., Snyder, A. Z., Powers, W. J., Gusnard, D. A., & Shulman, G. L. (2001). A default mode of brain function. *Proceedings of the National Academy of Sciences*, *98*(2), 676–682. <https://doi.org/10.1073/pnas.98.2.676>
- Rischka, L., Gryglewski, G., Pfaff, S., Vanicek, T., Hienert, M., Klöbl, M., Hartenbach, M., Haug, A., Wadsak, W., Mitterhauser, M., Hacker, M., Kasper, S., Lanzenberger, R., & Hahn, A. (2018). Reduced task durations in functional PET imaging with [18F]FDG approaching that of functional MRI. *NeuroImage*, *181*, 323–330. <https://doi.org/10.1016/j.neuroimage.2018.06.079>
- Shulman, R. G., Hyder, F., & Rothman, D. L. (2001). Lactate efflux and the neuroenergetic basis of brain function. *NMR in Biomedicine*, *14*(7–8), 389–396. <https://doi.org/10.1002/nbm.741>
- Simon, A. B., & Buxton, R. B. (2015). Understanding the dynamic relationship between cerebral blood flow and the BOLD signal: Implications for quantitative functional MRI. *NeuroImage*, *116*, 158–167. <https://doi.org/10.1016/j.neuroimage.2015.03.080>
- Smith, S. M., Jenkinson, M., Woolrich, M. W., Beckmann, C. F., Behrens, T. E. J., Johansen-Berg, H., Bannister, P. R., De Luca, M., Drobnjak, I., Flitney, D. E., Niazy, R. K., Saunders, J., Vickers, J., Zhang, Y., De Stefano, N., Brady, J. M., & Matthews, P. M. (2004). Advances in functional and structural MR image analysis and implementation as FSL. *NeuroImage*, *23*, S208–S219. <https://doi.org/10.1016/j.neuroimage.2004.07.051>
- Stiernman, L. J., Grill, F., Hahn, A., Rischka, L., Lanzenberger, R., Panes Lundmark, V., Riklund, K., Axelsson, J., & Rieckmann, A. (2021). Dissociations between glucose metabolism and blood oxygenation in the human default mode network revealed by simultaneous PET-fMRI. *Proceedings of the National Academy of Sciences*, *118*(27), e2021913118. <https://doi.org/10.1073/pnas.2021913118>
- Vafaei, M. S., Vang, K., Bergersen, L. H., & Gjedde, A. (2012). Oxygen consumption and blood flow coupling in human motor cortex during intense finger tapping: Implication for a role of lactate. *Journal of Cerebral Blood Flow & Metabolism*, *32*, 1859–1868. <https://doi.org/10.1038/jcbfm.2012.89>
- Vaishnavi, S. N., Vlassenko, A. G., Rundle, M. M., Snyder, A. Z., Mintun, M. A., & Raichle, M. E. (2010). Regional aerobic glycolysis in the human brain. *Proceedings of the National Academy of Sciences*, *107*(41), 17757–17762. <https://doi.org/10.1073/pnas.1010459107>
- Villien, M., Wey, H.-Y., Mandeville, J. B., Catana, C., Polimeni, J. R., Sander, C. Y., Zürcher, N. R., Chonde, D. B., Fowler, J. S., Rosen, B. R., & Hooker, J. M. (2014). Dynamic functional imaging of brain glucose utilization using fPET-FDG. *NeuroImage*, *100*, 192–199. <https://doi.org/10.1016/j.neuroimage.2014.06.025>
- Vlassenko, A. G., Rundle, M. M., & Mintun, M. A. (2006). Human brain glucose metabolism may evolve during activation: Findings from a modified FDG PET paradigm. *NeuroImage*, *33*(4), 1036–1041. <https://doi.org/10.1016/j.neuroimage.2006.06.065>
- Vriens, D., de Geus-Oei, L.-F., Oyen, W. J. G., & Visser, E. P. (2009). A Curve-Fitting Approach to Estimate the Arterial Plasma Input Function for the Assessment of Glucose Metabolic Rate and Response to Treatment. *Journal of Nuclear Medicine*, *50*(12), 1933–1939. <https://doi.org/10.2967/jnumed.109.065243>
- Wesolowski, R., Blockley, N. P., Driver, I. D., Francis, S. T., & Gowland, P. A. (2019). Coupling between cerebral blood flow and cerebral blood volume: Contributions of different vascular compartments. *NMR in Biomedicine*, *32*(3), e4061. <https://doi.org/10.1002/nbm.4061>

- Wu, H. (2003). Measurement of the Global Lumped Constant for 2-Deoxy-2-[18F]Fluoro-D-Glucose in Normal Human Brain Using [15O]Water and 2-Deoxy-2-[18F]Fluoro-D-Glucose Positron Emission Tomography Imaging A Method with Validation Based on Multiple Methodologies. *Molecular Imaging & Biology*, 5(1), 32–41. [https://doi.org/10.1016/S1536-1632\(02\)00122-1](https://doi.org/10.1016/S1536-1632(02)00122-1)
- Yablonskiy, D. A., & Haacke, E. M. (1994). Theory of NMR signal behavior in magnetically inhomogeneous tissues: The static dephasing regime. *Magnetic Resonance in Medicine*, 32(6), 749–763. <https://doi.org/10.1002/mrm.1910320610>
- Yeo, B. T., Krienen, F. M., Sepulcre, J., Sabuncu, M. R., Lashkari, D., Hollinshead, M., Roffman, J. L., Smoller, J. W., Zöllei, L., Polimeni, J. R., Fischl, B., Liu, H., & Buckner, R. L. (2011). The organization of the human cerebral cortex estimated by intrinsic functional connectivity. *Journal of Neurophysiology*, 106(3), 1125–1165. <https://doi.org/10.1152/jn.00338.2011>
- Zhang, J., Liu, T., Gupta, A., Spincemaille, P., Nguyen, T. D., & Wang, Y. (2015). Quantitative mapping of cerebral metabolic rate of oxygen (CMRO₂) using quantitative susceptibility mapping (QSM): Quantitative CMRO₂ Mapping Using QSM. *Magnetic Resonance in Medicine*, 74(4), 945–952. <https://doi.org/10.1002/mrm.25463>

3 PROJECT II: Negative BOLD signals do not necessarily indicate reduced oxygen metabolism – a quantitative MRI study

The current chapter includes the research article “Negative BOLD signals do not necessarily indicate reduced oxygen metabolism – a quantitative MRI study”. This article is currently under preparation for submission, so the authors retain the copyright for the manuscript. If the manuscript will be accepted for publication, it will be subject to the Copyright terms of the respective journal.

Authors

Samira M. Epp, Gabriel Castrillón, Beija Yuan, Jessica Andrews-Hanna, Christine Preibisch, Valentin Riedl

Contributions

SME, as the author of this thesis, was responsible for study design, participant organization, data collection, data analysis, manuscript drafting, writing & editing and figures. GC assisted with data curation and manuscript editing, BY with modeling, JAH with manuscript editing and design counseling, CP with sequence optimization, manuscript editing and mqBOLD data analysis pipeline, VR was responsible for the project conceptualization, supervision, funding and manuscript editing.

My contribution to this manuscript in detail:

For this manuscript, I was responsible for programming the tasks, piloting of all mqBOLD sequences and conceptualization of the task design, data collection & participant organization, data preprocessing & all analyses in this manuscript, interpretation of results, figure creation and manuscript writing.

Negative BOLD signals in default mode regions do not necessarily indicate reduced oxygen metabolism – a quantitative MRI study

Samira M. Epp^{1,2}, Gabriel Castrillón¹, Beija Yuan³, Jessica Andrews-Hanna⁴, Christine Preibisch¹, Valentin Riedl^{1,5}

1 Department of Neuroradiology, Neuroimaging Center, Technical University of Munich, Munich, Germany

2 Graduate School of Systemic Neurosciences, Ludwig-Maximilians-University, Munich, Germany

3 Department of Bioengineering, University of California, San Diego, California, USA

4 Department of Psychology, University of Arizona, Tucson, AZ, USA

5 Department of Neuroradiology, Friedrich-Alexander-University, Erlangen, Germany

ABSTRACT

In human neuroimaging, blood oxygen level dependent (BOLD) functional magnetic resonance imaging (fMRI) is the most widely employed method to identify changes in brain activity during experimentally controlled tasks. The BOLD signal is sensitive to the oxygenation of venous blood, more precisely to the deoxyhemoglobin (dHb) level of brain tissue. Tissue oxygenation depends on the exact interplay between neuronal activity and blood flow as well as between neuronal activity and oxygen metabolism, which the BOLD signal alone cannot resolve. The cerebral metabolic rate of oxygen (CMRO₂), in turn, reflects oxidative metabolism in the brain, a true physiological marker for neuronal activity. In this study, we used multi-parametric MRI to quantify CMRO₂ as a proxy for neuronal activity. Participants performed different cognitive tasks that induced well-known patterns of BOLD signal increases and decreases. BOLD signal *decreases* during a calculation task as well as *increases* during an autobiographical memory task were primarily localized in regions of the default mode network (DMN). BOLD signal *increases* during both the memory and the calculation task, and compared to an active and a passive baseline, were mostly accompanied by concomitant *increases* in CMRO₂ across voxels, with only 7 - 35% mismatch across voxels. On the contrary, 46 - 64% of DMN voxels that showed BOLD decreases did *not* show concomitant CMRO₂ decreases, but stable or increased CMRO₂. Thus, while some clusters within the DMN showed concomitant CMRO₂ decreases, our data point towards a metabolic heterogeneity within the DMN that was not captured by the BOLD signal. Our data fits well to the biophysical Davis model, which predicts that both negative and positive BOLD signals can occur despite opposing sign of the CMRO₂ response. Yet, dissociations between the signs of the BOLD and CMRO₂ amplitudes question our common interpretation of BOLD signal changes in terms of neuronal activity. By comparing fMRI BOLD with CMRO₂, this study provides evidence that this dissociation in oxidative metabolism and BOLD signal specifically affects *negative* BOLD responses. Thus, caution has to be exercised when interpreting negative BOLD signals as reduced excitatory brain activity. We advocate for the use of quantitative fMRI in future research.

Keywords: *Multiparametric, quantitative MRI (mqBOLD); default mode network (DMN); negative BOLD response (NBR); fMRI BOLD; cerebral rate of oxygen (CMRO₂); cerebral blood flow (CBF); oxygen extraction fraction (OEF)*

INTRODUCTION

For over 30 years, functional magnetic resonance imaging (fMRI) has been used as a noninvasive tool to localize neuronal activity in the human brain. Neuronal signaling accounts for around 85% of brain energy metabolism (Attwell & Iadecola, 2002), which, in turn, relies on a constant supply of glucose and oxygen via arterial blood. As a result of oxygen uptake for energy metabolism, deoxyhemoglobin (dHb) concentration rises in venous blood. Functional MRI is sensitive to changes in dHb and measures the blood oxygenation-level dependent (BOLD) signal simultaneously in thousands of volume elements (voxels) covering the entire brain (Logothetis, 2003; Ogawa et al., 1990).

If dHb levels exclusively reflected energy metabolism, BOLD signal changes could be interpreted as changes in neuronal activity. However, the canonical positive BOLD response is elicited by luxury perfusion, meaning that it is caused by an overcompensatory increase in cerebral blood flow (CBF), which outweighs the increase in oxygen consumption. Thus, paradoxically, the positive BOLD response reflects a *decrease* in dHb in venous blood at sites of neuronal activity. But dHb levels crucially depend on details of coupling between neuronal activity and perfusion (neurovascular coupling) and between neuronal activity and oxygen metabolism (neurometabolic coupling) (Hyder, 2010a), which the BOLD signal alone cannot resolve. The cerebral metabolic rate of oxygen (CMRO₂), in turn, reflects oxidative metabolism in the brain, a physiological marker for neuronal activity (Hoge & Pike, 2001). Most of the brain's energy needs are met via oxidative metabolism, which is the process that generates adenosine triphosphate (ATP) through oxygen and glucose (Hoge & Pike, 2001; Mangia et al., 2007; R. G. Shulman et al., 2001).

How exactly does neurovascular and neurometabolic coupling impact on the BOLD signal? In practice, each MRI voxel (typically 1-10 mm³) covers brain tissue with an unknown composition of arterial and venous blood vessels delivering oxygenated and draining deoxygenated blood. Therefore, the total amount of dHb at baseline in each voxel is unknown. On top of that, due to differences in vascular architecture (Gagnon et al., 2015), neurovascular coupling can be expected to vary between brain regions. More specifically, cerebral blood flow and volume have been found to change in a nonlinear manner with neuronal activity depending on the vascular composition and the concentration of metabolites mediating the neurovascular coupling (Attwell & Iadecola, 2002; Blockley et al., 2013a; Buxton, 2010a; Buxton et al., 2014a; Buxton & Frank, 1997; Kaplan et al., 2020). This means that an identical change in neuronal activity may result in different BOLD signal amplitudes across the cortex. In summary, the BOLD signal merely captures changes in dHb relative to an unknown baseline that depends on a variety of factors in addition to non-linear neurovascular coupling in each voxel.

Recent quantitative fMRI approaches aim to solve these uncertainties by capturing different aspects of cerebral hemodynamics with specific imaging sequences. Multiparametric, quantitative BOLD (mqBOLD) MRI is used to calculate the cerebral metabolic rate of oxygen (CMRO₂) from measurements of transverse relaxation rates T₂ and T₂^{*}, cerebral blood volume (CBV) as well as cerebral blood flow (CBF) (Bright et al., 2019; Christen et al., 2012; Kaczmarz, Hyder, et al., 2020; Kufer et al., 2022). CMRO₂ quantifies the absolute oxygen consumption on a voxel level in both baseline and task states. It is supposed to be driven largely by excitatory brain activity and task-induced increases in CMRO₂ are controlled by ATP turnover (Buxton, 2021; Buxton et al., 2014b; Lauritzen et al., 2012). Here, we used mqBOLD MRI in combination with classical BOLD fMRI to quantify the CMRO₂ changes underlying relative BOLD responses across brain regions and experimental conditions.

Yet, changes in the BOLD signal have been related to neuronal activity as well. Seminal work showed that positive BOLD responses relate to increased synaptic (measured by local field potentials, LFP) and spiking (measured by multi-unit activity, MUA) neuronal activity (Hillman, 2014; Hyder, 2010b; Logothetis, 2003, 2008). This has been shown in visual and primary sensory regions with dense capillaries and organized neuronal fields but does not necessarily hold true in

other regions such as associative areas (A. Ekstrom, 2010; A. D. Ekstrom, 2021; Harrison, 2002a). Crucially, the BOLD response is highly variable across the cortex because it depends on the vasculature, the hemoglobin content of the blood, the baseline of deoxygenated hemoglobin in this brain region and on the cerebral blood volume, which makes interpretation difficult (Blockley et al., 2013b; Buxton et al., 2014b; Buxton & Frank, 1997).

In particular, the detection of consistent negative BOLD responses, mainly in the so-called default-mode network (DMN), stimulated debate on the interpretation of BOLD signal changes. The DMN was originally defined as regions with decreased blood flow during sensory processing compared to passive states (G. L. Shulman et al., 1997). Since then, numerous studies reported BOLD signal decreases in DMN regions during a broad spectrum of sensory and cognitive processing compared to an uncontrolled, resting state condition (Buckner et al., 2008; Fox et al., 2005; Raichle, 2015; Raichle et al., 2001). Yet, DMN regions show positive BOLD responses during self-referential and other internally-oriented goal-directed tasks, in this case mostly compared to a matched control-task (Andrews-Hanna et al., 2014; Buckner et al., 2008; Spreng, 2012; Spreng et al., 2010, 2013). This led to the interpretation of the DMN as a network supporting internally-oriented cognition, which deactivates during externally-focused tasks that involve minimal internal mentation.

However, evidence that speaks for the interpretation of negative BOLD responses as decreases in neuronal activity is mixed. At least parts of the DMN showed suppressed activity in electrophysiological measurements: Macaques showed tonic suppression of single-unit-activity in 35%, but also enhancement in 9.4% of the neurons in the posterior cingulate cortex (PCC), part of the DMN, as well as suppressed LFP power during a passive visual stimulation task (Bentley et al., 2016; Hayden et al., 2009). Intracranial measurements in human patients with epilepsy discovered task-related suppression in gamma power in classical DMN areas during a visual search task (Ossandon et al., 2011). Gamma power was also suppressed in 24% of electrodes in posteromedial cortex during a calculation task, as well as increased in 33% during a self-episodic condition, while the other electrodes did not respond above threshold (Foster et al., 2012). While the electrophysiological macaque studies point towards a decrease in neuronal activity in at least parts of the DMN, suppression in gamma power is only an indirect marker for reduced spiking activity. Spiking activity, in turn, does rather reflect action potentials than general synaptic processing and has a comparatively small impact on energy consumption in the brain (Attwell & Iadecola, 2002; A. Ekstrom, 2010). Interestingly, a recent study did not find any evidence for decreased glucose metabolism in DMN areas, despite consistent BOLD signal 'deactivations', when comparing a working memory task to awake rest (Stiernman et al., 2021). Additionally, DMN deactivations have been related to physiological noise (Renvall et al., 2015) and prolonged hypoxia seems to drive both resting state CBF and task-induced BOLD responses specifically in the DMN in the opposite direction compared to the rest of the cortex (Lawley et al., 2017; Rogan et al., 2022; Rossetti et al., 2021a). These results suggests a fundamentally different neurovascular coupling in DMN regions.

In summary, there is strong evidence that positive BOLD responses are indicative for both increased neuronal spiking as well as increased synaptic activity in sensory cortices. However, there is no clear picture regarding BOLD *decreases*: do negative BOLD signals reliably capture decreases in synaptic and thus metabolic activity or do they arise due to deviations of the canonical neurovascular coupling mechanisms in certain brain regions?

In this study, we used multi-parametric MRI to quantify energy metabolism, more specifically CMRO₂, as a proxy for neuronal activity in brain areas showing positive and negative BOLD responses. To this end, we used cognitive tasks to induce well-known patterns of BOLD activations and deactivations. This allowed us to quantify task-induced changes in oxidative metabolism in comparison to BOLD signal changes within a range of cortical regions.

METHODS

Subjects

We acquired data of 47 healthy subjects for our main study, seven of whom had to be excluded because of apparent behavioral task difficulties, problems with contrast-agent application or severe motion artifacts in CBF or R2' data. Resting state (REST) data from a subset of 16 subjects were already evaluated with regard to oxygen diffusivity and published (Kufer et al., 2022). The two main tasks, calculation (CALC) and control (CTRL), were acquired for 40 healthy subjects (22 women, 18 men; mean age $32.1 \pm 9.2y$, all right-handed). All analyses including either autobiographical memory (MEM) or REST conditions were performed on a subset of 30 subjects (17 women, 13 men, mean age $32.2 \pm 9.6y$) from whom we acquired all four conditions. MRI was performed on a 3T Philips Elition Ingenia MR scanner (Philips Healthcare, Best, The Netherlands) using a 32-channel head-coil. The fMRI-only control study was performed on a separate cohort of 18 healthy subjects on a 3T Philips Ingenia MR scanner (Philips Healthcare, Best, The Netherlands), using an identically constructed 32-channel head coil (11 women, 7 men; mean age $28.1 \pm 5.0y$, all right-handed). Within the control study, we acquired BOLD fMRI data during prolonged task blocks compared to the main cohort. All participants gave informed written consent to procedures approved by the Ethics Review Board of the Klinikum Rechts der Isar, Technische Universität München.

Task design

Participants were lying in the scanner in a supine position and watched the task instructions on a screen behind the scanner via a mirror mounted on the head coil. Right hand responses were collected via a button box. Before entering the scanner, all subjects got the tasks explained, with emphasis on staying concentrated and giving correct responses rather than being fast, as well as practiced them on a computer outside of the scanning room. The CALC condition was designed to evoke negative BOLD responses in the DMN and positive BOLD responses in a task-positive network including frontoparietal control and dorsal attention networks (DAN). The CALC task was based on the design of Lin and colleagues (Lin et al., 2011) as a self-paced, continuous arithmetic task with a maximum response time of 10 seconds, so that participants had to continuously engage in calculations. A row of three numbers plus a question mark ($n_1, n_2, n_3, ?$) was presented that had to be continued, based on the following rule: $n_2 - n_1 = \text{DIFF}$, $n_2 = n_1 + (1 * \text{DIFF})$, $n_3 = n_2 + (2 * \text{DIFF})$, $? = n_3 + (3 * \text{DIFF})$. An exemplary row was 33 38 49 ?. Here, the difference between the first and the second number is 5 and $3 * 5$ is 15, so the right number is 64 ($49 + 15$). The participants had three response options. The autobiographical memory task was based on the task-design of Spreng and colleagues (DuPre et al., 2016; Spreng & Grady, 2010), where participants were asked to remember a specific event in the past. We aimed to match the visual input across all three tasks, thus using a written cue-word instead of a picture. Instructions were given to the participants to remember all details of any event in the past, which came to their minds, no matter how well it related to the cue-word. The cue-word was shown for a maximum of 15 seconds. To track how long it took the participants on average to remember an event, i.e., how easy it was for them to recover a memory, they were instructed to press the first button twice as soon as an event came to their minds. On average, it took the participants 2.5 ± 1 seconds to remember an event. If they could not remember any event or any more details, they were instructed to press the second and third button after each other in order to get a new cue-word. We employed this double-button pressing to match button presses across tasks. The CTRL condition was a task with low-level cognitive and attentional demands, where a row of random letters was shown for a fixed interval between 5.9 and 8.9 seconds and the participants had to decide via button-press if the first letter was a vowel or not. We employed CTRL as an active baseline, with matched visual input and button presses compared to the other two tasks, to employ a baseline without elevated activity in the DMN. While studies looking for DMN activations usually employ a matched control task as we did (Addis et al., 2007; Burianova et al., 2010; Burianova & Grady, 2007), studies looking at DMN deactivations, i.e., negative BOLD responses, usually compare a goal-directed task to the resting state (Lin et al., 2011; Pfefferbaum et al., 2011; Raichle et al., 2001).

This is why we also acquired REST data in 30 subjects, where a white fixation cross was presented on a black screen.

Image acquisition and experimental procedure

Multi-parametric, quantitative BOLD MRI included the following sequences:

A) Multi-echo spin-echo T2 mapping, only in CTRL; 3D gradient spin echo (GRASE) readout as described previously (Kaczmarz et al. 2020). 8 echoes with even-spaced echo times (TE): TE1 = Δ TE = 16ms; TR=251; $\alpha=90^\circ$; voxel size 2x2x3.3mm³; 35 slices (30 slices in 4 subjects); total acquisition time = 2:28min (for 35 slices)

B) Multi-echo gradient-echo T2* mapping, in all conditions; as described previously (Hirsch et al., 2014; Kaczmarz, Hyder, et al., 2020). 12 echoes, TE1 = Δ TE = 5ms; TR=2229ms; $\alpha=30^\circ$; voxel size 2x2x3mm³; gap 0.3mm; 35 slices (30 slices in 4 subjects). Correction for magnetic background gradients with a standard sinc-Gauss excitation pulse (Baudrexel et al., 2009; Hirsch & Preibisch, 2013); acquisition of half- and quarter-resolution data in k-space center for motion correction (Nöth et al., 2014); total acquisition time = 6:08min (for 35 slices).

C) Dynamic susceptibility imaging (DSC), in 30 subjects only during CTRL, in 10 subjects additionally during CALC; as described previously (Hedderich et al., 2019). Single-shot GRE-EPI; EPI factor 49; 80 dynamics; TR = 2.0s; $\alpha=60^\circ$; acquisition voxel size 2x2x3.5mm³; 35 slices (30 slices in 4 subjects). Injection of gadolinium-based contrast agent as a bolus after 5 dynamics, 0.1ml/kg, minimum 6ml, maximum 8ml per injection (i.e. 16ml for two injections in a row corresponding to a full clinical dosage), flow rate: 4ml/s, plus flushing with 25ml NaCl; total acquisition time = 2:49min (for 35 slices).

E) Pseudo-continuous arterial spin labeling (pCASL), in all conditions; following Alsop et al. (2015) and as implemented in Göttler et al. (2019) and Kaczmarz, Hyder et al. (2020). Post-labeling delay 1800ms, label duration 1800ms; 4 background suppression pulses; 2D EPI readout; TE=11ms; TR=4500ms; $\alpha=90^\circ$; 20 slices (16 slices in one subject); EPI factor 29; acquisition voxel size 3.28x3.5x6.0mm³; gap 0.6mm; 30 dynamics including a proton density weighted M0 scan; total acquisition time = 6:00min.

The BOLD fMRI task-localizer was acquired using single-shot EPI, EPI factor 43; voxel size = 3.0x3.0x3.0mm³; FOV 192x192x127.8mm³; TE=30ms; TR=1.2s; $\alpha=70^\circ$; 400 dynamic scans plus two dummy scans; 40 slices; parallel acquisition; total acquisition time: 8:05min. For susceptibility correction, an additional with B0 field map was acquired with two echoes; TR/TE1/TE2=525ms/6.0ms/9.8ms; 40 slices; parallel acquisition; $\alpha=60^\circ$; voxel size = 3.0x3.0x3.0mm³; FOV 192x192x127.8mm³; total acquisition time: 0:35s.

Additionally, a T1-weighted 3D MPRAGE pre-and post-gadolinium (TI/TR/TE/ α = 100ms/9ms/4ms/8[°]; 170 slices; FOV=240x252x170 mm³; voxel size 1.0x1.0x1.0mm³; acquisition time=2:05min) and T2-weighted 3D FLAIR (fluid-attenuated inversion recovery) image were acquired for anatomical reference and to exclude brain lesions (TR/TE/ α = 4800/293/40[°]; 140 slices; FOV=240x248.9x168 mm³; acquisition voxel size 1.2x1.2x1.2mm³; turbo spin-echo factor 170; inversion delay 1650ms; acquisition time=2:09min).

After giving informed written consent, a venous catheter was placed by a medical doctor and blood samples were taken and sent to our in-house clinical chemistry laboratory where hemoglobin, hematocrit (Hct) and creatinine values were analyzed. Before delivery of the contrast agent through the venous catheter at the end of the scanning session, creatinine values were requested and contrast agent was only applied if creatinine values were in a normal range to ensure healthy kidney function. Arterial oxygen saturation was measured via a pulse oximeter (Nonin 7500FO, Nonin Medical B.V., The Netherlands).

The 30 participants who performed all four conditions had two consecutive scanning sessions on the same day: In the first block, which took around one hour, participants completed all task condition runs i.e., all mqBOLD sequences except the DSC scan, in addition to an 8min BOLD fMRI

localizer, designed as a 30s-block-design with four repetitions per condition. For 17 subjects, the localizer fMRI scan was included in the second block instead of the first block. During a 15-25min break, participants completed a memory questionnaire, where they had to indicate how easy it was for them to remember concrete events of the MEM task (difficulty scale; 1='very easy', 2='rather easy', 3='rather difficult', 4='very difficult') and how detailed their memories were overall (concreteness scale; 1='very detailed', 2='rather detailed', 3='rather vague', 4='very vague'). On average, people scored 1.8 +/- 0.7 on the difficulty scale and 2.0 +/- 0.6 on the concreteness scale. This means that on average, it was rather easy for the subjects to remember a concrete event and the memory was rather detailed. This also matches with the reaction time: on average, it took participants only 2.5 ± 1s to remember an event. In the second session, which lasted 30min on average, a REST fMRI scan (not used in this study) along with a B0 scan and other structural scans (volumetric T2, MPRAGE, FLAIR, post-gadolinium MPRAGE, all used for basic clinical screening) were acquired. At the very end of the protocol and in the presence of a medical doctor, the contrast agent application for DSC MRI was performed via a venous catheter by means of a dedicated pump (Accutron MR, Medtron AG, Saarbrücken, Germany).

Within the independent control study cohort, we acquired only fMRI BOLD data as well as a MPRAGE scan during CALC, MEM and CTRL condition. Task blocks were 3min long with 1min interleaved CTRL blocks, all tasks were repeated four times. This resulted in a 33min continuous fMRI block, and participants were lying in the scanner for around 40min.

Quantitative parameter calculation using mqBOLD

The calculation of the quantitative parameter maps was performed with in-house scripts in Matlab and SPM12 (Wellcome Trust Centre for Neuroimaging, UCL, London, UK). Fig.1 displays all steps and subject-averaged parameter maps, median across gray-matter, with artifacts area masked, for each subject and condition in native space. Quantitative T2 and T2* maps were obtained by mono-exponential fits of the multi-echo spin and gradient echo data as described previously (Hirsch et al., 2014; Kaczmarz, Hyder, et al., 2020; Preibisch et al., 2008). Correction was performed for macroscopic magnetic background fields (Hirsch & Preibisch, 2013) and motion correction was performed using redundant acquisitions of k-space center (Nöth et al., 2014). R2' maps were calculated via

$$R2' = \frac{1}{T2^*} - \frac{1}{T2} \quad [1]$$

yielding the transverse, reversible relaxation rate that is dependent on the vascular dHb content (Blockley et al., 2013b, 2015; Bright et al., 2019). However, confounds from uncorrectable strong magnetic field inhomogeneities at air-tissue boundaries, iron deposition in deep GM structures as well as white matter structure need to be considered (Hirsch & Preibisch, 2013; Kaczmarz, Hyder, et al., 2020). The cerebral blood volume (CBV) was derived from DSC MRI via full integration of leakage-corrected $\Delta R2^*$ -curves (Boxermann, J.L., Schmainda, K.M., Weisskoff, R.M., 2006) and normalization to a white matter value of 2.5% (Leenders et al., 1990) as described previously (Hedderich et al., 2019; Kluge et al., 2016). From R2' and CBV parameter maps, the oxygen extraction fraction (OEF) was then calculated via the mqBOLD-approach (Christen et al., 2012; Hirsch et al., 2014; Yablonskiy & Haacke, 1994) as

$$OEF = \frac{R2'}{c \cdot CBV} \quad [2]$$

with $c = \gamma \cdot \frac{4}{3} \cdot \pi \cdot \Delta\chi_0 \cdot hct \cdot B_0$, the gyromagnetic ratio $\gamma = 2.675 \cdot 10^8 \text{ s}^{-1} \text{ T}^{-1}$, the susceptibility difference between fully deoxygenated and oxygenated hemoglobin of $\Delta\chi_0 = 0.264 \cdot 10^{-6}$, the magnetic field strength $B_0 = 3\text{T}$ and the small-vessel hematocrit hct , which was assumed to be 85% of our empirically measured (large-vessel) hematocrit values of each subject (Eichling et al., 1975; Hirsch et al., 2014). CBF maps were calculated from pCASL data as in (Alsop et al., 2015) to calculate

CBF from averaged, pairwise differences of motion-corrected label and control images and a proton-density weighted image.

Finally, for each subject and condition, we calculated CMRO2 in a voxel-wise manner by combining all parameter maps via Fick's principle:

$$\text{CMRO2} = \text{OEF} \cdot \text{CBF} \cdot \text{C}_a\text{O}_2 \quad [3]$$

where C_aO_2 is the oxygen carrying capacity of hemoglobin and was calculated as $\text{C}_a\text{O}_2 = 0.334 \cdot \text{Hct} \cdot 55.6 \cdot \text{O}_2\text{sat}$, with O_2sat being the oxygen saturation measured by the pulse oximeter (Bright et al., 2019; Ma et al., 2020). CBF was upscaled by 25% to account for systematic CBF underestimation due to four background-suppression pulses (Garcia et al., 2005; Mutsaerts et al., 2014). All parameter maps of each individual subject were registered to the first echo of their multi echo T2 data.

Estimation of a realistic CALC CBV surrogate

To be able to estimate CBV changes during CALC, we measured DSC data in our two main conditions, CALC and CTRL, in a subset of 10 subjects. These subjects received a full clinical dosage of contrast agent altogether. More than a full clinical dosage of contrast agent cannot be given in one session, so we could not acquire additional DSC data for the MEM and REST conditions. In this subset, due to technical reasons, we did not acquire oxygen saturation values empirically and assumed a value of 98%, which was the average across the remaining sample. From these measurements we determined the percent CBV changes (%CBV) of the CALC versus the CTRL condition across gray-matter for the individual subject brains, within 360 Glasser regions of interest (ROIs) (Glasser, 2016) to get more reliable estimates, and determined the median change per ROI across the 10 subjects. This ROI-wise map of average %CBV was then applied to the subject-specific CTRL CBV maps of the remaining 30 subjects, to calculate realistic CALC CBV surrogate maps. These were used in all analyses to calculate OEF and CMRO2 values during CALC. This approach could not be applied for the MEM condition, where we used CTRL CBV instead of a realistic MEM CBV surrogate.

Semi-quantitative CMRO2 estimation

The estimation of CMRO2 maps relies on a combination of $R2'$, CBV and CBF values. Due to unfavorable error propagation especially from $R2'$ measurements (see appendix in (Kaczmarz, Göttler, et al., 2020)), we also calculated semi-quantitative CMRO2 and OEF values from BOLD fMRI data using an approach presented by Fujita et al. (2006). This approach did not affect baseline CTRL and REST mapping of $R2'$, OEF and CMRO2, but only the MEM and CALC conditions. Instead of calculating $\Delta R2'$ using quantitative $R2'$ as measured by multi-echo T2* in the task conditions, we re-calculated $\Delta R2'$ as

$$\Delta R2' = -\frac{\Delta S}{S_0} \frac{1}{\text{TE} \cdot R2'_0} \quad [4]$$

with $\text{TE} = 30\text{ms}$, $R2'_0$ being the baseline $R2'$ and $\frac{\Delta S}{S_0}$ the BOLD signal change, derived from the fMRI BOLD localizer. $R2'$ in CALC and MEM was then re-calculated via $R2' = R2'_0 + (\Delta R2' \cdot R2'_0)$ and OEF and CMRO2 were re-calculated via [2] and [3]. This approach was repeated using the REST baseline instead of the CTRL baseline, so that depending on the contrasts we looked at we either used semi-quantitative CMRO2 maps derived from REST or CTRL baseline mapping. For CALC semi-quantitative CMRO2 calculation, realistic CALC CBV surrogate maps were used, see paragraph before, for MEM we used CTRL CBV maps. Thus, semi-quantitative compared to fully quantitative CMRO2 values in CALC conditions only differed in their usage of $\Delta R2'$ values that were inferred from BOLD fMRI signal changes.

Davis model

The Davis model was inspired by numerical BOLD signal simulations and describes how changes in the BOLD signal depend on changes in CBF, CMRO2, relying on M , α and β (Davis et al., 1998):

$$\frac{\Delta S}{S_0} = M \left[1 - \left(\frac{CBF}{CBF_0} \right)^{\alpha-\beta} \left(\frac{CMRO2}{CMRO2_0} \right)^\beta \right] \quad [5]$$

where α is a power-law exponent, relating changes in CBV to changes in CBF and β is dependent on the microvascular anatomy (Bright et al., 2019). Classically, $\alpha = 0.38$ was used, (Grubb et al., 1974) but currently used values are much lower. For the visualization in Fig. 4A we used $\alpha = -0.05$ and $\beta = 0.98$, suggested for measurements on a 3T scanner with a TE = 30ms. These are optimized parameters derived from rodents and simulations, rather reflecting fitting parameters than real biophysiological meaning (Gagnon et al., 2016). M is commonly referred to as a quantification of the maximum BOLD signal change that would occur if all dHb was washed out of the vessels, it is dependent on the baseline physiology and OEF in baseline (Blockley et al., 2013b). The Davis model was conceived for calibration of fMRI experiments. To this end, M is estimated via combined measurement of CBF and BOLD responses to a vasoactive stimulus, mostly hypercapnia. By assuming α and β , fractional change in CMRO2 can be calculated from combined BOLD signal and CBF measurements (Blockley et al., 2013b; Chen et al., 2022; Germuska & Wise, 2019).

fMRI processing and task analysis

The BOLD fMRI localizer data was pre-processed using fMRIPrep 20.2.4 (Esteban, 2019) as a docker container, which is based on Nipype 1.6.1 (Gorgolewski et al., 2011). This included segmentation, estimation of motion-parameters and other confounds, susceptibility distortion correction, co-registration in native T1w space and normalization to MNI152 ICBM 2mm Non-linear 6th Generation Asymmetric Average Brain Stereotaxic Registration Model (Montreal Neurological Institute, McGill University). fMRIPrep is using FSL 5.0.9 (Jenkinson et al., 2012; Smith et al., 2004) boundary-based registration, BBR, to register BOLD fMRI EPI time series to T1w data, FSL FAST for brain tissue segmentation and spatial normalization to standard space using ANTs 2.3.3, (Avants et al., 2008) registration in a multiscale, mutual-information based, nonlinear registration scheme, concatenating all transforms and applying all registration steps at once. This final normalization matrix was then applied to all quantitative mqBOLD parameter maps, after 6-dof (degrees of freedom) co-registration to native T1w space, to transform all images to MNI 2mm standard space. Further, task-analysis was done following recommendations in (Esteban et al., 2020), setting up a general linear model (GLM) with CSF and white-matter signal, dvars, framewise-displacement and translations and rotations in x-, y- and z-axis as confounds, high-pass filter of 100s and 6mm smoothing. For analyses based on GLM masks, we used individual 1st level z-maps, $z > 2.5$ and on a group level the FWE-corrected z-maps, output from the 2nd level analysis based on the following contrasts: CALC-positive = CALC > CTRL or REST, CALC-negative = CALC < CTRL or REST, MEM-positive = MEM > CTRL, MEM-negative = MEM < CTRL.

Artifact and gray matter masking

To exclude voxels from artifact affected brain areas, we calculated the temporal signal-to-noise ratio (tSNR) from the fMRI BOLD images per subject and voxel in standard 2mm space. We then masked out voxels that were in the lowest 15th percentile in over 66% of participants. These were mainly located in common susceptibility areas, i.e., fronto- and temporo-basal brain areas. Additionally, we masked out the cerebellum and only considered voxels with a gray-matter (GM) probability bigger than 0.5. The final SNR-GM-mask in standard space was applied to the output of the GLM group analysis and to the input matrices for the partial least squares analyses. For the analyses in native space (Fig. 2C, Fig. S1C, Fig. S3C, last column on the right in all graphs), we additionally used native-space parameter maps to mask cerebrospinal-fluid influenced areas ($T2 > 90$ ms), susceptibility-influenced areas ($R2' > 9 \text{ s}^{-1}$), voxels with a high percentage of blood volume ($CBV > 1 \%$, probably driven by larger veins/arteries) and voxels with $T2' > 90$ ms, $OEF > 0.9$, $CBF > 90$ ml/100g/min.

Partial least squares analysis

Partial least squares analysis (PLS) analyses were run using the Python pyls library (Python Software Foundation, version 3.8). Mean-centered PLS is a data-reduction method that computes latent variables and corresponding brain patterns, which optimally relate brain signals to the experimental design, contrasting e.g., groups or conditions (McIntosh & Lobaugh, 2004). In our case, the input data matrix contained one row for each subject including all voxels within the SNR-GM-mask in standard 2mm space, and stacked conditions, e.g. CALC and CTRL. In the case of BOLD fMRI data, median values of percent signal change (deviation from either median across CTRL or REST) across 24s (20TRs) per task condition were used, excluding the first 6s per task block to account for the hemodynamic response lag. In the case of mqBOLD data, quantitative OEF, CBF or CMRO2 values per voxel and subject were used, for all conditions that were compared. With the help of a dummy-coding matrix, the pyls library computes within-condition averages which are column-wise mean-centered (Krishnan et al., 2011). This matrix, $R_{\text{mean-centered}} (q \times p)$, which comprises q conditions and p voxels, is then subjected to singular value decomposition, which results in:

$$R'_{\text{mean-centered}} = USV' \quad [6]$$

where $U_{p \times q}$ are the voxel weights (brain saliences), one row per latent variable (LV) i , that reflect how much this voxel contributes to the effect captured by LV_i . $V_{q \times q}$ are the task saliences (one row per LV) that indicate how each condition contributes to the spatial pattern identified by LV_i . $S_{q \times q}$ are the singular values per LV that reflect the strength of the relationship extracted by each LV_i (McIntosh & Mišić, 2013). The significance of the latent variables, i.e., the entire multivariate pattern, was tested via permutation tests (3000 permutations), the reliability of the brain saliences, i.e., the voxel's contribution to the latent variables, was deduced via bootstrap resampling (3000 samples). Brain regions showing significant effects are identified via the ratio of the brain saliences to the bootstrap standard error (BSR), where a $BSR > \pm 2$ is akin to a confidence interval of 95%, if the bootstrap distribution is normal (Krishnan et al., 2011; McIntosh & Mišić, 2013). In this paper, we used PLS analyses to perform group level statistics in order to identify brain regions that differentiate best between a task (CALC or MEM) and a baseline (CTRL or REST) condition. As the same analyses were applied to both BOLD fMRI and mqBOLD data, resulting statistical result maps could be compared across the different parameters. The statistical maps were thresholded with a BSR of ± 2 and only clusters with more than 30 voxels were kept for creating masks for ROI evaluations. Please note that for correct interpretation, BSR maps must be compared to the design scores (design variables multiplied by brain saliences) of each condition within each LV to know the direction of task differences that is captured within the BSR pattern. In this manuscript, a blue-red BSR pattern indicates a positive task effect, that is voxels with higher values during the task compared to the baseline, whereas blue voxels show the opposite contrast.

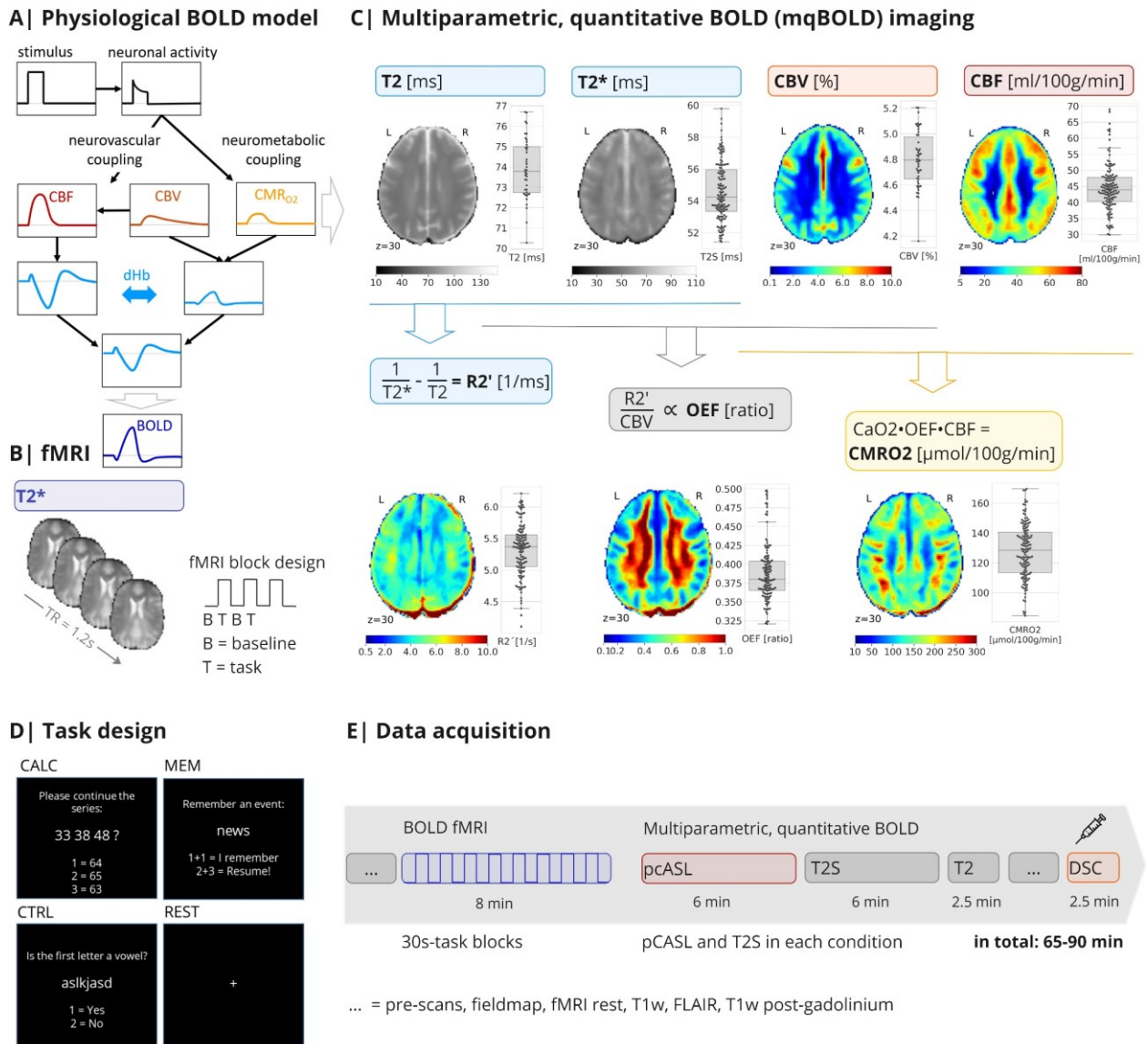


Figure 1. Hemodynamic model, task design and data acquisition. **A**) Physiological model of the BOLD signal. Increased neuronal activity causes elevated energy metabolism (CMRO₂) and blood volume (CBV) resulting in higher dHb in venous blood. At the same time cerebral blood flow (CBF) increases oxygen delivery, lowering dHb. **B**) Positive BOLD responses arise when CBF increases overcompensate oxygen consumption. **C**) Multi-parametric BOLD fMRI allows CMRO₂ measurement during different conditions via quantification of transverse relaxation times T₂ and T₂* as well as CBV and CBF. Subject-average parameter maps are displayed together with boxplots of average gray matter values per subject and condition (line, median; box limits, upper and lower quartiles). The reversible transverse relaxation rate (R₂') reflects the overall dHb content in a voxel. The oxygen extraction fraction (OEF) is proportional to the ratio of R₂' to CBV (from dynamic susceptibility contrast (DSC) MRI). Voxel-wise CMRO₂ is then obtained as the product of OEF, CBF (from pseudo-continuous arterial spin labeling, pCASL MRI), and the arterial oxygen content of blood (CaO₂). **D**) BOLD and mqBOLD data was acquired during four different conditions in the same imaging session: a calculation task (CALC) and an autobiographical memory task (MEM) as well as two baseline conditions, control (CTRL) and resting state (REST). **E**) During each imaging session, we acquired fMRI data with a 30s block design, as well as pCASL and T₂* during each condition (6min per condition), and T₂ and DSC MRI in CTRL (in 10 subjects, DSC was also acquired during CALC).

RESULTS

Modulation of directional BOLD signal intensity presumably also leads to concomitant changes in oxygen consumption. In order to quantify CMRO2 in brain areas exhibiting positive and negative BOLD responses, we performed multiparametric, quantitative BOLD (mqBOLD) and classical BOLD fMRI. According to the common interpretation of BOLD fMRI, we tested the following hypothesis: If regions with significant task-induced *positive* BOLD responses show *increased* oxygen metabolism as a result of increased neuronal activity, is the opposite also true for *negative* BOLD responses? Fig. 1A shows the canonical, physiological model of the positive BOLD signal that is expected in response to increased neuronal activity. We aimed to test whether negative BOLD signals also elicit concomitant, larger decreases in CBF and consistent, but smaller decreases in CMRO2. Subjects were scanned during four different conditions within the same imaging session (Fig 1.D). Our aim here was to 1) investigate DMN regions, which showed both *deactivations* during an externally oriented calculation task (CALC) as well as *activations* during an autobiographical memory task (MEM) in the fMRI BOLD signal 2) investigate frontoparietal control and dorsal attention regions in comparison, which showed CALC induced *increases* in the BOLD signal and to 3) investigate if our results differed when using an active control task (CTRL) versus a classical resting state (REST) baseline. Please note that in the following sections we use ‘CALC-positive_{CTRL}’ or ‘MEM-positive_{CTRL}’ and ‘CALC-negative_{CTRL}’ or ‘CALC-negative_{CTRL}’ to indicate regions which show a significant positive or negative BOLD signal change during CALC or MEM conditions, with the subscript indicating whether against CTRL or REST baselines. While our focus was on comparing the task-induced activation and deactivation patterns of the CALC versus the active CTRL task, a subgroup of 30 (out of 40) participants was also scanned during MEM and REST conditions.

All measured quantitative parameters covered biologically plausible ranges in gray-matter in the CTRL condition, and were very similar to literature values (Raichle et al., 2001; J. Zhang et al., 2015), see Table 1.

Table 1

Baseline CTRL values, mean \pm SD across subjects, within gray matter.

R2'	CBV	OEF	CBF	CMRO2
[1/s]	[%]	[ratio]	[ml/100g/min]	[μ mol/100g/min]
5.3 \pm 0.4	4.8 \pm 0.2	0.39 \pm 0.04	44.5 \pm 7.2	127.8 \pm 18.4

Concomitant CMRO2 changes in positive, but not in negative BOLD ROIs

In a first step, we performed group analyses on the BOLD fMRI data as well as on the mqBOLD data of all subjects in standard Talairach space to identify spatial maps of positive and negative task responses. Fig. 2A displays the CALC versus CTRL contrast, for the other task contrasts see Supplements. As we aimed to compare statistical analyses on the fMRI BOLD data to the mqBOLD data, we ran separate multivariate partial-least-squares (PLS) analyses for all contrasts and parameter maps, as the mqBOLD data are not time-resolved. As a comparison, we also ran a classical general linear model (GLM) on the fMRI BOLD data, which produced nearly identical statistical patterns, see Fig. S2 in the Supplements. All statistical maps in Fig. 2A represent bootstrap ratios, akin to z-values, within the first latent variable per PLS analysis, which was significant ($p < .001$) in all analyses. The fMRI BOLD voxel patterns revealed a pattern of positive BOLD signal changes (CALC-positive_{CTRL}, red) spanning fronto-parietal, dorsal attention and visual regions, and a pattern of negative BOLD signal changes including the DMN, but also auditory and somatosensory regions (CALC-negative_{CTRL}, blue), both consistent with the results of prior studies (Anticevic et al., 2012; Buckner et al., 2008; Fox et al., 2005). Separate PLS analyses applied to mqBOLD parameter maps,

contrasting absolute levels of CBF, OEF and CMRO2 during CALC versus CTRL, produced overall similar patterns of *positive* CBF, OEF, and CMRO2 changes (Fig. 2A, lower rows). Note that for canonical neurovascular coupling (increased CMRO2 and luxury perfusion), OEF decreases with higher neuronal activity, thus the color coding for OEF is inverted. The overlap of CALC-positive_{CTRL} and CALC-negative_{CTRL} maps with positive and negative CBF and CMRO2 maps revealed that there was an extended *positive* network showing both BOLD signal activations as well as CBF and CMRO2 increases, while there is nearly no overlap of the BOLD *deactivation* map with CBF or CMRO2 (Fig. 2B).

In order to better disentangle pure vascular from metabolic influences on BOLD signal changes, we displayed absolute mqBOLD parameter delta values, i.e. absolute CALC minus CTRL values per voxel, median across subjects, within the BOLD ROIs, i.e. thresholded and binarized BOLD group results, in Fig. 2C. The histograms show voxels within CALC-positive_{CTRL} (orange) and CALC-negative_{CTRL} (blue) BOLD ROIs with a median BOLD signal change of +0.33% and -0.21%, respectively. This means that the negative BOLD response is about 1/3 weaker than the positive BOLD response. This ratio should also be reflected in the other parameters - that is CBF, OEF and CMRO2 - if we expect neurovascular and neurometabolic coupling to be preserved for positive and negative BOLD responses. Yet, while we found consistent *increases* in CBF and CMRO2, and concomitant decreases in OEF, task-induced *decreases* were much weaker than expected. For an overview over all task-induced changes see Table 2. While we got significant CBF decreases, they were six times smaller weaker than expected, if we were to expect the negative CBF amplitudes to be 1/3 smaller than the positive CBF amplitudes, as the BOLD response suggests. While we got significant CMRO2 *increases*, CMRO2 decreases within CALC-negative_{CTRL} ROI were not significant.

To be more precise in terms of BOLD localization, we analyzed BOLD-fMRI and mqBOLD-parameters in native brain space, within the thresholded first-level GLM mask for each subject (Fig. 2C, right column). The average results for all parameter values are similar to the group level analysis above. Because individual first-level results are more specific than the group mask, we found generally higher median percent change amplitudes across subjects. Within individual CALC-positive_{CTRL} regions, CBF, CMRO2 increased and OEF decreased significantly, but we found no significant changes in CBF, OEF or CMRO2 within individual CALC-negative_{CTRL} regions across subjects. Thus, across subjects, there was no evidence for reduced CMRO2 nor CBF in regions with significant negative BOLD responses.

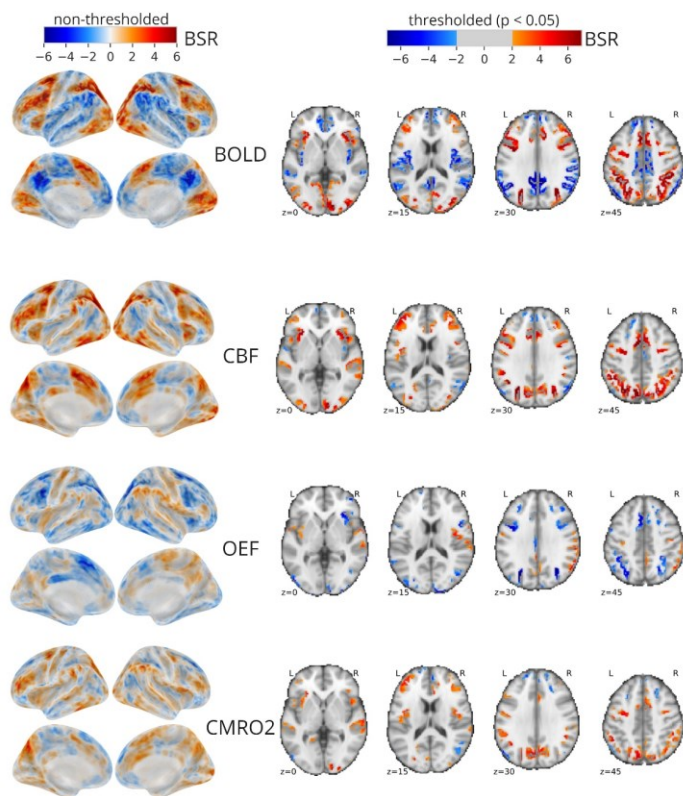
We replicated the same analyses with REST instead of CTRL as the baseline condition (see FigS1, Supplemental Material, and Table 2), obtaining very similar results. The group statistical maps show a high overlap of BOLD CALC-positive_{REST} regions with regions of CBF and CMRO2 *increases*, but little overlap of BOLD CALC-negative_{REST} with regions of CBF and CMRO2 *decreases*. We identified a similar range of positive BOLD signal changes with 0.42% in the CALC-positive_{REST} ROI and -0.19% in the CALC-negative_{REST} ROI on a group level in standard space. Thus, compared to REST, the negative BOLD amplitude is about half of the positive BOLD amplitude. Within the *positive* ROI, we found concomitant increases in CMRO2 and CBF and decreases in OEF. Within the *negative* ROI, we found concomitant decreases in CBF and CMRO2, changes in OEF were not significant. Yet, expecting the same positive-negative ratio as for the BOLD data, decreases in CBF and CMRO2 were nearly two times weaker than expected. In native space, CBF, CMRO2 and OEF showed concomitant changes in the positive ROIs across subjects, but changes were not significant across subjects for the negative native space ROIs.

As a control analysis, we additionally used BOLD GLM family-wise error (FWE) corrected group masks (CALC vs CTRL and CALC vs REST) instead of PLS group masks. FWE correction is considered overly conservative for fMRI group level analysis, it reduces the risk of false-positive BOLD voxels to a very minimum. This only changed our main results minimally and did not influence our interpretations, see Fig. S2 for GLM results versus Fig. 1 and Fig. S1 for PLS results.

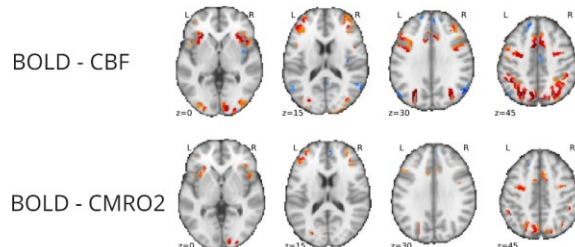
Finally, we analyzed regions that showed BOLD signal changes during MEM compared to CTRL. This contrast was successful in ‘activating’ regions of the DMN, as shown in the group results in Fig. S3A, and participants also showed wide-spread, significant increases in both CBF and CMRO2 group statistical maps. Within the MEM-positive ROI (see Table 2), as well as within individual first-level GLM masks, both CBF and CMRO2 increased significantly. CMRO2 increases during MEM were on average comparable to CMRO2 increases during CALC, however, we have to consider that we had no means of correcting for CBV increases during MEM because we had no subsample with contrast-agent injection during MEM, see Methods. Within MEM-negative ROIs, voxels showed significant decreases in CBF and CMRO2, although also here, decreases were three times (CBF) to four times (CMRO2) weaker than expected when considering the positive-negative BOLD ratio. Decreases in native space across subjects were not significant.

We summarize the discrepancy between BOLD-CBF and BOLD-CMRO2 coupling in negative versus positive BOLD regions in Fig. 2D (CALC vs CTRL), Fig. S1D (CALC vs. REST) and Fig. 3D (MEM vs. CTRL), for GLM masks see Fig S2B and D. If we assume that BOLD signal amplitude and sign reflect direction and strength of neuronal activity, we expect BOLD signal changes to be coupled to the same CBF and CMRO2 changes independent of brain regions, i.e. the ratio of CBF-BOLD and CMRO2-BOLD changes should be the same within positive and negative BOLD regions. The bar plots illustrate how CBF and CMRO2 percent-change amplitudes were related to BOLD percent-change amplitudes across subjects for positive versus negative regions BOLD regions, within standard space group masks and native space first-level masks. For this measure, we divided median CBF or CMRO2 percent-change values by BOLD percent-change values per subject, within the respective ROI. The coupling ratio thus shows to which changes in %CBF and %CMRO2 a 1% change in BOLD is empirically coupled to. Our null hypothesis was that this ratio should not differ between negative and positive BOLD regions. Our data rejected this assumption. They showed a consistent positive *BOLD-CBF* coupling between 9.0 (within native space CALC-REST masks) and 26.9 (within MEM-CTRL group ROI), as well as a consistent *BOLD-CMRO2* coupling between 5.7 (native-space CALC-REST masks) and 22.4 (MEM-CTRL group ROI). Yet, there was a lack of consistent coupling within CALC-negative regions, no matter if within group ROIs or native space masks. We only found consistent BOLD-CBF coupling within MEM-negative ROIs, between 4.0 (across subjects, native space) and 8.6 (across voxels, group ROI), although smaller than the BOLD-CBF coupling in positive BOLD ROIs.

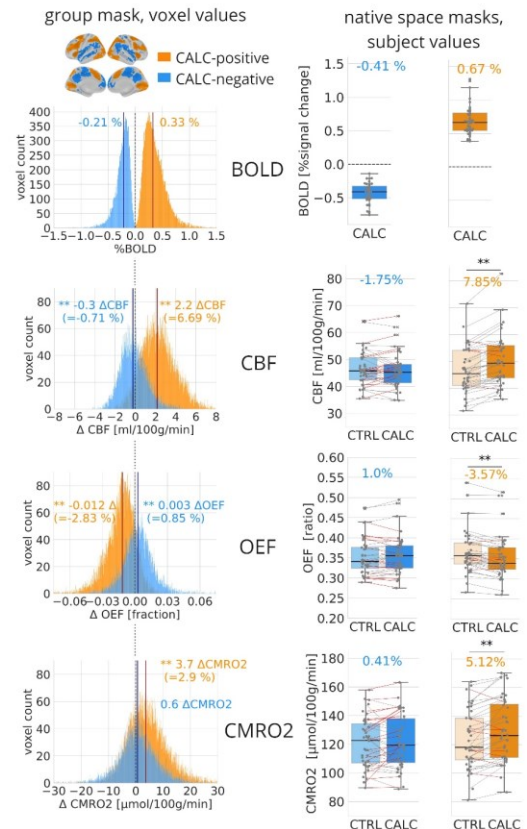
A| Group results: CALC vs CTRL



B| Overlap of BOLD fMRI- and mqBOLD-results



C| CALC-positive and negative BOLD voxels



D| BOLD-CBF and BOLD-CMRO2 coupling

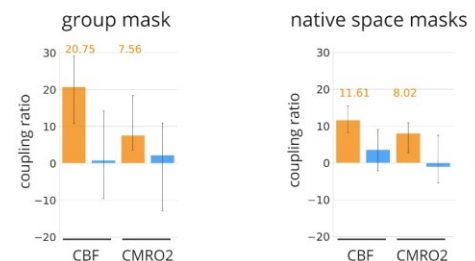


Figure 2. Negative BOLD responses do not imply reduced oxygen metabolism. **A|** Results of the PLS analyses of CALC versus CTRL for relative BOLD fMRI and quantitative mqBOLD parameters. Surface maps show non-thresholded statistical maps, output from the partial least squares analyses (PLS, values are bootstrap ratios=BSR, akin to z-values) within the first latent variable, significant in each analysis (permutation test, $p < .001$), see Methods. Red voxels indicate higher parameter values during CALC versus CTRL and blue voxels show the opposing contrast. Additionally, axial slices show reliable brain clusters, thresholded by a BSR ± 2 (akin to $p < .05$, cluster size >30 voxels) for BOLD-fMRI, CBF, OEF, and CMRO2. **B|** Maps show consistent overlap between CALC-positive BOLD regions and CBF and CMRO2 (red-orange) maps, but only very little overlap between CALC-negative BOLD regions and CBF or CMRO2 (blue) maps. **C| Left column:** Histograms show distribution of voxel delta values (CALC minus CTRL) within the binarized CALC-negative and CALC-positive BOLD group ROI (surface plot), median across subjects per voxel. Concomitant changes in CBF, OEF and CMRO2 were observed in both positive and negative ROIs, except for CMRO2 within the CALC-negative ROI. **** = $p < .001$.** **Right column:** Replication of results in native space. Each dot indicates a single subject's parameter value, median across voxels within CALC-negative and CALC-positive BOLD regions, 1st level GLM results (paired samples t-tests, **** = $p < .001$.** Red lines indicate subjects where the condition-related change in the parameter of interest deviates from the expected response indicated by the BOLD change. A median BOLD signal increase of 0.67% was accompanied by a significant increase in CBF, CMRO2 and decrease in OEF, while a BOLD decrease of -0.41% was not accompanied by any significant changes in mqBOLD parameters. **D|** Bar plots illustrate how CBF and CMRO2 percent-change amplitudes were related to BOLD percent-change amplitudes across subjects for CALC-positive versus CALC-negative regions within group ROIs and native space

1st level ROIs. On average, a 1% increase in the BOLD signal was coupled to a 20.8% increase in CBF and a 7.6% increase in CMRO2, within the CALC-positive ROI, and a 11.6% increase in CBF and a 8% increase in CMRO2 in native space positive ROIs, across subjects. Overall, positive BOLD responses were consistently coupled to increases in CBF and CMRO2 whereas negative BOLD responses were not consistently coupled to neither CBF nor CMRO2 (median parameters values within BOLD masks, coupling ratios on the subject level, error bar = 95% CI, 2000 bootstraps).

Table 2

Median values across voxels (IQR) within BOLD ROIs, original data, corrected for CBV.

base-line	BOLD ROI	BOLD %	CBF [ml/100g/min]		CMRO2 [μ mol/100g/min]		OEF [ratio]	
			base-line	Δ CBF % Δ CBF	base-line	Δ CMRO2 %CMRO2	base-line	Δ OEF %OEF
CTRL	CALC-pos	0.33% (0.25)	35.1 (7.8)	2.2** (2.3) 6.7% (6.5)	137.9 (48.0)	3.7** (9.3) 2.9% (6.9)	0.40 (0.15)	-0.011** (0.02) -2.8% (4.3)
	CALC-neg	-0.21% (0.16)	33.3 (8.7)	-0.3** (1.7) -0.7% (5.4)	126.6 (52.7)	n.s.	0.39 (0.16)	0.003 (0.02) 0.9% (4.4)
REST	CALC-pos	0.42% (0.51)	34.6 (8.1)	2.5** (3.0) 8.0% (9.9)	138.5 (51.2)	5.4** (12.5) 2.6% (7.2)	0.41 (0.17)	-0.012** (0.02) -2.5% (4.7)
	CALC-neg	-0.19% (0.25)	34.4 (9.4)	-0.7** (2.2) -2.0% (6.5)	124.2 (53.1)	-1.5** (10.8) -0.6% (8.0)	0.39 (0.16)	n.s.
CTRL	MEM-pos	0.22% (0.23)	36.5 (8.7)	2.3** (2.0) 6.8% (5.3)	136.1 (45.5)	5.9** (8.6) 5.3% (6.5)	0.39 (0.13)	-0.006** (0.01) -1.3% (3.8)
	MEM-neg	-0.15% (0.15)	34.6 (6.5)	-0.5** (1.1) -1.6% (3.6)	128.3 (48.6)	-0.8** (6.1) -0.3% (5.3)	0.38 (0.15)	0.004** (0.01) 1.3% (3.3)

Note. This table reports median values across voxels within each BOLD ROI, based on subject-averaged voxel values. Absolute CBF, CMRO2 and OEF are displayed both in the baseline and as delta values (task minus baseline), along with percent change values for each contrast. As voxel values were not normally distributed, median values along with interquartile ranges (IQR) are reported. ** $p < .001$, based on two-sample related permutation tests, 2000 permutations.

Usage of semi-quantitative CMRO2 in CALC and MEM conditions

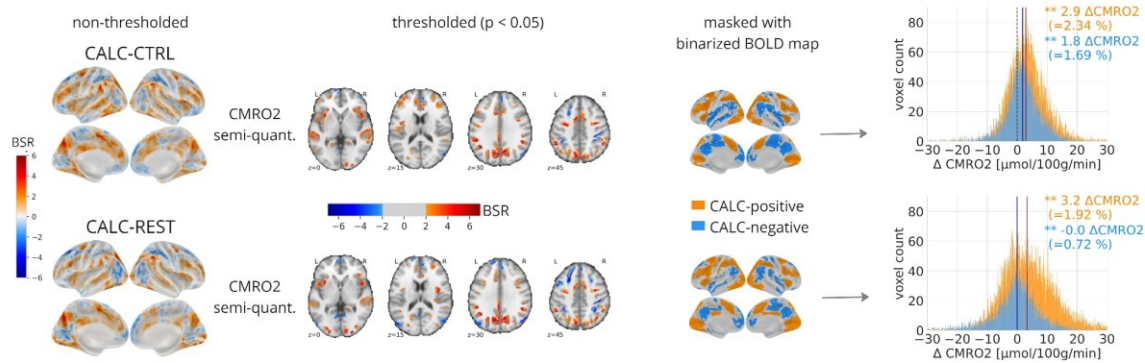
We acquired relative (BOLD) and quantitative (mqBOLD) MRI data in the same subjects and during the same imaging session. Still, task durations differed across sequences to achieve an optimal signal-to-noise ratio for each of the MRI-sequences. During BOLD fMRI, the block length for each task was 30 seconds, while the block duration during mqBOLD MRI lasted between four to six minutes. We therefore tested whether prolonged stimulation lead to a habituation effect in the acquired BOLD fMRI data. We acquired data from an independent sample of subjects (N = 18) that continuously performed the CALC and MEM task for three minutes, interleaved by 1min CTRL blocks. Additionally, we performed a time-resolved analysis of the six-minute blocks of CBF measurement from pCASL

imaging acquired in the main cohort. The two analyses revealed stable BOLD signal and CBF levels across several minutes of continuous task engagement (Fig. S4). We found an initial peak in the BOLD response, but after around 30s, positive and negative BOLD responses reached a stable plateau throughout task performance. We also observed stability of the CBF signal in all tasks throughout the entire measurement. In summary, metabolic and hemodynamic effects were stable over several minutes of task engagement, without habituation effects. This allowed us to use BOLD percent signal change data to optimize our CMRO2 calculation, as described in the next section.

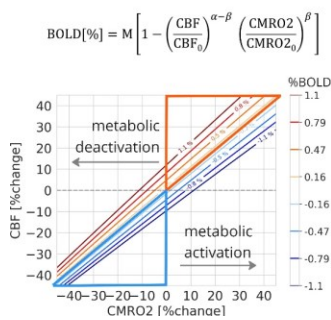
The mqBOLD protocol allows to quantify oxygen metabolism, yet has some disadvantages. First, it is time-consuming as it requires T2* mapping and pCASL acquisition for each task condition, requiring long scanning sessions. Second, prolonged data acquisition makes the technique prone to motion artifacts, especially for non-dynamic T2* mapping (Nöth et al., 2014). Third, T2* mapping is strongly influenced by background magnetic field gradients that need to be corrected (Hirsch & Preibisch, 2013). Finally, the calculation of R2', OEF and CMRO2 from several underlying parameter maps results in a rather low signal-to-noise ratio (SNR) (Hirsch et al., 2014; Kaczmarz, Hyder, et al., 2020). We therefore additionally implemented a semi-quantitative approach where $\Delta R2^*$ was approximated from BOLD fMRI data, see Methods (Fujita et al., 2006). Semi-quantitative $\Delta R2^*$ benefits from motion correction and offers a higher SNR due to repeated task conditions, even at a reduced total measurement time compared to mqBOLD MRI. Fig. 3A demonstrates comparable distributions and amplitudes of CMRO2 changes across the cortex for the semi-quantitative approach as compared to the fully quantitative approach. By repeating PLS group analyses with the semi-quantitative CMRO2 data, Fig. 3A shows that our main results were still valid and even strengthened. The CALC task induced a widespread pattern of CMRO2 increases, even in brain regions with negative BOLD responses. In CALC-negative ROIs, semi-quantitative CMRO2 increased significantly compared to CTRL (1.69%) and REST (0.72%). This is in contrast to the fully quantitative CMRO2 data, where CMRO2 did not show significant changes compared to CTRL, but decreases significantly by -0.6% compared to REST.

Starting from here (from Fig. 3B and Fig. S5), we used semi-quantitative CMRO2 maps instead of fully quantitative CMRO2 maps for the CALC and MEM conditions. Baseline REST and CTRL CMRO2 maps remained unchanged.

A| Replication of group results with semi-quantitative CMRO2



B| Davis model



C| Empirical data

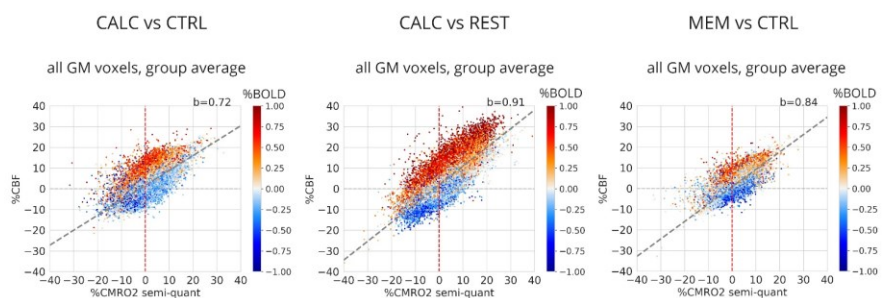


Figure 3. Semi-quantitative approach. **A|** Group results, replicating results in Fig. 2A with semi-quantitative CMRO2 data, using an approximation of $\Delta R2^*$ from BOLD fMRI instead of long-block T2*-mapping for the calculation of CMRO2. Group maps looked very similar for the quantitative versus semi-quantitative approach. As before, we found significant CMRO2 increases for voxels within CALC-positive ROIs (orange histograms), using CTRL (upper row) or REST (lower row) as baseline. Within CALC-negative BOLD ROIs, for both the CTRL and the REST baseline, there was a significant *increase* in CMRO2 across all voxels ($p < .001$, two-sample related permutation test, 2000 permutations). **B|** Visualization of the Davis model. BOLD responses (%BOLD) are plotted in relation to changes in CBF and CMRO2 (%CBF and %CMRO2), using $M=10$, $a=-0.05$, $b=0.98$. According to the model, the sign and amplitude of the BOLD response depends on the combined changes in CBF and CMRO2. Roughly, positive %BOLD requires that oxygen delivery via CBF surpasses oxygen consumption, which results in a canonical positive BOLD response, displayed in the orange triangle in the upper right corner. This canonical response is also assumed for negative BOLD changes, here again CBF decreases surpass CMRO2 decreases, displayed in the blue triangle in the lower left corner. **C|** Empirical data from semi-quantitative CMRO2, plotting %CMRO2 against %CBF, calculated as the median across all subjects ($N = 40$ for CALC vs. CTRL, $N=30$ for CALC vs. REST and MEM vs. CTRL), for all gray matter voxels. Please note that experimental data accurately replicated the model for positive (red) and negative (blue) BOLD changes across the whole range of CBF and CMRO2 changes, also outside of canonical neurovascular coupling.

Fit of our empirical data to the Davis model

Next, we sought to interpret our data through the lens of the Davis model (Davis et al., 1998). We wanted to see if and how our empirical data fit to this model approach, which relates changes in the BOLD signal to changes in perfusion and oxygen consumption. The Davis model reflects the compound nature of the BOLD signal as outlined in Fig. 1A and is mainly used in calibrated MRI studies (Blockley et al., 2013a; Griffeth & Buxton, 2011) to calculate CMRO2 changes from combined measurements of BOLD signal and CBF. However, the Davis model has so far not been experimentally validated with fully quantitative CBF and CMRO2 data in humans. Fig. 3B shows the model equation and visualizes it for a range of percent BOLD signal changes (%BOLD, colored lines) in relation to percent CBF and CMRO2 changes (%CBF, %CMRO2). Canonical coupling as described in Fig. 1A, featuring higher increase of CBF than CMRO2, resulting in positive BOLD changes, are only to be found in a small part of the graph, on the left side of the diagonal in the first quadrant (orange triangle

in the plot). However, this graphical display also illustrates combinations of CBF and CMRO2 changes that do not coincide with the canonical physiological BOLD model. The graph shows that decreases in CMRO2 may well be accompanied by positive BOLD responses, while negative BOLD responses may actually go along with increased CMRO2, which is also the most accepted explanation for the 'initial dip' due to faster CMRO2 dynamics (Simon & Buxton, 2015). This dissociation between the sign of BOLD and CMRO2 changes can be the result of a lack of CBF 'overshoot' or due to opposing directions of CBF and CMRO2 changes; this is possible because neuronal activity triggers CBF and CMRO2 in parallel.

When plotting empirical %BOLD vs. %CBF and %CMRO2 (Fig. 3C) across all voxels of the brain, median across subjects comparing CALC to CTRL, our results closely resembled dependencies between metabolism, perfusion and associated BOLD signal changes as predicted by the Davis model. This was reflected by the similar slope of the %BOLD contours in Fig. 3B compared to 3C and the dividing line between positive (red) and negative (blue) BOLD responses in the %CBF and %CMRO2 parameter space. Notably, as implied in the Davis model, a substantial number of voxels with negative BOLD responses, blue in the scatterplots, showed CMRO2 changes with opposing sign, i.e. metabolic activations or CMRO2 increases, being located on the right of the red line, and vice versa for voxels with positive BOLD responses. The close resemblance of our empirical data to predictions of the Davis model, made us confident in a) the robustness and validity of the Davis model outside of the calibrated BOLD approach b) the robustness of our semi-quantitative CMRO2 data, based on the mqBOLD approach.

Dissociations between BOLD and CMRO2 changes

Next, we wanted to know how many voxels within the BOLD group ROIs showed dissociations in their BOLD and CMRO2 responses, and where exactly these voxels were located. Fig. 3C shows all gray-matter voxels independent of their significance, Fig. 4A only shows voxels within CALC-positive_{CTRL} (upper plot) and CALC-negative_{CTRL} (lower plot) BOLD ROIs. Please note that this is the same data as in Fig 2C, only the CALC CMRO2 data are semi-quantitative, as shown in Fig. 3A. In the violet rectangles, we illustrated and quantified the ratio of voxels where the sign of %BOLD opposes that of %CMRO2. In the following, we call voxels with opposing sign in %BOLD and %CMRO2 'deviant voxels'. This analysis revealed that 30% of the CALC-positive_{CTRL} and 66% of the CALC-negative_{CTRL} BOLD voxels did not show concomitant increases or decreases in oxygen metabolism, respectively (pie-plots in Fig. 4B). Moreover, these deviant voxels spread across the full range of BOLD signal amplitudes and do not only comprise voxels with weak %BOLD (bar plots in Fig. 4B). Voxels within the DMN showed virtually the same proportion of deviant voxels as the bigger, non-restricted negative BOLD ROIs (DMN voxels are summarized in the black-contoured pie-plots).

The brain slices in Fig. 4B show where deviant voxels (in violet) were located. Within CALC-negative_{CTRL} regions, a larger cluster was located in auditory regions, while smaller clusters of deviant voxels were found throughout the whole DMN (black contours show the DMN as defined by (Yeo et al., 2011)). In the CALC-negative_{CTRL} brain slices in Fig. 4B, it seems that smaller clusters within the DMN are preserved that show BOLD as well as CMRO2 decreases (pale blue color). To make sure to be looking at significant CMRO2 decreases, we replicated this plot in Fig S6A, now only plotting regions with both significant BOLD and CMRO2 changes on the group level (voxels within the overlap in Fig. 1B). Thus restricted, generally only very few voxels with significant CMRO2 decreases were left and as much as 89% of CALC-negative_{CTRL} BOLD voxels actually showed deviant CMRO2 responses, i.e. increases in CMRO2. In the positive domain, within CALC-positive BOLD regions, when restricted to significant CMRO2 voxels, the number of deviant voxels dropped from 30% to 6% (pie-plots in Fig. 4D versus Fig. S6). Within the MEM-positive ROI (Fig. 4C), we found 14% of deviant voxels, allocated across the whole range of BOLD amplitude changes.

Even though our main baseline was the CTRL condition, DMN 'deactivations' have usually been shown compared to a passive resting-state instead of an active control task (Raichle et al., 2001). Thus, we replicated Fig. 4 with the REST baseline in Fig. S5. The scatterplot revealed a similar slope,

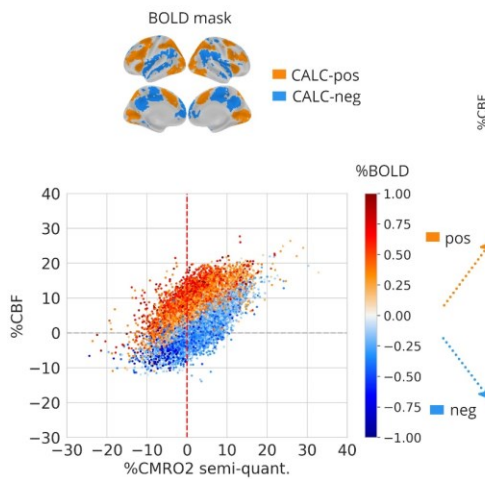
yet with a broader range of values in both directions, i.e. maximum CBF and CMRO2 values of -20/30% and -20/25% compared to -10/20% and -15/15% as in Fig. 4B (CTRL). While the percentage of voxels within CALC-negative_{REST} BOLD ROIs with deviant %CMRO2 diminished, particularly because auditory clusters were not present anymore, still nearly half (48%) of all BOLD voxels did not show coinciding decreases in oxygen consumption, and 46% of voxels that were located within the DMN. These deviant voxels were present across the whole BOLD amplitude range (quartiles in the bar plots in Fig. S5A), but less so for higher BOLD amplitudes. Restricting the BOLD ROI to areas that also showed significant CMRO2 changes increased the ratio of deviant voxels to 57% (Fig. S6B). In summary, the analysis with the REST instead of the CTRL shows a shift of the voxel distribution along the BOLD contours of the Davis-model, but overall replicates the above reported results, although with a decreased ratio of deviant voxels, which still amounts to nearly 50%.

In summary, regions with significant positive BOLD changes seemed to be a quite reliable indicator for increased oxygen consumption. On the other hand, there was a substantial number of voxels with dissociations between BOLD and CMRO2 responses, specifically within negative BOLD ROI. Only 52% of the voxels within negative BOLD ROIs showed concomitant, decreased oxygen consumption, in the best-case scenario against the REST baseline, and only 34% against the CTRL baseline.

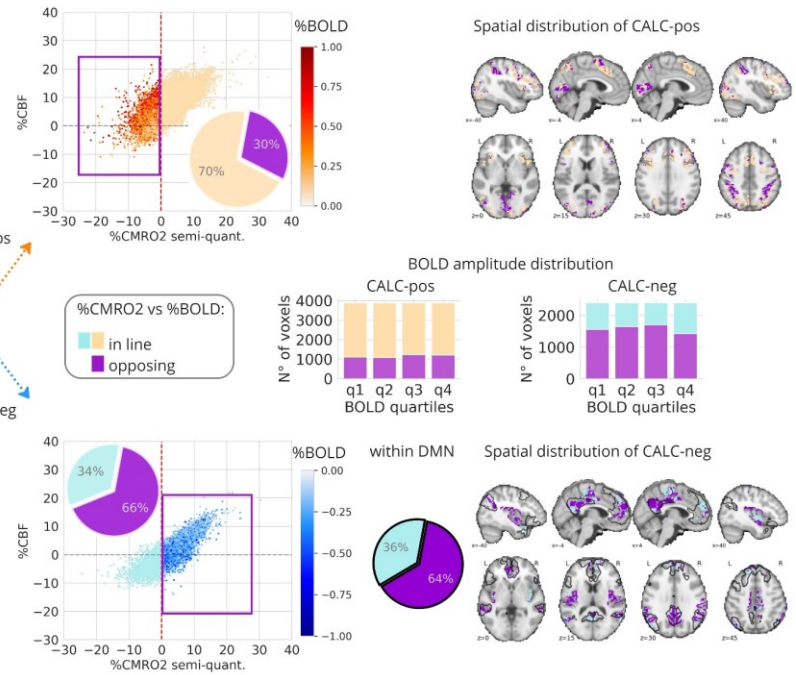
Deviant BOLD and CMRO2 responses were not explained by differences in vascularization

Yet, differences between regions, such as different vascularization, baseline metabolism or flow, can influence the BOLD response (Buxton et al., 2014b). Thus, we sought to restrict our analyses to one ROI that shows both BOLD decreases and increases, in order for regional differences to not play a role in the result interpretation. To this end, we included only voxels that showed both a significant BOLD increase during MEM (Fig. S7, left) as well as a significant BOLD decrease during CALC (Fig. S6, right). 96% of these 1317 voxels were located within the DMN. For this selected set of voxels, we identified a ratio of 7% voxels within CALC-positive BOLD regions that showed deviant %CMRO2 responses versus 64% deviant voxels within CALC-negative BOLD ROIs. Thus, while BOLD increases in this DMN ROI coincided by 93% with increases in oxygen consumption, a substantial amount of the same voxels showed negative BOLD responses during CALC in the presence of increased CMRO2 (64%). That means that we found a decoupling between BOLD responses and CMRO2 during MEM versus CALC within the same regions. This difference between negative and positive BOLD responses must thus be characteristic of either this special set of DMN regions or of negative BOLD responses in general.

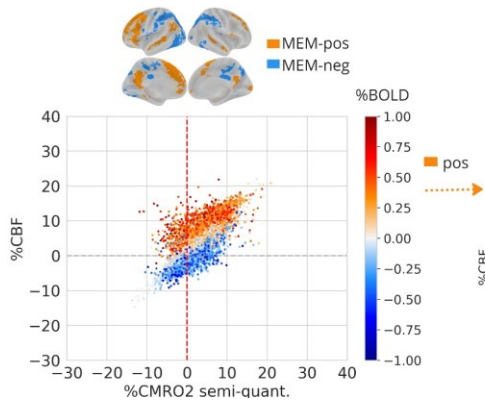
A| Empirical data: CALC vs CTRL



B| CALC vs CTRL: metabolism opposing %BOLD in CALC-positive vs CALC-negative BOLD regions



C| Empirical data: MEM vs CTRL



D| MEM vs CTRL: metabolic increases in MEM-positive BOLD regions

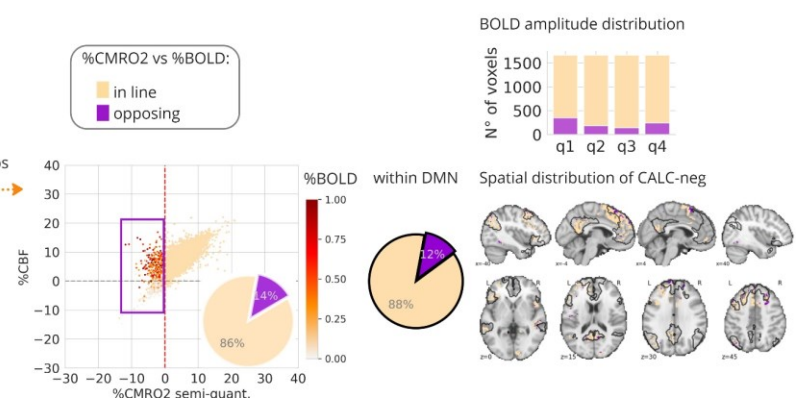


Figure 4. Positive and negative BOLD responses in relation to CBF and CMRO2 changes. **A|** Empirical data from semi-quantitative CMRO2 within CALC-positive and CALC-negative BOLD ROIs, compared to the CTRL baseline, group mask as shown in the surface plot. %CMRO2 is plotted against %CBF, colors indicate %BOLD, calculated for each voxel as the median across all subjects (N = 40). **B|** Negative and positive BOLD voxels are plotted separately. Voxels where the sign of %BOLD accorded with the sign of %CMRO2 are depicted in pale colors. Voxels where the BOLD signal changes opposes the sign of %CMRO2, i.e. deviant voxels, are depicted in violet color, in the scatter plots, barplots and brain plots. The pie-plots reflect the percentage of deviant voxels, violet rectangle. Our results showed that 30% of voxels with positive %BOLD were not accompanied by %CMRO2 increases, and 66% of voxels with negative %BOLD were not accompanied by a decrease in %CMRO2. Axial slices illustrate where these voxels were distributed and barplots show that they were equally distributed across the range of BOLD signal amplitudes with q1-q4 summarizing voxels from the lowest to highest BOLD quartiles. For negative %BOLD voxels, DMN contours are depicted in black in the brain slices together with the black-contoured pie-plot, which only contains DMN voxels. Within the DMN, 64% of voxels with BOLD decreases show deviant CMRO2 increases. **C|** Empirical data from semi-quantitative CMRO2 within MEM-positive and MEM-negative BOLD ROIs, compared to the CTRL baseline, group mask as shown in the surface plot. %CMRO2 is plotted against %CBF, colors indicate %BOLD, calculated for each voxel as the median across all subjects (N = 30). **D|** Only voxels with significant %BOLD increases are shown. As in B, violet color highlights voxels with deviating %BOLD and %CMRO2 responses. 14% of all MEM-positive BOLD voxels showed deviating %CMRO2 and these were distributed across all BOLD quartiles. Within the brain slices, the DMN is

depicted by black contours, and voxels within the DMN are shown in the black contoured pie-plot. Of these DMN voxels, only 12% of voxels showed opposing %CMRO2.

Median task-evoked responses

In Fig. 5 the results of this study are summarized, comparing BOLD signal changes to underlying changes in CMRO2 and CBF within MEM and CALC positive (orange) and negative (blue) BOLD ROIs, using CTRL as a baseline. We identified a consistent increase in the BOLD signal during CALC and MEM and concomitant increases in CBF and CMRO2 (orange bars). Please note that, differently to the values in Table 2, these values were based on semi-quantitative CMRO2. Additionally, voxels with negative BOLD responses within the BOLD-*positive* ROIs and voxels with positive BOLD responses within the BOLD-*negative* ROIs, even though these were part of the PLS group result ROI, were not considered. This only concerned a few voxels. Finally, in order to compare the MEM vs. CTRL and the CALC vs. CTRL contrasts, we calculated both MEM and CALC CMRO2 without accounting for changes in CBV. However, this only had minor influence on the CMRO2 responses, increasing them from 2.4% (with CBV correction) to 2.6% and decreasing them in CALC-negative regions from 1.7% to 1.5%.

On average, median CBF and CMRO2 increases across voxels within positive BOLD ROIs – but taking up to 30% of deviant BOLD voxels into account – suggested a consistent constructive coupling of BOLD and CBF going along with increased metabolic activity, i.e., CMRO2. Interestingly, MEM and CALC conditions lead to similar flow increases (6.5% vs 6.6%) but MEM induced a higher CMRO2 increase (4% vs 2.6%) than CALC. This discrepancy of CMRO2 amplitudes could explain the weaker BOLD increases in the MEM-positive compared to the CALC-positive ROI (0.33% vs 0.22%).

For a different set of voxels (blue bars), we identified a consistent pattern of negative BOLD responses during CALC and MEM, which was not accompanied by metabolic deactivation, i.e., a decreases in CMRO2. Within CALC-negative regions, the oxygen consumption even increased, on average. Together with a rather small CBF decrease of -0.8%, this could explain the strong BOLD signal decrease. In accordance with predictions from the Davis model, BOLD signal changes are strongest when the signs of CBF and CMRO2 responses are opposing. On the contrary, in the MEM-negative ROI, negative BOLD responses seemed to be the result of pure vascular effects, i.e. of CBF decreases (1.5%) with nearly no changes in CMRO2 (0.2%). When taking REST instead of CTRL as the baseline (Fig. S8A), we got a stronger decrease in CBF during CALC (-2.3%), but CMRO2 changes around zero, also pointing towards a mainly vascular effect behind these BOLD decreases.

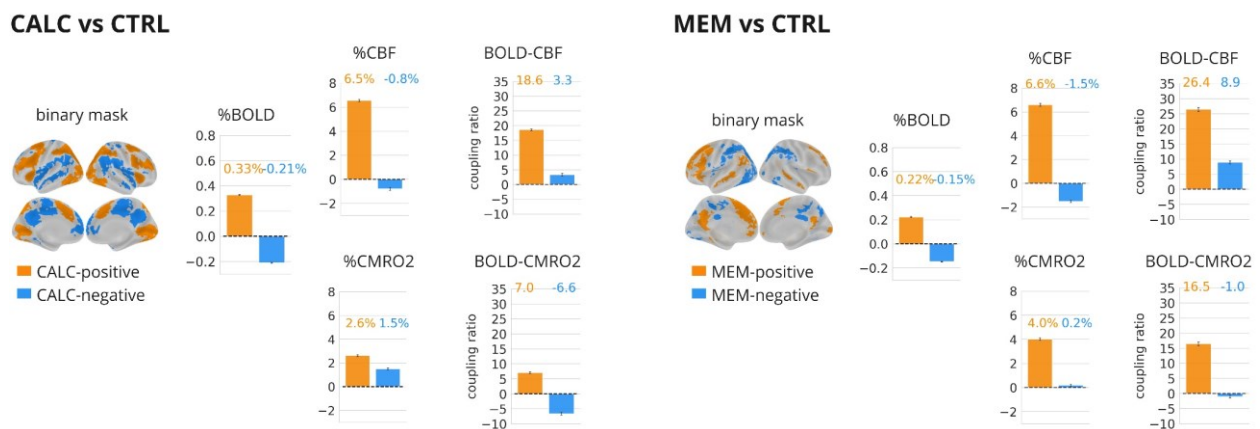


Figure 5. Median %BOLD, %CBF and %CMRO2 responses within positive and negative BOLD ROIs. Barplots are summarizing voxel distributions within the CALC vs. CTRL and MEM vs. CTRL ROIs as plotted in the 3D brains on the left, median across subjects, summarizing results in Fig. 4. Error bars display 95% CI of percent signal change values across voxels, 2000 permutations. During CALC vs CTRL as well as during MEM vs CTRL, we find regions with both significant %BOLD increases (orange) as well as decreases (blue). Orange

bars show a significant, median increase in %BOLD, %CBF and %CMRO2 across voxels in both contrasts. Blue bars show %BOLD decreases, as well as small %CBF decreases (-0.8% for CALC vs. CTRL, -1.5% for MEM vs. CTRL), but either stable %CMRO2 for MEM vs CTRL (0.2%) or even increased %CMRO2 for CALC vs CTRL (1.5%). The last column in both contrasts quantifies the amplitude changes in %CBF and %CMRO2 to which a median change of 1% BOLD signal is coupled, across voxels. Within positive BOLD ROIs (orange), a 1% increase in BOLD is coupled to an increase in %CBF of 18.6% (CALC vs CTRL) or 26.4% (MEM vs CTRL) and an increase in %CMRO2 of 7.0% (CALC vs CTRL) or 16.5% (MEM vs CTRL). The MEM task thus elicits similar CBF and higher CMRO2 responses than the CALC task (vs CTRL). Within negative BOLD ROIs (blue), a 1% decrease in BOLD is coupled to a CBF decrease of 3.3% (CALC vs CTRL) or 8.9% (MEM vs CTRL), so the coupling factor is much smaller than for %BOLD increases. This is even more pronounced for BOLD-CMRO2 coupling within CALC-negative and MEM-negative ROIs. On average, a 1% BOLD decrease is coupled to a 1% CMRO2 decrease within MEM-negative regions, and even goes hand in hand with an average increase in %CMRO2 of 6.6% within CALC-negative regions, so we do not find the same coupling factor for negative BOLD responses as for positive BOLD responses. Please note that CALC-negative and MEM-positive regions partly overlap in the DMN, as shown in Fig. S7.

DISCUSSION

In this study, we used fully quantified measures of CMRO2 to assess whether significant BOLD signal changes accurately reflect changes in oxidative metabolism, a direct physiological marker that indicates increased synaptic activity (A. Ekstrom, 2010; A. D. Ekstrom, 2021). We were especially interested in BOLD signal decreases in the DMN and therefore employed an autobiographical memory task to ‘activate’ DMN regions as well as a calculation task to ‘deactivate’ DMN regions. DMN ‘activation’ studies usually employ an active baseline to control for visual input (Addis et al., 2007; Burianova & Grady, 2007; Spreng & Grady, 2010), DMN ‘deactivation’ studies traditionally use the passive resting state as a baseline as defined by early PET studies (Raichle et al., 2001). While we advocate for using an active baseline that controls for visual input and motor output, in this study, for the sake of comparison to other DMN studies, we employed both REST and CTRL baselines and replicated all CALC analyses also with the REST baseline, see supplementary materials.

To our knowledge, this study is the first to measure CMRO2 fully quantitatively with a cognitive design instead of visual or motor stimulation. Recent studies employed this technique in patient populations where larger effects are to be expected (Göttler et al., 2019; Kaczmarz, Hyder, et al., 2020). While there have been calibrated BOLD studies with gas inhalation using a cognitive design (Gauthier et al., 2012; Goodwin et al., 2009; Restom et al., 2008), calibration studies in general rely on several assumptions (Gauthier & Fan, 2019). First, it is assumed that the breathing manipulation does not affect the rate of oxidative metabolism. Second, calibration studies assume a fixed rate of CBF-CBV coupling across subjects and brain regions and rely on changes in BOLD and CBF to calculate fractional changes in CMRO2 via the Davis model (see Methods, formula [4]). Absolute levels of CMRO2 can be measured by dual calibration (Ma et al., 2020; Wise et al., 2013). A newer n-back study additionally included fractional CBV changes via vascular space occupancy (VASO) measurements, but without gas calibration and thus without full quantification (Y. Zhang et al., 2021). We bypassed the assumptions inherent to calibrated BOLD studies and aimed for a quantified mapping of CMRO2 in baseline and task states. This was possible by A) mapping oxygen extraction (OEF) via R2’ mapping in all conditions plus measurement of total CBV via contrast agent injection, B) measuring participants’ CBF via pCASL, C) measuring participants’ arterial oxygenation levels with pulse oximetry and D) measuring participants’ hematocrit levels in venous blood, used for both the OEF calculation as well as for the calculation of the arterial oxygen content of blood (CaO2, see Methods). This allowed us to combine all parameters via Fick’s formula and quantify CMRO2 in all conditions, without relying on the Davis model and fixed CBV-CBF coupling. All parameter values were in the expected range (Table 1).

Our whole-brain group results showed consistent CALC-positive and MEM-positive BOLD networks with overall concomitant changes in all parameters (CBF, OEF and CMRO2) on the group

level across voxels (standard space) as well as across subjects in native space (Fig. 2). It is worth noting that the localization of CALC-positive and MEM-positive ROIs depends on the parameter we look at; in CBV, we see a lateralization of the red-orange activation maps compared to BOLD (Fig. 2A) and even more in CMRO2. On the other hand, while we found extensive CALC-negative BOLD regions, we did not find a consistent CALC-negative network using CBF and especially CMRO2 data, here only a few small clusters showed significant decreases (Fig. 2B). Overall, across voxels in standard space as well as across subjects in native space, voxels in BOLD-negative ROIs did not show significant CMRO2 decreases versus CTRL. When compared to REST, CMRO2 decreases within BOLD ROIs were significant but negligibly small. CBF decreases within CALC-negative BOLD ROIs were small but significant (except across subjects in native space), see Fig. 2 and Fig. S1 and S3. These CBF and CMRO2 decreases, if present, were around two to six times smaller than expected, if one assumed the same BOLD-CBF and BOLD-CMRO2 coupling in task-positive as in task-negative BOLD ROIs. Using the GLM FWE-corrected group mask instead of the group mask from the PLS analysis did not change these results. This leads to the assumption that positive BOLD signal changes are indeed the result of canonical neurovascular and neurometabolic coupling and represent increased neuronal activity, while negative BOLD signal changes do not necessarily reflect decreased oxygen consumption.

We then aimed to explain the lack of consistent CMRO2 decreases in regions with consistent BOLD signal decreases by predictions of the theoretical biophysical Davis model (Fig. 3 and 4). Although we did not use the Davis model to calculate our empirical CMRO2 data, this biophysical model relates BOLD-signal changes to changes in CMRO2 and CBF and visualizes how sign and amplitude of the BOLD signal depend on the exact interplay between CBF and CMRO2 changes. First, we see a striking resemblance of our empirical data with predictions of the Davis model, for percent-signal changes across grey-matter voxels in all contrasts (Fig 3). As we aimed to answer the question whether BOLD signal changes are a reliable indicator for concomitant metabolic changes, we restricted further analyses to significant BOLD ROIs. Second, the large percentage of voxels within CALC-negative regions that showed a dissociation of (negative) %BOLD and (positive) %CMRO2 (roughly half of the voxels against REST and about 2/3 of the voxels against CTRL) explained the lack of overall CMRO2 decreases seen in Fig. 3A. In CALC-positive regions, only around 6-35% of all voxels showed deviant %CMRO2 responses. These dissociations did not only affect voxels with weak BOLD amplitudes or non-significant CMRO2 responses. The difference in the percentage of deviant voxels in CALC-positive compared to CALC-negative ROIs became even more prominent when restricting them to regions with significant CMRO2 changes (Fig. S6). Further, while deviant voxels were clustered in auditory regions (CALC vs CTRL), there were also large clusters of deviant voxels in all parts of the DMN, both against REST and CTRL. Posterior DMN seemed to be more affected by dissociations between %CMRO2 and %BOLD than anterior DMN (Fig. 4B, S5A).

A common limitation of studies investigating negative BOLD responses and comparing them to their positive counterpart is the comparison of different ROIs, which may be affected by differences in baseline oxygenation and vascularization that influence the BOLD response (Ances et al., 2008; Buxton et al., 2014b; Simon & Buxton, 2015). We could identify an area within the DMN on the group level that showed both significant BOLD signal decreases during CALC as well as increases during MEM, named here CALC-MEM-overlap ROI (Fig. S7). Nevertheless, despite showing decreases in %BOLD during CALC, around two-thirds of these voxels showed deviant %CMRO2 increases, similar to what we found for the larger CALC-negative ROI. However, nearly all voxels (93%) showed both increases in %BOLD and concomitantly in %CMRO2 during MEM. Because these voxels showed, on average, large flow as well as CMRO2 increases, missing evidence for decreased %CMRO2 during CALC cannot be explained by a limited range of vascular dynamics in these regions or limited sensitivity of the pCASL sequence employed, as it did reliably catch flow increases. One might still argue that negative BOLD responses are lower than positive BOLD responses, which makes it more difficult to measure them reliably because of lower SNR. While this argument is hard to refute, we saw that rather low BOLD signal changes do not necessarily indicate low amplitudes of underlying CBF or CMRO2 changes. While voxels within the CALC-MEM-overlap ROI showed, on average, only

small BOLD increases (0.16%), these were coupled to rather large flow (6%) and CMRO2 (4.1%) increases, while the larger BOLD decrease (-0.22%) was not caused by a flow decrease (-0.5% only), but by an increase in CMRO2 (1.8%). We saw the same deviant BOLD-CBF and BOLD-CMRO2 coupling in the larger CALC-negative regions, which makes us assume that it is not the low SNR in these regions being the cause for absent or small CBF and CMRO2 decreases, but rather true effects.

In general, while positive BOLD changes in our empirical data could be explained by canonical hemodynamic coupling with luxury perfusion, overcompensating for increases in CMRO2, negative BOLD changes did not fit to a model of reversed hemodynamic coupling as was suggested by Raichle (Raichle et al., 2001). Rather, as summarized in Fig. 5, overall BOLD signal decreases reflected either mainly vascular effects, i.e. decreases in %CBF, or a combination of decreases in %CBF and increases in %CMRO2, leading to an even stronger negative BOLD response, in accordance with the Davis model. This implicates that decreases in the BOLD signal are no reliable proxy for decreased oxidative metabolism, i.e. do not necessarily reflect decreased neuronal activity, while BOLD signal increases are a more reliable proxy for increased oxygen metabolism. Yet, while metabolic decreases in our data were in general not very prominent, parts of the DMN still showed decreased CMRO2 during CALC, especially when compared to REST. These clusters with concomitant CMRO2 decreases were present in prefrontal, medial and lateral parts of the DMN, but were much smaller than the extended CALC-negative BOLD regions would suggest. On the other hand, large parts within the DMN showed *increased* metabolic activity during CALC, opposed to BOLD decreases. This explained why, on average, we did not find decreases in %CMRO2 across voxels within the entire BOLD ROI. Our data confirmed that the DMN is a heterogeneous region, as multiple studies have emphasized in the past (Andrews-Hanna et al., 2014; DiNicola et al., 2019; Leech et al., 2011). In extension of the Stiernman study (2021), (Godbersen et al., 2023) recently could show that metabolic decreases in DMN regions depend on the task employed. While dorsal PCC regions, although quite small in extent, consistently showed decreases in glucose consumption in externally guided tasks, a working memory task seemed to relate to increases in glucose consumption in ventral PCC. The authors suggested that cognitive control as during the working memory task induced a metabolically expensive suppression in vmPCC, and that heightened activity in the frontoparietal network is correlated to heightened metabolism in vmPCC. In our data, we also saw a division between dorsal parts of the PCC, that rather show CMRO2 decreases, and ventral parts without concomitant CMRO2 decreases, similar to (Leech et al., 2011). This could be explained by characteristics of our calculation task, where participants had to keep the differential number in mind in order to calculate the solution, similar to a working memory task. The division of voxels with increased and decreased %CMRO2 in posterior regions of the DMN could point towards a segregation of the DMN that has been found in recent papers, but needs further investigation (Braga & Buckner, 2017; Daitch & Parvizi, 2018).

Finally, when comparing MEM-positive to CALC-positive regions, we saw a similar average increase in %CBF, but a stronger average increase in %CMRO2 in MEM-positive regions. Differences of CBF-CMRO2 coupling in the MEM-CTRL contrast could be explained by characteristics of the MEM task that affected %CMRO2 more than it affected %CBF. While it has been shown that e.g. attention strongly modulates %CMRO2, but less so %CBF (Moradi et al., 2012), this explanation does not hold for the MEM task compared to the CALC task. On the other hand, different CBF-CMRO2 coupling in MEM-positive versus CALC-positive regions points towards a lower n-ratio in the MEM-positive regions, with less overcompensation of CBF. This lower n-ratio could be region- and thus DMN-specific. As the hippocampus has been shown to have a different n-ratio because of microvascular differences (Shaw et al., 2021), a similar mechanism could be at play in regions of the DMN. Kim and Ogawa explicitly stated that 'in areas where vascular reactivity is hampered, a negative BOLD response is likely due to increased CMRO2 without a concomitant increase in CBF', and also other studies state this possibility (A. D. Ekstrom, 2021; Harrison, 2002b; Kim & Ogawa, 2012). Thus, despite seeing a similar CBF increase in MEM-positive (DMN) as in CALC-positive regions, the blood flow response would have been even stronger in DMN regions if the vascularization was similar. Also, studies of the Mullins group point towards differences in the architecture of DMN regions, who

showed that neurovascular coupling specifically in DMN regions was reverted during hypoxia (Lawley et al., 2017; Rogan et al., 2022; Rossetti et al., 2021b). All in all, evidence points into the direction of vascular differences in the DMN, which influence CBF and BOLD responses. Further research, looking at negative and positive BOLD responses and their underlying metabolism in regions of the DMN compared to primary cortices with dense vascularization, is needed to confirm this hypothesis.

Limitations

Even though we aimed to measure all parameters influencing our CMRO2 estimations as extensively as possible, this study also faces some limitations. While most studies do not measure subject-specific CBV in baseline and task conditions, but interpolate it from CBF changes (Blockley et al., 2013b), we quantified CBV per subject. Contrast agent could only be injected to healthy participants up to a clinical threshold (0.2ml /kg), so we could only measure CBV in up to two conditions (with half the dosage each), which we did for 10 participants in CALC and CTRL, and then interpolated CBV changes to the rest of the participants. This could not be done for the MEM and REST conditions, so for these conditions we used CBV CTRL values for CMRO2 calculation and did not take possible changes in CBV into account. This affected OEF calculation and means that increases or decreases in CMRO2 including MEM or REST conditions might be overestimated as they were not corrected for CBV changes. However, when we compared CMRO2 responses during CALC with and without CBV correction, this only had minor influence on the CMRO2 response, so we are confident that this possible overestimation did not affect our main results. On the other hand, we might be overly conservative by correcting for (total) CBV increases, underestimating CMRO2 changes in CALC-CTRL regions. This is because we measured total CBV instead of venous CBV, and arterial vasodilation may account for 30-70% of total CBV increase, but is of no interest for CMRO2 calculation (Drew, 2019; Hua et al., 2019; Huber et al., 2019a). All in all, it is important to take venous CBV changes into account, so we propose for future measurements to quantify CBV in the baseline via contrast agent injection, but to measure relative changes in CBV in all conditions via VASO (vascular space occupancy, (Huber et al., 2018)), or even better only measure dynamic changes in venous CBV. Further, BOLD, T2' and CBF were all measured via separate sequences to get optimal sensitivity for each sequence. This resulted in prolonged measurement time and we cannot be sure that we measured the exact same processes in all parameters, as they were not acquired simultaneously. Newer studies using multi-echo sequences claim improved sensitivity for simultaneous measurement of CBF and BOLD and contain the possibility to also extract quantitative T2* (Devi et al., 2022; K. Zhang et al., 2019), which would reduce scanning time drastically.

Also, $\Delta R2^*$ measurements and thus OEF and CMRO2 are relatively noisy. This why we decided to approximate $\Delta R2^*$ via $\Delta BOLD$ from Fig. 3 onwards. The excellent fit of semi-quantitative %CMRO2 to predictions from the Davis model made us confident that this approach worked. We cannot rule out that a fully quantitative evaluation of %CMRO2 would have been more ambiguous in its interpretation because of noisy $\Delta R2'$ which impacts on CMRO2. Nevertheless, we propose that future research fully quantifies $R2'$, OEF and CMRO2 in the baseline, but makes use of relative ΔCBV (via VASO) and $\Delta R2'$ (via fMRI BOLD) to quantify CMRO2 in task states.

Finally, it is well known that gradient-echo BOLD fMRI is biased towards by pial, draining veins containing large amounts of dHb. It is thus less sensitive towards the locus of interest, i.e. changes in dHb within capillaries (Beckett et al., 2020; De Martino et al., 2013). CMRO2 should localize changes in neuronal activity better than BOLD fMRI (Huber et al., 2019b). These factors may also explain why %BOLD and %CMRO2 in single voxels do not necessarily match.

CONCLUSION

To date, it is broadly accepted that CBF and CMRO₂ are not directly coupled, but neuronal activity is coupled to both CBF and CMRO₂ in parallel (Attwell & Iadecola, 2002; Blockley et al., 2013b; Buxton, 2010b, 2021; Kaplan et al., 2020). It is therefore unlikely that the compound BOLD signal, being influenced by both CBF and CMRO₂ changes, linearly scales with metabolic synaptic activity, ubiquitously across the whole cortex and across subjects.

In this study, we confirmed that BOLD signal changes do not necessarily match changes in metabolic synaptic activity as measured by CMRO₂. This is especially true for BOLD areas showing negative task-related BOLD decreases: while there is no total accordance between the sign of %BOLD and %CMRO₂ in general, we found 6-35% of *positive* BOLD voxels showing deviant %CMRO₂ decreases compared to a larger percentage of 48-89% of *negative* BOLD voxels showing deviant %CMRO₂ increases.

Our results concerning the DMN confirm findings from a recent study that didn't find decreases in metabolism (glucose consumption) in the DMN despite significant BOLD 'deactivations' (Stiernman et al., 2021). Yet, our study extends these findings by measuring absolute, voxel-wise CBF and CMRO₂. On average within BOLD ROIs, we found no or only very weak evidence for decreased activity in DMN regions. Yet, when localizing deviant %CMRO₂ voxels, we found that there were clusters in the DMN that showed decreases in oxidative metabolism, while others showed increases. This points towards the existence of different subregions within the DMN with different metabolic signatures, which were not captured by a uniform negative BOLD signal, and will need further investigation.

All in all, this study fundamentally questions the commonly accepted interpretation of positive and specifically negative BOLD responses as indicators for increased and decreased neuronal activity, and might settle arguments regarding the interpretation of negative BOLD responses. Further, it strengthens recent efforts to extend or even replace fMRI BOLD measurements by parameters that reflect real biophysiological processes (Chen et al., 2022; Devi et al., 2022; A. D. Ekstrom, 2021; Huber et al., 2019b; Kufer et al., 2022).

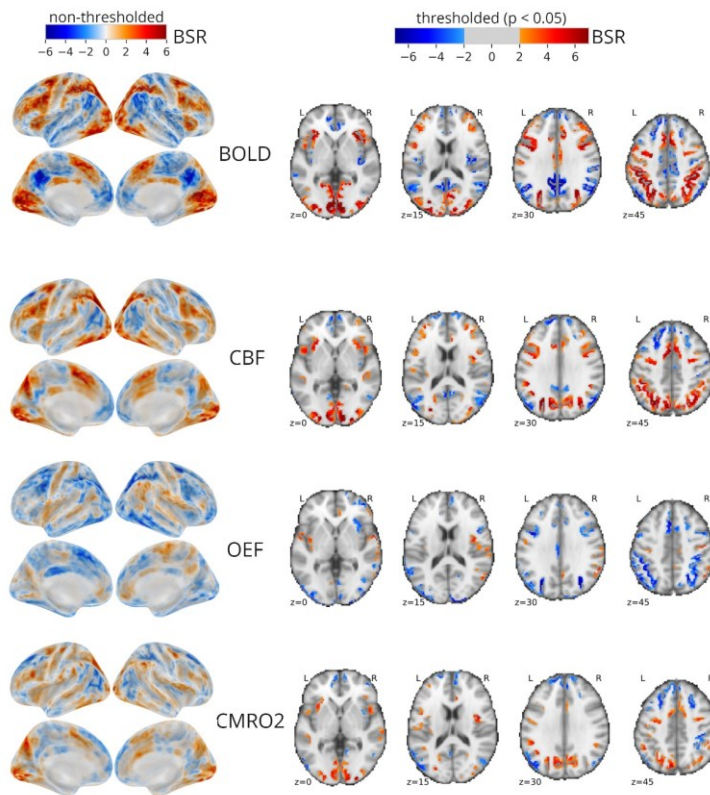
FUNDING

CP: funded by the Deutsche Forschungsgemeinschaft (DFG, German Research Foundation) – Projektnummer 395030489.

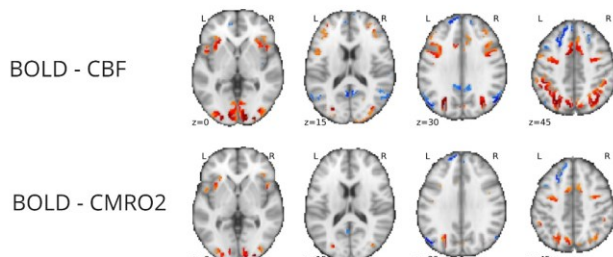
VR: funded by the European Research Council (ERC) under the European Union's Horizon 2020 research and innovation program (ERC Starting Grant, ID 759659)

SUPPLEMENTARY MATERIAL

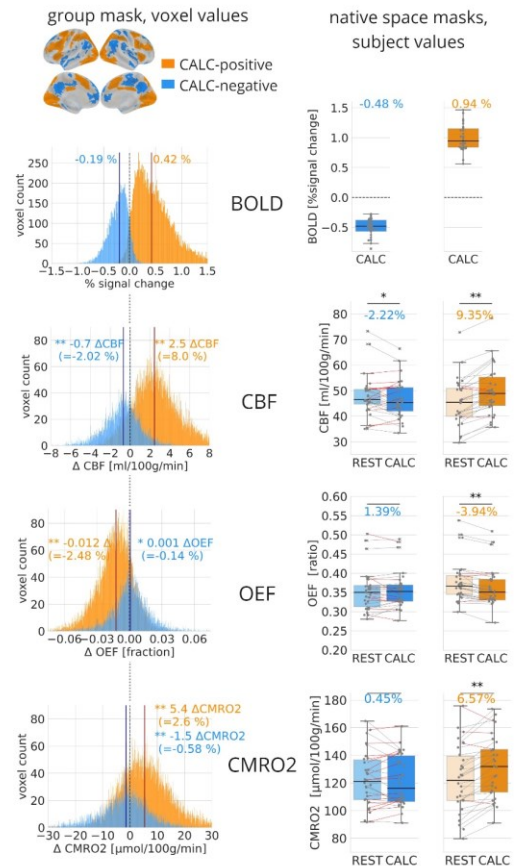
A | Group results: CALC vs REST



B | Overlap of BOLD fMRI- and mqBOLD-results



C | CALC-positive and negative BOLD voxels



D | BOLD-CBF and BOLD-CMRO2 coupling

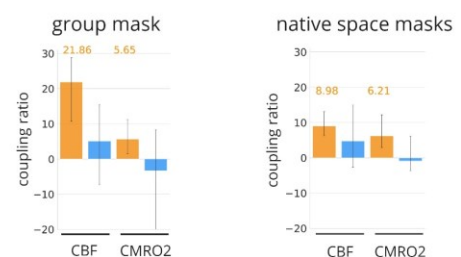
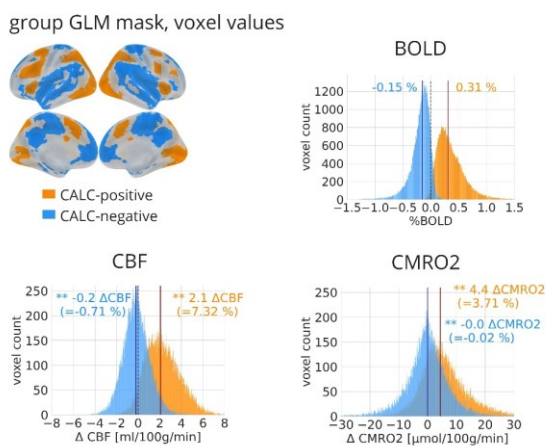


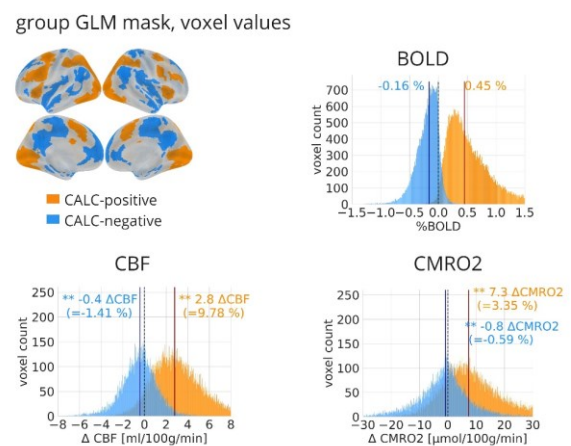
Figure S1. Replication of Fig. 2 with REST baseline. **A** | Results of the PLS analyses of CALC versus REST for relative BOLD fMRI and quantitative mqBOLD parameters. Surface maps show non-thresholded statistical maps, output from the partial least squares analyses (PLS, values are bootstrap ratios=BSR, akin to z-values) within the first latent variable, significant in each analysis (permutation test, $p < .001$), see Methods. Red voxels indicate higher parameter values during CALC versus REST and blue voxels show the opposite contrast. Additionally, axial slices show reliable brain clusters, thresholded by a BSR < -2 and > 2 (bootstrap ratio akin to $p < .05$, cluster size > 30 voxels) for BOLD-fMRI, CBF, OEF, and CMRO2. **B** | Maps show consistent overlap between CALC-positive BOLD regions and CBF and CMRO2 (red-orange) maps, and smaller overlap between CALC-negative BOLD regions and CBF or CMRO2 (blue) maps. **C** | **Left column**: Histograms show voxels within the binarized CALC-negative and CALC-positive BOLD group ROI and their distribution for the different mqBOLD parameter delta values (CALC minus REST), median across subjects per voxel. See also Table 2 for an overview over all values. A median BOLD signal increase of 0.42% related to a significant increase in CBF (2.5 ml/100g/min) and CMRO2 (5.4 $\mu\text{mol}/100\text{g}/\text{min}$) with a corresponding decrease in OEF (-0.012). A median BOLD signal decrease of -0.19% related to a significant decrease in CBF (-0.7 ml/100g/min) with an increase in OEF (0.001, $p < 0.05$), and a small, but significant overall CMRO2 decrease (-1.5 $\mu\text{mol}/100\text{g}/\text{min}$, permutation tests on delta values, $** = p < .001$). **Right column**: Replication of results in native space. Each dot indicates a

single subject's parameter value, median across voxels within CALC-negative and CALC-positive BOLD regions (paired samples t-tests, $** = p < .001$, $* = p < .05$). Red lines indicate subjects where the condition-related change in the parameter of interest deviated from the expected response indicated by the BOLD change. Again, a median BOLD signal increase of 0.94% was accompanied by a significant increase in CBF, CMRO2 and decrease in OEF, while a BOLD decrease of -0.48% was only accompanied by a significant change in CBF. **D]** Bar plots illustrate how CBF and CMRO2 percent-change amplitudes were related to BOLD percent-change amplitudes across subjects for CALC-positive versus CALC-negative regions within standard space group masks and native space 1st level masks. On average, a 1% increase in the BOLD signal was e.g. coupled to a 21.86% increase in CBF, within the CALC-positive group mask, across subjects. Overall, positive BOLD responses were consistently coupled to increases in CBF and CMRO2 whereas negative BOLD responses were not consistently coupled to neither CBF nor CMRO2 (median parameters values within BOLD masks, coupling ratios on the subject level, error bar=95% CI, 2000 bootstraps).

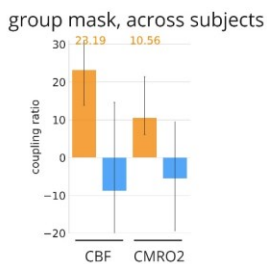
A] CALC vs CTRL: positive and negative BOLD voxels



C] CALC vs REST: positive and negative BOLD voxels



B] BOLD-CBF and BOLD-CMRO2 coupling



D] BOLD-CBF and BOLD-CMRO2 coupling

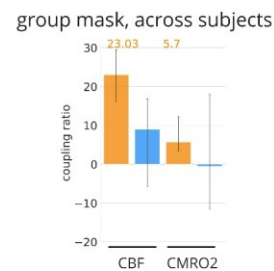
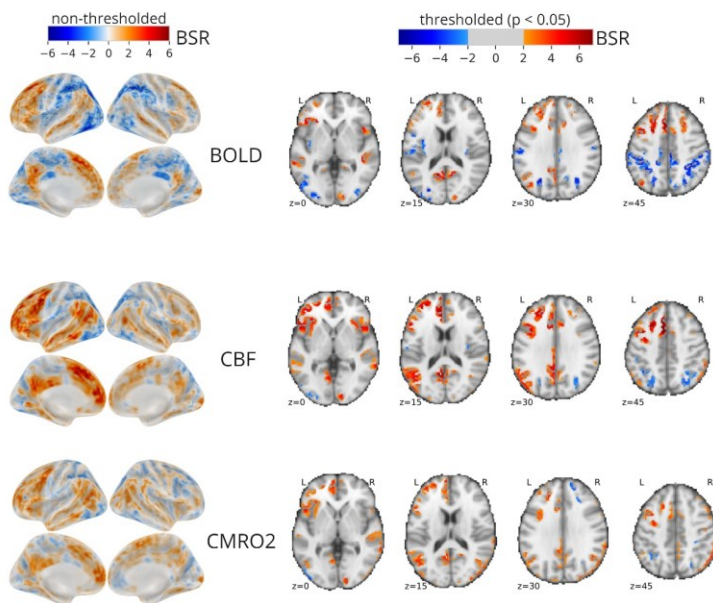


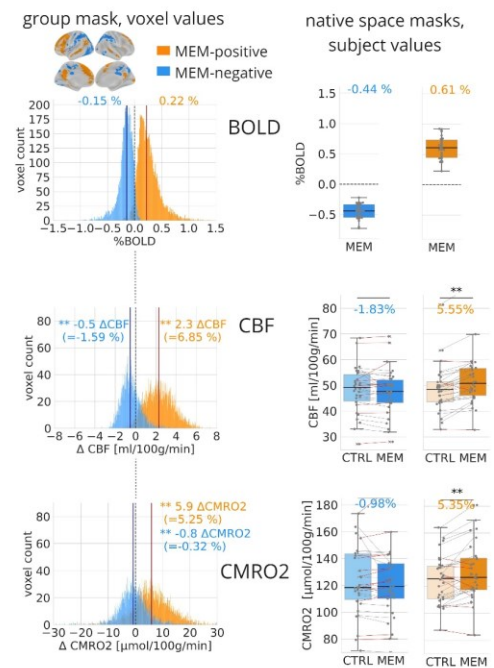
Figure S2. Replication of Fig. 2C and Fig. S1 C within GLM group mask. **A]** Histograms show voxels within the binarized CALC-negative and CALC-positive BOLD GLM group ROI and their distribution for the different mqBOLD parameter delta values (CALC minus CTRL), median across subjects per voxel. A median BOLD signal increase of 0.31% related to a significant increase in CBF (2.1 ml/100g/min) and CMRO2 (4.4 μ mol/100g/min). A median BOLD signal decrease of -0.15% related to a significant decrease in CBF (-0.2 ml/100g/min) and a very small, but significant CMRO2 decrease across voxels (-0.02%), permutation tests on delta values, $** = p < .001$). **B]** Bar plots illustrate how CBF and CMRO2 percent-change amplitudes were related to BOLD percent-change amplitudes across subjects for CALC-positive versus CALC-negative regions within standard space group ROIs. On average, a 1% increase in the BOLD signal was coupled to a 23.19% increase in CBF and a 10.56% increase in CMRO2, within the CALC-positive group mask, across subjects. Overall, positive BOLD responses were consistently coupled to increases in CBF and CMRO2 whereas negative BOLD responses were not consistently coupled to neither CBF nor CMRO2 (median parameters values within BOLD masks, coupling ratios on the subject level, error bar=95% CI, 2000 bootstraps). **C]** Histograms show voxels within the binarized CALC-negative and CALC-positive BOLD GLM group mask and their distribution for the different mqBOLD parameter delta values (CALC minus REST), median across subjects per voxel. A median BOLD signal increase of 0.45% related to a significant increase in CBF (2.8 ml/100g/min) and CMRO2 (7.3 μ mol/100g/min). A

median BOLD signal decrease of -0.16% related to a significant decrease in CBF (-0.4 ml/100g/min) and a small, but significant CMRO2 decrease across voxels (-0.8 $\mu\text{mol}/100\text{g}/\text{min}$), permutation tests on delta values, ** = $p < 0.001$). **D**] Bar plots illustrate how CBF and CMRO2 percent-change amplitudes were related to BOLD percent-change amplitudes across subjects for CALC-positive versus CALC-negative regions within standard space group masks. On average, a 1% increase in the BOLD signal was coupled to a 23.03% increase in CBF and a 5.7% increase in CMRO2, within the CALC-positive group mask, across subjects. Overall, positive BOLD responses were consistently coupled to increases in CBF and CMRO2 whereas negative BOLD responses were not consistently coupled to neither CBF nor CMRO2 (median parameters values within BOLD masks, coupling ratios on the subject level, error bar=95% CI, 2000 bootstraps).

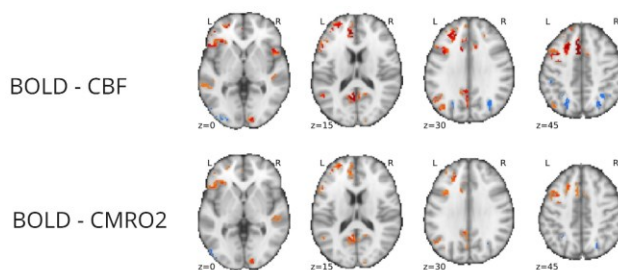
A] Group results: MEM vs CTRL



C] MEM-positive and negative BOLD voxels



B] Overlap of BOLD fMRI- and mqBOLD-results



D] BOLD-CBF and BOLD-CMRO2 coupling

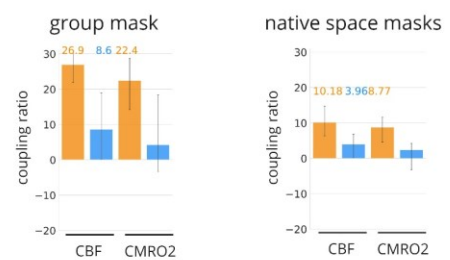
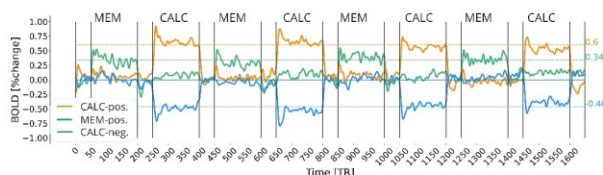


Figure S3. Replication of Fig. 2 with MEM vs. CTRL conditions. **A**] Results of the PLS analyses of MEM versus CTRL for relative BOLD fMRI and quantitative mqBOLD parameters. Surface maps show non-thresholded statistical maps, output from the partial least squares analyses (PLS, values are bootstrap ratios=BSR, akin to z-values) within the first latent variable, significant in each analysis (permutation test, $p < .001$), see Methods. Red voxels indicate higher parameter values during MEM versus CTRL and blue voxels show the opposite contrast. Additionally, axial slices show reliable brain clusters, thresholded by a BSR < -2 and > 2 (bootstrap ratio akin to $p < .05$, cluster size > 30 voxels) for BOLD-fMRI, CBF, OEF, and CMRO2. **B**] Maps show consistent overlap between CALC-positive BOLD regions and CBF and CMRO2 (red-orange) maps, and smaller overlap between CALC-negative BOLD regions and CBF or CMRO2 (blue) maps. **C**] **Left column:** Histograms show voxels within the binarized MEM-negative and MEM-positive BOLD group ROI and their distribution for the different mqBOLD parameter delta values (MEM minus CTRL), median across subjects per voxel. See also Table 2 for an overview over all values. A median BOLD signal increase of 0.22% related to a significant increase in

CBF (2.3 ml/100g/min) and CMRO2 (5.9 $\mu\text{mol}/100\text{g}/\text{min}$). A median BOLD signal decrease of -0.15% related to a significant, but small decrease in CBF (-0.5 ml/100g/min) and CMRO2 (-0.8 $\mu\text{mol}/100\text{g}/\text{min}$, permutation tests on delta values, $** = p < .001$). **Right column:** Replication of results in native space. Each dot indicates a single subject's parameter value, median across voxels within MEM-negative and MEM-positive BOLD regions (paired samples t-tests, $** = p < .001$). Red lines indicate subjects where the condition-related change in the parameter of interest deviates from the expected response indicated by the BOLD change. Again, a median BOLD signal increase of 0.61% was accompanied by a significant increase in CBF and CMRO2, while a BOLD decrease of -0.44% was not accompanied by significant changes in CBF or CMRO2 across subjects. **D|** Bar plots illustrate how CBF and CMRO2 percent-change amplitudes were related to BOLD percent-change amplitudes across subjects for CALC-positive versus CALC-negative regions within standard space group masks and native space 1st level masks. On average, a 1% increase in the BOLD signal was coupled to a 26.9% increase in CBF and a 22.4% increase in CMRO2, within the CALC-positive group mask, across subjects. Overall, positive BOLD responses were consistently coupled to increases in CBF and CMRO2 whereas negative BOLD responses were not consistently coupled to neither CBF nor CMRO2 changes (median parameters values within BOLD masks, coupling ratios on the subject level, error bar=95% CI, 2000 bootstraps).

A| Sustained activation during long-block CALC and MEM

Control study (N=18), BOLD fMRI only



Main study (N=30), stability of pCASL long blocks

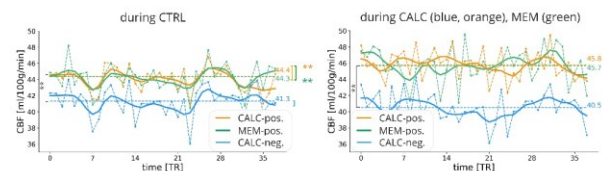


Fig. S4. Control analyses. A| Left: Median time-course of BOLD fMRI signal extracted from individual ROIs (GLM 1st level contrast maps, $z > 2.5$, native space, duration (task/baseline): three/one minutes) and averaged across subjects ($N = 18$, independent control sample). CALC > CTRL, orange; CALC < CTRL, blue; MEM > CTRL, green. BOLD signal peaks at the beginning of each task block and then stabilize at an elevated level during the entire task duration. **Right:** Median CBF time-course within CALC-positive (orange), CALC-negative (blue) and MEM-positive (green) ROIs averaged across all subjects from the main study ($N = 40$; $N = 30$ for MEM). The left plot shows time-courses within the different ROIs during CTRL and the right plot shows time-courses within the same ROIs during task. CALC-negative during CALC, blue, CALC-positive during CALC, orange, MEM-positive during MEM, green. Within all conditions and ROIs, CBF was stable during 6min of acquisition. Replicating the results in Fig. 2C and S3C, there was a significant increase in CBF from CTRL to both CALC and MEM, within MEM-positive and CALC-positive ROIs, respectively, indicated by ****** in the plot.

A| Empirical data: CALC vs REST

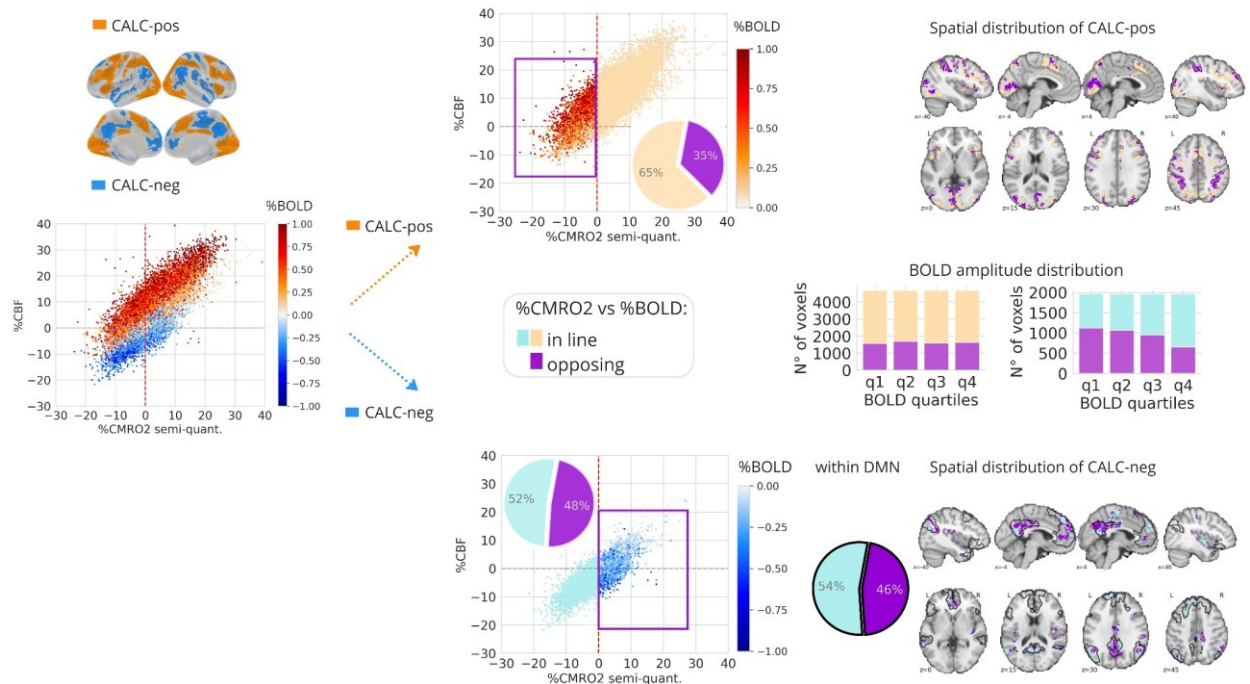
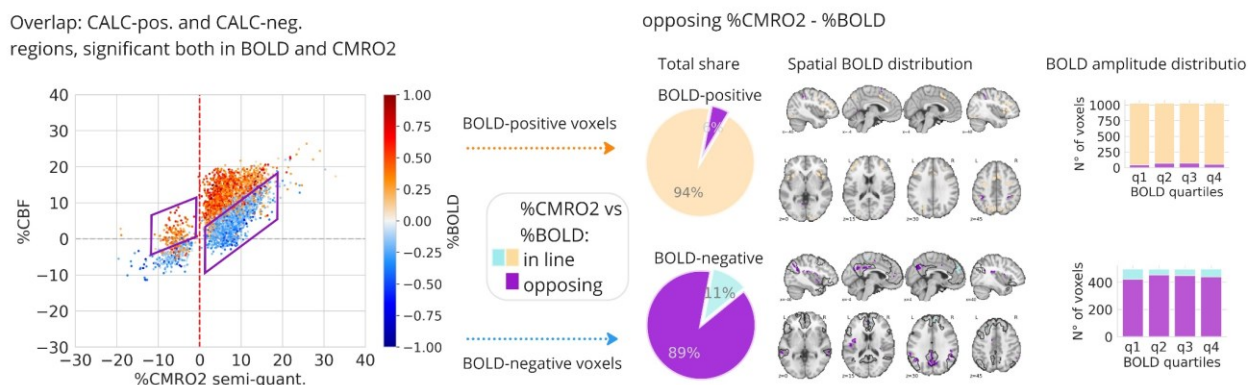


Figure S5. Replication of Fig. 4 with REST baseline. Positive and negative BOLD responses in relation to CBF- and CMRO2 changes. A| Empirical data from semi-quantitative CMRO2, plotting %CMRO2 against %CBF (CALC vs REST), calculated as the median across all subjects ($N = 30$) per voxel. Only voxels within CALC-positive and CALC-negative ROIs are plotted, group ROIs are shown in blue and orange in the surface brain plot. Voxels where the sign of %BOLD accords with the sign of %CMRO2 are plotted in pale colors. Voxels where the BOLD signal changes opposes the sign of %CMRO2, i.e. deviant voxels, are indicated by violet color, in the scatter plots, bar-plots and brain plots. The pie-plots reflect the percentage of deviant voxels within all significant BOLD voxels. Our results showed that 35% of voxels with positive %BOLD were not accompanied by %CMRO2 increases, and 48% of voxels with negative %BOLD were not accompanied by a decrease in %CMRO2. Axial and sagittal brain slices illustrate where these voxels were distributed and bar-plots show that they were distributed across the whole range of BOLD signal amplitudes with q1-q4 summarizing voxels from the lowest to highest BOLD quartiles. Black contours in the lower plot outline the DMN and the pie-plot with black contours summarizes all voxels that were located within the DMN. Within the DMN, 46% of all voxels with significant %BOLD decreases show opposing %CMRO2, i.e. CMRO2 increases.

A | Semi-quant; Empirical data: CALC vs CTRL, regions with significant %BOLD and %CMRO2



B | Empirical data: CALC vs REST, regions with significant %BOLD and %CMRO2

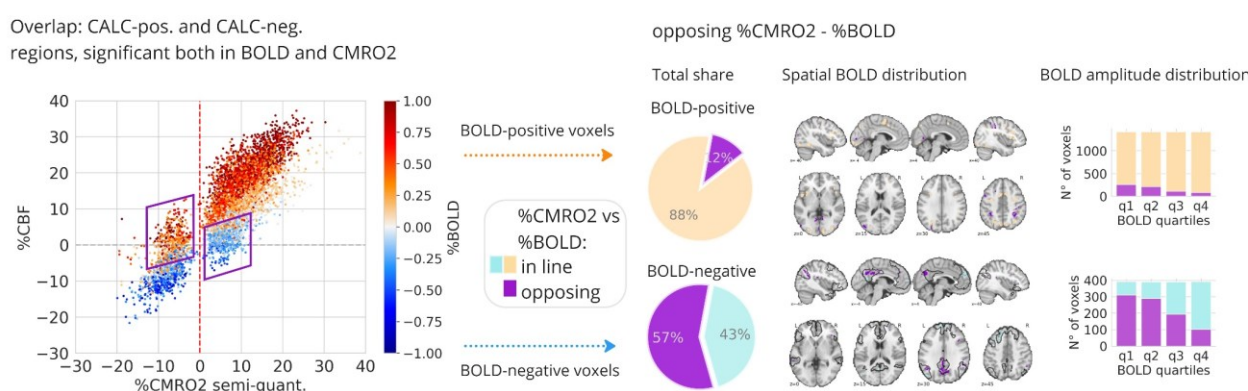


Figure S6. Replication of Fig. 4B and C within significant CALC-pos. and CALC-neg. BOLD and CMRO2 overlap regions. A | Overlap voxels, showing both significant change in BOLD as in CMRO2, are shown. Color codes for %BOLD. Voxels where the sign of %BOLD accords with the sign of %CMRO2 are plotted in pale colors. Voxels where the BOLD signal changes opposes the sign of %CMRO2, i.e. deviant voxels, are indicated by violet color, in the scatter plots, bar-plots and brain plots. The pie-plots reflect the percentage of deviant voxels within all voxels in the scatterplot, separately for BOLD-positive and BOLD-negative voxels. Our results show that 6% of voxels with positive %BOLD were not accompanied by %CMRO2 increases, and 89% of voxels with negative %BOLD were not accompanied by a decrease in %CMRO2. Axial slices illustrate where these voxels were distributed and barplots show that they were equally distributed across the range of BOLD signal amplitudes with q1-q4 summarizing voxels from the lowest to highest BOLD quartiles. **B |** Replication of A, but with REST as the baseline condition. Empirical data from semi-quantitative CMRO2, plotting %CMRO2 against %CBF (CALC vs REST), calculated as the median across all subjects (N = 30) per voxel. Voxels where the BOLD signal changes opposes the sign of %CMRO2, i.e. deviant voxels, were indicated by violet color, in the scatter plots, bar-plots and brain plots. The pie-plots reflect the percentage of deviant voxels within all voxels in the scatterplot, separately for BOLD-positive and BOLD-negative voxels. Our results showed that 12% of voxels with positive %BOLD were not accompanied by %CMRO2 increases, and 57% of voxels with negative %BOLD were not accompanied by a decrease in %CMRO2. Axial slices illustrate where these voxels were distributed and barplots show how they were distributed across the range of BOLD signal amplitudes with q1-q4 summarizing voxels from the lowest to highest BOLD quartiles, with a tendency for higher negative BOLD amplitudes containing less deviating voxels.

Overlap voxels: MEM-pos and CALC-neg (vs CTRL)

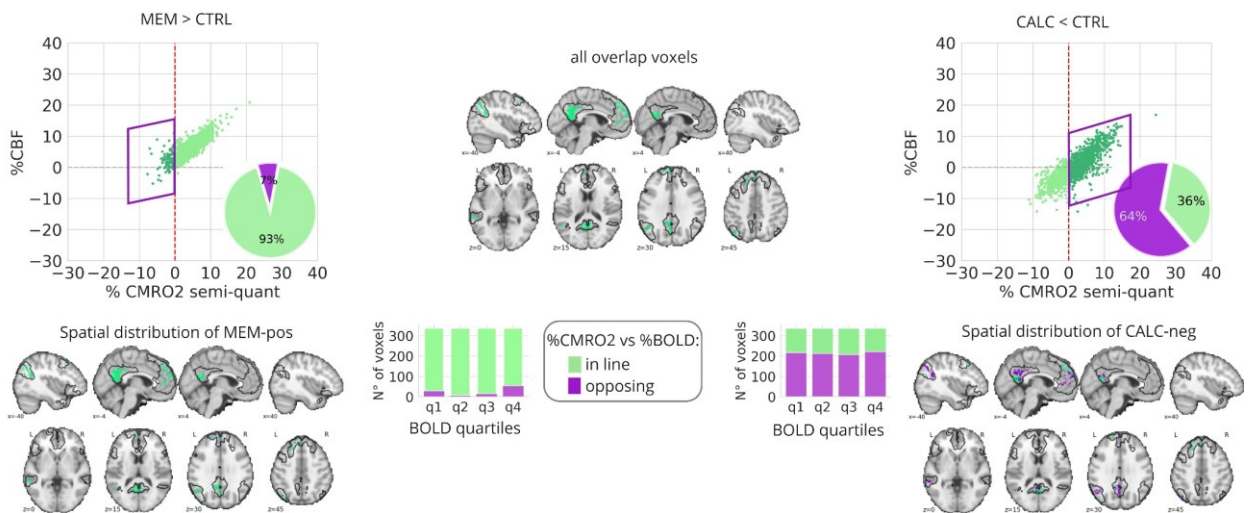
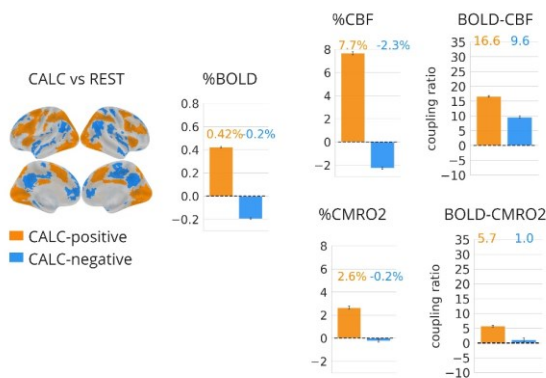


Figure S7. Overlap between CALC-negative and MEM-positive voxels. Both scatterplots show the same subset of voxels (brain slices in the middle) that displayed significant positive BOLD responses during MEM vs CTRL (left plot) and significant negative BOLD responses during CALC vs CTRL (right plot), 96% of these voxels were located within the DMN. During MEM, only 7% of these voxels exhibited opposing %CMRO2 decreases, despite positive %BOLD (violet in the pie-chart), while 64% exhibited opposing %CMRO2 during CALC, i.e. increases in %CMRO2 despite negative %BOLD, pie-plot in the right graph. Again, deviant CMRO2 responses were distributed across the whole range of BOLD signal amplitudes (bar plots) and the brain slices show where the deviating voxels were located (in violet) in both contrasts.

A | CALC vs REST



B | MEM-pos / CALC-neg overlap voxels

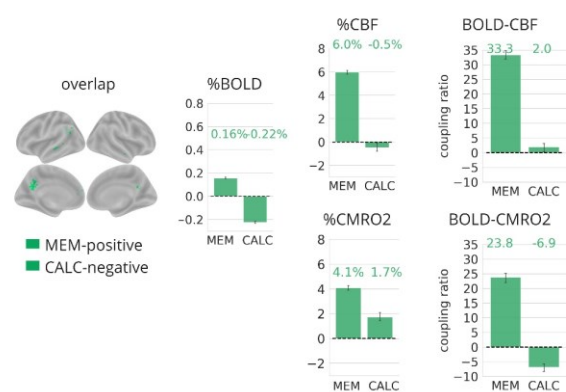


Figure S8. Summary of Fig. S5 and S7, showing median %BOLD, %CBF and %CMRO2 responses within CALC-positive and CALC-negative BOLD ROIs as well as within the overlap ROI. Barplots are summarizing voxel distributions, median across 30 subjects, within the CALC vs REST ROIs (A) as well as within the MEM-positive / CALC-negative overlap ROIs (B) as plotted in the 3D brains. Error bars display 95% CI of percent signal change values across voxels, 2000 permutations. **A |** During CALC vs REST, we found regions with both significant %BOLD increases (orange) as well as decreases (blue). Orange bars show a significant, median increase in %BOLD (0.42%), as well as a 7.7% increase in CBF and a 2.7% increase in CMRO2 across voxels in the same region. This resulted in a BOLD-CBF coupling of 16.6 and a BOLD-CMRO2 coupling of 5.7. Within CALC-negative regions (blue), a median decrease of -0.2% in the BOLD signal was coupled to -2.3% decrease in CBF, resulting in a BOLD-CBF coupling of 9.6 across voxels. The median CMRO2 response within this ROI was only -0.2%, resulting in a BOLD-CMRO2 coupling of 1.0. Both BOLD-CBF and especially BOLD-CMRO2 coupling was much higher within CALC-positive than within CALC-negative regions. **B |** The same voxels were displayed in green and plotted during MEM (vs CTRL) as well as during CALC (vs CTRL). During MEM, these voxels displayed a median BOLD signal increase of 0.16%, together with a CBF increase of 6% and a CMRO2

increase of 4.1%, resulting in a BOLD-CBF coupling of 33.3 and a BOLD-CMRO2 coupling of 23.8. In contrast, during CALC, these voxels displayed a median BOLD signal decrease of -0.22%, together with a small CBF decrease (0.5%) and a CMRO2 increase of 1.7%. This resulted in BOLD-CBF coupling factor of 2, much smaller than during MEM, and a BOLD-CMRO2 coupling of -6.9. This inversed coupling factor indicates that negative BOLD responses during CALC were coupled, on average, to CMRO2 increases, thus the opposite mechanism that we would expect. Please note that %CMRO2 during CALC was not corrected for CBV increases, in order to be comparable to MEM increases.

REFERENCES

- Addis, D. R., Wong, A. T., & Schacter, D. L. (2007). Remembering the past and imagining the future: Common and distinct neural substrates during event construction and elaboration. *Neuropsychologia*, *45*(7), 1363–1377. <https://doi.org/10.1016/j.neuropsychologia.2006.10.016>
- Alsop, D. C., Detre, J. A., Golay, X., Günther, M., Hendrikse, J., Hernandez-Garcia, L., Lu, H., MacIntosh, B. J., Parkes, L. M., Smits, M., van Osch, M. J. P., Wang, D. J. J., Wong, E. C., & Zaharchuk, G. (2015). Recommended implementation of arterial spin-labeled perfusion MRI for clinical applications: A consensus of the ISMRM perfusion study group and the European consortium for ASL in dementia: Recommended Implementation of ASL for Clinical Applications. *Magnetic Resonance in Medicine*, *73*(1), 102–116. <https://doi.org/10.1002/mrm.25197>
- Ances, B. M., Leontiev, O., Perthen, J. E., Liang, C., Lansing, A. E., & Buxton, R. B. (2008). Regional differences in the coupling of cerebral blood flow and oxygen metabolism changes in response to activation: Implications for BOLD-fMRI. *NeuroImage*, *39*(4), 1510–1521. <https://doi.org/10.1016/j.neuroimage.2007.11.015>
- Andrews-Hanna, J. R., Saxe, R., & Yarkoni, T. (2014). Contributions of episodic retrieval and mentalizing to autobiographical thought: Evidence from functional neuroimaging, resting-state connectivity, and fMRI meta-analyses. *NeuroImage*, *91*, 324–335. <https://doi.org/10.1016/j.neuroimage.2014.01.032>
- Anticevic, A., Cole, M. W., Murray, J. D., Corlett, P. R., Wang, X.-J., & Krystal, J. H. (2012). The role of default network deactivation in cognition and disease. *Trends in Cognitive Sciences*, *16*(12), 584–592. <https://doi.org/10.1016/j.tics.2012.10.008>
- Attwell, D., & Iadecola, C. (2002). The neural basis of functional brain imaging signals. *Trends in Neurosciences*, *25*(12), 621–625.
- Avants, B., Epstein, C., Grossman, M., & Gee, J. (2008). Symmetric diffeomorphic image registration with cross-correlation: Evaluating automated labeling of elderly and neurodegenerative brain. *Medical Image Analysis*, *12*(1), 26–41. <https://doi.org/10.1016/j.media.2007.06.004>
- Baudrexel, S., Volz, S., Preibisch, C., Klein, J. C., Steinmetz, H., Hilker, R., & Deichmann, R. (2009). Rapid single-scan T_2^* -mapping using exponential excitation pulses and image-based correction for linear background gradients: T_2^* Mapping With Field Gradient Correction. *Magnetic Resonance in Medicine*, *62*(1), 263–268. <https://doi.org/10.1002/mrm.21971>
- Beckett, A. J. S., Dadakova, T., Townsend, J., Huber, L., Park, S., & Feinberg, D. A. (2020). Comparison of BOLD and CBV using 3D EPI and 3D GRASE for cortical layer functional MRI at 7 T. *Magnetic Resonance in Medicine*, *84*(6), 3128–3145. <https://doi.org/10.1002/mrm.28347>
- Bentley, W. J., Li, J. M., Snyder, A. Z., Raichle, M. E., & Snyder, L. H. (2016). Oxygen Level and LFP in Task-Positive and Task-Negative Areas: Bridging BOLD fMRI and Electrophysiology. *Cerebral Cortex*, *26*(1), 346–357. <https://doi.org/10.1093/cercor/bhu260>
- Blockley, N. P., Griffeth, V. E. M., Simon, A. B., & Buxton, R. B. (2013a). A review of calibrated blood oxygenation level-dependent (BOLD) methods for the measurement of task-induced changes in brain oxygen metabolism: A REVIEW OF CALIBRATED BOLD METHODS. *NMR in Biomedicine*, *26*(8), 987–1003. <https://doi.org/10.1002/nbm.2847>
- Blockley, N. P., Griffeth, V. E. M., Simon, A. B., & Buxton, R. B. (2013b). A review of calibrated blood oxygenation level-dependent (BOLD) methods for the measurement of task-induced changes in

- brain oxygen metabolism: A REVIEW OF CALIBRATED BOLD METHODS. *NMR in Biomedicine*, 26(8), 987–1003. <https://doi.org/10.1002/nbm.2847>
- Blockley, N. P., Griffeth, V. E. M., Simon, A. B., Dubowitz, D. J., & Buxton, R. B. (2015). Calibrating the BOLD response without administering gases: Comparison of hypercapnia calibration with calibration using an asymmetric spin echo. *NeuroImage*, 104, 423–429. <https://doi.org/10.1016/j.neuroimage.2014.09.061>
- Boxermann, J.L., Schmainda, K.M., Weisskoff, R.M. (2006). Relative Cerebral Blood Volume Maps Corrected for Contrast Agent Extravasation Significantly Correlate with Glioma Tumor Grade, Whereas Uncorrected Maps Do Not. *American Journal of Neuroradiology*, 27(4), 859–867.
- Braga, R. M., & Buckner, R. L. (2017). Parallel Interdigitated Distributed Networks within the Individual Estimated by Intrinsic Functional Connectivity. *Neuron*, 95(2), 457–471.e5. <https://doi.org/10.1016/j.neuron.2017.06.038>
- Bright, M. G., Croal, P. L., Blockley, N. P., & Bulte, D. P. (2019). Multiparametric measurement of cerebral physiology using calibrated fMRI. *NeuroImage*, 187, 128–144. <https://doi.org/10.1016/j.neuroimage.2017.12.049>
- Buckner, R., Andrews-Hanna, J., & Schacter, D. (2008). The Brain's Default Network: Anatomy, Function, and Relevance to Disease. *Annals of the New York Academy of Sciences*, 1124, 1–38.
- Burianova, H., & Grady, C. L. (2007). Common and Unique Neural Activations in Autobiographical, Episodic, and Semantic Retrieval. *Journal of Cognitive Neuroscience*, 19(9), 1520–1534. <https://doi.org/10.1162/jocn.2007.19.9.1520>
- Burianova, H., McIntosh, A. R., & Grady, C. L. (2010). A common functional brain network for autobiographical, episodic, and semantic memory retrieval. *NeuroImage*, 49(1), 865–874. <https://doi.org/10.1016/j.neuroimage.2009.08.066>
- Buxton, R. B. (2010a). Interpreting oxygenation-based neuroimaging signals: The importance and the challenge of understanding brain oxygen metabolism. *Frontiers in Neuroenergetics*. <https://doi.org/10.3389/fnene.2010.00008>
- Buxton, R. B. (2010b). Interpreting oxygenation-based neuroimaging signals: The importance and the challenge of understanding brain oxygen metabolism. *Frontiers in Neuroenergetics*. <https://doi.org/10.3389/fnene.2010.00008>
- Buxton, R. B. (2021). *The thermodynamics of thinking: Connections between neural activity, energy metabolism and blood flow*.
- Buxton, R. B., & Frank, L. R. (1997). A Model for the Coupling between Cerebral Blood Flow and Oxygen Metabolism during Neural Stimulation. *Journal of Cerebral Blood Flow & Metabolism*, 17(1), 64–72. <https://doi.org/10.1097/00004647-199701000-00009>
- Buxton, R. B., Griffeth, V. E. M., Simon, A. B., & Moradi, F. (2014a). Variability of the coupling of blood flow and oxygen metabolism responses in the brain: A problem for interpreting BOLD studies but potentially a new window on the underlying neural activity. *Frontiers in Neuroscience*, 8. <https://doi.org/10.3389/fnins.2014.00139>
- Buxton, R. B., Griffeth, V. E. M., Simon, A. B., & Moradi, F. (2014b). Variability of the coupling of blood flow and oxygen metabolism responses in the brain: A problem for interpreting BOLD studies but potentially a new window on the underlying neural activity. *Frontiers in Neuroscience*, 8. <https://doi.org/10.3389/fnins.2014.00139>

- Chen, J. J., Uthayakumar, B., & Hyder, F. (2022). Mapping oxidative metabolism in the human brain with calibrated fMRI in health and disease. *Journal of Cerebral Blood Flow & Metabolism*, 42(7), 1139–1162. <https://doi.org/10.1177/0271678X221077338>
- Christen, T., Schmiedeskamp, H., Straka, M., Bammer, R., & Zaharchuk, G. (2012). Measuring brain oxygenation in humans using a multiparametric quantitative blood oxygenation level dependent MRI approach. *Magnetic Resonance in Medicine*, 68(3), 905–911. <https://doi.org/10.1002/mrm.23283>
- Daitch, A. L., & Parvizi, J. (2018). Spatial and temporal heterogeneity of neural responses in human posteromedial cortex. *Proceedings of the National Academy of Sciences*, 115(18), 4785–4790. <https://doi.org/10.1073/pnas.1721714115>
- Davis, T. L., Kwong, K. K., Weisskoff, R. M., & Rosen, B. R. (1998). Calibrated functional MRI: Mapping the dynamics of oxidative metabolism. *Proceedings of the National Academy of Sciences*, 95(4), 1834–1839. <https://doi.org/10.1073/pnas.95.4.1834>
- De Martino, F., Zimmermann, J., Muckli, L., Ugurbil, K., Yacoub, E., & Goebel, R. (2013). Cortical Depth Dependent Functional Responses in Humans at 7T: Improved Specificity with 3D GRASE. *PLoS ONE*, 8(3), e60514. <https://doi.org/10.1371/journal.pone.0060514>
- Devi, R., Lepsien, J., Lorenz, K., Schlumm, T., Mildner, T., & Möller, H. E. (2022). Multi-echo investigations of positive and negative CBF and concomitant BOLD changes. *NeuroImage*, 263, 119661. <https://doi.org/10.1016/j.neuroimage.2022.119661>
- DiNicola, L. M., Braga, R. M., & Buckner, R. L. (2019). *Parallel Distributed Networks Dissociate Episodic and Social Functions Within the Individual* [Preprint]. Neuroscience. <https://doi.org/10.1101/733048>
- Drew, P. J. (2019). Vascular and neural basis of the BOLD signal. *Current Opinion in Neurobiology*, 58, 61–69. <https://doi.org/10.1016/j.conb.2019.06.004>
- DuPre, E., Luh, W.-M., & Spreng, R. N. (2016). Multi-echo fMRI replication sample of autobiographical memory, prospection and theory of mind reasoning tasks. *Scientific Data*, 3(1), 160116. <https://doi.org/10.1038/sdata.2016.116>
- Eichling, J. O., Raichle, M. E., Grubb, R. L., Larson, K. B., & Ter-Pogossian, M. M. (1975). In vivo determination of cerebral blood volume with radioactive oxygen-15 in the monkey. *Circulation Research*, 37(6), 707–714. <https://doi.org/10.1161/01.RES.37.6.707>
- Ekstrom, A. (2010). How and when the fMRI BOLD signal relates to underlying neural activity: The danger in dissociation. *Brain Research Reviews*, 62(2), 233–244. <https://doi.org/10.1016/j.brainresrev.2009.12.004>
- Ekstrom, A. D. (2021). Regional variation in neurovascular coupling and why we still lack a Rosetta Stone. *Philosophical Transactions of the Royal Society B: Biological Sciences*, 376(1815), 20190634. <https://doi.org/10.1098/rstb.2019.0634>
- Esteban, O. (2019). fMRIPrep: A robust preprocessing pipeline for functional MRI. *Nature Methods*, 16, 14.
- Esteban, O., Ciric, R., Finc, K., Blair, R. W., Markiewicz, C. J., Moodie, C. A., Kent, J. D., Goncalves, M., DuPre, E., Gomez, D. E. P., Ye, Z., Salo, T., Valabregue, R., Amlien, I. K., Liem, F., Jacoby, N., Stojić, H., Cieslak, M., Urchs, S., ... Gorgolewski, K. J. (2020). Analysis of task-based functional MRI data

preprocessed with fMRIPrep. *Nature Protocols*, 15(7), 2186–2202.
<https://doi.org/10.1038/s41596-020-0327-3>

Foster, B. L., Dastjerdi, M., & Parvizi, J. (2012). Neural populations in human posteromedial cortex display opposing responses during memory and numerical processing. *Proceedings of the National Academy of Sciences*, 109(38), 15514–15519. <https://doi.org/10.1073/pnas.1206580109>

Fox, M. D., Snyder, A. Z., Vincent, J. L., Corbetta, M., & Raichle, M. E. (2005). The human brain is intrinsically organized into dynamic, anticorrelated functional networks. *Proceedings of the National Academy of Sciences of the United States of America*, 6.

Fujita, N., Matsumoto, K., Tanaka, H., Watanabe, Y., & Murase, K. (2006). Quantitative study of changes in oxidative metabolism during visual stimulation using absolute relaxation rates. *NMR in Biomedicine*, 19(1), 60–68. <https://doi.org/10.1002/nbm.1001>

Gagnon, L., Sakad i, S., Lesage, F., Musacchia, J. J., Lefebvre, J., Fang, Q., Yucel, M. A., Evans, K. C., Mandeville, E. T., Cohen-Adad, J., Polimeni, J. R., Yaseen, M. A., Lo, E. H., Greve, D. N., Buxton, R. B., Dale, A. M., Devor, A., & Boas, D. A. (2015). Quantifying the Microvascular Origin of BOLD-fMRI from First Principles with Two-Photon Microscopy and an Oxygen-Sensitive Nanoprobe. *Journal of Neuroscience*, 35(8), 3663–3675. <https://doi.org/10.1523/JNEUROSCI.3555-14.2015>

Gagnon, L., Sakadžić, S., Lesage, F., Pouliot, P., Dale, A. M., Devor, A., Buxton, R. B., & Boas, D. A. (2016). Validation and optimization of hypercapnic-calibrated fMRI from oxygen-sensitive two-photon microscopy. *Philosophical Transactions of the Royal Society B: Biological Sciences*, 371(1705), 20150359. <https://doi.org/10.1098/rstb.2015.0359>

Garcia, D. M., Duhamel, G., & Alsop, D. C. (2005). Efficiency of inversion pulses for background suppressed arterial spin labeling. *Magnetic Resonance in Medicine*, 54(2), 366–372.
<https://doi.org/10.1002/mrm.20556>

Gauthier, C. J., Desjardins-Crépeau, L., Madjar, C., Bherer, L., & Hoge, R. D. (2012). Absolute quantification of resting oxygen metabolism and metabolic reactivity during functional activation using QUO2 MRI. *NeuroImage*, 63(3), 1353–1363.
<https://doi.org/10.1016/j.neuroimage.2012.07.065>

Gauthier, C. J., & Fan, A. P. (2019). BOLD signal physiology: Models and applications. *NeuroImage*, 187, 116–127. <https://doi.org/10.1016/j.neuroimage.2018.03.018>

Germuska, M., & Wise, R. G. (2019). Calibrated fMRI for mapping absolute CMRO2: Practicalities and prospects. *NeuroImage*, 187, 145–153. <https://doi.org/10.1016/j.neuroimage.2018.03.068>

Glasser, M. F. (2016). *A multi-modal parcellation of human cerebral cortex*. 11.
<https://doi.org/10.1038/nature18933>

Goodwin, J. A., Vidyasagar, R., Balanos, G. M., Bulte, D., & Parkes, L. M. (2009). Quantitative fMRI using hyperoxia calibration: Reproducibility during a cognitive Stroop task. *NeuroImage*, 47(2), 573–580. <https://doi.org/10.1016/j.neuroimage.2009.04.064>

Gorgolewski, K., Burns, C. D., Madison, C., Clark, D., Halchenko, Y. O., Waskom, M. L., & Ghosh, S. S. (2011). Nipype: A Flexible, Lightweight and Extensible Neuroimaging Data Processing Framework in Python. *Frontiers in Neuroinformatics*, 5. <https://doi.org/10.3389/fninf.2011.00013>

Göttler, J., Kaczmarz, S., Kallmayer, M., Wustrow, I., Eckstein, H.-H., Zimmer, C., Sorg, C., Preibisch, C., & Hyder, F. (2019). Flow-metabolism uncoupling in patients with asymptomatic unilateral carotid

- artery stenosis assessed by multi-modal magnetic resonance imaging. *Journal of Cerebral Blood Flow & Metabolism*, 39(11), 2132–2143. <https://doi.org/10.1177/0271678X18783369>
- Griffeth, V. E. M., & Buxton, R. B. (2011). A theoretical framework for estimating cerebral oxygen metabolism changes using the calibrated-BOLD method: Modeling the effects of blood volume distribution, hematocrit, oxygen extraction fraction, and tissue signal properties on the BOLD signal. *NeuroImage*, 58(1), 198–212. <https://doi.org/10.1016/j.neuroimage.2011.05.077>
- Grubb, R. L., Raichle, M. E., Eichling, J. O., & Ter-Pogossian, M. M. (1974). The Effects of Changes in Pa CO₂ Cerebral Blood Volume, Blood Flow, and Vascular Mean Transit Time. *Stroke*, 5(5), 630–639. <https://doi.org/10.1161/01.STR.5.5.630>
- Harrison, R. V. (2002a). Blood Capillary Distribution Correlates with Hemodynamic-based Functional Imaging in Cerebral Cortex. *Cerebral Cortex*, 12(3), 225–233. <https://doi.org/10.1093/cercor/12.3.225>
- Harrison, R. V. (2002b). Blood Capillary Distribution Correlates with Hemodynamic-based Functional Imaging in Cerebral Cortex. *Cerebral Cortex*, 12(3), 225–233. <https://doi.org/10.1093/cercor/12.3.225>
- Hayden, B. Y., Smith, D. V., & Platt, M. L. (2009). Electrophysiological correlates of default-mode processing in macaque posterior cingulate cortex. *Proceedings of the National Academy of Sciences*, 106(14), 5948–5953. <https://doi.org/10.1073/pnas.0812035106>
- Hedderich, D., Kluge, A., Pyka, T., Zimmer, C., Kirschke, J. S., Wiestler, B., & Preibisch, C. (2019). Consistency of normalized cerebral blood volume values in glioblastoma using different leakage correction algorithms on dynamic susceptibility contrast magnetic resonance imaging data without and with preload. *Journal of Neuroradiology*, 46(1), 44–51. <https://doi.org/10.1016/j.neurad.2018.04.006>
- Hillman, E. M. C. (2014). Coupling Mechanism and Significance of the BOLD Signal: A Status Report. *Annual Review of Neuroscience*, 37(1), 161–181. <https://doi.org/10.1146/annurev-neuro-071013-014111>
- Hirsch, N. M., & Preibisch, C. (2013). T2* Mapping with Background Gradient Correction Using Different Excitation Pulse Shapes. *American Journal of Neuroradiology*, 34(6), E65–E68. <https://doi.org/10.3174/ajnr.A3021>
- Hirsch, N. M., Toth, V., Förchler, A., Kooijman, H., Zimmer, C., & Preibisch, C. (2014). Technical considerations on the validity of blood oxygenation level-dependent-based MR assessment of vascular deoxygenation: BOLD-BASED ASSESSMENT OF VASCULAR DEOXYGENATION. *NMR in Biomedicine*, 27(7), 853–862. <https://doi.org/10.1002/nbm.3131>
- Hoge, R. D., & Pike, G. B. (2001). Oxidative metabolism and the detection of neuronal activation via imaging. *Journal of Chemical Neuroanatomy*, 22(1–2), 43–52. [https://doi.org/10.1016/S0891-0618\(01\)00114-4](https://doi.org/10.1016/S0891-0618(01)00114-4)
- Hua, J., Liu, P., Kim, T., Donahue, M., Rane, S., Chen, J. J., Qin, Q., & Kim, S.-G. (2019). MRI techniques to measure arterial and venous cerebral blood volume. *NeuroImage*, 187, 17–31. <https://doi.org/10.1016/j.neuroimage.2018.02.027>
- Huber, L., Ivanov, D., Handwerker, D. A., Marrett, S., Guidi, M., Uludağ, K., Bandettini, P. A., & Poser, B. A. (2018). Techniques for blood volume fMRI with VASO: From low-resolution mapping towards

- sub-millimeter layer-dependent applications. *NeuroImage*, 164, 131–143.
<https://doi.org/10.1016/j.neuroimage.2016.11.039>
- Huber, L., Uludağ, K., & Möller, H. E. (2019a). Non-BOLD contrast for laminar fMRI in humans: CBF, CBV, and CMRO2. *NeuroImage*, 197, 742–760. <https://doi.org/10.1016/j.neuroimage.2017.07.041>
- Huber, L., Uludağ, K., & Möller, H. E. (2019b). Non-BOLD contrast for laminar fMRI in humans: CBF, CBV, and CMRO2. *NeuroImage*, 197, 742–760. <https://doi.org/10.1016/j.neuroimage.2017.07.041>
- Hyder, D. S. F. (2010a). Neurovascular and neurometabolic couplings in dynamic calibrated fMRI: Transient oxidative neuroenergetics for block-design and event-related paradigms. *Frontiers in Neuroenergetics*. <https://doi.org/10.3389/fnene.2010.00018>
- Hyder, D. S. F. (2010b). Neurovascular and neurometabolic couplings in dynamic calibrated fMRI: transient oxidative neuroenergetics for block-design and event-related paradigms. *Frontiers in Neuroenergetics*, 2. <https://doi.org/10.3389/fnene.2010.00018>
- Jenkinson, M., Beckmann, C. F., Behrens, T. E. J., Woolrich, M. W., & Smith, S. M. (2012). FSL. *NeuroImage*, 62(2), 782–790. <https://doi.org/10.1016/j.neuroimage.2011.09.015>
- Kaczmarz, S., Göttler, J., Zimmer, C., Hyder, F., & Preibisch, C. (2020). Characterizing white matter fiber orientation effects on multi-parametric quantitative BOLD assessment of oxygen extraction fraction. *Journal of Cerebral Blood Flow & Metabolism*, 40(4), 760–774.
<https://doi.org/10.1177/0271678X19839502>
- Kaczmarz, S., Hyder, F., & Preibisch, C. (2020). Oxygen extraction fraction mapping with multi-parametric quantitative BOLD MRI: Reduced transverse relaxation bias using 3D-GraSE imaging. *NeuroImage*, 220, 117095. <https://doi.org/10.1016/j.neuroimage.2020.117095>
- Kaplan, L., Chow, B. W., & Gu, C. (2020). Neuronal regulation of the blood–brain barrier and neurovascular coupling. *Nature Reviews Neuroscience*, 21(8), 416–432.
<https://doi.org/10.1038/s41583-020-0322-2>
- Kim, S.-G., & Ogawa, S. (2012). Biophysical and Physiological Origins of Blood Oxygenation Level-Dependent fMRI Signals. *Journal of Cerebral Blood Flow & Metabolism*, 32(7), 1188–1206.
<https://doi.org/10.1038/jcbfm.2012.23>
- Kluge, A., Lukas, M., Toth, V., Pyka, T., Zimmer, C., & Preibisch, C. (2016). Analysis of three leakage-correction methods for DSC-based measurement of relative cerebral blood volume with respect to heterogeneity in human gliomas. *Magnetic Resonance Imaging*, 34(4), 410–421.
<https://doi.org/10.1016/j.mri.2015.12.015>
- Krishnan, A., Williams, L. J., McIntosh, A. R., & Abdi, H. (2011). Partial Least Squares (PLS) methods for neuroimaging: A tutorial and review. *NeuroImage*, 56(2), 455–475.
<https://doi.org/10.1016/j.neuroimage.2010.07.034>
- Kufer, J., Preibisch, C., Epp, S., Göttler, J., Schmitzer, L., Zimmer, C., Hyder, F., & Kaczmarz, S. (2022). Imaging effective oxygen diffusivity in the human brain with multiparametric magnetic resonance imaging. *Journal of Cerebral Blood Flow & Metabolism*, 42(2), 349–363.
<https://doi.org/10.1177/0271678X211048412>
- Lauritzen, M., Mathiesen, C., Schaefer, K., & Thomsen, K. J. (2012). Neuronal inhibition and excitation, and the dichotomic control of brain hemodynamic and oxygen responses. *NeuroImage*, 62(2), 1040–1050. <https://doi.org/10.1016/j.neuroimage.2012.01.040>

- Lawley, J. S., Macdonald, J. H., Oliver, S. J., & Mullins, P. G. (2017). Unexpected reductions in regional cerebral perfusion during prolonged hypoxia: Hypoxia and regional cerebral blood flow. *The Journal of Physiology*, *595*(3), 935–947. <https://doi.org/10.1113/JP272557>
- Leech, R., Kamourieh, S., Beckmann, C. F., & Sharp, D. J. (2011). Fractionating the Default Mode Network: Distinct Contributions of the Ventral and Dorsal Posterior Cingulate Cortex to Cognitive Control. *Journal of Neuroscience*, *31*(9), 3217–3224. <https://doi.org/10.1523/JNEUROSCI.5626-10.2011>
- Leenders, K. L., Perani, D., Lammertsma, A. A., Heather, J. D., Buckingham, P., Jones, T., Healy, M. J. R., Gibbs, J. M., Wise, R. J. S., Hatazawa, J., Herold, S., Beaney, R. P., Brooks, D. J., Spinks, T., Rhodes, C., & Frackowiak, R. S. J. (1990). CEREBRAL BLOOD FLOW, BLOOD VOLUME AND OXYGEN UTILIZATION: NORMAL VALUES AND EFFECT OF AGE. *Brain*, *113*(1), 27–47. <https://doi.org/10.1093/brain/113.1.27>
- Lin, P., Hasson, U., Jovicich, J., & Robinson, S. (2011). A Neuronal Basis for Task-Negative Responses in the Human Brain. *Cerebral Cortex*, *21*(4), 821–830. <https://doi.org/10.1093/cercor/bhq151>
- Logothetis, N. K. (2003). The Underpinnings of the BOLD Functional Magnetic Resonance Imaging Signal. *The Journal of Neuroscience*, *23*(10), 3963–3971. <https://doi.org/10.1523/JNEUROSCI.23-10-03963.2003>
- Logothetis, N. K. (2008). What we can do and what we cannot do with fMRI. *Nature*, *453*(7197), 869–878. <https://doi.org/10.1038/nature06976>
- Ma, Y., Sun, H., Cho, J., Mazerolle, E. L., Wang, Y., & Pike, G. B. (2020). Cerebral OEF quantification: A comparison study between quantitative susceptibility mapping and dual-gas calibrated BOLD imaging. *Magnetic Resonance in Medicine*, *83*(1), 68–82. <https://doi.org/10.1002/mrm.27907>
- Mangia, S., Tkáč, I., Gruetter, R., Van De Moortele, P.-F., Maraviglia, B., & Ugurbil, K. (2007). Sustained neuronal activation raises oxidative metabolism to a new steady-state level: Evidence from ¹H NMR spectroscopy in the human visual cortex. *Journal of Cerebral Blood Flow & Metabolism*, *27*, 1055–1063. <https://doi.org/10.1038/sj.jcbfm.9600401>
- McIntosh, A. R., & Lobaugh, N. J. (2004). Partial least squares analysis of neuroimaging data: Applications and advances. *NeuroImage*, *23*, S250–S263. <https://doi.org/10.1016/j.neuroimage.2004.07.020>
- McIntosh, A. R., & Mišić, B. (2013). Multivariate Statistical Analyses for Neuroimaging Data. *Annual Review of Psychology*, *64*(1), 499–525. <https://doi.org/10.1146/annurev-psych-113011-143804>
- Moradi, F., Buračas, G. T., & Buxton, R. B. (2012). Attention strongly increases oxygen metabolic response to stimulus in primary visual cortex. *NeuroImage*, *59*(1), 601–607. <https://doi.org/10.1016/j.neuroimage.2011.07.078>
- Mutsaerts, H. J. M. M., Steketee, R. M. E., Heijtel, D. F. R., Kuijter, J. P. A., van Osch, M. J. P., Majoie, C. B. L. M., Smits, M., & Nederveen, A. J. (2014). Inter-Vendor Reproducibility of Pseudo-Continuous Arterial Spin Labeling at 3 Tesla. *PLoS ONE*, *9*(8), e104108. <https://doi.org/10.1371/journal.pone.0104108>
- Nöth, U., Volz, S., Hattingen, E., & Deichmann, R. (2014). An improved method for retrospective motion correction in quantitative T2* mapping. *NeuroImage*, *92*, 106–119. <https://doi.org/10.1016/j.neuroimage.2014.01.050>

- Ogawa, S., Lee, T. M., Kay, A. R., & Tank, D. W. (1990). Brain magnetic resonance imaging with contrast dependent on blood oxygenation. *Proceedings of the National Academy of Sciences*, *87*(24), 9868–9872. <https://doi.org/10.1073/pnas.87.24.9868>
- Ossandon, T., Jerbi, K., Vidal, J. R., Bayle, D. J., Henaff, M.-A., Jung, J., Minotti, L., Bertrand, O., Kahane, P., & Lachaux, J.-P. (2011). Transient Suppression of Broadband Gamma Power in the Default-Mode Network Is Correlated with Task Complexity and Subject Performance. *Journal of Neuroscience*, *31*(41), 14521–14530. <https://doi.org/10.1523/JNEUROSCI.2483-11.2011>
- Pfefferbaum, A., Chanraud, S., Pitel, A.-L., Muller-Oehring, E., Shankaranarayanan, A., Alsop, D. C., Rohlfing, T., & Sullivan, E. V. (2011). Cerebral Blood Flow in Posterior Cortical Nodes of the Default Mode Network Decreases with Task Engagement but Remains Higher than in Most Brain Regions. *Cerebral Cortex*, *21*(1), 233–244. <https://doi.org/10.1093/cercor/bhq090>
- Preibisch, C., Volz, S., Anti, S., & Deichmann, R. (2008). Exponential excitation pulses for improved water content mapping in the presence of background gradients. *Magnetic Resonance in Medicine*, *60*(4), 908–916. <https://doi.org/10.1002/mrm.21730>
- Raichle, M. E. (2015). The Brain's Default Mode Network. *Annual review of neuroscience*, *38*(1), 433–447. <https://doi.org/10.1146/annurev-neuro-071013-014030>
- Raichle, M. E., MacLeod, A. M., Snyder, A. Z., Powers, W. J., Gusnard, D. A., & Shulman, G. L. (2001). A default mode of brain function. *Proceedings of the National Academy of Sciences*, *98*(2), 676–682. <https://doi.org/10.1073/pnas.98.2.676>
- Renvall, V., Nangini, C., & Hari, R. (2015). All that glitters is not BOLD: Inconsistencies in functional MRI. *Scientific Reports*, *4*(1), 3920. <https://doi.org/10.1038/srep03920>
- Restom, K., Perthen, J. E., & Liu, T. T. (2008). Calibrated fMRI in the medial temporal lobe during a memory-encoding task. *NeuroImage*, *40*(4), 1495–1502. <https://doi.org/10.1016/j.neuroimage.2008.01.038>
- Rogan, M., Friend, A. T., Rossetti, G. M., Edden, R., Mikkelsen, M., Oliver, S. J., Macdonald, J. H., & Mullins, P. G. (2022). Hypoxia alters posterior cingulate cortex metabolism during a memory task: A 1H fMRS study. *NeuroImage*, *260*, 119397. <https://doi.org/10.1016/j.neuroimage.2022.119397>
- Rossetti, G. M., d'Avossa, G., Rogan, M., Macdonald, J. H., Oliver, S. J., & Mullins, P. G. (2021a). Reversal of neurovascular coupling in the default mode network: Evidence from hypoxia. *Journal of Cerebral Blood Flow & Metabolism*, *41*(4), 805–818. <https://doi.org/10.1177/0271678X20930827>
- Rossetti, G. M., d'Avossa, G., Rogan, M., Macdonald, J. H., Oliver, S. J., & Mullins, P. G. (2021b). Reversal of neurovascular coupling in the default mode network: Evidence from hypoxia. *Journal of Cerebral Blood Flow & Metabolism*, *41*(4), 805–818. <https://doi.org/10.1177/0271678X20930827>
- Shaw, K., Bell, L., Boyd, K., Grijseels, D. M., Clarke, D., Bonnar, O., Crombag, H. S., & Hall, C. N. (2021). Neurovascular coupling and oxygenation are decreased in hippocampus compared to neocortex because of microvascular differences. *Nature Communications*, *12*(1), 3190. <https://doi.org/10.1038/s41467-021-23508-y>
- Shulman, G. L., Fiez, J. A., Corbetta, M., Buckner, R. L., Miezin, F. M., Raichle, M. E., & Petersen, S. E. (1997). Common Blood Flow Changes across Visual Tasks: II. Decreases in Cerebral Cortex. *Journal of cognitive neuroscience*, *9*(5), 648–663. <https://doi.org/10.1162/jocn.1997.9.5.648>
- Shulman, R. G., Hyder, F., & Rothman, D. L. (2001). Lactate efflux and the neuroenergetic basis of brain function. *NMR in Biomedicine*, *14*(7–8), 389–396. <https://doi.org/10.1002/nbm.741>

- Simon, A. B., & Buxton, R. B. (2015). Understanding the dynamic relationship between cerebral blood flow and the BOLD signal: Implications for quantitative functional MRI. *NeuroImage*, *116*, 158–167. <https://doi.org/10.1016/j.neuroimage.2015.03.080>
- Smith, S. M., Jenkinson, M., Woolrich, M. W., Beckmann, C. F., Behrens, T. E. J., Johansen-Berg, H., Bannister, P. R., De Luca, M., Drobnjak, I., Flitney, D. E., Niazy, R. K., Saunders, J., Vickers, J., Zhang, Y., De Stefano, N., Brady, J. M., & Matthews, P. M. (2004). Advances in functional and structural MR image analysis and implementation as FSL. *NeuroImage*, *23*, S208–S219. <https://doi.org/10.1016/j.neuroimage.2004.07.051>
- Spreng, R. N. (2012). The Fallacy of a “Task-Negative” Network. *Frontiers in Psychology*, *3*. <https://doi.org/10.3389/fpsyg.2012.00145>
- Spreng, R. N., & Grady, C. L. (2010). Patterns of Brain Activity Supporting Autobiographical Memory, Prospection, and Theory of Mind, and Their Relationship to the Default Mode Network. *Journal of Cognitive Neuroscience*, *22*(6), 1112–1123. <https://doi.org/10.1162/jocn.2009.21282>
- Spreng, R. N., Sepulcre, J., Turner, G. R., Stevens, W. D., & Schacter, D. L. (2013). Intrinsic Architecture Underlying the Relations among the Default, Dorsal Attention, and Frontoparietal Control Networks of the Human Brain. *Journal of Cognitive Neuroscience*, *25*(1), 74–86. https://doi.org/10.1162/jocn_a_00281
- Spreng, R. N., Stevens, W. D., Chamberlain, J. P., Gilmore, A. W., & Schacter, D. L. (2010). Default network activity, coupled with the frontoparietal control network, supports goal-directed cognition. *NeuroImage*, *53*(1), 303–317. <https://doi.org/10.1016/j.neuroimage.2010.06.016>
- Stiernman, L. J., Grill, F., Hahn, A., Rischka, L., Lanzenberger, R., Panes Lundmark, V., Riklund, K., Axelsson, J., & Rieckmann, A. (2021). Dissociations between glucose metabolism and blood oxygenation in the human default mode network revealed by simultaneous PET-fMRI. *Proceedings of the National Academy of Sciences*, *118*(27), e2021913118. <https://doi.org/10.1073/pnas.2021913118>
- Wise, R. G., Harris, A. D., Stone, A. J., & Murphy, K. (2013). Measurement of OEF and absolute CMRO₂: MRI-based methods using interleaved and combined hypercapnia and hyperoxia. *NeuroImage*, *83*, 135–147. <https://doi.org/10.1016/j.neuroimage.2013.06.008>
- Yablonskiy, D. A., & Haacke, E. M. (1994). Theory of NMR signal behavior in magnetically inhomogeneous tissues: The static dephasing regime. *Magnetic Resonance in Medicine*, *32*(6), 749–763. <https://doi.org/10.1002/mrm.1910320610>
- Yeo, B. T., Krienen, F. M., Sepulcre, J., Sabuncu, M. R., Lashkari, D., Hollinshead, M., Roffman, J. L., Smoller, J. W., Zöllei, L., Polimeni, J. R., Fischl, B., Liu, H., & Buckner, R. L. (2011). The organization of the human cerebral cortex estimated by intrinsic functional connectivity. *Journal of Neurophysiology*, *106*(3), 1125–1165. <https://doi.org/10.1152/jn.00338.2011>
- Zhang, J., Liu, T., Gupta, A., Spincemaille, P., Nguyen, T. D., & Wang, Y. (2015). Quantitative mapping of cerebral metabolic rate of oxygen (CMRO₂) using quantitative susceptibility mapping (QSM): Quantitative CMRO₂ Mapping Using QSM. *Magnetic Resonance in Medicine*, *74*(4), 945–952. <https://doi.org/10.1002/mrm.25463>
- Zhang, K., Sturm, V. J., Buschle, L. R., Hahn, A., Yun, S. D., Jon Shah, N., Bendszus, M., Heiland, S., Schlemmer, H. P., Ziener, C. H., & Kurz, F. T. (2019). Dual-contrast pCASL using simultaneous gradient-echo/spin-echo multiband EPI. *Magnetic Resonance Imaging*, *57*(November 2018), 359–367. <https://doi.org/10.1016/j.mri.2018.11.018>

Zhang, Y., Du, W., Yin, Y., Li, H., Liu, Z., Yang, Y., Han, Y., & Gao, J.-H. (2021). Impaired cerebral vascular and metabolic responses to parametric N-back tasks in subjective cognitive decline. *Journal of Cerebral Blood Flow & Metabolism*, 41(10), 2743–2755.
<https://doi.org/10.1177/0271678X211012153>

4 General discussion

The goal of this thesis was to investigate brain metabolism in terms of quantitative oxygen and glucose consumption across different task states in healthy human participants. The first section summarizes and discusses the results of Project I, a simultaneous fPET and mqBOLD study that measured stimulation-induced increases in fMRI BOLD, CMRO2 and CMRglc in the visual cortex. The second section summarizes and discusses the results of Project II, an mqBOLD study that investigated the metabolic basis of task-induced fMRI BOLD activation and deactivation patterns in terms of oxygen consumption. Finally, the limitations and key findings of both projects are summarized.

4.1 Implications of Project I

In the first study, we used an integrated PET-MR scanner for the simultaneous measurement of mqBOLD and fPET, yielding quantified CMRO2 and CMRglc maps per subject during resting state (REST) and visual stimulation (STIM). This is, to our knowledge, the first study to quantify both metrics simultaneously during the same scanning session in more than one condition. All measured parameters were in biologically plausible ranges. We found task-induced, significant increases in CBF, CBV, CMRO2 and CMRglc on the group level in the occipital cortex.

We also found quite large stimulation-induced increases in total CBV (12.5%), measured by intravenous contrast agent injection. It has been reported that especially in visual and somatosensory cortices, the vascularization is quite dense compared to association cortices, resulting in high increases in BOLD, flow and volume, or generally a higher vascular responsiveness to be expected (Ances et al., 2008; A. D. Ekstrom, 2021; Harrison, 2002). Both CBF and CBV changes influence the calculation of CMRO2 maps in opposing directions. If not corrected for arterial CBV increases, CMRO2 responses will be underestimated, because only venous CBV increases are relevant for the calculation of the oxygen extraction fraction and ultimately CMRO2 (S.-G. Kim et al., 1999; S.-G. Kim & Ogawa, 2012). This is why we restricted CBV increases to 30% of the total CBV changes, following a study that employed visual stimulation on a 7T scanner, which found that only 29% of total CBV increases were venous (Huber et al., 2014). Of note, our CBF increases were unexpectedly low, 11.5% on the group level (27.6% within the smaller fPET ROI), in contrast to literature values ranging between 30 and 65% (Donahue et al., 2009; Fujita et al., 2006; Hoge & Pike, 2001; A.-L. Lin et al., 2010; Liu et al., 2019; Mintun et al., 2001; R. G. Shulman et al., 2001; Simon & Buxton, 2015), and in the same range as CBV increases. Thus, CMRO2 increases on the group level were not significant when considering total CBV changes. However, after correcting for arterial CBV, CMRO2 increased significantly by 3.3% within the larger BOLD ROI and 8.3% increase within the smaller fPET ROI. Still, these increases are on the lower end of literature values. As just mentioned, this was most probably due to our low task-induced CBF increases. The pCASL sequence used at the PET-MR scanner employed automatic instead of manual planning of the labeling plane, which probably reduced labeling efficiency, together with a rather low SNR of the 12k head-coil. Further, CBF increases measured by pCASL are underestimated in comparison to CBF increases measured by PET (Warnock et al., 2018), which also may partly explain why our CBF increases are lower than CBF increases during visual stimulation measured via PET (P. Fox et al., 1988, S. 198; Mintun et al., 2001). Yet, other studies employing ASL measurements also measured CBF increases around 50-60% (Donahue et al., 2009; Fujita et al., 2006; A.-L. Lin et al., 2010), but usually in an overlap ROI with both significant CBF and BOLD activation. The choice of ROI influences average CMRO2 responses. The

more focal the ROI, the higher the average CMRO₂ and CMRglc responses, as we can also see in our data comparing the larger BOLD ROI to the more focal fPET ROI.

Conversely, CBF and CMRglc increases were very similar, 11.5% and 8.2% within the larger BOLD ROI, 27.6% and 31% within the more focal fPET ROI, speaking in favor of a close coupling between CBF and CMRglc during focal neuronal activity, as described in the literature (P. Fox et al., 1988; Newberg et al., 2005; Paulson et al., 2010). However, as noted above, CBF increases were rather weak. But also the CMRglc values might suffer from a lower SNR of fPET compared to bolus PET (Jamadar, Ward, Carey, et al., 2019; Jamadar, Ward, Li, et al., 2019).

Finally, we found a significant decrease in oxygen-to-glucose index (OGI) within the visual task ROIs, indicating increased levels of non-oxidative glucose metabolism. This is in line with other studies finding lower task-induced OGI (Mintun et al., 2002; R. G. Shulman et al., 2001; Vafaee et al., 2012) as well as spectroscopy studies finding higher levels of lactate, indicating aerobic glycolysis, during prolonged visual stimulation (Bednařík et al., 2015; Mangia et al., 2007). However, we have to consider that both CMRglc and CMRO₂ values, and thus also the OGI, were averages over prolonged visual stimulation blocks of 5 - 7.5min. Unfortunately, with fPET and mqBOLD, the temporal resolution of both the CMRglc and the CMRO₂ measurements is several minutes and does not reach the temporal resolution of fMRI BOLD. Studies measuring prolonged visual stimulation found variable CMRO₂ and lactate increases over different time-courses. While Moradi & Buxton (Moradi & Buxton, 2013) found that CBF and even more CMRO₂ response *decreased* during prolonged stimulation, comparing 45s to 8s intervals, Mintun and colleagues (Mintun et al., 2002) found *increases* in CMRO₂ across prolonged stimulation, but comparing 1min to 25min of stimulation. Others have found that lactate levels reached peak after 3min and then returned to baseline, also pointing into the direction of *increases* in oxidative metabolism or CMRO₂ over time (Frahm et al., 1996). Mangia and colleagues (Mangia et al., 2007) found *sustained* steady-state lactate levels over the time-courses of 5 and 10min visual stimulation, which would speak in favor of sustained CMRO₂ consumption over time. It is thus not clear whether we should expect CMRO₂ consumption to adapt, reach steady state levels or increase over time. Still, overall CMRO₂ increases would be expected, because even in presence of aerobic glycolysis, most of the metabolic needs are met via oxidative metabolism (Hoge & Pike, 2001; Mangia et al., 2007).

Overall, we could show that simultaneous acquisition of CMRO₂ and CMRglc is feasible in healthy subjects, comparing blocks of resting state to blocks of visual stimulation. We found task-induced, significant increases in CMRglc and smaller, but significant increases in CMRO₂ in visual ROIs. This made us confident to examine task-induced changes in CMRO₂ during a more complex cognitive design, although skipping simultaneous fPET measurements for the sake of decreasing drop-out rates, time needs and generally simplifying the study set-up.

4.2 Implications of Project II

In the second study, we used fully quantified measures of CMRO₂ to assess whether significant BOLD signal changes accurately reflected changes in oxidative metabolism. We were especially interested in BOLD signal decreases in the default mode network (DMN) and therefore employed an autobiographical memory task (MEM) to 'activate' DMN regions as well as a calculation task (CALC) to 'deactivate' DMN regions. Instead of simple visual stimulation, we used a complex cognitive design. Task-induced changes were compared to both an active control (CTRL) as well as a passive resting state (REST) baseline.

Task-induced changes in the BOLD signal

We were successful in eliciting large, consistent BOLD *increases* mainly in visual, frontoparietal control and dorsal attention networks as well as BOLD *decreases* in DMN regions as well as parts of auditory and somatomotor networks, comparing CALC versus CTRL or REST. These patterns were what we aimed for and reproduced the so-called ‘task-negative’ versus ‘task-positive’ fMRI BOLD networks as described by (M. D. Fox et al., 2005). Average BOLD-negative amplitudes were about two-thirds (versus CTRL) to half (versus REST) of average BOLD-positive amplitudes. During MEM, compared to CTRL, the BOLD signal showed an opposed pattern. Here, parts of the DMN showed BOLD signal *increases*, although the pattern was not as extensive and more left-lateralized than the BOLD-negative pattern during CALC, as also found in the literature (Davey et al., 2016). In contrast, parts of frontoparietal control and dorsal attention networks showed BOLD signal *decreases*. Again, the amplitude of BOLD *decreases* was about two-thirds of the amplitude of BOLD *increases*.

Task-induced changes in blood flow

As the blood flow is a major driver for BOLD signal changes, we expected to find similar changes in CBF as in the BOLD data. This was the case for the positive task contrasts, where we found strong CBF increases during CALC and MEM. For negative task contrasts, the picture was not as clear. As described in the introduction, the DMN was first discovered in PET data, showing decreased CBF in a range of active compared to passive tasks, and replicated with ASL measurements (A.-L. Lin et al., 2010; Pfefferbaum et al., 2011; G. L. Shulman, FIEZ, et al., 1997). Thus, we expected to find CBF decreases in DMN regions. In our data, CBF decreases were more consistent during CALC when compared to REST than when compared to CTRL. Yet, when compared to the active control task, the extent of significant CBF-negative regions was quite small. On average, CBF-negative ROIs were much more focal than the extended BOLD-negative ROIs. Across all voxels within the BOLD-negative ROI, CBF decreased significantly, but decreases were rather small, only 12-30% of CBF *increases*.

Task-induced changes in oxygen consumption

As expected in canonical neurovascular coupling, we expected to get concomitant increases in CMRO₂ in regions with BOLD increases. Even though the relative share of nonoxidative metabolism has been shown to increase during task execution, still most of the increased energy needs are met via oxidative metabolism (Hoge & Pike, 2001). First, we were successful in showing task-induced changes in CMRO₂ with a cognitive design. Our whole-brain group results showed regions with consistent task-induced *increases* in BOLD as well as extended regions with *increases* in CMRO₂ during CALC (versus both CTRL and REST) and during MEM (versus CTRL), overlapping with BOLD-positive regions. On the other hand, the CMRO₂ data only showed a few small clusters with significant *decreases*. Yet, as described in the introduction, the empirical basis of negative BOLD signals is still unclear. It has been suggested by Raichle that negative BOLD responses are the result of inverted neurovascular and neurometabolic coupling and thus are based on large decreases in CBF and smaller decreases in CMRO₂ (Raichle et al., 2001). Our data did not support this assumption. A recent study comparing CMRglc and fMRI BOLD responses specifically in DMN versus frontoparietal and DAN areas also showed larger regional overlap for activations than for deactivations (Godbersen et al., 2023). We therefore aimed to quantify to which extent the negative and positive group BOLD ROIs mirrored concomitant decreases and increases in oxygen consumption. While BOLD-*positive* voxels

on average showed significant *increases* of 2.6% (CALC vs. REST or CTRL) up to 4% (MEM vs. CTRL), BOLD-*negative* voxels showed, on average, only very small CMRO2 decreases (-0.2% CALC vs. REST) or even *increases* (1.5% CALC vs. CTRL). This led us to conclude that, while positive BOLD signal changes represent increased oxidative metabolism, negative BOLD signal changes do not necessarily reflect decreased oxygen consumption. This result supports a recent FDG-PET study, showing consistent BOLD decreases in a working memory task compared to a resting state, but without concomitant decreases in glucose metabolism (Stiernman et al., 2021). There is also empirical evidence from animal studies that negative BOLD signals can arise despite increased or stable levels of neuronal activity (Schridde et al., 2008; Shih et al., 2011; Takata et al., 2018). Second, we suspected different coupling mechanisms for negative and positive BOLD responses. This contradicts the assumptions of Raichle and colleagues (Raichle et al., 2001), who simply assumed inverted coupling underlying negative BOLD. To explain the occurrence of negative BOLD signal changes despite stable CMRO2, we compared our empirical data to predictions of the Davis model. The empirical data fit very well to the theoretical model as visualized in Fig. M1|B. On average, between half and two-thirds of all voxels with significant BOLD *decreases* did show *increases* in CMRO2 (displayed as d) and e) in Fig. M1|B). It makes sense that increases in CMRO2 correlate with negative BOLD when not compensated by CBF changes, as oxygen consumption increases dHb levels in the venous blood. In our data, BOLD signal decreases reflected either mainly vascular effects, i.e. decreases in fractional CBF, or a combination of decreases in fractional CBF and increases in fractional CMRO2. As both of these mechanisms increase dHb levels, even small changes in this combination can lead to substantial BOLD signal decreases.

The default mode network – a heterogeneous region

Nevertheless, the picture is more complex when looking at the different voxels that make up the large BOLD-negative ROI. While metabolic decreases in our data were in general not very prominent, parts of the DMN still showed decreased CMRO2 during CALC, especially when compared to REST. These clusters with concomitant CMRO2 decreases were present in all main parts of the DMN, but were much smaller than the extended CALC-negative BOLD regions. Conversely, substantial parts of BOLD-negative DMN regions showed increased CMRO2 (about half to two-third of the voxels). This lets us conclude that the DMN is a heterogeneous network, as multiple studies have emphasized in the past (Andrews-Hanna et al., 2014b; DiNicola et al., 2019; Leech et al., 2011). Our data suggest that the DMN does not suspend its activity as a whole network during externally oriented tasks, but rather increases its activity in some parts while reducing its activity in other parts. This view also fits with several functional connectivity studies, which found that parts of the DMN were recruited during executive function and that especially frontoparietal network activity was coupled to DMN activity to support goal-directed action (A. C. Chen et al., 2013; Crittenden et al., 2015; González-García et al., 2018; Spreng et al., 2010, 2013; Vatansever et al., 2015). A recent study, comparing CMRglc and fMRI BOLD during a Tetris task as well as a working memory task found that, found that both tasks exhibited consistent BOLD deactivation in the DMN. Nevertheless, while small parts of dorsal posterior cingulate (PCC) also showed decreases in CMRglc during the Tetris task, other parts of ventro-medial PCC (vmPCC) showed increases in CMRglc (Godbersen et al., 2023), as previously reported (Stiernman et al., 2021). The authors suggested that cognitive control as during the working memory task induces a metabolically expensive suppression in vmPCC, and that heightened activity in the frontoparietal network is correlated to heightened metabolism in vmPCC. In our data, we also see a division between dorsal parts of the PCC, that rather show CMRO2 decreases, an ventral parts without concomitant CMRO2 decreases, similar to (Leech et al., 2011). This could be explained by

characteristics of our calculation task, where participants had to keep the differential number in mind in order to calculate the solution, similar to a working memory task. But this hypothesis remains speculation and needs to be tested by comparison to a different task without working memory load.

Possible explanations for the dissociations in CMRO2 and BOLD

Thus, heterogeneity within the DMN has been found in several studies but is usually explained by task differences. Yet, these hypotheses do not explain the biophysical basics that have to be met for a negative BOLD signal to occur despite increases in metabolism. The biophysical Davis model predicts that dissociations of BOLD and CMRO2 responses are possible in both the positive and negative domain. Yet, our empirical data shows that this is more often the case for negative BOLD responses. This could be region-specific, or inherent to negative BOLD responses in general. As mentioned in the introduction, the Davis model already implies some non-linearities of CBF-CMRO2-BOLD coupling in the negative domain. The spacing of contours in Fig. M1|B gets smaller when the BOLD response is negative, but also when both CBF and CMRO2 responses are negative. This implicates that relatively small *decreases* in CBF and CMRO2 can already cause a BOLD response with a larger absolute amplitude than the same *increases* in CBF and CMRO2. Thus, based on the Davis model, we assume slight differences in CBF-CMRO2-BOLD coupling in the negative domain.

Additionally, research suggests that DMN regions might have a different architecture than other cortical regions. Mullins and colleagues (Lawley et al., 2017; Rogan et al., 2022; Rossetti et al., 2021b) found hypoxia-induced reversal of task-induced BOLD patterns specifically in the DMN despite stable neuronal activity, although this could not be measured but was concluded from stable behavioral results. The reversal of the BOLD pattern, i.e. negative BOLD during the memory task, thus may have resulted from constant metabolic demands, but reduced flow increases due to hypoxia so that CBF increases were smaller than CMRO2 increases, leading to a negative BOLD response. Yet, task-induced CBF responses were not measured during hypoxia in comparison to normoxia, so these explanations remain speculative. Partly, their could be explained by differences in vascular responsiveness in the DMN. The dynamic range of blood flow and blood volume is influenced by the density of vessels, and in turn stronger BOLD responses are expected in regions with denser vascularization (Ances et al., 2008; A. D. Ekstrom, 2021; Harrison, 2002). But whether differences in vascularization are specific to DMN regions and sufficient to reverse the BOLD response in hypoxia needs to be tested.

We tried to address the question of restricted vascular responsiveness of DMN regions by identifying an area within the DMN on the group level that showed both significant BOLD signal *decreases* during CALC as well as *increases* during MEM. In this way, differences underlying the positive versus negative BOLD response cannot be explained by a difference in vascularization. In this ROI, the average positive BOLD response was +0.16%, thus smaller in amplitude than the negative BOLD response with -0.22% and in the same range as negative BOLD amplitudes during CALC. Nevertheless, despite consistent *negative* BOLD responses, two-thirds of the voxels showed CMRO2 *increases* during CALC. Despite the rather small BOLD *increase*, oxygen consumption within this area was higher than in BOLD-positive areas during CALC. Firstly, this shows that the amplitude of BOLD response is not indicative of the amplitude of the CMRO2 response. Secondly, this also shows that the underlying metabolic differences between negative and positive BOLD were not simply a problem of reduced sensitivity due to smaller negative BOLD amplitudes in negative BOLD regions. Additionally, this result speaks in favor of restricted vascular responses in the DMN, as a larger

CMRO2 increase in this DMN overlap region is coupled to a relatively weaker flow response, thus we have a smaller CBF-CMRO2 coupling in the DMN compared to frontoparietal or DAN regions. In summary, a combination of both explanations, different neurovascular coupling in the negative domain as well as restricted vascular responsiveness of DMN regions, seems plausible, although perhaps not sufficient.

Furthermore, differences in localization of negative BOLD responses versus CMRO2 responses can occur due to different reasons. First, researchers showed the occurrence of negative BOLD effects in voxels with high proportions of venous blood and CSF, e.g. close to pial veins downstream from activated sites (Bianciardi et al., 2011). Also, while oxygen is consumed at the site of neuronal activity, changes in CBF (and CBV) are more widespread (Attwell & Iadecola, 2002; Kaplan et al., 2020), yet it is not clear how this fact would influence positive and negative BOLD responses differently.

CBF and CMRO2 as indicators of the excitation-inhibition balance

Another biological explanation for negative BOLD responses is inhibitory activity. Studies confirmed that GABA concentration increased with BOLD signal deactivations in the PCC, a core region of the DMN (Koush et al., 2021b) and that higher GABA levels at baseline correlate with stronger BOLD deactivations in the PCC (Hu et al., 2013). Yet, in every voxel, inhibitory and excitatory activity is present. A modeling study has shown that negative BOLD responses can arise from different scenarios of increases in excitatory versus inhibitory activity. If only inhibitory activity is increased, with no decrease or even small increases in overall excitatory activity, a negative BOLD response arises in combination with an *increase* in CMRO2 (Sotero & Trujillo-Barreto, 2007). Yet, with the same increase of inhibitory activity as just described, if overall excitatory activity drops below baseline levels, strong negative BOLD signals arise together with CMRO2 *decreases*. In this case, increased activity of inhibitory neurons leads to overall suppression of excitatory activity in a larger population. This latter case can explain BOLD decreases in small parts of the DMN where we found concomitant CMRO2 decreases. Yet, only the first scenario of active suppression without decreases in overall excitatory activity can explain the results in large parts of the DMN where we found negative BOLD response with stable or increased CMRO2. In general, CMRO2 is supposed to be largely driven by excitatory activity, while CBF is influenced by both excitatory and inhibitory activity (Buxton, 2021; Buxton et al., 2014). CMRO2 and CBF are driven in parallel, and controlled by different mechanisms, see review by (Lauritzen et al., 2012). Thus, the exact balance of inhibition and excitation per voxel is crucial for the resulting CBF, CMRO2 and finally BOLD changes. For future studies that study the basics of BOLD signal increases and decreases, measures of GABA, glutamate and lactate together with CBF and CMRO2 may be necessary to shed light on underlying processes.

Conclusions of Study II

All in all, positive BOLD signals are mostly coupled to increases in oxidative metabolism, whereas negative BOLD signals are no reliable proxy for decreases in oxidative metabolism. While increases in oxygen consumption can go hand in hand with active inhibition, even together with small increases in excitatory activity, they are not compatible with overall decreased neuronal activity. Thus, from a negative BOLD response alone we cannot infer reduced neuronal activity levels.

4.3 Limitations

The aim of both projects described in this thesis was to fully quantify both CMRglc and CMRO2. To meet this goal, we acquired subject-specific hematocrit, changes in R2' and CBF as well as changes in total CBV. However, since CMRglc and CMRO2 cannot be measured directly, the full quantification of both parameters is still relying on some assumptions:

To gain subject specific maps of CMRglc, subjects got [¹⁸F]-FDG injected intravenously, while subject-specific arterial input functions were derived via continuous arterial sampling. The quantification of CMRglc then relied on Patlak modeling to deduce Ki maps, which were then multiplied by plasma glucose values and divided by a lumped constant (LC). The exact CMRglc values thus depend on the LC used, and different values between 0.4 and 0.8 have been proposed, see review of (Knudsen et al., 2004). However, a recent study suggested that the LC is also dependent on the physiological state, so that CMRglc during activation may be overestimated by up to 50% (Angleys et al., 2018). In our study, with a LC of 0.65 (Wu, 2003) we got global grey-matter CMRglc values of 27.4 $\mu\text{mol}/100\text{g}/\text{min}$, which is in the expected range, but depends on the LC used. Additionally, we cannot be sure whether task-induced increases in CMRglc were over-estimated.

On the other hand, the calculation of CMRO2 relies on Fick's principle. This formula calculates CMRO2 from a multiplication of oxygen delivery, product of CBF and the arterial oxygen content of blood, with oxygen extraction, OEF. To calculate CMRO2, only the venous contributions to OEF are relevant as they quantify how much of the oxygen was used, assuming that arterial CBV is fully oxygenated. However, with contrast-agent CBV measurements, we only measured total CBV and had no means for estimating the venous contributions in the baseline or during task states. Studies estimated that at baseline 70-80% of total CBV is venous, but that the majority of task-induced total CBV increases is arterial (Hua et al., 2019). A 7T study estimated 29% of total CBV increases during a visual task being venous (Huber et al., 2014). Depending on the measured changes in total CBV in contrast to changes in CBF, this can have a big influence on the calculation of CMRO2, as large increases in CBV will result in smaller estimates of CMRO2. During visual stimulation in Project I, we measured large total increases in CBV in visual cortex, with big influences on our CMRO2 estimation. In contrast, in Project II, CBV increases did not play a crucial part in our CMRO2 estimation. Comparing CMRO2 changes after correction for total CBV changes, versus without correcting for CBV changes, only resulted in a 0.2% difference; CMRO2 percent change values were 2.6% (positive ROI) and 1.5% (negative ROI) in the uncorrected case, versus 2.4% and 1.7% in the corrected case. The conclusion of this is twofold: first, stimulus-induced CBV changes in visual cortex are larger than task-induced CBV changes in association areas as the frontoparietal control networks and the DMN. Second, in Study I, our measured CBV changes were in the same range as the CBF changes, leading to the massive influence on the CMRO2 calculation. We assume that the pCASL sequence on the Siemens scanner with the 12k head-coil had a lower SNR than equal measurements on the Philips scanner in Study II, with a 32k head-coil. Additionally, the labeling efficiency was probably higher at the Philips scanner, where we planned the labeling plane manually, while this was done automatically in Study I. We conclude that high sensitivity of CBF measurements as well as the exact measurement of venous volume changes are crucial to correctly estimate CMRO2.

Another limitation of both studies is the lack of time resolution in both CMRglc and CMRO2 measurements. Task changes were estimated during blocks of 5-7 minutes, and these task blocks had to be repeated at least twice (for T2* and pCASL measurements), so adaptation effects cannot be excluded. We tried to test this in a control sample, included in Study II, by measuring fMRI BOLD changes during extended 3min task blocks. Here, we did not find any adaptation effect. Additionally,

we looked at time-resolved CBF and could not find an adaptation effect within any of the task conditions either. Yet, we do not know how CBV and $R2'$ and finally CMRO2 changes behave over time. Even though it is in theory possible to calculate CMR_{glc} in smaller task blocks of 1min (Jamadar, Ward, Carey, et al., 2019; Rischka et al., 2018), the signal-to-noise ratio makes it hard to detect and quantify task-induced changes. Concerning CMRO2 quantification, $R2'$ and CBV measurements via multi-echo T2* and dynamic susceptibility mapping made shorter task blocks impossible.

Furthermore, CBF as well as $R2'$ measurements are rather noisy and due to unfavorable error propagation this also affected CMRO2 calculation. It could be argued that due to the low signal-to-noise ratio we did not find CBF and CMRO2 deactivations in BOLD-negative ROIs in Study II. Yet, with the same methods, we were able to find CBF and CMRO2 *increases* in BOLD-*positive* ROIs. Albeit the amplitude of negative BOLD responses was roughly about two-thirds of the positive BOLD response, amplitudes of CBF and CMRO2 changes were much lower than two-thirds of CBF and CMRO2, which speaks against similar CBF-CMRO2 coupling within positive and negative BOLD ROIs and cannot simply be explained by a lower SNR.

Finally, $R2'$, CBV, CBF and BOLD measurements were done sequentially and not simultaneously. Even though there are dual-echo EPI sequences to measure CBF and BOLD simultaneously, this usually is at the expense of sensitivity loss of one of the signals. However, newer methods claim to achieve similar sensitivity with a multi-echo approach, with the potential to even derive $\Delta R2^*$ (Devi et al., 2022a).

5 Outlook

Three main aspects of mqBOLD as presented in this work have to be addressed for it to be broadly applicable. First, acquisition duration has to be reduced. The long scan time primarily stems from sequential measurements of T2, T2*, pCASL and DSC in all conditions (except for T2, only measured in baseline). Simultaneous measurements of at least some of the sequences could improve efficiency while measuring exactly the same processes. Recent developments with multi-echo simultaneous ASL EPI-BOLD sequences have shown improved sensitivity for mapping CBF changes. Devi and colleagues could show improved Δ CBF mapping with a pCASL-prepared ME-DEPICTING sequence while the contrast-to-noise ratio of the simultaneously measured BOLD signal was not affected (Devi et al., 2022a). This multi-echo sequence also allows for absolute $R2^*$ mapping, thus, only additional measurements of baseline T2 as well as baseline and task CBV would be necessary. Alternatively, $\Delta R2'$ could be estimated from BOLD signal changes, as shown in Study II, with additional baseline $R2'$ mapping to quantify the changes (Fujita et al., 2006), as shown in Study II, for an overview over $R2'$ mapping methods see (J. J. Chen et al., 2022). The advantage of these approaches is that only absolute baseline values need to be quantified, while $\Delta T2^*$ can be measured simultaneously with CBF changes during task conditions in a block-design. In the case of Study II, this would have saved additional pCASL measurements of three conditions, corresponding to 18 min. Likewise, VASO (vascular space occupancy) sequences are able to measure BOLD and CBV simultaneously (Huber et al., 2019), which would still require additional baseline CBV and $R2'$ mapping as well as CBF measurements.

Second, measuring the temporal dynamics of CMRO2 and its underlying parameters is crucial to gain understanding of the underlying processes that drive oxygen consumption. The main limitation here is the SNR of the CBF measurements as well as the non-dynamic nature of multi-echo T2* mapping. The aforementioned multi-echo EPI approach could be a solution to mapping both $\Delta T2^*$

and ΔCBF in a time-resolved manner. Likewise, VASO could be used to map fractional CBV changes during blocks employing several conditions in a time-resolved manner. In summary, a goal in future studies should be to measure time-resolved changes in CMRO_2 , for example by combining baseline quantification of CBV and R_2' with time-resolved simultaneous measurements of T_2^* and ASL plus time-resolved VASO-CBV.

Third, the main limitation to measure absolute CMRO_2 in the baseline as well as in different task states is the quantification of baseline OEF. Baseline OEF, CBF and ultimately CMRO_2 values are affected by various diseases as well as healthy ageing (J. J. Chen et al., 2022; Hashem & Dunn, 2021). This can influence temporal dynamics and amplitudes of the BOLD signal and even vary across healthy subjects. BOLD signal amplitudes are especially not comparable between healthy subjects and certain patient groups, so quantitative measurements of baseline oxygenation can be a valuable tool in the clinical routine (Buxton, 2010; Buxton et al., 2014; Hashem & Dunn, 2021; Simon & Buxton, 2015). Yet, absolute quantification via MRI remains a challenge. Calibrated fMRI studies either assume a fixed baseline OEF value or employ both hypercapnia and hyperoxia to map absolute baseline CMRO_2 , so-called dual calibrated BOLD (Germuska & Wise, 2019; Merola et al., 2018; Rodgers et al., 2016). In the mqBOLD framework, OEF is calculated via R_2' mapping and DSC measurements. Non-invasive CBV mapping is also possible, for an overview over different arterial and venous CBV measurement methods see (Hua et al., 2019). For future research, the goal should be to quantify absolute CBV in the baseline condition and map venous CBV changes in task conditions. VASO sequences are able to measure fractional changes in total CBV in several conditions and measurement of fractional venous CBV can be done by a few techniques including e.g. venous refocusing for volume estimation (VERVE) (Hua et al., 2019). So, in order to quantify absolute baseline CMRO_2 , either a combination of R_2' and absolute CBV in the baseline, or direct mapping of baseline OEF e.g. via Velocity-Selective Excitation with Arterial Nulling (VSEAN) is necessary (Hashem & Dunn, 2021; Jiang & Lu, 2022; Liu et al., 2019). In this work, we aimed for full quantification by measuring total CBV with an intravenous gadolinium-based contrast agent. This procedure requires venous injection of contrast agent, but provides good SNR. Additional measurements of subject specific venous hematocrit values made our calculations more accurate. In future studies, other, non-invasive procedures should be further explored and applied to cognitive designs in order to compare results to the mqBOLD approach used here.

Finally, additional measurements of glucose consumption together with CMRO_2 measurements provide important insights about oxidative versus non-oxidative metabolism across brain regions and in different task states. While this is relevant to gain further understanding about metabolic processes in the brain, quantitative fPET measurements require invasive injection of radioactive tracers plus arterial blood sampling. Because of the complex study setup and needs for a PET-MR scanner, simultaneous measurements of CMRO_2 and CMR_{glc} are, to date, not ready for extensive application. To further gain insight into non-oxidative metabolism, non-invasive spectroscopy measurements of lactate may be of interest in future research (R. G. Shulman et al., 2001). Additionally, the contribution of inhibitory and excitatory neuronal activity to task-induced increases in CBF, OEF and CMRO_2 via measurements of GABA and glutamate levels are promising (Hu et al., 2013; Koush et al., 2021b).

6 Conclusions

The absolute quantification of oxygen and glucose consumption is a promising tool for further understanding different mechanisms triggered by different types of neuronal activity in the human brain, as well as investigating impaired metabolism in different disease states. Absolute quantification enables the comparison of baseline brain metabolism across the cortex within the same subject, but also across subjects or across different populations. While the absolute measurement of glucose consumption requires a PET scanner and is relatively invasive, recent developments allow CMRO₂ mapping in a non-invasive way using MRI. The mqBOLD approach, with prospects to achieve baseline mapping of venous CBV, is a powerful tool for gaining insights about cognitive brain processes and disease processes. In contrast to fMRI BOLD, CMRO₂ is a physiological signal and directly measures oxidative brain metabolism, which is supposed to be more localized and is happening at the exact site of neuronal activation as opposed to BOLD and CBF measurements. Improvements of measurement time by simultaneously measuring some of the needed parameters may make CMRO₂ acquisitions also clinically relevant.

With this body of work, we have shown that CMRO₂ measurements in healthy human subjects, using the mqBOLD approach, are sensitive enough to show task-induced changes in a cognitive design. Further, by comparing fMRI BOLD with CMRO₂, we provided evidence that negative BOLD responses are not necessarily indicative of reduced oxygen metabolism and thereby not indicative of reduced excitatory brain activity. Rather, while parts of the DMN showed task-induced decreases in oxygen metabolism, around half to two-thirds of DMN voxels with BOLD-signal decreases actually showed increased oxygen consumption, which may be an indicator of active inhibitory suppression. Additional measurements of GABA and glutamate may be necessary to test this hypothesis. Additionally, improved time resolution will be important for future studies to shed light on the timings of task-induced changes.

All in all, the presented findings fundamentally questions our commonly accepted interpretation of positive, but specifically negative BOLD responses as indicators for increased and decreased neuronal activity, and might settle arguments regarding the interpretation of negative BOLD responses.

REFERENCES

- 1 Aanerud, J., Borghammer, P., Chakravarty, M. M., Vang, K., Rodell, A. B., Jónsdóttir, K. Y., Møller, A., Ashkanian, M., Vafae, M. S., Iversen, P., Johannsen, P., & Gjedde, A. (2012). Brain Energy Metabolism and Blood Flow Differences in Healthy Aging. *Journal of Cerebral Blood Flow & Metabolism*, *32*(7), 1177–1187. <https://doi.org/10.1038/jcbfm.2012.18>
- 2 Ances, B. M., Leontiev, O., Perthen, J. E., Liang, C., Lansing, A. E., & Buxton, R. B. (2008). Regional differences in the coupling of cerebral blood flow and oxygen metabolism changes in response to activation: Implications for BOLD-fMRI. *NeuroImage*, *39*(4), 1510–1521. <https://doi.org/10.1016/j.neuroimage.2007.11.015>
- 3 Andrews-Hanna, J. R. (2012). The Brain's Default Network and Its Adaptive Role in Internal Mentation. *The Neuroscientist*, *18*(3), 251–270. <https://doi.org/10.1177/1073858411403316>
- 4 Andrews-Hanna, J. R., Reidler, J. S., Sepulcre, J., Poulin, R., & Buckner, R. L. (2010). Functional-Anatomic Fractionation of the Brain's Default Network. *Neuron*, *65*(4), 550–562. <https://doi.org/10.1016/j.neuron.2010.02.005>
- 5 Andrews-Hanna, J. R., Saxe, R., & Yarkoni, T. (2014a). Contributions of episodic retrieval and mentalizing to autobiographical thought: Evidence from functional neuroimaging, resting-state connectivity, and fMRI meta-analyses. *NeuroImage*, *91*, 324–335. <https://doi.org/10.1016/j.neuroimage.2014.01.032>
- 6 Andrews-Hanna, J. R., Saxe, R., & Yarkoni, T. (2014b). Contributions of episodic retrieval and mentalizing to autobiographical thought: Evidence from functional neuroimaging, resting-state connectivity, and fMRI meta-analyses. *NeuroImage*, *91*, 324–335. <https://doi.org/10.1016/j.neuroimage.2014.01.032>
- 7 Angleys, H., Jespersen, S. N., & Østergaard, L. (2018). The effects of capillary transit time heterogeneity on the BOLD signal. *Human Brain Mapping*, *39*(6), 2329–2352. <https://doi.org/10.1002/hbm.23991>
- 8 Anticevic, A., Cole, M. W., Murray, J. D., Corlett, P. R., Wang, X.-J., & Krystal, J. H. (2012). The role of default network deactivation in cognition and disease. *Trends in Cognitive Sciences*, *16*(12), 584–592. <https://doi.org/10.1016/j.tics.2012.10.008>
- 9 Anticevic, A., Repovs, G., Shulman, G. L., & Barch, D. M. (2010). When less is more: TPJ and default network deactivation during encoding predicts working memory performance. *NeuroImage*, *49*(3), 2638–2648. <https://doi.org/10.1016/j.neuroimage.2009.11.008>
- 10 Attwell, D., & Iadecola, C. (2002). The neural basis of functional brain imaging signals. *Trends in Neurosciences*, *25*(12), 621–625.
- 11 Baudrexel, S., Volz, S., Preibisch, C., Klein, J. C., Steinmetz, H., Hilker, R., & Deichmann, R. (2009). Rapid single-scan T_2^* -mapping using exponential excitation pulses and image-based correction for linear background gradients: T_2^* Mapping With Field Gradient Correction. *Magnetic Resonance in Medicine*, *62*(1), 263–268. <https://doi.org/10.1002/mrm.21971>
- 12 Beckett, A. J. S., Dadakova, T., Townsend, J., Huber, L., Park, S., & Feinberg, D. A. (2020). Comparison of BOLD and CBV using 3D EPI and 3D GRASE for cortical layer functional MRI at 7 T. *Magnetic Resonance in Medicine*, *84*(6), 3128–3145. <https://doi.org/10.1002/mrm.28347>

- 13 Bednařík, P., Tkáč, I., Giove, F., DiNuzzo, M., Deelchand, D. K., Emir, U. E., Eberly, L. E., & Mangia, S. (2015). Neurochemical and BOLD Responses during Neuronal Activation Measured in the Human Visual Cortex at 7 Tesla. *Journal of Cerebral Blood Flow & Metabolism*, *35*(4), 601–610. <https://doi.org/10.1038/jcbfm.2014.233>
- 14 Bentley, W. J., Li, J. M., Snyder, A. Z., Raichle, M. E., & Snyder, L. H. (2016). Oxygen Level and LFP in Task-Positive and Task-Negative Areas: Bridging BOLD fMRI and Electrophysiology. *Cerebral Cortex*, *26*(1), 346–357. <https://doi.org/10.1093/cercor/bhu260>
- 15 Bianciardi, M., Fukunaga, M., van Gelderen, P., de Zwart, J. A., & Duyn, J. H. (2011). Negative BOLD-fMRI Signals in Large Cerebral Veins. *Journal of Cerebral Blood Flow & Metabolism*, *31*(2), 401–412. <https://doi.org/10.1038/jcbfm.2010.164>
- 16 Blazey, T., Snyder, A. Z., Goyal, M. S., Vlassenko, A. G., & Raichle, M. E. (2018). A systematic meta-analysis of oxygen-to-glucose and oxygen-to-carbohydrate ratios in the resting human brain. *PLOS ONE*, *13*(9), e0204242. <https://doi.org/10.1371/journal.pone.0204242>
- 17 Blazey, T., Snyder, A. Z., Su, Y., Goyal, M. S., Lee, J. J., Vlassenko, A. G., Arbeláez, A. M., & Raichle, M. E. (2018). Quantitative positron emission tomography reveals regional differences in aerobic glycolysis within the human brain. *Journal of Cerebral Blood Flow & Metabolism*, *0271678X1876700*. <https://doi.org/10.1177/0271678X18767005>
- 18 Blockley, N. P., Griffeth, V. E. M., & Buxton, R. B. (2012). A general analysis of calibrated BOLD methodology for measuring CMRO₂ responses: Comparison of a new approach with existing methods. *NeuroImage*, *60*(1), 279–289. <https://doi.org/10.1016/j.neuroimage.2011.11.081>
- 19 Blockley, N. P., Griffeth, V. E. M., Simon, A. B., & Buxton, R. B. (2013). A review of calibrated blood oxygenation level-dependent (BOLD) methods for the measurement of task-induced changes in brain oxygen metabolism: A REVIEW OF CALIBRATED BOLD METHODS. *NMR in Biomedicine*, *26*(8), 987–1003. <https://doi.org/10.1002/nbm.2847>
- 20 Blockley, N. P., Griffeth, V. E. M., Simon, A. B., Dubowitz, D. J., & Buxton, R. B. (2015). Calibrating the BOLD response without administering gases: Comparison of hypercapnia calibration with calibration using an asymmetric spin echo. *NeuroImage*, *104*, 423–429. <https://doi.org/10.1016/j.neuroimage.2014.09.061>
- 21 Boillat, Y., Xin, L., van der Zwaag, W., & Gruetter, R. (2020). Metabolite concentration changes associated with positive and negative BOLD responses in the human visual cortex: A functional MRS study at 7 Tesla. *Journal of Cerebral Blood Flow & Metabolism*, *40*(3), 488–500. <https://doi.org/10.1177/0271678X19831022>
- 22 Boorman, L., Kennerley, A. J., Johnston, D., Jones, M., Zheng, Y., Redgrave, P., & Berwick, J. (2010). Negative Blood Oxygen Level Dependence in the Rat: A Model for Investigating the Role of Suppression in Neurovascular Coupling. *Journal of Neuroscience*, *30*(12), 4285–4294. <https://doi.org/10.1523/JNEUROSCI.6063-09.2010>
- 23 Bright, M. G., Croal, P. L., Blockley, N. P., & Bulte, D. P. (2019). Multiparametric measurement of cerebral physiology using calibrated fMRI. *NeuroImage*, *187*, 128–144. <https://doi.org/10.1016/j.neuroimage.2017.12.049>
- 24 Buckner, R., Andrews-Hanna, J., & Schacter, D. (2008). The Brain's Default Network: Anatomy, Function, and Relevance to Disease. *Annals of the New York Academy of Sciences*, *1124*, 1–38.

- 25 Buckner, R. L., & DiNicola, L. M. (2019). The brain's default network: Updated anatomy, physiology and evolving insights. *Nature Reviews Neuroscience*, *20*(10), 593–608. <https://doi.org/10.1038/s41583-019-0212-7>
- 26 Bulte, D. P., Kelly, M., Germuska, M., Xie, J., Chappell, M. A., Okell, T. W., Bright, M. G., & Jezzard, P. (2012). Quantitative measurement of cerebral physiology using respiratory-calibrated MRI. *NeuroImage*, *60*(1), 582–591. <https://doi.org/10.1016/j.neuroimage.2011.12.017>
- 27 Buxton, R. B. (2010). Interpreting oxygenation-based neuroimaging signals: The importance and the challenge of understanding brain oxygen metabolism. *Frontiers in Neuroenergetics*. <https://doi.org/10.3389/fnene.2010.00008>
- 28 Buxton, R. B. (2021). *The thermodynamics of thinking: Connections between neural activity, energy metabolism and blood flow*.
- 29 Buxton, R. B., Griffeth, V. E. M., Simon, A. B., & Moradi, F. (2014). Variability of the coupling of blood flow and oxygen metabolism responses in the brain: A problem for interpreting BOLD studies but potentially a new window on the underlying neural activity. *Frontiers in Neuroscience*, *8*. <https://doi.org/10.3389/fnins.2014.00139>
- 30 Buxton, R. B., Uludağ, K., Dubowitz, D. J., & Liu, T. T. (2004). Modeling the hemodynamic response to brain activation. *NeuroImage*, *23*, S220–S233. <https://doi.org/10.1016/j.neuroimage.2004.07.013>
- 31 Byrne, J. H., Heidelberger, R., & Waxham, M. N. (Hrsg.). (2014). *From molecules to networks: An introduction to cellular and molecular neuroscience* (Third edition). Elsevier/AP, Academic Press is an imprint of Elsevier.
- 32 Castrillon, G., Epp, S., Bose, A., Fraticelli, L., Hechler, A., Belenya, R., Ranft, A., Yakushev, I., Utz, L., Sundar, L., Rauschecker, J. P., Preibisch, C., Kurcyus, K., & Riedl, V. (2023). *An energy costly architecture of neuromodulators for human brain evolution and cognition* [Preprint]. *Neuroscience*. <https://doi.org/10.1101/2023.04.25.538209>
- 33 Chen, A. C., Oathes, D. J., Chang, C., Bradley, T., Zhou, Z.-W., Williams, L. M., Glover, G. H., Deisseroth, K., & Etkin, A. (2013). Causal interactions between fronto-parietal central executive and default-mode networks in humans. *Proceedings of the National Academy of Sciences*, *110*(49), 19944–19949. <https://doi.org/10.1073/pnas.1311772110>
- 34 Chen, J. J., & Pike, G. B. (2009). BOLD-specific cerebral blood volume and blood flow changes during neuronal activation in humans: BOLD-SPECIFIC CHANGES IN CBV AND CBF. *NMR in Biomedicine*, *22*(10), 1054–1062. <https://doi.org/10.1002/nbm.1411>
- 35 Chen, J. J., Uthayakumar, B., & Hyder, F. (2022). Mapping oxidative metabolism in the human brain with calibrated fMRI in health and disease. *Journal of Cerebral Blood Flow & Metabolism*, *42*(7), 1139–1162. <https://doi.org/10.1177/0271678X221077338>
- 36 Christen, T., Schmiedeskamp, H., Straka, M., Bammer, R., & Zaharchuk, G. (2012). Measuring brain oxygenation in humans using a multiparametric quantitative blood oxygenation level dependent MRI approach. *Magnetic Resonance in Medicine*, *68*(3), 905–911. <https://doi.org/10.1002/mrm.23283>
- 37 Crittenden, B. M., Mitchell, D. J., & Duncan, J. (2015). Recruitment of the default mode network during a demanding act of executive control. *ELife*, *4*, e06481. <https://doi.org/10.7554/eLife.06481>

- 38 Daselaar, S. M., Prince, S. E., & Cabeza, R. (2004). When less means more: Deactivations during encoding that predict subsequent memory. *NeuroImage*, 23(3), 921–927. <https://doi.org/10.1016/j.neuroimage.2004.07.031>
- 39 Davey, C. G., Pujol, J., & Harrison, B. J. (2016). Mapping the self in the brain's default mode network. *NeuroImage*, 132, 390–397. <https://doi.org/10.1016/j.neuroimage.2016.02.022>
- 40 Davis, T. L., Kwong, K. K., Weisskoff, R. M., & Rosen, B. R. (1998). Calibrated functional MRI: Mapping the dynamics of oxidative metabolism. *Proceedings of the National Academy of Sciences*, 95(4), 1834–1839. <https://doi.org/10.1073/pnas.95.4.1834>
- 41 Deery, H. A., Di Paolo, R., Moran, C., Egan, G. F., & Jamadar, S. D. (2023). Lower brain glucose metabolism in normal ageing is predominantly frontal and temporal: A systematic review and pooled effect size and activation likelihood estimates meta-analyses. *Human Brain Mapping*, 44(3), 1251–1277. <https://doi.org/10.1002/hbm.26119>
- 42 Devi, R., Lepsien, J., Lorenz, K., Schlumm, T., Mildner, T., & Möller, H. E. (2022a). Multi-echo investigations of positive and negative CBF and concomitant BOLD changes. *NeuroImage*, 263, 119661. <https://doi.org/10.1016/j.neuroimage.2022.119661>
- 43 Devi, R., Lepsien, J., Lorenz, K., Schlumm, T., Mildner, T., & Möller, H. E. (2022b). Multi-echo investigations of positive and negative CBF and concomitant BOLD changes. *NeuroImage*, 263, 119661. <https://doi.org/10.1016/j.neuroimage.2022.119661>
- 44 Di, X., & Biswal, and Alzheimer's Disease Neu, B. B. (2012). Metabolic Brain Covariant Networks as Revealed by FDG-PET with Reference to Resting-State fMRI Networks. *Brain Connectivity*, 2(5), 275–283. <https://doi.org/10.1089/brain.2012.0086>
- 45 DiNicola, L. M., Braga, R. M., & Buckner, R. L. (2019). *Parallel Distributed Networks Dissociate Episodic and Social Functions Within the Individual* [Preprint]. Neuroscience. <https://doi.org/10.1101/733048>
- 46 Donahue, M. J., Blicher, J. U., Østergaard, L., Feinberg, D. A., MacIntosh, B. J., Miller, K. L., Günther, M., & Jezzard, P. (2009). Cerebral blood flow, blood volume, and oxygen metabolism dynamics in human visual and motor cortex as measured by whole-brain multi-modal magnetic resonance imaging. *Journal of cerebral blood flow and metabolism*, 29(11), 1856–1866. <https://doi.org/10.1038/jcbfm.2009.107>
- 47 Drew, P. J. (2019). Vascular and neural basis of the BOLD signal. *Current Opinion in Neurobiology*, 58, 61–69. <https://doi.org/10.1016/j.conb.2019.06.004>
- 48 Ekstrom, A. (2010). How and when the fMRI BOLD signal relates to underlying neural activity: The danger in dissociation. *Brain Research Reviews*, 62(2), 233–244. <https://doi.org/10.1016/j.brainresrev.2009.12.004>
- 49 Ekstrom, A. D. (2021). Regional variation in neurovascular coupling and why we still lack a Rosetta Stone. *Philosophical Transactions of the Royal Society B: Biological Sciences*, 376(1815), 20190634. <https://doi.org/10.1098/rstb.2019.0634>
- 50 Engl, E., & Attwell, D. (2015). Non-signalling energy use in the brain. *The Journal of Physiology*, 593(16), 3417–3429. <https://doi.org/10.1113/jphysiol.2014.282517>
- 51 Foster, B. L., Dastjerdi, M., & Parvizi, J. (2012). Neural populations in human posteromedial cortex display opposing responses during memory and numerical processing. *Proceedings of*

- the National Academy of Sciences*, 109(38), 15514–15519.
<https://doi.org/10.1073/pnas.1206580109>
- 52 Fox, K. C. R., Foster, B. L., Kucyi, A., Daitch, A. L., & Parvizi, J. (2018). Intracranial Electrophysiology of the Human Default Network. *Trends in Cognitive Sciences*, 22(4), 307–324. <https://doi.org/10.1016/j.tics.2018.02.002>
 - 53 Fox, M. D., Snyder, A. Z., Vincent, J. L., Corbetta, M., & Raichle, M. E. (2005). The human brain is intrinsically organized into dynamic, anticorrelated functional networks. *Proceedings of the National Academy of Sciences of the United States of America*, 6.
 - 54 Fox, P., Raichle, M., Mintun, M., & Dence, C. (1988). Nonoxidative glucose consumption during focal physiologic neural activity. *Science*, 241(4864), 462–464. <https://doi.org/10.1126/science.3260686>
 - 55 Fox, P. T., & Raichle, M. E. (1986a). Focal physiological uncoupling of cerebral blood flow and oxidative metabolism during somatosensory stimulation in human subjects. *Proceedings of the National Academy of Sciences*, 83(4), 1140–1144. <https://doi.org/10.1073/pnas.83.4.1140>
 - 56 Fox, P. T., & Raichle, M. E. (1986b). Focal physiological uncoupling of cerebral blood flow and oxidative metabolism during somatosensory stimulation in human subjects. *Proceedings of the National Academy of Sciences*, 83(4), 1140–1144. <https://doi.org/10.1073/pnas.83.4.1140>
 - 57 Frahm, J., Krüger, G., Merboldt, K. D., & Kleinschmidt, A. (1996). Dynamic uncoupling and recoupling of perfusion and oxidative metabolism during focal brain activation in man. *Magnetic Resonance in Medicine*, 35(2), 143–148. <https://doi.org/10.1002/mrm.1910350202>
 - 58 Fujita, N. (2003). Quantitative mapping of cerebral deoxyhemoglobin content using MR imaging. *NeuroImage*, 20(4), 2071–2083. <https://doi.org/10.1016/j.neuroimage.2003.06.002>
 - 59 Fujita, N., Matsumoto, K., Tanaka, H., Watanabe, Y., & Murase, K. (2006). Quantitative study of changes in oxidative metabolism during visual stimulation using absolute relaxation rates. *NMR in Biomedicine*, 19(1), 60–68. <https://doi.org/10.1002/nbm.1001>
 - 60 Gagnon, L., Sakadžić, S., Lesage, F., Pouliot, P., Dale, A. M., Devor, A., Buxton, R. B., & Boas, D. A. (2016). Validation and optimization of hypercapnic-calibrated fMRI from oxygen-sensitive two-photon microscopy. *Philosophical Transactions of the Royal Society B: Biological Sciences*, 371(1705), 20150359. <https://doi.org/10.1098/rstb.2015.0359>
 - 61 Germuska, M., & Wise, R. G. (2019). Calibrated fMRI for mapping absolute CMRO₂: Practicalities and prospects. *NeuroImage*, 187, 145–153. <https://doi.org/10.1016/j.neuroimage.2018.03.068>
 - 62 Gilbert, S. J., Bird, G., Frith, C. D., & Burgess, P. W. (2012). Does “Task Difficulty” Explain “Task-Induced Deactivation?”. *Frontiers in Psychology*, 3. <https://doi.org/10.3389/fpsyg.2012.00125>
 - 63 Godbersen, G. M., Klug, S., Wadsak, W., Pichler, V., Raitanen, J., Rieckmann, A., Stiernman, L., Cocchi, L., Breakspear, M., Hacker, M., Lanzenberger, R., & Hahn, A. (2023). Task-evoked metabolic demands of the posteromedial default mode network are shaped by dorsal attention and frontoparietal control networks. *eLife*, 12, e84683. <https://doi.org/10.7554/eLife.84683>
 - 64 Goense, J., Merkle, H., & Logothetis, N. K. (2012). High-Resolution fMRI Reveals Laminar Differences in Neurovascular Coupling between Positive and Negative BOLD Responses. *Neuron*, 76(3), 629–639. <https://doi.org/10.1016/j.neuron.2012.09.019>

- 65 González-García, C., Flounders, M. W., Chang, R., Baria, A. T., & He, B. J. (2018). Content-specific activity in frontoparietal and default-mode networks during prior-guided visual perception. *ELife*, 7. <https://doi.org/10.7554/eLife.36068>
- 66 Gordon, E. M., Laumann, T. O., Marek, S., Raut, R. V., Gratton, C., Newbold, D. J., Greene, D. J., Coalson, R. S., Snyder, A. Z., Schlaggar, B. L., Petersen, S. E., Dosenbach, N. U. F., & Nelson, S. M. (2020). Default-mode network streams for coupling to language and control systems. *Proceedings of the National Academy of Sciences*, 202005238. <https://doi.org/10.1073/pnas.2005238117>
- 67 Göttler, J., Kaczmarz, S., Kallmayer, M., Wustrow, I., Eckstein, H.-H., Zimmer, C., Sorg, C., Preibisch, C., & Hyder, F. (2019). Flow-metabolism uncoupling in patients with asymptomatic unilateral carotid artery stenosis assessed by multi-modal magnetic resonance imaging. *Journal of Cerebral Blood Flow & Metabolism*, 39(11), 2132–2143. <https://doi.org/10.1177/0271678X18783369>
- 68 Greicius, M. D., Krasnow, B., Reiss, A. L., & Menon, V. (2003). Functional connectivity in the resting brain: A network analysis of the default mode hypothesis. *Proceedings of the National Academy of Sciences*, 100(1), 253–258. <https://doi.org/10.1073/pnas.0135058100>
- 69 Griffeth, V. E. M., Blockley, N. P., Simon, A. B., & Buxton, R. B. (2013). A New Functional MRI Approach for Investigating Modulations of Brain Oxygen Metabolism. *PLoS ONE*, 8(6), e68122. <https://doi.org/10.1371/journal.pone.0068122>
- 70 Griffeth, V. E. M., Perthen, J. E., & Buxton, R. B. (2012). *Prospects for Quantitative fMRI: Investigating the Effects of Caffeine on Baseline Oxygen Metabolism and the Response to a Visual Stimulus in Humans*. 21.
- 71 Griffeth, V. E. M., Simon, A. B., & Buxton, R. B. (2015). The coupling of cerebral blood flow and oxygen metabolism with brain activation is similar for simple and complex stimuli in human primary visual cortex. *NeuroImage*, 104, 156–162. <https://doi.org/10.1016/j.neuroimage.2014.10.003>
- 72 Grubb, R. L., Raichle, M. E., Eichling, J. O., & Ter-Pogossian, M. M. (1974). The Effects of Changes in Pa CO₂ Cerebral Blood Volume, Blood Flow, and Vascular Mean Transit Time. *Stroke*, 5(5), 630–639. <https://doi.org/10.1161/01.STR.5.5.630>
- 73 Gu, H., Hu, Y., Chen, X., He, Y., & Yang, Y. (2019a). Regional excitation-inhibition balance predicts default-mode network deactivation via functional connectivity. *NeuroImage*, 185, 388–397. <https://doi.org/10.1016/j.neuroimage.2018.10.055>
- 74 Gu, H., Hu, Y., Chen, X., He, Y., & Yang, Y. (2019b). Regional excitation-inhibition balance predicts default-mode network deactivation via functional connectivity. *NeuroImage*, 185, 388–397. <https://doi.org/10.1016/j.neuroimage.2018.10.055>
- 75 Hahn, A., Breakspear, M., Rischka, L., Wadsak, W., Godbersen, G. M., Pichler, V., Michenthaler, P., Vanicek, T., Hacker, M., Kasper, S., Lanzenberger, R., & Cocchi, L. (2020). Reconfiguration of functional brain networks and metabolic cost converge during task performance. *ELife*, 9, e52443. <https://doi.org/10.7554/eLife.52443>
- 76 Hahn, A., Gryglewski, G., Nics, L., Hienert, M., Rischka, L., Vranka, C., Sigurdardottir, H., Vanicek, T., James, G. M., Seiger, R., Kautzky, A., Silberbauer, L., Wadsak, W., Mitterhauser, M., Hacker, M., Kasper, S., & Lanzenberger, R. (2016). Quantification of Task-Specific Glucose Metabolism with Constant Infusion of 18F-FDG. *Journal of Nuclear Medicine*, 57(12), 1933–1940. <https://doi.org/10.2967/jnumed.116.176156>

- 77 Hahn, A., Gryglewski, G., Nics, L., Rischka, L., Ganger, S., Sigurdardottir, H., Vranka, C., Silberbauer, L., Vanicek, T., Kautzky, A., Wadsak, W., Mitterhauser, M., Hartenbach, M., Hacker, M., Kasper, S., & Lanzenberger, R. (2017). Task-relevant brain networks identified with simultaneous PET/MR imaging of metabolism and connectivity. *Brain Structure and Function*. <https://doi.org/10.1007/s00429-017-1558-0>
- 78 Harrison, R. V. (2002). Blood Capillary Distribution Correlates with Hemodynamic-based Functional Imaging in Cerebral Cortex. *Cerebral Cortex*, *12*(3), 225–233. <https://doi.org/10.1093/cercor/12.3.225>
- 79 Hashem, M., & Dunn, J. F. (2021). Brain Oximetry and the Quest for Quantified Metabolic Rate: Applications Using MRI and Near-Infrared Spectroscopy. *Applied Magnetic Resonance*, *52*(10), 1343–1377. <https://doi.org/10.1007/s00723-021-01345-y>
- 80 Hayden, B. Y., Smith, D. V., & Platt, M. L. (2009). Electrophysiological correlates of default-mode processing in macaque posterior cingulate cortex. *Proceedings of the National Academy of Sciences*, *106*(14), 5948–5953. <https://doi.org/10.1073/pnas.0812035106>
- 81 He, X., & Yablonskiy, D. A. (2007). Quantitative BOLD: Mapping of human cerebral deoxygenated blood volume and oxygen extraction fraction: Default state. *Magnetic Resonance in Medicine*, *57*(1), 115–126. <https://doi.org/10.1002/mrm.21108>
- 82 Henriksen, O. M., Gjedde, A., Vang, K., Law, I., Aanerud, J., & Rostrup, E. (2021). Regional and interindividual relationships between cerebral perfusion and oxygen metabolism. *Journal of Applied Physiology*, *130*(6), 1836–1847. <https://doi.org/10.1152/jappphysiol.00939.2020>
- 83 Henriksen, O. M., Vestergaard, M. B., Lindberg, U., Aachmann-Andersen, N. J., Lisbjerg, K., Christensen, S. J., Rasmussen, P., Olsen, N. V., Forman, J. L., Larsson, H. B. W., & Law, I. (2018). Interindividual and regional relationship between cerebral blood flow and glucose metabolism in the resting brain. *Journal of Applied Physiology*, *125*(4), 1080–1089. <https://doi.org/10.1152/jappphysiol.00276.2018>
- 84 Hillman, E. M. C. (2014). Coupling Mechanism and Significance of the BOLD Signal: A Status Report. *Annual Review of Neuroscience*, *37*(1), 161–181. <https://doi.org/10.1146/annurev-neuro-071013-014111>
- 85 Hirsch, N. M., & Preibisch, C. (2013). T2* Mapping with Background Gradient Correction Using Different Excitation Pulse Shapes. *American Journal of Neuroradiology*, *34*(6), E65–E68. <https://doi.org/10.3174/ajnr.A3021>
- 86 Hirsch, N. M., Toth, V., Förchler, A., Kooijman, H., Zimmer, C., & Preibisch, C. (2014). Technical considerations on the validity of blood oxygenation level-dependent-based MR assessment of vascular deoxygenation: BOLD-BASED ASSESSMENT OF VASCULAR DEOXYGENATION. *NMR in Biomedicine*, *27*(7), 853–862. <https://doi.org/10.1002/nbm.3131>
- 87 Hoge, R. D., & Pike, G. B. (2001). Oxidative metabolism and the detection of neuronal activation via imaging. *Journal of Chemical Neuroanatomy*, *22*(1–2), 43–52. [https://doi.org/10.1016/S0891-0618\(01\)00114-4](https://doi.org/10.1016/S0891-0618(01)00114-4)
- 88 Hu, Y., Chen, X., Gu, H., & Yang, Y. (2013). Resting-State Glutamate and GABA Concentrations Predict Task-Induced Deactivation in the Default Mode Network. *Journal of Neuroscience*, *33*(47), 18566–18573. <https://doi.org/10.1523/JNEUROSCI.1973-13.2013>

- 89 Hua, J., Liu, P., Kim, T., Donahue, M., Rane, S., Chen, J. J., Qin, Q., & Kim, S.-G. (2019). MRI techniques to measure arterial and venous cerebral blood volume. *NeuroImage*, *187*, 17–31. <https://doi.org/10.1016/j.neuroimage.2018.02.027>
- 90 Huang, S. C., Phelps, M. E., Hoffman, E. J., Sideris, K., Selin, C. J., & Kuhl, D. E. (1980). Noninvasive determination of local cerebral metabolic rate of glucose in man. *American Journal of Physiology-Endocrinology and Metabolism*, *238*(1), E69–E82. <https://doi.org/10.1152/ajpendo.1980.238.1.E69>
- 91 Huber, L., Goense, J., Kennerley, A. J., Ivanov, D., Krieger, S. N., Lepsien, J., Trampel, R., Turner, R., & Möller, H. E. (2014). Investigation of the neurovascular coupling in positive and negative BOLD responses in human brain at 7T. *NeuroImage*, *97*, 349–362. <https://doi.org/10.1016/j.neuroimage.2014.04.022>
- 92 Huber, L., Uludağ, K., & Möller, H. E. (2019). Non-BOLD contrast for laminar fMRI in humans: CBF, CBV, and CMRO₂. *NeuroImage*, *197*, 742–760. <https://doi.org/10.1016/j.neuroimage.2017.07.041>
- 93 Huijbers, W., Vannini, P., Sperling, R. A., C.M., P., Cabeza, R., & Daselaar, S. M. (2012). Explaining the encoding/retrieval flip: Memory-related deactivations and activations in the posteromedial cortex. *Neuropsychologia*, *50*(14), 3764–3774. <https://doi.org/10.1016/j.neuropsychologia.2012.08.021>
- 94 Hyder, D. S. F. (2010a). Neurovascular and neurometabolic couplings in dynamic calibrated fMRI: Transient oxidative neuroenergetics for block-design and event-related paradigms. *Frontiers in Neuroenergetics*. <https://doi.org/10.3389/fnene.2010.00018>
- 95 Hyder, D. S. F. (2010b). Neurovascular and neurometabolic couplings in dynamic calibrated fMRI: transient oxidative neuroenergetics for block-design and event-related paradigms. *Frontiers in Neuroenergetics*, *2*. <https://doi.org/10.3389/fnene.2010.00018>
- 96 Hyder, F., Chase, J. R., Behar, K. L., Mason, G. F., Siddeek, M., Rothman, D. L., & Shulman, R. G. (1996). Increased tricarboxylic acid cycle flux in rat brain during forepaw stimulation detected with ¹H[¹³C]NMR. *Proceedings of the National Academy of Sciences*, *93*(15), 7612–7617. <https://doi.org/10.1073/pnas.93.15.7612>
- 97 Hyder, F., Herman, P., Bailey, C. J., Møller, A., Globinsky, R., Fulbright, R. K., Rothman, D. L., & Gjedde, A. (2016). Uniform distributions of glucose oxidation and oxygen extraction in gray matter of normal human brain: No evidence of regional differences of aerobic glycolysis. *Journal of Cerebral Blood Flow & Metabolism*, *36*(5), 903–916. <https://doi.org/10.1177/0271678X15625349>
- 98 Jamadar, S. D., Ward, P. G., Carey, A., McIntyre, R., Parkes, L., Sasan, D., Fallon, J., Li, S., Chen, Z., & Egan, G. F. (2019). *Constant Infusion Radiotracer Administration for High Temporal Resolution Positron Emission Tomography (PET) of the Human Brain: Application to [18F]-Fluorodeoxyglucose PET (FDG-PET)* [Preprint]. Neuroscience. <https://doi.org/10.1101/667352>
- 99 Jamadar, S. D., Ward, P. G., Li, S., Sforzini, F., Baran, J., Chen, Z., & Egan, G. F. (2019). Simultaneous task-based BOLD-fMRI and [18-F] FDG functional PET for measurement of neuronal metabolism in the human visual cortex. *NeuroImage*, *189*, 258–266. <https://doi.org/10.1016/j.neuroimage.2019.01.003>
- 100 Jamadar, S. D., Zhong, S., Carey, A., McIntyre, R., Ward, P. G. D., Fornito, A., Premaratne, M., Jon Shah, N., O'Brien, K., Stäb, D., Chen, Z., & Egan, G. F. (2021). Task-evoked simultaneous FDG-PET

- and fMRI data for measurement of neural metabolism in the human visual cortex. *Scientific Data*, 8(1), 267. <https://doi.org/10.1038/s41597-021-01042-2>
- 101 Jiang, D., & Lu, H. (2022). Cerebral oxygen extraction fraction MRI: Techniques and applications. *Magnetic Resonance in Medicine*, 88(2), 575–600. <https://doi.org/10.1002/mrm.29272>
- 102 Kaczmarz, S., Hyder, F., & Preibisch, C. (2020). Oxygen extraction fraction mapping with multi-parametric quantitative BOLD MRI: Reduced transverse relaxation bias using 3D-GraSE imaging. *NeuroImage*, 220, 117095. <https://doi.org/10.1016/j.neuroimage.2020.117095>
- 103 Kaplan, L., Chow, B. W., & Gu, C. (2020). Neuronal regulation of the blood–brain barrier and neurovascular coupling. *Nature Reviews Neuroscience*, 21(8), 416–432. <https://doi.org/10.1038/s41583-020-0322-2>
- 104 Kernbach, J. M., Yeo, B. T. T., Smallwood, J., Margulies, D. S., Thiebaut de Schotten, M., Walter, H., Sabuncu, M. R., Holmes, A. J., Gramfort, A., Varoquaux, G., Thirion, B., & Bzdok, D. (2018). Subspecialization within default mode nodes characterized in 10,000 UK Biobank participants. *Proceedings of the National Academy of Sciences*, 115(48), 12295–12300. <https://doi.org/10.1073/pnas.1804876115>
- 105 Kety, S. S., & Schmidt, C. F. (1945). THE DETERMINATION OF CEREBRAL BLOOD FLOW IN MAN BY THE USE OF NITROUS OXIDE IN LOW CONCENTRATIONS. *American Journal of Physiology-Legacy Content*, 143(1), 53–66. <https://doi.org/10.1152/ajplegacy.1945.143.1.53>
- 106 Kim, H. (2012). A dual-subsystem model of the brain's default network: Self-referential processing, memory retrieval processes, and autobiographical memory retrieval. *NeuroImage*, 61(4), 966–977. <https://doi.org/10.1016/j.neuroimage.2012.03.025>
- 107 Kim, S.-G., & Ogawa, S. (2012). Biophysical and Physiological Origins of Blood Oxygenation Level-Dependent fMRI Signals. *Journal of Cerebral Blood Flow & Metabolism*, 32(7), 1188–1206. <https://doi.org/10.1038/jcbfm.2012.23>
- 108 Kim, S.-G., Rostrup, E., Larsson, H. B. W., Ogawa, S., & Paulson, O. B. (1999). Determination of relative CMRO₂ from CBF and BOLD changes: Significant increase of oxygen consumption rate during visual stimulation. *Magnetic Resonance in Medicine*, 41(6), 1152–1161. [https://doi.org/10.1002/\(SICI\)1522-2594\(199906\)41:6<1152::AID-MRM11>3.0.CO;2-T](https://doi.org/10.1002/(SICI)1522-2594(199906)41:6<1152::AID-MRM11>3.0.CO;2-T)
- 109 Knudsen, G. M., Rostrup, E., & Hasselbalch, S. G. (2004). Quantitative PET for assessment of cerebral blood flow and glucose consumption under varying physiological conditions. *International Congress Series*, 1265, 189–200. <https://doi.org/10.1016/j.ics.2004.04.025>
- 110 Koshino, H., Minamoto, T., Ikeda, T., Osaka, M., Otsuka, Y., & Osaka, N. (2011). Anterior Medial Prefrontal Cortex Exhibits Activation during Task Preparation but Deactivation during Task Execution. *PLoS ONE*, 6(8), e22909. <https://doi.org/10.1371/journal.pone.0022909>
- 111 Koush, Y., de Graaf, R. A., Kupers, R., Dricot, L., Ptito, M., Behar, K. L., Rothman, D. L., & Hyder, F. (2021a). Metabolic underpinnings of activated and deactivated cortical areas in human brain. *Journal of Cerebral Blood Flow & Metabolism*, 41(5), 986–1000. <https://doi.org/10.1177/0271678X21989186>
- 112 Koush, Y., de Graaf, R. A., Kupers, R., Dricot, L., Ptito, M., Behar, K. L., Rothman, D. L., & Hyder, F. (2021b). Metabolic underpinnings of activated and deactivated cortical areas in human brain. *Journal of Cerebral Blood Flow & Metabolism*, 41(5), 986–1000. <https://doi.org/10.1177/0271678X21989186>

- 113 Kufer, J., Preibisch, C., Epp, S., Göttler, J., Schmitzer, L., Zimmer, C., Hyder, F., & Kaczmarz, S. (2022). Imaging effective oxygen diffusivity in the human brain with multiparametric magnetic resonance imaging. *Journal of Cerebral Blood Flow & Metabolism*, *42*(2), 349–363. <https://doi.org/10.1177/0271678X211048412>
- 114 Kushner, M. J., Rosenquist, A., Alavi, A., Rosen, M., Dann, R., Fazekas, F., Bosley, T., Greenberg, J., & Reivich, M. (1988). Cerebral metabolism and patterned visual Stimulation: A positron emission tomographic study of the human visual cortex. *Neurology*, *38*(1), 89–89. <https://doi.org/10.1212/WNL.38.1.89>
- 115 Lauritzen, M., Mathiesen, C., Schaefer, K., & Thomsen, K. J. (2012). Neuronal inhibition and excitation, and the dichotomic control of brain hemodynamic and oxygen responses. *NeuroImage*, *62*(2), 1040–1050. <https://doi.org/10.1016/j.neuroimage.2012.01.040>
- 116 Lawley, J. S., Macdonald, J. H., Oliver, S. J., & Mullins, P. G. (2017). Unexpected reductions in regional cerebral perfusion during prolonged hypoxia: Hypoxia and regional cerebral blood flow. *The Journal of Physiology*, *595*(3), 935–947. <https://doi.org/10.1113/JP272557>
- 117 Leech, R., Braga, R., & Sharp, D. J. (2012). Echoes of the Brain within the Posterior Cingulate Cortex. *Journal of Neuroscience*, *32*(1), 215–222. <https://doi.org/10.1523/JNEUROSCI.3689-11.2012>
- 118 Leech, R., Kamourieh, S., Beckmann, C. F., & Sharp, D. J. (2011). Fractionating the Default Mode Network: Distinct Contributions of the Ventral and Dorsal Posterior Cingulate Cortex to Cognitive Control. *Journal of Neuroscience*, *31*(9), 3217–3224. <https://doi.org/10.1523/JNEUROSCI.5626-10.2011>
- 119 Leech, R., & Sharp, D. J. (2014). The role of the posterior cingulate cortex in cognition and disease. *Brain*, *137*(1), 12–32. <https://doi.org/10.1093/brain/awt162>
- 120 Liang, X., Zou, Q., He, Y., & Yang, Y. (2013). Coupling of functional connectivity and regional cerebral blood flow reveals a physiological basis for network hubs of the human brain. *Proceedings of the National Academy of Sciences*, *110*(5), 1929–1934. <https://doi.org/10.1073/pnas.1214900110>
- 121 Lin, A.-L., Fox, P. T., Hardies, J., Duong, T. Q., & Gao, J.-H. (2010). Nonlinear coupling between cerebral blood flow, oxygen consumption, and ATP production in human visual cortex. *Proceedings of the National Academy of Sciences*, *107*(18), 8446–8451. <https://doi.org/10.1073/pnas.0909711107>
- 122 Lin, A.-L., Fox, P. T., Yang, Y., Lu, H., Tan, L.-H., & Gao, J.-H. (2008). Evaluation of MRI models in the measurement of CMRO₂ and its relationship with CBF. *Magnetic Resonance in Medicine*, *60*(2), 380–389. <https://doi.org/10.1002/mrm.21655>
- 123 Lin, P., Hasson, U., Jovicich, J., & Robinson, S. (2011). A Neuronal Basis for Task-Negative Responses in the Human Brain. *Cerebral Cortex*, *21*(4), 821–830. <https://doi.org/10.1093/cercor/bhq151>
- 124 Liu, E. Y., Guo, J., Simon, A. B., Haist, F., Dubowitz, D. J., & Buxton, R. B. (2019). The potential for gas-free measurements of absolute oxygen metabolism during both baseline and activation states in the human brain. *NeuroImage*, *116*342. <https://doi.org/10.1016/j.neuroimage.2019.116342>

- 125 Logothetis, N. K. (2003). The Underpinnings of the BOLD Functional Magnetic Resonance Imaging Signal. *The Journal of Neuroscience*, 23(10), 3963–3971. <https://doi.org/10.1523/JNEUROSCI.23-10-03963.2003>
- 126 Logothetis, N. K. (2008). What we can do and what we cannot do with fMRI. *Nature*, 453(7197), 869–878. <https://doi.org/10.1038/nature06976>
- 127 Logothetis, N. K., Pauls, J., Augath, M., Trinath, T., & Oeltermann, A. (2001). *Neurophysiological investigation of the basis of the fMRI signal*. 412.
- 128 Lowry, J. P., & Fillenz, M. (1997). Evidence for uncoupling of oxygen and glucose utilization during neuronal activation in rat striatum. *The Journal of Physiology*, 498(2), 497–501. <https://doi.org/10.1113/jphysiol.1997.sp021875>
- 129 Madsen, P. L., Hasselbalch, S. G., Hagemann, L. P., Olsen, K. S., Bülow, J., Holm, S., Wildschjødtz, G., Paulson, O. B., & Lassen, N. A. (1995). Persistent Resetting of the Cerebral Oxygen/Glucose Uptake Ratio by Brain Activation: Evidence Obtained with the Kety—Schmidt Technique. *Journal of Cerebral Blood Flow & Metabolism*, 15(3), 485–491. <https://doi.org/10.1038/jcbfm.1995.60>
- 130 Magistretti, P. J., & Allaman, I. (2018). Lactate in the brain: From metabolic end-product to signalling molecule. *Nature Reviews Neuroscience*, 19(4), 235–249. <https://doi.org/10.1038/nrn.2018.19>
- 131 Magistretti, P. J., & Pellerin, L. (1999). Cellular mechanisms of brain energy metabolism and their relevance to functional brain imaging. *Philosophical transactions of the Royal Society of London. Series B, Biological sciences*, 354(1387), 1155–1163. <https://doi.org/10.1098/rstb.1999.0471>
- 132 Mangia, S., Tkáč, I., Gruetter, R., Van De Moortele, P.-F., Maraviglia, B., & Ugurbil, K. (2007). Sustained neuronal activation raises oxidative metabolism to a new steady-state level: Evidence from ¹H NMR spectroscopy in the human visual cortex. *Journal of Cerebral Blood Flow & Metabolism*, 27, 1055–1063. <https://doi.org/10.1038/sj.jcbfm.9600401>
- 133 Mason, M. F., Norton, M. I., Van Horn, J. D., Wegner, D. M., Grafton, S. T., & Macrae, C. N. (2007). Wandering Minds: The Default Network and Stimulus-Independent Thought. *Science*, 315(5810), 393–395. <https://doi.org/10.1126/science.1131295>
- 134 Mayer, J. S., Roebroeck, A., Maurer, K., & Linden, D. E. J. (2009). Specialization in the default mode: Task-induced brain deactivations dissociate between visual working memory and attention. *Human Brain Mapping*, NA-NA. <https://doi.org/10.1002/hbm.20850>
- 135 Mayhew, S. D., Coleman, S. C., Mullinger, K. J., & Can, C. (2022a). Across the adult lifespan the ipsilateral sensorimotor cortex negative BOLD response exhibits decreases in magnitude and spatial extent suggesting declining inhibitory control. *NeuroImage*, 253, 119081. <https://doi.org/10.1016/j.neuroimage.2022.119081>
- 136 Mayhew, S. D., Coleman, S. C., Mullinger, K. J., & Can, C. (2022b). Across the adult lifespan the ipsilateral sensorimotor cortex negative BOLD response exhibits decreases in magnitude and spatial extent suggesting declining inhibitory control. *NeuroImage*, 253, 119081. <https://doi.org/10.1016/j.neuroimage.2022.119081>
- 137 Merola, A., Germuska, M. A., Murphy, K., & Wise, R. G. (2018). Assessing the repeatability of absolute CMRO₂, OEF and haemodynamic measurements from calibrated fMRI. *NeuroImage*, 173, 113–126. <https://doi.org/10.1016/j.neuroimage.2018.02.020>

- 138 Mevel, K., Chételat, G., Eustache, F., & Desgranges, B. (2011). The Default Mode Network in Healthy Aging and Alzheimer's Disease. *International Journal of Alzheimer's Disease*, 2011, 1–9. <https://doi.org/10.4061/2011/535816>
- 139 Minoshima, S., Giordani, B., Berent, S., Frey, K. A., Foster, N. L., & Kuhl, D. E. (1997). Metabolic reduction in the posterior cingulate cortex in very early Alzheimer's disease. *Annals of Neurology*, 42(1), 85–94. <https://doi.org/10.1002/ana.410420114>
- 140 Mintun, M. A., Lundstrom, B. N., Snyder, A. Z., Vlassenko, A. G., Shulman, G. L., & Raichle, M. E. (2001). Blood flow and oxygen delivery to human brain during functional activity: Theoretical modeling and experimental data. *Proceedings of the National Academy of Sciences*, 98(12), 6859–6864. <https://doi.org/10.1073/pnas.111164398>
- 141 Mintun, M. A., Raichle, M. E., & Martin, W. R. W. (1984). Brain Oxygen Utilization Measured with 0- 15 Radiotracers and Positron Emission Tomography. *The Journal of Nuclear Medicine*, 25(2).
- 142 Mintun, M. A., Vlassenko, A. G., Shulman, G. L., & Snyder, A. Z. (2002). Time-Related Increase of Oxygen Utilization in Continuously Activated Human Visual Cortex. *NeuroImage*, 16(2), 531–537. <https://doi.org/10.1006/nimg.2002.1114>
- 143 Mohan, A., Roberto, A. J., Mohan, A., Lorenzo, A., Jones, K., Carney, M. J., Liogier-Weyback, L., Hwang, S., & Lapidus, K. A. B. (o. J.). *The Significance of the Default Mode Network (DMN) in Neurological and Neuropsychiatric Disorders: A Review*.
- 144 Moon, H. S., Jiang, H., Vo, T. T., Jung, W. B., Vazquez, A. L., & Kim, S.-G. (2021). Contribution of Excitatory and Inhibitory Neuronal Activity to BOLD fMRI. *Cerebral Cortex*, 31(9), 4053–4067. <https://doi.org/10.1093/cercor/bhab068>
- 145 Moradi, F., Buračas, G. T., & Buxton, R. B. (2012). Attention strongly increases oxygen metabolic response to stimulus in primary visual cortex. *NeuroImage*, 59(1), 601–607. <https://doi.org/10.1016/j.neuroimage.2011.07.078>
- 146 Moradi, F., & Buxton, R. B. (2013). Adaptation of cerebral oxygen metabolism and blood flow and modulation of neurovascular coupling with prolonged stimulation in human visual cortex. *NeuroImage*, 82, 182–189. <https://doi.org/10.1016/j.neuroimage.2013.05.110>
- 147 Mosconi, L. (2005). Brain glucose metabolism in the early and specific diagnosis of Alzheimer's disease: FDG-PET studies in MCI and AD. *European Journal of Nuclear Medicine and Molecular Imaging*, 32(4), 486–510. <https://doi.org/10.1007/s00259-005-1762-7>
- 148 Mullinger, K. J., Mayhew, S. D., Bagshaw, A. P., Bowtell, R., & Francis, S. T. (2014). Evidence that the negative BOLD response is neuronal in origin: A simultaneous EEG–BOLD–CBF study in humans. *NeuroImage*, 94, 263–274. <https://doi.org/10.1016/j.neuroimage.2014.02.029>
- 149 Newberg, A. B., Wang, J., Rao, H., Swanson, R. L., Wintering, N., Karp, J. S., Alavi, A., Greenberg, J. H., & Detre, J. A. (2005). Concurrent CBF and CMRGlc changes during human brain activation by combined fMRI – PET scanning. *NeuroImage*, 28(2), 500–506. <https://doi.org/10.1016/j.neuroimage.2005.06.040>
- 150 Ogawa, S., Lee, T. M., Kay, A. R., & Tank, D. W. (1990). Brain magnetic resonance imaging with contrast dependent on blood oxygenation. *Proceedings of the National Academy of Sciences*, 87(24), 9868–9872. <https://doi.org/10.1073/pnas.87.24.9868>
- 151 Ogawa, S., Menon, R. S., Tank, D. W., Kim, S. G., Merkle, H., Ellermann, J. M., & Ugurbil, K. (1993). Functional brain mapping by blood oxygenation level-dependent contrast magnetic resonance

- imaging. A comparison of signal characteristics with a biophysical model. *Biophysical Journal*, 64(3), 803–812. [https://doi.org/10.1016/S0006-3495\(93\)81441-3](https://doi.org/10.1016/S0006-3495(93)81441-3)
- 152 Ossandon, T., Jerbi, K., Vidal, J. R., Bayle, D. J., Henaff, M.-A., Jung, J., Minotti, L., Bertrand, O., Kahane, P., & Lachaux, J.-P. (2011). Transient Suppression of Broadband Gamma Power in the Default-Mode Network Is Correlated with Task Complexity and Subject Performance. *Journal of Neuroscience*, 31(41), 14521–14530. <https://doi.org/10.1523/JNEUROSCI.2483-11.2011>
- 153 Pasley, B. N., Inglis, B. A., & Freeman, R. D. (2007). Analysis of oxygen metabolism implies a neural origin for the negative BOLD response in human visual cortex. *NeuroImage*, 36(2), 269–276. <https://doi.org/10.1016/j.neuroimage.2006.09.015>
- 154 Passow, S., Specht, K., Adamsen, T. C., Biermann, M., Brekke, N., Craven, A. R., Ersland, L., Grüner, R., Kleven-Madsen, N., Kvernenes, O.-H., Schwarzlmüller, T., Olesen, R. A., & Hugdahl, K. (2015). Default-mode network functional connectivity is closely related to metabolic activity: Metabolic Activity and DMN Connectivity. *Human Brain Mapping*, 36(6), 2027–2038. <https://doi.org/10.1002/hbm.22753>
- 155 Paulson, O. B., Hasselbalch, S. G., Rostrup, E., Knudsen, G. M., & Pelligrino, D. (2010). Cerebral Blood Flow Response to Functional Activation. *Journal of Cerebral Blood Flow & Metabolism*, 30(1), 2–14. <https://doi.org/10.1038/jcbfm.2009.188>
- 156 Pfefferbaum, A., Chanraud, S., Pitel, A.-L., Muller-Oehring, E., Shankaranarayanan, A., Alsop, D. C., Rohlfing, T., & Sullivan, E. V. (2011). Cerebral Blood Flow in Posterior Cortical Nodes of the Default Mode Network Decreases with Task Engagement but Remains Higher than in Most Brain Regions. *Cerebral Cortex*, 21(1), 233–244. <https://doi.org/10.1093/cercor/bhq090>
- 157 Preibisch, C., Volz, S., Anti, S., & Deichmann, R. (2008). Exponential excitation pulses for improved water content mapping in the presence of background gradients. *Magnetic Resonance in Medicine*, 60(4), 908–916. <https://doi.org/10.1002/mrm.21730>
- 158 Raichle, M. E., MacLeod, A. M., Snyder, A. Z., Powers, W. J., Gusnard, D. A., & Shulman, G. L. (2001). A default mode of brain function. *Proceedings of the National Academy of Sciences*, 98(2), 676–682. <https://doi.org/10.1073/pnas.98.2.676>
- 159 Reivich, M., Kuhl, D., Wolf, A., Greenberg, J., Phelps, M., Ido, T., Casella, V., Fowler, J., Hoffman, E., Alavi, A., Som, P., & Sokoloff, L. (1979). The [18F]fluorodeoxyglucose method for the measurement of local cerebral glucose utilization in man. *Circulation Research*, 44(1), 127–137. <https://doi.org/10.1161/01.RES.44.1.127>
- 160 Renvall, V., Nangini, C., & Hari, R. (2015). All that glitters is not BOLD: Inconsistencies in functional MRI. *Scientific Reports*, 4(1), 3920. <https://doi.org/10.1038/srep03920>
- 161 Restom, K., Perthen, J. E., & Liu, T. T. (2008). Calibrated fMRI in the medial temporal lobe during a memory-encoding task. *NeuroImage*, 40(4), 1495–1502. <https://doi.org/10.1016/j.neuroimage.2008.01.038>
- 162 Rischka, L., Godbersen, G. M., Pichler, V., Michenthaler, P., Klug, S., Klöbl, M., Ritter, V., Wadsak, W., Hacker, M., Kasper, S., Lanzenberger, R., & Hahn, A. (2021). Reliability of task-specific neuronal activation assessed with functional PET, ASL and BOLD imaging. *Journal of Cerebral Blood Flow & Metabolism*, 0271678X2110205. <https://doi.org/10.1177/0271678X211020589>
- 163 Rischka, L., Gryglewski, G., Pfaff, S., Vanicek, T., Hienert, M., Klöbl, M., Hartenbach, M., Haug, A., Wadsak, W., Mitterhauser, M., Hacker, M., Kasper, S., Lanzenberger, R., & Hahn, A. (2018). Reduced task durations in functional PET imaging with [18F]FDG approaching that of

- functional MRI. *NeuroImage*, 181(June), 323–330.
<https://doi.org/10.1016/j.neuroimage.2018.06.079>
- 164 Rodgers, Z. B., Detre, J. A., & Wehrli, F. W. (2016). MRI-based methods for quantification of the cerebral metabolic rate of oxygen. *Journal of Cerebral Blood Flow & Metabolism*, 36(7), 1165–1185. <https://doi.org/10.1177/0271678X16643090>
- 165 Rogan, M., Friend, A. T., Rossetti, G. M., Edden, R., Mikkelsen, M., Oliver, S. J., Macdonald, J. H., & Mullins, P. G. (2022). Hypoxia alters posterior cingulate cortex metabolism during a memory task: A 1H fMRS study. *NeuroImage*, 260, 119397.
<https://doi.org/10.1016/j.neuroimage.2022.119397>
- 166 Rossetti, G. M., d’Avossa, G., Rogan, M., Macdonald, J. H., Oliver, S. J., & Mullins, P. G. (2021a). Reversal of neurovascular coupling in the default mode network: Evidence from hypoxia. *Journal of Cerebral Blood Flow & Metabolism*, 41(4), 805–818.
<https://doi.org/10.1177/0271678X20930827>
- 167 Rossetti, G. M., d’Avossa, G., Rogan, M., Macdonald, J. H., Oliver, S. J., & Mullins, P. G. (2021b). Reversal of neurovascular coupling in the default mode network: Evidence from hypoxia. *Journal of Cerebral Blood Flow & Metabolism*, 41(4), 805–818.
<https://doi.org/10.1177/0271678X20930827>
- 168 Scherr, M., Utz, L., Tahmasian, M., Pasquini, L., Grothe, M. J., Rauschecker, J. P., Grimmer, T., Drzezga, A., Sorg, C., & Riedl, V. (2019). Effective connectivity in the default mode network is distinctively disrupted in Alzheimer’s disease-A simultaneous resting-state FDG-PET/fMRI study. *Human Brain Mapping*. <https://doi.org/10.1002/hbm.24517>
- 169 Schridde, U., Khubchandani, M., Motelow, J. E., Sangahalli, B. G., Hyder, F., & Blumenfeld, H. (2008). Negative BOLD with Large Increases in Neuronal Activity. *Cerebral Cortex*, 18(8), 1814–1827. <https://doi.org/10.1093/cercor/bhm208>
- 170 Shaw, K., Bell, L., Boyd, K., Grijseels, D. M., Clarke, D., Bonnar, O., Crombag, H. S., & Hall, C. N. (2021). Neurovascular coupling and oxygenation are decreased in hippocampus compared to neocortex because of microvascular differences. *Nature Communications*, 12(1), 3190.
<https://doi.org/10.1038/s41467-021-23508-y>
- 171 Shih, Y.-Y. I., Wey, H.-Y., De La Garza, B. H., & Duong, T. Q. (2011). Striatal and Cortical BOLD, Blood Flow, Blood Volume, Oxygen Consumption, and Glucose Consumption Changes in Noxious Forepaw Electrical Stimulation. *Journal of Cerebral Blood Flow & Metabolism*, 31(3), 832–841. <https://doi.org/10.1038/jcbfm.2010.173>
- 172 Shmuel, A., Yacoub, E., Pfeuffer, J., Van de Moortele, P.-F., Adriany, G., Hu, X., & Ugurbil, K. (2002). Sustained Negative BOLD, Blood Flow and Oxygen Consumption Response and Its Coupling to the Positive Response in the Human Brain. *Neuron*, 36(6), 1195–1210.
[https://doi.org/10.1016/S0896-6273\(02\)01061-9](https://doi.org/10.1016/S0896-6273(02)01061-9)
- 173 Shu, C. Y., Herman, P., Coman, D., Sangahalli, B. G., Wang, H., Juchem, C., Rothman, D. L., de Graaf, R. A., & Hyder, F. (2016). Brain region and activity-dependent properties of M for calibrated fMRI. *NeuroImage*, 125, 848–856.
<https://doi.org/10.1016/j.neuroimage.2015.10.083>
- 174 Shulman, G. L., Astafiev, S. V., McAvoy, M. P., d’Avossa, G., & Corbetta, M. (2007). Right TPJ Deactivation during Visual Search: Functional Significance and Support for a Filter Hypothesis. *Cerebral Cortex*, 17(11), 2625–2633. <https://doi.org/10.1093/cercor/bhl170>

- 175 Shulman, G. L., Corbetta, M., Buckner, R. L., Fiez, J. A., Miezin, F. M., Raichle, M. E., & Petersen, S. E. (1997). Common Blood Flow Changes across Visual Tasks: I. Increases in Subcortical Structures and Cerebellum but Not in Nonvisual Cortex. *Journal of Cognitive Neuroscience*, 9(5), 624–647. <https://doi.org/10.1162/jocn.1997.9.5.624>
- 176 Shulman, G. L., FIEZ, J. A., Corbetta, M., Buckner, R. L., Miezin, F. M., Raichle, M. E., & Petersen, S. E. (1997). Common Blood Flow Changes across Visual Tasks: II. Decreases in Cerebral Cortex. *Journal of cognitive neuroscience*, 9(5), 648–663. <https://doi.org/10.1162/jocn.1997.9.5.648>
- 177 Shulman, R. G., Hyder, F., & Rothman, D. L. (2001). Lactate efflux and the neuroenergetic basis of brain function. *NMR in Biomedicine*, 14(7–8), 389–396. <https://doi.org/10.1002/nbm.741>
- 178 Simon, A. B., & Buxton, R. B. (2015). Understanding the dynamic relationship between cerebral blood flow and the BOLD signal: Implications for quantitative functional MRI. *NeuroImage*, 116, 158–167. <https://doi.org/10.1016/j.neuroimage.2015.03.080>
- 179 Singh, K. D., & Fawcett, I. P. (2008). Transient and linearly graded deactivation of the human default-mode network by a visual detection task. *NeuroImage*, 41(1), 100–112. <https://doi.org/10.1016/j.neuroimage.2008.01.051>
- 180 Singhal, I., Soni, A. K., & Srinivasan, N. (2020). *Default(y) Mode Network: Important regions of DMN do not survive alterations in flip angles* [Preprint]. Neuroscience. <https://doi.org/10.1101/2020.07.09.196568>
- 181 Smallwood, J., Brown, K., Baird, B., & Schooler, J. W. (2012). Cooperation between the default mode network and the frontal-parietal network in the production of an internal train of thought. *Brain Research*, 1428, 60–70. <https://doi.org/10.1016/j.brainres.2011.03.072>
- 182 Sokoloff, L. (2008a). The physiological and biochemical bases of functional brain imaging. *Cognitive Neurodynamics*, 2(1), 1–5. <https://doi.org/10.1007/s11571-007-9033-x>
- 183 Sokoloff, L. (2008b). The physiological and biochemical bases of functional brain imaging. *Cognitive Neurodynamics*, 2(1), 1–5. <https://doi.org/10.1007/s11571-007-9033-x>
- 184 Sokoloff, L., Mangold, R., Wechsler, R. L., Kennedy, C., & Kety, S. S. (1955). THE EFFECT OF MENTAL ARITHMETIC ON CEREBRAL CIRCULATION AND METABOLISM 1. *Journal of Clinical Investigation*, 34(7 Pt 1), 1101–1108. <https://doi.org/10.1172/JCI103159>
- 185 Sotero, R. C., & Trujillo-Barreto, N. J. (2007). Modelling the role of excitatory and inhibitory neuronal activity in the generation of the BOLD signal. *NeuroImage*, 35(1), 149–165. <https://doi.org/10.1016/j.neuroimage.2006.10.027>
- 186 Spreng, R. N., Sepulcre, J., Turner, G. R., Stevens, W. D., & Schacter, D. L. (2013). Intrinsic Architecture Underlying the Relations among the Default, Dorsal Attention, and Frontoparietal Control Networks of the Human Brain. *Journal of Cognitive Neuroscience*, 25(1), 74–86. https://doi.org/10.1162/jocn_a_00281
- 187 Spreng, R. N., Stevens, W. D., Chamberlain, J. P., Gilmore, A. W., & Schacter, D. L. (2010). Default network activity, coupled with the frontoparietal control network, supports goal-directed cognition. *NeuroImage*, 53(1), 303–317. <https://doi.org/10.1016/j.neuroimage.2010.06.016>
- 188 Stefanovic, B., Warnking, J. M., & Pike, G. B. (2004). Hemodynamic and metabolic responses to neuronal inhibition. *NeuroImage*, 22(2), 771–778. <https://doi.org/10.1016/j.neuroimage.2004.01.036>

- 189 Stiernman, L. J., Grill, F., Hahn, A., Rischka, L., Lanzenberger, R., Panes Lundmark, V., Riklund, K., Axelsson, J., & Rieckmann, A. (2021). Dissociations between glucose metabolism and blood oxygenation in the human default mode network revealed by simultaneous PET-fMRI. *Proceedings of the National Academy of Sciences*, *118*(27), e2021913118. <https://doi.org/10.1073/pnas.2021913118>
- 190 Takata, N., Sugiura, Y., Yoshida, K., Koizumi, M., Hiroshi, N., Honda, K., Yano, R., Komaki, Y., Matsui, K., Suematsu, M., Mimura, M., Okano, H., & Tanaka, K. F. (2018). Optogenetic astrocyte activation evokes BOLD fMRI response with oxygen consumption without neuronal activity modulation. *Glia*, *66*(9), 2013–2023. <https://doi.org/10.1002/glia.23454>
- 191 Ter-Pogossian, M. M., Phelps, M. E., Hoffman, E. J., & Mullani, N. A. (1975). A Positron-Emission Transaxial Tomograph for Nuclear Imaging (PETT). *Radiology*, *114*(1), 89–98. <https://doi.org/10.1148/114.1.89>
- 192 Tomasi, D., & Volkow, N. D. (2011). Functional connectivity hubs in the human brain. *NeuroImage*, *57*(3), 908–917. <https://doi.org/10.1016/j.neuroimage.2011.05.024>
- 193 Tomasi, D., Wang, G.-J., & Volkow, N. D. (2013). Energetic cost of brain functional connectivity. *Proceedings of the National Academy of Sciences*, *110*(33), 13642–13647. <https://doi.org/10.1073/pnas.1303346110>
- 194 Uludağ, K., Dubowitz, D. J., Yoder, E. J., Restom, K., Liu, T. T., & Buxton, R. B. (2004). Coupling of cerebral blood flow and oxygen consumption during physiological activation and deactivation measured with fMRI. *NeuroImage*, *23*(1), 148–155. <https://doi.org/10.1016/j.neuroimage.2004.05.013>
- 195 Vafaei, M. S., Vang, K., Bergersen, L. H., & Gjedde, A. (2012). Oxygen consumption and blood flow coupling in human motor cortex during intense finger tapping: Implication for a role of lactate. *Journal of Cerebral Blood Flow & Metabolism*, *32*, 1859–1868. <https://doi.org/10.1038/jcbfm.2012.89>
- 196 Vaishnavi, S. N., Vlassenko, A. G., Rundle, M. M., Snyder, A. Z., Mintun, M. A., & Raichle, M. E. (2010). Regional aerobic glycolysis in the human brain. *Proceedings of the National Academy of Sciences*, *107*(41), 17757–17762. <https://doi.org/10.1073/pnas.1010459107>
- 197 Vatansever, D., Menon, D. K., Manktelow, A. E., Sahakian, B. J., & Stamatakis, E. A. (2015). Default Mode Dynamics for Global Functional Integration. *The Journal of Neuroscience*, *35*(46), 15254–15262. <https://doi.org/10.1523/JNEUROSCI.2135-15.2015>
- 198 Villien, M., Wey, H.-Y., Mandeville, J. B., Catana, C., Polimeni, J. R., Sander, C. Y., Zürcher, N. R., Chonde, D. B., Fowler, J. S., Rosen, B. R., & Hooker, J. M. (2014). Dynamic functional imaging of brain glucose utilization using fPET-FDG. *NeuroImage*, *100*, 192–199. <https://doi.org/10.1016/j.neuroimage.2014.06.025>
- 199 Vlassenko, A. G., Rundle, M. M., & Mintun, M. A. (2006). Human brain glucose metabolism may evolve during activation: Findings from a modified FDG PET paradigm. *NeuroImage*, *33*(4), 1036–1041. <https://doi.org/10.1016/j.neuroimage.2006.06.065>
- 200 Wang, S., Taren, A. A., Tepfer, L. J., & Smith, D. V. (2017). *Functional Parcellation of the Default Mode Network: A Large-Scale Meta-Analysis* [Preprint]. Neuroscience. <https://doi.org/10.1101/225375>
- 201 Warnock, G., Özbay, P. S., Kuhn, F. P., Nanz, D., Buck, A., Boss, A., & Rossi, C. (2018). Reduction of BOLD interference in pseudo-continuous arterial spin labeling: Towards quantitative fMRI.

Journal of Cerebral Blood Flow & Metabolism, 38(5), 847–856.
<https://doi.org/10.1177/0271678X17704785>

- 202 Wesolowski, R., Blockley, N. P., Driver, I. D., Francis, S. T., & Gowland, P. A. (2019). Coupling between cerebral blood flow and cerebral blood volume: Contributions of different vascular compartments. *NMR in Biomedicine*, 32(3), e4061. <https://doi.org/10.1002/nbm.4061>
- 203 Whittaker, J. R., Driver, I. D., Bright, M. G., & Murphy, K. (2016). The absolute CBF response to activation is preserved during elevated perfusion: Implications for neurovascular coupling measures. *NeuroImage*, 125, 198–207. <https://doi.org/10.1016/j.neuroimage.2015.10.023>
- 204 Wu, H. (2003). Measurement of the Global Lumped Constant for 2-Deoxy-2-[18F]Fluoro-D-Glucose in Normal Human Brain Using [15O]Water and 2-Deoxy-2-[18F]Fluoro-D-Glucose Positron Emission Tomography Imaging A Method with Validation Based on Multiple Methodologies. *Molecular Imaging & Biology*, 5(1), 32–41. [https://doi.org/10.1016/S1536-1632\(02\)00122-1](https://doi.org/10.1016/S1536-1632(02)00122-1)
- 205 Yablonskiy, D. A., & Haacke, E. M. (1994). Theory of NMR signal behavior in magnetically inhomogeneous tissues: The static dephasing regime. *Magnetic Resonance in Medicine*, 32(6), 749–763. <https://doi.org/10.1002/mrm.1910320610>
- 206 Yang, J., Ruchti, E., Petit, J.-M., Jourdain, P., Grenningloh, G., Allaman, I., & Magistretti, P. J. (2014). Lactate promotes plasticity gene expression by potentiating NMDA signaling in neurons. *Proceedings of the National Academy of Sciences*, 111(33), 12228–12233. <https://doi.org/10.1073/pnas.1322912111>
- 207 Zhang, Y., Yin, Y., Li, H., & Gao, J.-H. (2020). Measurement of CMRO₂ and its relationship with CBF in hypoxia with an extended calibrated BOLD method. *Journal of Cerebral Blood Flow & Metabolism*, 40(10), 2066–2080. <https://doi.org/10.1177/0271678X19885124>

ACKNOWLEDGEMENTS

First of all, I would like to thank my amazing supervisor Valentin for doing a great job in finding the right balance between supervision, support and providing possibilities to work independently. I really think I could not have found a better supervisor and a better working environment. Thanks to him, I never lost motivation on this long journey, even though COVID-19 gave me (and all my lab members) enough reasons to do so. Just in time, he, together with Gabi, initiated all the necessary infrastructural changes that made it possible to work on our data from home from the very beginning, which I am very grateful for. I will also never forget all the fun outings, retreats and hikes that we did as a lab and that made us grow together.

I also want to thank all of our lab members, a team that started small and keeps growing, but stays familiar and welcoming. Especially Gabriel and Kasia were a lot of fun and a great support in the beginning, Toni provided us all with self-made cake and André with discussions about statistics, and what I am most grateful for: the whole lab shares a great enthusiasm about food! Also thanks to all other members for sharing lunch conversations and ice cream, namely Laura, Roman, Mahnaz, Akhil and Jingxian, not to forget our lab adoptees Alyssa and Dani, with whom you can also have a great time outside of the lab.

I am also very thankful for the huge support of Christine from the very beginning and continuously throughout the years. I especially value her very honest and open attitude, which comes along with a cordial kindness. A big thank you also to Jessica, who supported us in DMN questions and to Lars, for supporting me through my TAC.

I also would like to thank the GSN, for providing financial support and an international, interdisciplinary and very welcoming environment through which I got to know Isabel, Cilia and Becky. We are also known in several mountain huts as the 'brains on tour' and continue exploring the mountains together.

Then, hugs go out to all members of the Möwennest: Matze, Silvi, Claudi, Marco, Aurelia, Romy, Gonza & Ryan, you are the best flat-mates one could dream of! I don't know how I would have survived through COVID and my PhD without you and all the chocolate, food and fun that comes along. An even bigger hug goes out to Max, who continuously supports me through all my journeys and adventures, inspires me to think critically and who bears with me when I am stressed and annoyed. I am grateful to be living in an environment that cares about each other, but also gets active about different (intersectional) social issues such as the climate crisis, capitalism, feminism and other important topics. I think that in the future, resilience will be more important than anything. Also, hugs go out to Dario for being a calm, yet inspiring island in turbulent PhD waters throughout the last months and to Steffi, Tom, Eva and the whole Klimacamp team for just being amazing.

Und nicht zuletzt möchte ich mich bei meiner Familie dafür bedanken, dass ihr mich zu einer kritischen und selbständigen Persönlichkeit gemacht habt. Danke an meine Eltern, dass ihr mich und generell uns Kinder bei den unterschiedlichsten Projekten und Träumen immer unterstützt und an uns geglaubt habt, und auch dafür, dass euch Äußerlichkeiten und Karriere nie wichtig waren. Umarmung auch an Rani und Tabi, ihr seid die besten Schwestis! Liebe Grüße von der Streberin.

CURRICULUM VITAE

School and university

- 10/2017 – 09/2023 **PhD student, Graduate School for Systemic Neurosciences;**
Ludwig-Maximilians-Universität, Munich, Germany
- 10/2012 - 06/2017 **Master of Science, Psychology;** Humboldt Universität, Berlin,
Germany
- 04/2013 – 12/2013 Stay abroad at Universidad Nacional de Córdoba, Argentina
- 10/2009 – 07/2012 **Bachelor of Science, Psychology;** Ludwig-Maximilians-Universität,
Munich, Germany
- 09/1999 – 06/2008 **Abitur (A-levels);** Gymnasium Vilshofen, Vilshofen a.d. Donau,
Germany

Professional experience

- 06/2018 – 06/2023 **Research associate, TUM Klinikum rechts der Isar,**
Neuroradiologie, Munich, Germany (neuroenergetics lab, PI:
Valentin Riedl)
- 06/2014 – 03/2018 **Student research assistant, Max-Planck-Institute for Human**
Development, Berlin, Germany (PI: Douglas Garrett)
- 06/2010 – 06/2012 **Working student at Siemens AG,** Learning Campus, Munich,
Germany

LIST OF PUBLICATIONS

Castrillón, G., **Epp, S.**, Bose, A., Fraticelli, L., Hechler, A., Belenya, R., Ranft, A., Yakushev, I., Utz, L., Sundar, L., Rauschecker, J. P., Preibisch, C., Kurcyus, K., & Riedl, V. (2023). An energy costly architecture of neuromodulators for human brain evolution and cognition [Preprint].

<https://doi.org/10.1101/2023.04.25.538209>

Eichhorn, H., Hammernik, K., Spieker, V., **Epp, S. M.**, Rueckert, D., Preibisch, C., Schnabel, J. A. (2023). Deep Learning-Based Detection of Motion-Affected k-Space Lines for T2*-Weighted MRI [Preprint].

<https://doi.org/10.48550/arXiv.2303.10987>

Kufer, J., Preibisch, C., **Epp, S.**, Göttler, J., Schmitzer, L., Zimmer, C., Hyder, F., & Kaczmarz, S. (2022). Imaging effective oxygen diffusivity in the human brain with multiparametric magnetic resonance imaging. *Journal of Cerebral Blood Flow & Metabolism*, 42(2), 349–363.

<https://doi.org/10.1177/0271678X211048412>

Garrett, D. D., Koosterman, N. A., **Epp, S. M.**, Chopurian, V., Kosciessa, J. Q., Waschke, L., Skowron, A., Shine, J. M., Perry, A., Salami, A., Rieckmann, A., Papenber, G., Wählin, Anders, Karalija, N., Andersson, M., Riklund, K., Lövdén, M., Bäckman, L., Nyber, L. & Lindenberger, U. (2022). Dynamic regulation of neural variability during working memory reflects dopamine, functional integration, and decision-making [Preprint]. *BioRxiv*, 2022.05.05.490687.

<https://doi.org/10.1101/2022.05.05.490687>

Garrett, D. D., **Epp, S. M.**, Kleemeyer, M., Lindenberger, U., & Polk, T. A. (2020). Higher performers upregulate brain signal variability in response to more feature-rich visual input. *Neuroimage*, 217, 116836.

<https://doi.org/10.1016/j.neuroimage.2020.116836>

Garrett, D. D., **Epp, S. M.**, Perry, A., & Lindenberger, U. (2018). Local temporal variability reflects functional integration in the human brain. *NeuroImage*, 183, 776–787.

<https://doi.org/10.1016/j.neuroimage.2018.08.019>

AFFIDAVIT / Eidesstattliche Versicherung

Hiermit versichere ich an Eides statt, dass ich die vorliegende Dissertation "Neuroenergetics and function of the default mode network – quantitative measurement of human brain metabolism“ selbstständig angefertigt habe, mich außer der angegebenen keiner weiteren Hilfsmittel bedient und alle Erkenntnisse, die aus dem Schrifttum ganz oder annähernd übernommen sind, als solche kenntlich gemacht und nach ihrer Herkunft unter Bezeichnung der Fundstelle einzeln nachgewiesen habe.

I hereby confirm that the dissertation "Neuroenergetics and function of the default mode network – quantitative measurement of human brain metabolism" is the result of my own work and that I have only used sources or materials listed and specified in the dissertation.

München, 14. Juni 2023

Munich, 14th of June 2023

Samira Maria Epp

DECLARATION OF AUTHOR CONTRIBUTIONS

Project I: Simultaneous measurement of oxygen and glucose consumption during visual stimulation in the human cortex

Samira M. Epp & Antonia Bose, Roman Belenya, Gabriel Castrillón, Katarzyna Kurcyus, Eric Ceballos Dominguez, Andreas Ranft, Eliana Salas Villa, Moritz Bursche, Christine Preibisch, Valentin Riedl

Samira M. Epp, as the author of this thesis, is the shared first author of this manuscript together with Antonia Bose.

SME & AB were responsible for data collection, design optimization, participant organization, data analysis, SME wrote the manuscript with contributions of AB, GC and VR, and finalized all figures. RB performed the quantification of the fPET data, GC assisted with data analysis, data management and manuscript editing, KK assisted with data collection and conceptualization of the design, ECD assisted with the quantification of the fPET data, AR was the responsible medical doctor during data collection, ESV helped with the quantification of the fPET data, MB helped with data collection, CP was responsible for sequence optimization and for the mqBOLD analysis pipeline, VR supervised the project, was responsible for conceptualization, funding and manuscript review.

My contribution to this manuscript in detail:

For this manuscript, I was, together with AB, responsible for the project organization, all data collection & subject management, optimization of design and data quality checks. Further, I analyzed the imaging data via partial least squares analyses and calculated the OGI on the final CMRO2 and CMRglc maps. Finally, I interpreted all final analyses, wrote the manuscript draft, with contributions of AB, and finalized all figures.

Munich, 14th of June 2023

Samira Maria Epp

Antonia Bose

Prof. Dr. med. Valentin Riedl

Project II: Simultaneous measurement of oxygen and glucose consumption during visual stimulation in the human cortex

Samira M. Epp & Antonia Bose, Roman Belenya, Gabriel Castrillón, Katarzyna Kurcyus, Eric Ceballos Dominguez, Andreas Ranft, Eliana Salas Villa, Moritz Bursche, Christine Preibisch, Valentin Riedl

Samira M. Epp, as the author of this thesis, is the shared first author of this manuscript together with Antonia Bose.

SME & AB were responsible for data collection, design optimization, participant organization, data analysis, SME wrote the manuscript with contributions of AB, GC and VR, and finalized all figures. RB performed the quantification of the fPET data, GC assisted with data analysis, data management and manuscript editing, KK assisted with data collection and conceptualization of the design, ECD assisted with the quantification of the fPET data, AR was the responsible medical doctor during data collection, ESV helped with the quantification of the fPET data, MB helped with data collection, CP was responsible for sequence optimization and for the mqBOLD analysis pipeline, VR supervised the project, was responsible for conceptualization, funding and manuscript review.

My contribution to this manuscript in detail:

For this manuscript, I was, together with AB, responsible for the project organization, all data collection & subject management, optimization of design and data quality checks. Further, I analyzed the imaging data via partial least squares analyses and calculated the OGI on the final CMRO₂ and CMRglc maps. Finally, I interpreted all final analyses, wrote the manuscript draft, with contributions of AB, and finalized all figures.

Munich, 14th of June 2023

Samira Maria Epp

Prof. Dr. med. Valentin Riedl